

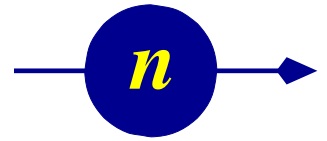


Technical University of Denmark

DTU



McStas



- CAMEA –
Continuous Angle
Multi-Energy
Analysis – An
Inelastic Neutron
Spectrometer for
the European
Spallation Source



PAUL SCHERRER INSTITUT



ÉCOLE POLYTECHNIQUE
FÉDÉRALE DE LAUSANNE

CAMEA – Continuous Angle Multi-Energy Analysis – Spectrometer Concept Phase Report

Abstract:

CAMEA is an indirect geometry spectrometer conceived by a Danish (Copenhagen University, Technical University of Denmark) and Swiss (École Polytechnique Fédérale de Lausanne, Paul Scherrer Institut) Collaboration for the European Spallation Source (ESS), Lund, Sweden. The CAMEA instrument concept has been selected for construction at the ESS, subject to a feasibility study. This document is the final report for the concept phase of the CAMEA instrument project for the European Spallation Source. The material contained within this report represents updated versions of all of the reports submitted for the instrument proposal to the ESS, from which CAMEA was selected for construction.

Contents:

In this report each chapter represents a report that was submitted as part of the instrument proposal. The page numbering of this final report is indicated in the top right hand corner in blue text, with other page numbering being internal number of the individual report.

The chapters of this report are as follows:

- 1) Instrument Proposal
- 2) Concept and Science Case
- 3) Demand for CAMEA
- 4) Simulations and Kinetic Calculations
- 5) Analytical Calculations for CAMEA
- 6) Guide Report
- 7) Benching Mark CAMEA
- 8) CAMEA Comparison to direct Time-of-Flight Spectrometer
- 9) Building and Testing a Prototype for CAMEA
- 10) Pyrolytic Graphite Experimental Results
- 11) Technical Solutions
- 12) Costing Report

Additionally to conclude this phase of the CAMEA project:

- 13) Executive Summary of the Project Achievements

Page Numbering

Chapter 1 - Instrument Proposal	8
EXECUTIVE SUMMARY	11
1. INSTRUMENT PROPOSAL	12
1.1 Instrument Capability and Performance Summary	12
1.1.1 Scientific Impact	13
1.1.2 User Base and Demand	18
1.1.3 Strategy and Uniqueness	19
1.2 Description of Instrument Concept and Performance	21
1.2.1 Instrument Description – Overall description of the proposed instrument	21
1.2.2. Instrument Performance – Quantitative performance of proposed instrument	32
1.3 Technical Maturity	39
1.3.1 Guide	39
1.3.2 Choppers	39
1.3.3 Sample and Sample Environment	39
1.3.4 Analysers	40
1.3.5 Detectors	41
1.3.6 Electronics	42
1.3.7 Shielding	42
1.4 Costing	42
References	44
2. LIST OF ABBREVIATIONS	47
Chapter 2 Concept and Science Case	48
Abstract	50
1) Concept	53
1a) Motivation	53

1b) Existing Spectrometers that address the science case of CAMEA	54
1c) CAMEA Instrument Concept	55
1d) Instrument Parameters	58
1e) Advantages of Multi-analyser System	59
1f) Polarization analysis	61
2) Experimenting Capabilities of CAMEA	62
3) CAMEA for Science	74
4) Concluding Remarks	86
References	87

Chapter 3 Demand for CAMEA 90

i) Letters of support	92
ii) List of supporters of CAMEA	104
iii) Survey of for CAMEA capability	105

Chapter 4 Simulations and Kinetic Calculations 106

1 Introduction	109
2 Working model	110
3 Coverage	111
4 The Chopper system	117
5 Analysers	122
6 Detectors	128
7 Additional issues on Analyzer-Detector interaction	129
8 Time Resolved measurements	137
9 The Prototype	138
10 Conclusion	138

Chapter 5	Analytical Calculations for CAMEA	139
1	Introduction	141
2	Primary resolution	141
3	Resolution of the secondary instrument	144
4	Resolution ellipsoid	146
5	Conclusions	148
	References	149
Chapter 6	Guide Report	150
1	Guide for CAMEA proposal	151
1.1	Guide description	151
1.2	Guide geometry	151
1.3	Phase space on sample	151
1.4	Moderator height	151
1.5	Line-of-sight	152
1.6	Coating	152
1.7	Performance - Brilliance transfer	153
1.8	Performance - Absolute units	154
	Figures of performance of proposed guide	155
Chapter 7	Benching Mark CAMEA	162
	Benching mark CAMEA's incident neutron flux and solid angle coverage against present multiplexed triple axis spectrometers and indirect geometry inelastic neutron spectrometers	163
Chapter 8	CAMEA Comparison to direct Time-of-Flight Spectrometer	169
	Contents	
1	Introduction	170

2 Kinematic flux calculations	170
3 Flux simulations	171
4 Background	172
5 Other experimental issues	176
5.1 Coverage	176
5.2 High Resolution	176
5.3 Time Resolution	177
5.4 Thermal Measurements	177
5.5 Bragg peaks	177
6 Conclusions	177
Chapter 9 Building and Testing a Prototype for CAMEA		178
1 Introduction	180
2 Description	180
3 Aligning and calibrating the prototype	183
4 Measurements	187
5 Conclusions	193
References	193
Chapter 10 Pyrolytic Graphite Experimental Results		194
1 Introduction	196
2 PG Alignments	196
3 Reflectivity and Transmissions Measurement	199
4 Cooled PG Experiments	200
5 Outlook	206
References	206

Chapter 11	Technical Solutions	207
1 Introduction	208
2 Sample area	208
3 The Analyser-detector tank	209
4 Analysers	212
5 Beam vanes	212
6 Detectors	212
7 Magnetic materials	213
Chapter 12	Costing Report	214
1. Guides and shielding	216
2. CAMEA spectrometer	219
3. Sample environment for CAMEA	224
4. Manpower	225
5. Summary of construction costs	225
6. Conclusion	227
Chapter 13	Executive Summary of the CAMEA Project Achievements	228

ESS Instrument Construction Proposal CAMEA

Please read the call for instrument proposals found at europeanspallationsource.se/instruments2013 and the "Preparation and Review of an Instrument Construction Proposal" to guide you in preparing your instrument construction proposal.

	Name (name, title, e-mail address)	Affiliation (name of institution, address)
Proposer	Henrik Ronnow, Prof., Henrik.ronnow@epfl.ch	EPFL SB ICMP LQM PH D2 455 (Bâtiment PH) Station 3 CH-1015 Lausanne Switzerland
Co-proposers	Kim Lefmann, Prof., lefmann@fys.ku.dk Niels Bech Christensen, Prof. nbch@fysik.dtu.dk Christof Niedermayer, Prof., christof.niedermayer@psi.ch Fanni Jurányi, Dr., fanni.juranyi@psi.ch Márton Markó, Dr. marton.marko@psi.ch Jonas Okkels Birk, Mr., jonaso@fys.ku.dk Mads Bertelsen, Mr., mads.bertelsen@gmail.com	University of Copenhagen, Universitetsparken 5, DK 2100 København Ø, Denmark Technical University of Denmark, Fysikvej, 311 DK-2800, Kgs. Lyngby, Denmark Paul Scherrer Institute, 5232 Villigen – PSI, Switzerland Paul Scherrer Institute, 5232 Villigen – PSI, Switzerland Paul Scherrer Institute, 5232 Villigen PSI, Switzerland University of Copenhagen, Universitetsparken 5, DK 2100 København Ø, Denmark Niels Bohr Institute, Universitetsparken 5, DK 2100 København Ø, Denmark

Document Number MXName
 Project Name CAMEA
 Date 05/05/2014
 Revision Final Version
 State MXCurrent Copy

	Jacob Larsen, Dr., jacb@fysik.dtu.dk	Technical University of Denmark, Fysikvej, 311 DK-2800, Kgs. Lyngby, Denmark
	Paul Gregory Freeman, Dr., paul.freeman@epfl.ch	EPFL SB ICMP LQM, CH-1015 Lausanne, Switzerland.
ESS coordinator	Arno Hiess	

Note: All proposals received by ESS will be included as Expressions of Interest for In-kind contributions. ESS will use this information for planning purposes and the proposer or affiliated organization is not obligated to materially contribute to the project.

The following table is used to track the ESS internal distribution of the submitted proposal.

	Name
Document submitted to	Ken Andersen
Distribution	SAC, Dimitri Argyriou, Oliver Kirstein, Arno Hiess, Robert Connatser, Sindra Petersson Årsköld, Richard Hall-Wilton, Phillip Bentley, Iain Sutton, Thomas Gahl, relevant STAP

MXType.Localized
Document Number Final Porposal
Project Name CAMEA
Date 05/05/2014

ENCLOSURES

Concept and Science Case

Scientific Demand for CAMEA

Bench Marking

Guide Report

Simulation and Kinematic Calculations

Comparison to the Cold Chopper Spectrometer

Analytical Calculations for CAMEA

Building and testing Prototype for CAMEA

Pyrolytic Graphite Experimental Results

Technical Solutions

Costing Report

MXType.Localized
Document Number Final Proposal
Project Name CAMEA
Date 05/05/2014

EXECUTIVE SUMMARY

We propose the construction of a highly innovative spectrometer – **CAMEA** – offering **Continuous Angular and Multiple Energy Analysis**. Combining indirect time-of-flight with multiple consecutive analyser arrays, this instrument will provide massive flux on the sample and strongly enhanced efficiency in detecting neutrons scattered in the horizontal plane. The combination yields a spectrometer with completely unprecedented performance - with **gains from 2 up to 4 orders of magnitude compared to current state of the art**.

This increase in neutron detection efficiency will bring current fields of neutron spectroscopy to a new level, and will open the powerful technique of neutron spectroscopy to new scientific communities. While ~1000mm³ samples is currently the practical limit for neutron spectroscopy **CAMEA makes it possible to study <1mm³ samples**. Furthermore, being optimized for collecting the maximum number of neutrons scattered in the horizontal plane, CAMEA is superior in combination with large split-coil magnets and anvil-type high-pressure cells. The dramatic reduction in required sample size and the extreme conditions capabilities will enable a series of new possibilities:

- Neutron spectroscopy will become a powerful tool in the discovery of new functionally advanced materials, including search for new superconductors, multiferroics, thermo-electrics etc.
- Neutron spectroscopy will become possible at pressures >10 GPA both at low temperature for tuning fundamental electronic states of matter and at high temperatures, which will attract the fields of planetary science to use neutron scattering under geophysically relevant conditions.
- The study of molecular dynamics in biological matter will become feasible.
- Complete mapping of excitation spectra will become possible in higher magnetic fields than currently possible
- Excitation maps can be measured sufficiently fast that in-situ and real-time studies become possible with 20 micro-second stroboscopic time-resolution.

The strong scientific case for CAMEA is described in this proposal, in the dedicated Science Case Report, and documented by letters of support from leading scientists in **research fields ranging from fundamental quantum magnetism and correlated electron physics over materials discovery and planetary sciences to life sciences**.

While the complete CAMEA instrument is highly innovative and goes beyond any previous similar multiplexing crystal analyser instrument, each of its technical solutions have already been implemented in different instruments. Furthermore, the results of the extensive analytic and Monte-Carlo simulations of the instrument and its performance, including resolution and background, have been verified by dedicated prototyping, as we detail in enclosed reports. This provides very **high confidence that the instrument can be built with a very low risk level**, and that it will perform as predicted. In summary, **CAMEA will lift neutron spectroscopy to a new level of applicability, thereby contributing to the goal that ESS will enable new science hitherto uncharted**.

MXType.Localized
 Document Number Final Porposal
 Project Name CAMEA
 Date 05/05/2014

TABLE OF CONTENTS

ENCLOSURES	3
Executive Summary	4
Table of Contents	5
1. Instrument Proposal	5
1.1 Instrument Capability and Performance Summary	5
1.2 Description of Instrument Concept and Performance	13
1.3 Technical Maturity	31
1.4 Costing.....	34
2. List of Abbreviations	39

1. INSTRUMENT PROPOSAL

1.1 Instrument Capability and Performance Summary

We propose an indirect geometry neutron spectrometer optimized for high efficiency neutron counting rates within the horizontal scattering plane to be constructed as one of the instruments at the ESS. To obtain the highest count rate we use a 165 m long guide and take advantage of the full neutron flux of a medium bandwidth of incident neutron wavelengths. The analyser concept is called CAMEA, the Continuous Angle Multi-Energy Analysis spectrometer, and it utilizes the high transmission rate of neutron analyser crystals to place 10 arcs of analyser crystals behind each other to detect different final neutron energies of scattered neutrons, over a large angular range. The analyser arcs are placed at distances of 1 – 1.8 m from the sample position, scattering neutrons downwards into position sensitive detectors to detect both the horizontal scattering direction and energy.

The analysers give the instrument an energy resolution somewhat better than most cold neutron triple axis spectrometers, $\Delta E/E$ of 1.2-4.2 %, similar to the typical energy resolution of direct geometry time-of-flight cold neutron chopper spectrometers. We have optimized the instrument to study excitations of materials in the energy range of 0-20 meV, with an extended range up to 60 meV. The optimization is ideally suited to the needs of the established research communities in quantum magnetism and strongly correlated electron systems. Optimization for a horizontal scattering plane is chosen as this scattering plane matches well with the restricted neutron access of complex sample environments, such as cryomagnets and high pressure anvil cells. Optimization for working with complex sample environments also opens the possibility for the instrument to perform in-situ and time-dependent studies of excitations. In the Supplementary Material, we show that CAMEA has a count rate for down-scattered neutrons 20 times higher than cold direct Time of Flight spectrometers on identical guides when using extreme sample environment, and a factor 1.5 times higher when no sample environment is used. The instrument concept was invented following scientific needs within several communities [Scientific demand for CAMEA]. The instrument performance and

MXType.Localized
Document Number Final Proposal
Project Name CAMEA
Date 05/05/2014

optimization have been determined by the use of computer simulations. Analytic calculations were performed in parallel to the simulations to gain an understanding of the simulation results. A prototype of the secondary spectrometer has been built in combination with an existing time-of-flight spectrometer and was extensively tested with neutrons. The prototype testing has been used to develop techniques for construction and formulating the method for commissioning this instrument type. The prototyping also confirmed the validity of our computer simulations and analytical calculations.

This instrument project is developed as a Swiss-Danish work package. The contributors are based at the University of Copenhagen (KU, Denmark), the Technical University of Denmark (DTU, Denmark), École Polytechnique Fédérale de Lausanne (EPFL, Switzerland), and the Paul Scherrer Institut (PSI, Switzerland). The work unit has considerable experience in inelastic neutron instrumentation (RITA-2; Focus; Mars at PSI, IN8; IN22 at ILL; EXED at HZB). Work in the proposal has been carried out from September 2011 to 31st March 2014 and has been developed with the aid of scientific feedback from the Indirect Geometry Spectrometers Scientific and Technical Advisory Panel of the ESS.

1.1.1 Scientific Impact

The central goal of our proposed instrument is to make maximum use of the neutron flux from the ESS pulse with high energy resolution, to achieve the highest possible neutron count rates within a horizontal scattering plane, with a high signal-to-noise ratio. Scientific output from this instrument will include studies that present neutron instrumentation cannot achieve. CAMEA has gain factors in the orders of 1000 compared to existing instruments [bench marking].

Material Discovery: The ability to study samples down to 1mm³ [bench marking] will promote the technique of neutron spectroscopy from its current role of examining well established compounds to become an integrated part of the iterative process to discover new materials classes. Not only will neutron spectroscopy be applicable much earlier after a material is discovered, it will also become possible for materials synthesized under conditions that will never produce large crystals, such as high-pressure synthesis (which is how the highest T_c iron-based superconductors were first crystalized) and hydrothermal synthesis (which is how the best known realization of a kagome quantum magnet is synthesized)[concept and science case]. This will lead to input from inelastic neutron scattering immediately after materials are discovered, or directly lead to discovery of materials. At present a large amount of experimental and theoretical work is wasted due to incorrect assumptions made about the spin and lattice interactions in materials, inelastic neutron scattering unambiguously resolves these issues.

Quantum Magnetism, High Definition Mapping: The good energy and momentum resolution will enable high definition mapping of excitations in the scattering plane, greatly facilitating interpretation of complex excitation spectra. In systems such as quantum magnets there is often a weak continuum of excitations spread across large areas of reciprocal space. The detailed structure of this continuum that can be measured by neutron spectroscopy presently is inferior to that which can be theoretically predicted. High definition mapping with high count rates on CAMEA will bridge this gap to test our fundamental understanding of

MXType.Localized
Document Number Final Proposal
Project Name CAMEA
Date 05/05/2014

quantum magnetism, leading to both detailed tests of theories and the identification of new quantum phenomena.

Rapid Mapping to Study Critical Transitions: The high count rate and essentially complete angular and energy coverage in a single acquisition will enable continuous parametric scanning of excitations. At phase transition boundaries, current instrumentation can only be used to map out excitation spectra at a few selected positions on the two sides of the phase transitions, whereas rapid mapping of excitations by CAMEA will resolve the evolution of spectra as the control parameter (temperature, magnetic field etc.) is tuned continuously across the phase transition. CAMEA can be aligned on a specific excitation and study that excitation dependence of a sample parameter in a continuous manner, equivalent to a temperature ramp in powder neutron diffraction.

Time Resolved Studies: With a time resolution of $\sim 20 \mu\text{s}$, see section 1.2.2.1 CAMEA opens up the possibility for studying the time evolution of excitations following a change of parameters, such as a laser pulse, an electric field pulse etc. This time resolution is for instance sufficient to capture the magnetic field dependence during a pulsed magnet cycle[concept and science case].

Due to the long-pulsed nature of ESS, any particular wavelength will impinge on the sample over a time span of 3 ms, during which, the mean wavelength varies only slightly. Hence, a particular value of scattering vector and energy transfer is probed during 3 ms, with a time resolution at least 100 times better. In this way, CAMEA gains over the direct time-of-flight spectrometers, which chop the incident beam, so that an incident pulse will probe one specific energy only during some tens of μs . Hence, to examine a particular signal over 3 ms, with the same time resolution as CAMEA, requires on a direct geometry spectrometer 100 settings of the time-delay.

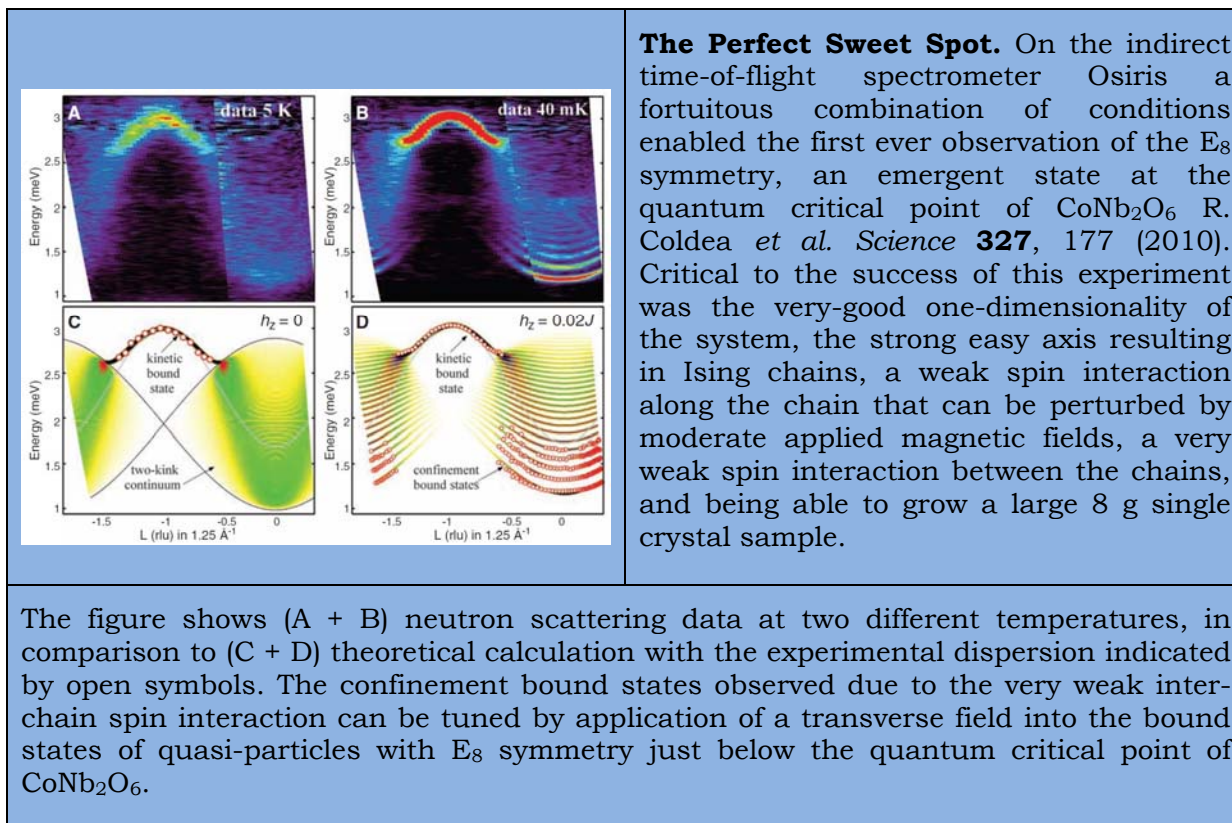
The time resolved capabilities of CAMEA will allow for pump-probe experiments to study the out-of-equilibrium evolution of systems, of relevance to functional materials for energy research, such as catalysts. It will also enable studies of the response of soft matter to external stimuli such as light.

Complex Sample Environment and Small Samples: The CAMEA instrument has been designed to achieve a high signal-to-noise ratio with complex sample environment by minimizing the background count rate. In direct geometry time-of-flight spectrometers, a neutron that scatters elastically off the sample environment may enter the neutron detectors with a time offset that will be misinterpreted as inelastic scattering[Comparison to Cold Chopper]. Even if this background signal on direct geometry spectrometers can be reduced by radial collimators, the elastic scattering from complex sample environment may render parts of the inelastic spectra unusable. In this respect, CAMEA will have two advantages: 1) The tightly defined neutron flight path (by shielding and collimation) reduces visibility of the sample environment and diffuse background scattering. 2) The long primary flight path ensures that any time offset from elastic sample environment scattering does not place background neutrons in the inelastic spectrum.

CAMEA will use a series of absorbing jaws in the guide to control the incoming beam divergence. This concept has been implemented on the WISH instrument at ISIS [Chapon11] and together with traditional slits close to the sample it will also

MXType.Localized
 Document Number Final Porposal
 Project Name CAMEA
 Date 05/05/2014

allow a very good definition of the beam spot. A small beam size is vital for studying small samples of crystals that do not exist in large size, e.g. newly discovered materials. A small beam size is also essential for studies in pressure cells where the sample volume is very limited. With CAMEA at ESS we will be able to study excitations in 1 mm³ sized samples [bench marking].



Magnetism Under Applied Magnetic Fields: This instrument represents a significant advancement for inelastic neutron scattering in scientific fields where application of a strong magnetic field is required. In quantum magnetism and strongly correlated systems the cleanest way to study transitions, and reach new magnetic phases of matter is to use a tuning variable. In the case of using applied magnetic fields this instrument creates the ability to scan across the transition to determine the nature of magnetic quantum phase transitions [concept and science case].

Magnetism Under Extreme Pressure: Applying extreme pressures to study materials is presently of minimal use in inelastic neutron scattering due to the limited sample volume that can be used in pressure cells. By allowing spectroscopy on smaller samples, CAMEA will open the door to systematic studies of excitation spectra up to very high pressures. Pressures of 1-10 GPa are sufficient to induce measurable changes in hopping integrals that govern electronic motion between states and hence effects the electronic interactions driving phase transitions. By changing the hopping integral we will therefore allow testing interpretations and theories predicting materials' magnetic and electronic properties. In this fashion, the unique scientific output from studies under pressure will become a significant evolution in neutron scattering.

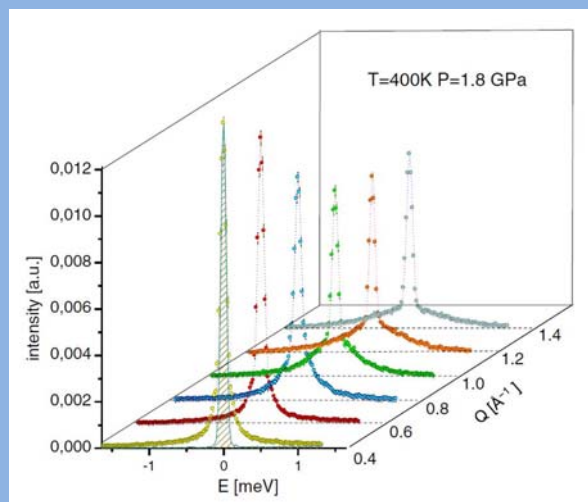
MXType.Localized
Document Number Final Proposal
Project Name CAMEA
Date 05/05/2014

Functional Materials: CAMEA has many advantages for studying complex materials with properties that have potential for practical applications. The rapid mapping capability of CAMEA provides a way to scan many materials providing a way to explore complete series of materials which will direct the evolution in material design, of e.g. thermoelectric materials, fuel cell materials and molecular magnets. Use of radial collimation on CAMEA to remove the visibility of the sample environments allows functional materials to be studied in-situ. In-situ studies on CAMEA will for instance investigate working components of fuel-cells, batteries, magnetic cooling systems, and the processing of materials. By the use of the beam definition jaws, a well-defined incident neutron beam will enable the scanning with precision down to 3 mm the in-situ performance across the active volume.

Soft Matter: Inelastic neutron scattering from soft matter has previously concentrated on neutron spin echo techniques to determine materials elasticity and compressibility, while quasi-elastic neutron scattering (QENS) is used to study incoherent motions of the molecules in materials. Incoherent processes in molecules include vibrations, rotations, librations (hindered rotations) and diffusion. Molecular dynamic computer models have however evolved to describe molecule behaviour over the complete energy and wavevector range of inelastic neutron scattering. Inelastic neutron scattering is developing into studies of collective (hence wave-vector-dependent) dynamics in soft matter. For example in membranes, collective dynamics are believed to drive transport of molecules, pore opening, membrane fusions and protein-protein interactions [Rheinstädter12]. Inelastic neutron scattering is required to measure the dispersion of these collective motions [Rheinstädter04]. In soft matter research CAMEA will study incoherent processes with moderate resolution QENS, compared to ultra-high energy resolution backscattering QENS, and provide high resolution measurements of the collective dynamics in soft matter. At CAMEA soft matter experiments will take advantage of the small sample capability, the efficient screening of background from sample environments on CAMEA, and the ability of polarization analysis to separate coherent and incoherent motions. Furthermore, CAMEA provides the ability for time resolved studies of soft matter stimulated out of equilibrium using pump-probe techniques.

Geoscience: There exist a great hitherto unaccommodated interest to study lattice dynamics in simple material under extreme pressure, and for geo- and planetary science related studies such as hydrogen diffusion in materials of the Earth's upper mantle. CAMEA is ideally suited for both purposes. Despite the fact that water is vital for life on Earth we have little knowledge on the extent of the water cycle in the Earth's mantle, with estimates on the water in the mantle varying from ten percent to two and a half times the water on the Earth's surface. The uptake of water into the material of the Earth's mantle greatly influences the properties of the materials, which has consequences for flow of material and sound velocities in the mantle, studying these materials has the potential to provide great insight into plate-tectonics and seismic activity[concept and science case, Hirschmann12].

The Hidden Water Cycle. Little is known about the behaviour of water under extreme conditions, and how far into the interior of planets the water cycle goes. Researchers are only presently able to study the dynamics of pure water under gigapascal pressure and elevated temperatures in an energy range well suited to CAMEA. To understand water's effects on the Earth's mantle and the hidden water cycle, CAMEA will be able to measure the dynamics of hydrogen in the extreme conditions of Earth's upper mantle, where water concentrations may be at the one percent level and greatly influence the properties of the Earth's mantle [D. G. Pearson *et. al.*, Nature **507**, 221 (2014)].



Inelastic neutron scattering of the dynamics of water under high pressure and temperature. [L. E. Bove *et. al.*, Phys. Rev. Lett. **111**, 185901 (2013)].

Complimentary Techniques: Development of x-ray scattering techniques has led to complementarity and occasional competition with inelastic neutron scattering in measuring excitations. X-ray scattering techniques have the advantage of being able to study small samples typically down to 100 μm . However, inelastic X-ray scattering (IXS) cannot readily observe phonon modes involving light elements, and the best energy resolution that is achieved is 0.8 meV compared to below 20 μeV for CAMEA. Resonant Inelastic X-ray Scattering (RIXS) can be used to study magnetic excitations but today's 30 meV resolution is poor and fundamental limitations makes it highly unlikely that resolution will improve below 5-10 meV even by 2020. Furthermore, the soft x-rays used will be unable to penetrate complex sample environments, and it will be difficult to achieve low temperatures significantly below 10 K due to sample heating. Last, the long x-ray wavelength needed to access the most important L-edge of transition metals provides a fundamentally limited coverage in reciprocal space. It is therefore clear that the wavevector and energy dependencies that can be obtained by cold inelastic neutron scattering are unique.

Grand Challenges: In 2007 in the USA the National Research Council of the National Academies produced a report commissioned by the Department of Energy, and the National Science Foundation, on the grand challenges in condensed matter and materials physics for the coming decade[grand_challenges]. The grand challenges identified in this report remain for the next decade and beyond. Of the six grand challenges that were identified, three can be directly addressed by CAMEA with capabilities far beyond present instrumentation i) How do complex phenomena emerge from simple ingredients? ii) How to meet the energy demand of future generations, and iii) What happens far from equilibrium and why? In magnetism a prominent way to discover emergent phenomena is the use of extreme environments

MXType.Localized
Document Number Final Proposal
Project Name CAMEA
Date 05/05/2014

to tune the magnetic interactions in materials, which CAMEA is ideally suited for. The ability of CAMEA for studies on functional materials in-situ in the components of fuel-cells, batteries, magnetic refrigeration, superconductors and the processing of materials, address the challenge of future energy demands. In-situ experimentation on CAMEA, including time resolved studies, will enable novel experiments providing insight into out of equilibrium processes, in both functional materials, in fundamental model materials and in the complex behaviour of soft matter.

1.1.2 User Base and Demand

The proposed instrument addresses the needs of multiple user communities in condensed matter physics, especially but far from exclusively in magnetism. Inelastic neutron scattering has provided a unique experimental tool for the investigation of the wavevector and energy dependence of magnetic fluctuations in electronically complex materials. In research fields such as quantum magnetism and high temperature superconductivity the results of inelastic neutron scattering provide unique information that often lead to break-through understandings. By understanding the magnetism of correlated electron systems we gain fundamental knowledge that may provide vital insight for conceiving materials for devices in the future. An illustrative analogy is how the development of the theory of electrons in solids, notably semi-conductors, enabled the development of solid state devices such as the transistor.

We have studied the user base and demand for the proposed instrument, as can be found in the report “concept and science case”. The correlated electron and magnetism research fields dominate the user community of many inelastic neutron spectrometers, as can be observed in the publication lists for these spectrometers. Despite the significant increase in the number of spectrometers available for studying the magnetic excitations, the user demand for beamtime has continued to grow outpacing the availability of beamtime. Currently, one third of the user beamtime on cold neutron spectrometers in Europe is conducted with application of magnetic fields – for which the CAMEA instrument is ideally suited. With present neutron instrumentation studies of magnetism under extreme pressures is virtually non-existent due to the limitation on sample size, a shortcoming which will be addressed by the enhanced performance of CAMEA.

Indeed, there is a strong existing neutron scattering user community eagerly awaiting to use CAMEA to perform spectroscopy of materials under extreme pressures, and there is no existing spectrometer to perform these experiments [ESS-Symposium on Spin Dynamics 12]. On top of the existing demand, we expect emergence of research communities within a number of topics, which do not present have established neutron user communities due to lack of proper instrumentation: In-situ measurements of excitations; time resolved studies (i.e. pulsed magnetic/electric fields); excitations in soft matter aligned by high fields; and high pressure and high temperature studies of materials (geo- and planetary sciences).

The strongest present demand for CAMEA clearly comes from the magnetism community, but as shown above there is a strong potential for a scientific impact in

MXType.Localized
 Document Number Final Porposal
 Project Name CAMEA
 Date 05/05/2014

other fields of research. These communities will grow with the capabilities of the ESS, and further increase the demand for beamtime on CAMEA.

1.1.3 Strategy and Uniqueness

The instrument we are proposing here fits into the strategy of the indirect spectroscopy to provide instrumentation that covers from high resolution low energy studies, over medium energy resolution studies to high energies. CAMEA bridges the dynamic energy range from the ultra-high resolution low energy studies of backscattering spectroscopy to that of medium resolution vibrational spectroscopy. This instrument also provides additional experimental capabilities compared to the capabilities of cold direct geometry time-of-flight chopper spectrometers. In particular CAMEA can fulfil the demand by the magnetism user community for an inelastic spectrometer that can perform experiments under extreme conditions [ESS-SymposiumonSpinDynamics12].

Instrument	CAMEA Flux Gain	CAMEA Analyser $\pm 1.4^\circ$ Solid Angle Gain [§]	CAMEA Gain Factor
IN14 with Flatcone	105	27.7	2910
PANDA with Flatcone*	947	27.7	26200
THALES with Flatcone [#]	51	27.7	1410
MACS ⁺	36	17.8	640
OSIRIS	554	7.7	4270
IRIS	1500	8.4	12600
PRISMA	>20 [≡]	82.4	>1650

[§]The full multiplied gain factor is only applicable for cases where the entire coverage of $S(q, \omega)$ is scientifically relevant. The solid angle gain includes a comparison of the total analyser coverage of CAMEA corrected for transmission efficiency of the CAMEA analysers, conservatively estimate as a total gain factor of 7.1 for the 10 analysers.

*Flatcone is not available at FRM-II for PANDA. The CAMEA flux gain is in comparison to PANDA using a monochromator with vertical focusing only.

[#]This gain factor is reduced to 135 for THALES using a CAMEA type secondary spectrometer.

⁺ Flux gain compares CAMEA to the low energy resolution, high flux thermal setup of MACS.

[≡]The absolute flux of Prisma is unknown, and this gain factor is a very conservative estimate.

Table 1: The flux and solid angle performance gain of CAMEA compared to multiplexed triple axis and indirect geometry spectrometers [Bench marking].

At present there exists no other neutron spectrometer like the one we are proposing for ESS. Previous indirect spectrometers such as PRISMA (ISIS) and CQS (Los

MXType.Localized
Document Number Final Porposal
Project Name CAMEA
Date 05/05/2014

Alamos) worked with variable final neutron energies but only analysed one neutron energy at a specific scattering angle. For spectrometers the successful development of position sensitive detectors led to the development of direct geometry chopper spectrometers over indirect geometry spectrometers. The strength of direct geometry chopper spectrometers is in measuring excitations over large volumes of reciprocal space. However, direct geometry chopper spectrometers cannot concentrate on specific areas or planes of reciprocal space. CAMEA maps out scattering planes by performing a sample rotation. In the event that the area of reciprocal space of interest is known, the sample rotation scanned by CAMEA can be significantly smaller than a 90° or 180° rotation required to map out all of the reciprocal plane. When working with sample environments that have restricted neutron access only a fraction of the detectors of direct geometry chopper spectrometers are illuminated, so CAMEA's in-plane optimization scans excitations at 20 times higher count rates than corresponding direct ToF spectrometers when the vertical access is limited to $\pm 2^\circ$ (see Comparison_to_the_Cold_Chopper_Spectrometer section 3.1). The indirect geometry spectrometer we are proposing provides a way to concentrate on measuring excitations in specific scattering planes, and is well matched to performing experiments in sample environments that have restricted neutron access. The instrument we propose can be seen as an advanced evolution of multiplexed triple-axis spectrometers (TAS) with multiple analyser channels that have been developed in the last decade [Rodriguez08, Kempa06]. It multiplexes both in angle and in energies, and it exploits the time-of flight method for incident energy determination. Building this instrument at the 5 MW source at the ESS delivers neutron spectroscopy with count rates largely surpassing any existing spectrometers. In table one we highlight the gain factor that CAMEA achieves over both multiplexed TAS and present indirect geometry spectrometers.

This instrument concept incorporates a large sample space that is necessary for sample environments such as cryomagnets, and provides adaptability to accommodate complex sample environment for in-situ studies. The use of a collimated secondary flight path also reduces the visibility of the complex sample environment, which would otherwise produce large quantities of structured background signal. To provide an extended energy range we will use a new order sorting chopper technique and the second order reflections of the analyser crystals, we expect that for in-situ studies of phonons the extended energy and q range will be of great importance.

MXType.Localized
 Document Number Final Porposal
 Project Name CAMEA
 Date 05/05/2014

1.2 Description of Instrument Concept and Performance

1.2.1 Instrument Description

Primary Spectrometer	
Moderator	Cold
Wavelength range (Energy range)	1 Å to 8 Å (81.8 meV to 1.3 meV)
Bandwidth at sample position	1.7 Å
Guide length and shape	165 m - Parabolic feeder to double elliptical guide
Line-of-sight removal	Kink between elliptical guide sections
Number of choppers	7, operating from 840 rpm to 12600 rpm
Incoming divergence	2.0° vertical, 1.5° horizontal
Divergence control	5 divergence jaws integrated in guide
Incoming energy resolution	Adjustable from 0.1 % to 3 % at 5 meV
Sample	
Maximum flux on sample position	1.8×10^{10} n/s/cm ² /1.7 Å
Wavevector range at elastic position (including PG(004) reflections)	PG(002) reflections: 0.058 Å ⁻¹ to 3.6 Å ⁻¹ PG(004) reflections: 0.12 Å ⁻¹ to 7.26 Å ⁻¹
Background count rate	< 5e-5 compared to elastic signal of vanadium (result from prototype testing)
Beam size at sample position	1.5 cm * 1.5 cm
Beam size optimization	0.1 cm * 0.1 cm - 1 cm * 1 cm
Sample environment space	90 cm diameter, side access possible
Magnetic fields	>20T, >10T with 10GPa, 0.1K-350K
Pressure	30GPa with 5mm ³ sample, T=3-2000K 10GPa with 50mm ³ sample, T=0.1-1800K
Secondary Spectrometer	
Collimation	Radial collimation after sample. Cross talk collimation in secondary spectrometer.
Filter	Removable cooled Be-filter before analyzers
Analyzer crystals	2 m ² cooled pyrolytic graphite (PG) - 60" mosaicity, using (002) and (004) reflections
Detectors	2.5 m ² Position sensitive ³ He at 7 bar
Number of analyzer arcs	10
Number of analyzer-detector segments	15 (9° per segment, 6° active)
Sample to analyzer distances	1.00 m to 1.79 m
Analyzer to detector distances	0.80 m to 1.45 m
Horizontal angular coverage	3°-135°
Horizontal angular resolution	0.79° to 0.46°
Vertical angular coverage	±1.4°
Final neutron energy range	PG(002): 2.5 meV to 8.0 meV PG(002)+PG(004): 2.5 meV to 32 meV
Secondary energy resolution	0.77 % to 1.3 %
Time resolution	20 μs
Neutron polarization and analysis	Polarizing supermirrors

MXType.Localized
Document Number Final Porposal
Project Name CAMEA
Date 05/05/2014

ESS-CAMEA is a new cold-neutron inverse-geometry time-of-flight spectrometer concept. It combines several different techniques to achieve an unprecedented high count rate in the horizontal scattering plane together with good resolution.

First, the inverse time-of-flight primary spectrometer ensures that the sample receives a broad incoming wavelength band, where we have the flexibility to choose between good incoming energy resolution, or a high flux mode that utilises the entire ESS long-pulse.

After the sample, analysers arranged in arcs around the sample ensures that a large fraction of the in-plane scattering angles are covered. Each analyser bank covers 6° and reflects neutrons down towards position sensitive detectors in order to combine a large angular coverage with good angular resolution. Further the analysers are focusing in the vertical direction to increase the covered solid angle.

CAMEA uses 10 concentric PG analyser arcs to reflect 10 energy bands towards the detectors, thereby increasing the energy-coverage greatly.

Finally a new multi wavelength analyser technique enables separation of the reflected neutrons from each analyser arc into 3 separate bands thereby both increasing the energy-coverage and improving the resolution.

In the following we will describe each feature in more detail. An overview of the instrument is seen in figure 1.

CAMEA will have two modes for selecting the energy coverage of the measurement, and two modes of resolution for both energy coverages.

The **Maximum Coverage Mode** uses the order sorting chopper pairs to avoid any overlapping of the neutrons selected by the first or second order scattering of the analysers. The order sorting choppers reduce the incident intensity, but provide increased q and energy range in a one-shot measurement.

The **Focused Mode** uses Be filter between the sample and analysers, while the order sorting choppers are stopped. In this mode the full incident intensity and the first 7 out of 10 analysers are used. This mode gives high intensity in a limited q and energy range.

After selection of the energy coverage mode, a choice of resolution setting is made:

The **Resolution Matching Mode** employs the pulse shaping chopper in order to provide matching between primary and secondary resolution at a given energy transfer. It is possible to match the resolutions up to an energy transfer of 20 meV, though at a more moderate flux than in the high flux mode.

The **Maximum Flux Mode** opens the pulse shaping choppers to use the full pulse. This produces an even higher flux but relaxes the Energy resolution to $\Delta E/E=4\%$ at 5 meV elastic scattering.

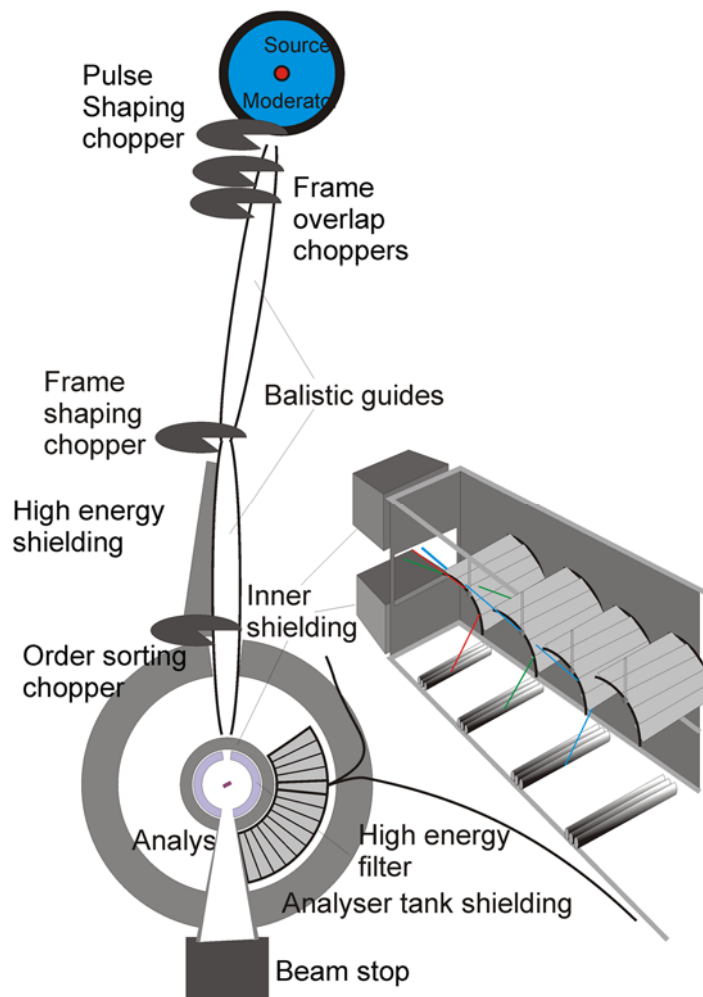


Figure 1: An overview of the CAMEA instrument (not to scale). Two long ballistic guides lead the neutrons from moderator to sample. The guides are kinked by a small angle to avoid direct line-of-sight. The sample is surrounded by the analyser-detector chamber that covers a large angle within the horizontal plane. A cross section of one multi-analyser-detector module is shown as an insert. The positions of the most important choppers are sketched.

1.2.1.1 Moderator and Guide

CAMEA is optimized for the study of excitations in the energy range 0-20 meV, and the analyser settings cover the energy range 2.5-8 meV. The most frequently used incident energies will cover the energy range 1.6-28 meV, or in wavelength 1.7-7 Å. Since much of the science case covers magnetism and correlated electrons, many experiments will be performed at low temperatures. Hence, CAMEA is designed mostly for energy down-scattering, while the quasi-elastic range is still covered.

MXType.Localized
 Document Number Final Porposal
 Project Name CAMEA
 Date 05/05/2014

We choose to use the ESS cold moderator, which covers the desired wavelength range well. We have discarded the use of the bispectral beam extraction system [jacobsen13, zendler12], to eliminate risk. In a bispectral system, degradation of the first reflecting supermirrors very close to the moderator would lead to a dramatic loss of cold neutrons and would potentially compromise the whole instrument.

A key strength of CAMEA is the possibility to combine good resolution and (q, ω) coverage with a higher intensity in each channel than direct time-of-flight instruments. To take full advantage of this feature the instrument needs to be long. If the instrument was moved to half distance and used a frame multiplication system the intensity for a given (q, ω) pixel would be halved, but the coverage in incoming wavelength doubled. It is however also possible for a long instrument to trade flux for coverage by rotating the choppers at a lower frequency thus skipping every second pulse. The opposite is not possible for frame multiplication instruments. So we have chosen an instrument with a length of 165 m as this is the natural length where the 71 ms frame can be filled by one pulse for all resolutions, when the pulse-shaping chopper is placed at the minimum position of 6.5 m [schober08, lefmann13]. This gives a 1.7 Å wide wavelength band. In the high-flux mode, the instrument can run even without using the pulse-shaping chopper.

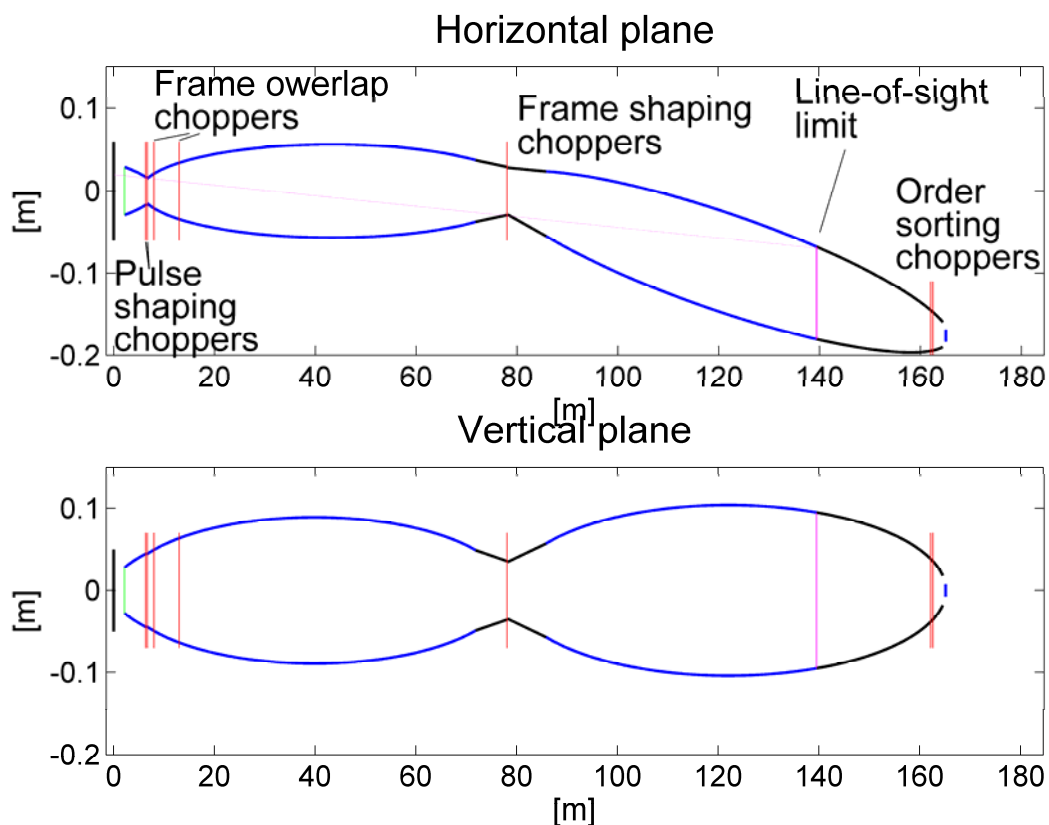


Figure 2: Sketch of guide and chopper system as seen from above.

MXType.Localized
Document Number Final Proposal
Project Name CAMEA
Date 05/05/2014

The guide geometry was chosen by using the guide simulation package GuideBot for McStas [bertelsen14] that allowed investigation and optimization of about 150 different guide geometries as well as many different parameters. The final choice was a guide without line of sight to the sample with very good transport capabilities and a smooth beam profile both in real space and in divergence space.

For the beam extraction system, CAMEA uses a pinhole with a "feeder" guide piece close to the moderator [bertelsen13] for the horizontal part (See figure 2). The vertical part of the beam extraction is an expanding parabola. This extraction system feeds a double ballistic guide [Guide Report]. We have selected the guide system from the requirements that the illuminated beam spot is $15 \times 15 \text{ mm}^2$ and that the desired divergence is $\pm 1.0^\circ$ vertical and $\pm 0.75^\circ$ horizontal. Optimising for a smaller beam spot would only give marginal higher central flux, at the expense of the possibility to measure samples as large as 15 mm diameter. A combination of analytical calculations, and GuideBot optimizations led us to choose a 30 mm wide pinhole, after a gap for the pulse shaping chopper at 6.5 m. The guide opening is 98 mm tall at 6.6 m (see also section 1.3.1).

The guides have a maximum width of 0.23 m in the vertical part and 0.15 m in the horizontal direction. The guide sections are kinked with respect to each other by 0.056° in the horizontal plane to avoid direct line-of-sight through the guide [cussen13]. The kink point is narrow, $50 \times 95 \text{ mm}^2$, and is shielded for additional suppression of the fast neutron background. For further background suppression, a tungsten beam block (equivalent to a stopped T-zero chopper) may be inserted in the "fat" part of the first guide with flux reduction below 10%, but resulting in a factor 10 background suppression [filges13].

1.2.1.2 Chopper System

The pulse shaping chopper pair is placed as close to the moderator as possible at 6.5 m and will run in the same direction at 14-210 Hz. The chopper has a diameter of 700 mm with an opening angle of 170° . This makes it possible to use the entire ESS pulse in a high flux mode or reduce the opening to improve the resolution. An opening time of 0.08 ms will be needed to achieve good resolution at typical high energies (20 meV), matching the resolution contribution of the 5 meV analyser (54 μeV). To achieve the short opening times with a good pulse shape it is necessary to increase the chopper frequency to 210 Hz.

Both frame overlap and the extra pulses generated when running the pulse shaping chopper will be removed by two 14 Hz choppers placed 8 and 13 m from the moderator, see figure 3. The diameter of these choppers is 700 mm.

A 14 Hz band-defining chopper, 700 mm diameter and with a 158° opening, is placed at the kink point where the guide is narrow. This allows for a precise definition of the wavelength band.

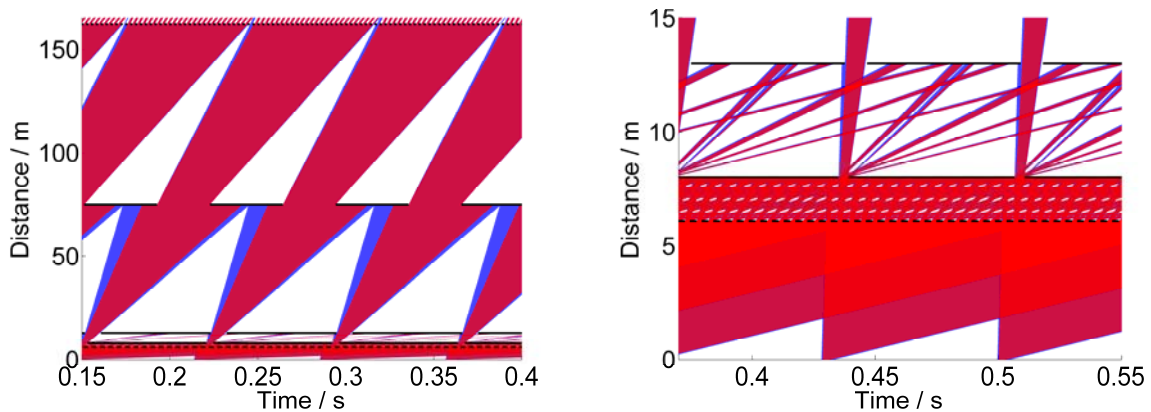


Figure 3: Left: Time-distance diagram of the CAMEA guide system; right: Zoom of the first 15 m. The pulse is shaped by the first chopper pair at 6.5 m, while the next two choppers are eliminating frame overlap and the shaping of the wavelength band is done by the last chopper. The chopper close to the sample is an “order sorting chopper” to be detailed in fig. 4.

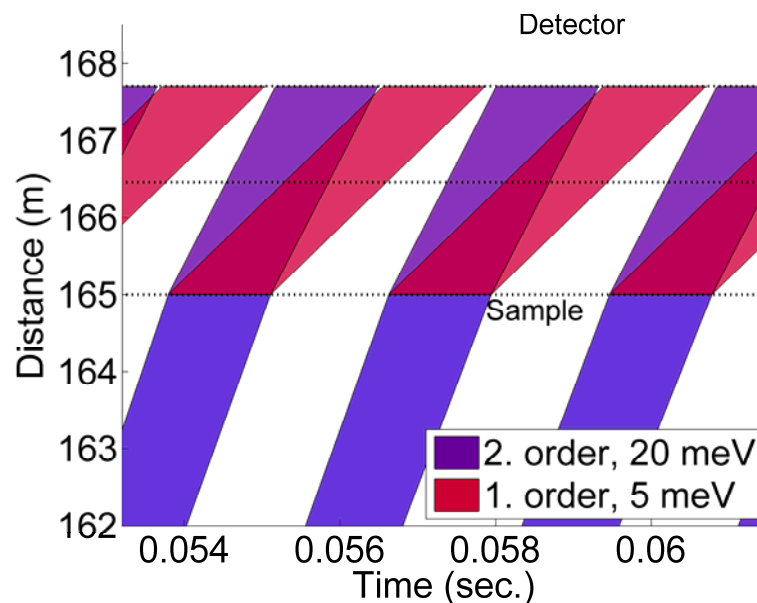


Figure 4: Time-of-flight diagram of the order sorting chopper. At 162 m the chopper divides the pulse into about 25 pulses, at 3 m the neutrons hit the sample and scatters. After that only neutrons that can reflect on the analyser (166.46 m) as first or second order scattering is displayed. The two different velocities will be fully separated at the sample position. The white gaps between the pulses will be filled with overlapping signals mainly due to the choppers open and closing time. The Time-of-Flight diagrams are different for each analyser, here the 7th analyser ($E_f = 5$ meV) is displayed.

At 3 m before the sample we place an optional double chopper. This "order-sorting chopper" has two openings of 80° and spins with 180Hz. The effect of this chopper is to allow for time-of-flight discrimination of second-order scattering from the

MXType.Localized
Document Number Final Porposal
Project Name CAMEA
Date 05/05/2014

analyser crystals. This method is illustrated in fig. 4. By changing the opening time of the chopper it is additionally possible to discriminate first and second order scattering as well as third order scattering if needed. The flight paths in the secondary instrument are chosen to give the same flight time for each analysed energy, thus one setting of the order sorting chopper will select the first and second order scattering of all of the 10 analyser arrays. The chopper frequency is not a multiple of 14 Hz to ensure that the entire wavelength band is uniformly covered (in this case in just 7 pulses).

1.2.1.3 Sample and Sample Environment

CAMEA is optimized for single crystal experiments. The sample is placed on a sample table of the type known from triple-axis instruments with a double goniometer and translational stages. We have designed the instrument for sample sizes of $10 \times 10 \text{ mm}^2$ or smaller, but have aimed for a slightly larger beam size of $15 \times 15 \text{ mm}^2$ to allow for homogeneous illumination during sample rotation, which we foresee to be a frequent mode of operation.

The sample table will be prepared for holding a large cryomagnet, i.e. with no magnetic parts. The sample table can rotate, but when using bulk sample environment with a designated incoming beam path, the sample rotation will take place on a stick inside the sample environment, as is common practice, e.g. in the Oxford 15 T magnets.

We aim for the most extreme values of sample parameters we can obtain at the time of purchase. Presently, 16 T is the largest commercially available magnetic field (plus 2.0 T Dy boosters of the HZB type). However, magnets with high-temperature superconducting tapes will most likely become available within the coming 6-8 years, lifting the field limit to around 25 T [oxford13].

The magnets and cryostats will be equipped with variable temperature inserts for 2-350 K temperatures, and with dilution refrigerator inserts for temperatures down to 30 mK.

Sample sticks will be available to provide an additional electrical field up to 10 kV/mm. For performing high pressure studies at low temperatures Paris-Edinburgh cells achieving 10 GPa at 3 K are currently available, and design improvements will lead to lower base temperatures <300 mK. High temperature studies desire a pressure cell capable of reaching 30 GPa and > 2000 K, that can be developed from the 97 GPa pressure cells used for neutron diffraction at the SNS.

To provide flexibility in extreme environments a 10 cm wide bore vertical split coil superconducting magnet (>10 T) for a pressure cell (>3 GPa) that can be cooled to <1K is feasible with current technology. This sample environment will provide a large volume of parameter space to explore.

Since CAMEA will be an ultra-high flux instrument, sample activation must be taken seriously. We have designed a movable transport cylinder for active samples, see section 1.3.3.

1.2.1.4 Secondary Spectrometer Tank

The analyser-detector set-up is enclosed in the wedge-shaped secondary spectrometer tank. The inner radius of the tank is 0.50 m, with an outer radius of 3 m. The tank covers 3-135° scattering angle in one scattering direction. A sketch of the tank is shown as figure 5. There is an upgrade possibility to install another tank to the other scattering direction, which could be a medium resolution diffractometer specialized in in-plane scattering.

The analyser-detector module inside the tank is positioned on rails so that it can rotate to slightly different scattering angles. This is necessary to cover the dark angles between analyser arrays, discussed in the next sections. The tank is under vacuum to reduce air scattering and to allow cooling the analysers; details in next sections.

The module consist of 15 segments each covering 9° with a 6° active area. The first segment will be a special half size segment to get as close as possible to the direct beam.

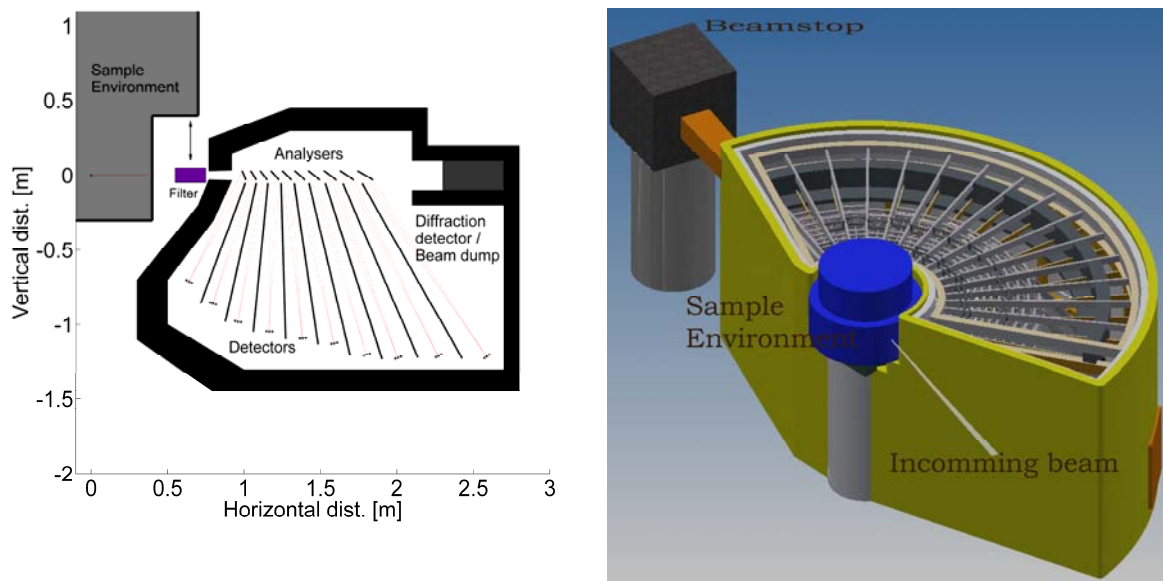


Figure 5: Left: A vertical cut of the secondary spectrometer tank. The sample is at the left, and the neutrons travel from there through the filter. Then the neutrons pass through single-focusing analyser arrays, until scattered towards the detectors. Right: Technical drawing of the tank. The beam enters from bottom-right in the picture.

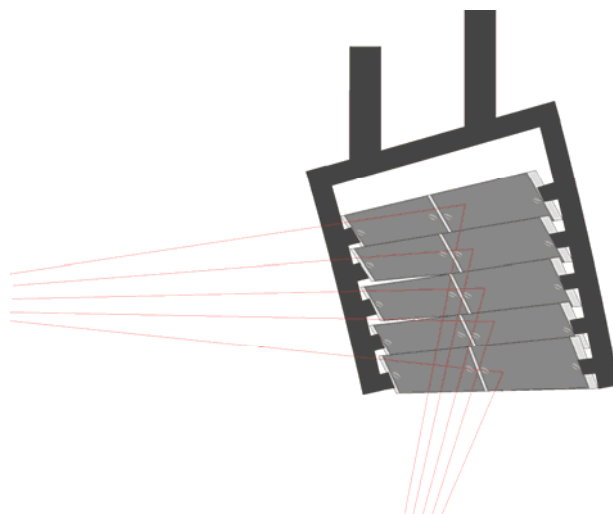


Figure 6: Illustration of analyser arrangement. The PG analysers are mounted on Si wafers that are in turn mounted on an Al frame. The individual PG crystals are aligned to the Si beforehand using small Al spacers if needed. The analysers closest to the sample will have 7 wafers each carrying 3 analyser crystals. These numbers increase to 11 wafers each carrying 5 crystals for analysers furthest from the sample.

1.2.1.5 Analyser-Detector Geometry

One truly novel part of the CAMEA spectrometer is the analyser-detector arrangement. We use thin (1 mm) pyrolytic graphite of medium grade (60 arc minutes mosaic). These crystals have a good cold-neutron reflectivity, 60-70%, and importantly a high transmission. We can therefore place 10 analyser arcs behind each other, scattering at slightly different angles (and henceforth final neutron energies), as sketched in Fig. 5. This allows for detection of a large fraction of the neutrons scattered within the horizontal plane.

The analysers employ vertical Rowland focusing much like the horizontal focusing of a TAS analyser (See figure 6). The PG is held in place by Si wafers on aluminium holders that ensures the focusing condition.

The detectors are 1/2 inch (12.5 mm) ^3He tubes, with 5 mm resolution along the tube - or similar technology depending on ESS detector policy and the He-3 situation. The analyser-detector distance is around 1 m, matched for each scattered wavelength to comply with restrictions from the order-sorting scheme. We position 3 detector tubes in parallel to measure additional energies. The energy resolution is, in fact, determined solely by distance collimation (i.e. the collimation arising from the small angles that detector, analyser and sample see each other under due to their small sizes and the long distances between them). Neutrons with slightly different energies are scattered at different Bragg angles - and reach in turn different detector tubes. The extended PG mosaicity ensures reasonable reflectivity for all directions [birk14]. This effect is illustrated in Fig. 7.

MXType.Localized
 Document Number Final Porposal
 Project Name CAMEA
 Date 05/05/2014

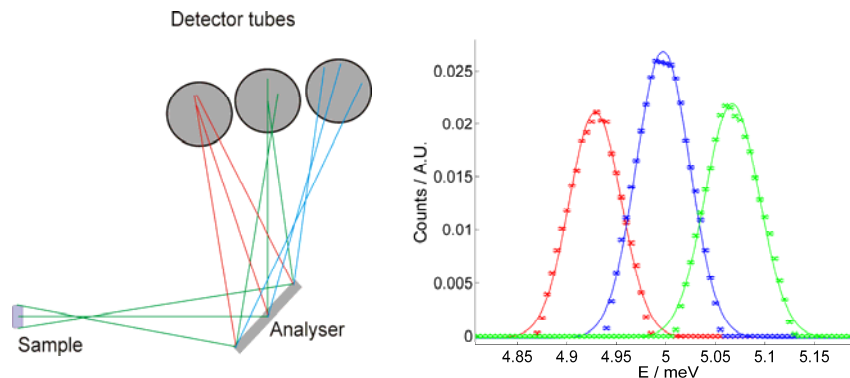


Figure: 7: An analyser crystal with relaxed mosaicity will reflect a band of different energies in slightly different directions. The left panel illustrates the principle for a single analyser crystal and 3 detector tubes. Right panel shows a simulation of how the principle works if the single crystal is replaced by a focusing analyser. The detector consists of a system of three 1/2 inch detector tubes. Simulations show that several energies from the same analyser crystal can be separated; thus improving resolution compared to a big-detector scheme, but without losing intensity.

Since space is needed for the analyser mounts, there are "dark" angles, not covered by the analysers in any particular setting. In the experiment, the dark angles are covered by moving the whole analyser-detector setup by a few degrees. With 3 settings all angles can be covered twice as all analyser arcs each has at least 67% angular coverage.

In total, the secondary spectrometer tank will deploy 2.4 m² detectors and 2 m² PG crystals.

1.2.1.6 Shielding, Filter, and Collimators

To reduce background, we employ a number of known techniques. As discussed earlier, the guide system is designed by the pinhole concept to reduce background from fast neutrons. To further minimize the background contributors, we place a 10 m "get lost tube" after the instrument, to stop the remaining fast neutrons only at a position far from the detectors.

To eliminate unwanted neutrons at the sample position, the guide is designed to transport as few unwanted neutrons as possible. In addition, to tailor the beam, we use the WISH "divergence jaws" method [chapon11]. Both jaws and slits before the sample will use boron as absorber to lower the energy of the secondary gamma radiation.

Background considerations will be integrated into the design of the central sample environment, i.e. magnets and pressure cells, so that walls are thinned in the beam path and bulky material is covered by neutron absorbing Gd paint and possibly with build-in radial collimators.

MXType.Localized
Document Number Final Porposal
Project Name CAMEA
Date 05/05/2014

Most of the neutrons scattering from the sample environment will be absorbed in a radial collimator, which is placed in the "nose" part of the secondary analyser tank. For experiments where secondary energies higher than 5 meV are not needed, a 10 cm thick Be filter (with its own radial collimator) can replace the radial collimator. Two radial collimators will be available for CAMEA, one for 15 mm by 15 mm samples and one for 5 mm by 5 mm samples.

Cross-talk and other background events inside the tank will be minimized by a careful materials choice for the components inside the tank. Placing absorbing walls between analyser modules and by placing collimation between each analyser and the corresponding detectors, radially as well as vertically. Such a type of shielding, albeit on a smaller scale, was found to strongly reduce the background level of the RITA-2 spectrometer at PSI [lefmann06,bahl06].

The tank itself will consist of an Al pressure vessel, with 30 cm borated polyethylene on the outside and a Cd layer on the inside to reduce penetration of fast, epithermal, and thermal neutrons. In addition, the detectors will be mounted in Cd-clad detector housings with a directional field-of-view towards the analyser modules.

1.2.1.7 Polarization Analysis

For polarizing the incoming neutron beam CAMEA will have a guide changer that places into the guide a short supermirror polarizer. To cover the largest possible wavelength band an s-bender supermirror polarizer will be used. This polarizer will give a highly stable time-independent polarized neutron beam. The flipping of the incoming beam can be achieved by a field flipper as used on D3 at the ILL in conjunction with high field magnets[D3].

To analyse the polarization of the scattered neutron beam we will employ a polarization supermirror analyser. A wide angle ^3He polarization analyser was considered, but this is unable to work with the majority of required sample environments, or in stray magnetic fields. A polarization supermirror analyser will analyse the neutron polarization in front of the 10 PG analysers which will then analyse the energies of the scattered neutrons. We will use a supermirror polarization analyser that has been developed by PSI for the HYSPEC instrument at SNS, that is to be used in conjunction with a 14 T cryomagnet.

The cost estimate of the supermirror polarize to cover all scattering angles is 2.1 M€ (PSI). This system is however can be modular, so that the polarization analyser is built form individual sections for each analyser segment. An initial polarization analyser could be built to cover 5 of the 15 analyser segments.

1.2.2. Instrument Performance

1.2.2.1 Model of the Back-end

We have performed a thorough investigation of the back-end performance by McStas simulations [Simulations and Kinematic Calculations], analytical calculations [Resolution Calculations], and measurements on a prototype built inside the MARS ToF backscattering spectrometer at PSI [Prototype Report]. This has led to the numbers shown in table 2.

E_{Analyser} (meV)	2.5	2.8	3.1	3.5	4.0	4.5	5.0	5.5	6.5	8.0
$D_{\text{Sample-Analyser}}$ (m)	1.00	1.06	1.13	1.20	1.28	1.37	1.46	1.56	1.67	1.79
$D_{\text{Analyser-Detector}}$ (m)	0.80	0.90	1.00	1.05	1.10	1.15	1.25	1.30	1.35	1.45
E_f resolution (μeV)	19	23	27	33	41	49	54	61	79	104
E_f resolution (%)	0.77	0.83	0.85	0.94	1.02	1.08	1.09	1.12	1.21	1.30
Outgoing Angular resolution (degrees)	0.79	0.77	0.75	0.71	0.65	0.61	0.59	0.55	0.51	0.46
Time resolution (μs)	37	28	23	22	22	22	21	22	21	19

Table 2: The main numbers of the secondary spectrometer. Only the middle detector in each detector bank is shown. The side detectors will look at an energy approximately one HWHM away and have the same resolutions. For second order reflections the absolute energy resolutions are multiplied with 4 while the time resolutions are multiplied with approximately 0.8.

1.2.2.2 Flux and Coverage

At the high flux mode the instrument will receive a (simulated) flux of up to 1.8×10^{10} n/s/cm²/1.7 Å on the sample (above 1.4×10^{10} n/s/cm²/1.7 Å for any 1.7 Å wavelength band fully between 1.7 Å and 5.0 Å), for the specified guide delivering a total divergence of $1.5^\circ \times 2.0^\circ$. Comparing to a triple-axis spectrometer on the same source, the flux should be around a factor 30 higher, as divergences match and we have here a wavelength band of 1.7 Å, where a triple-axis would integrate over 0.05 Å. This matches well with the predicted values of the new THALES at ILL, where the maximal flux is 4×10^8 n/s/cm², given the rule of thumb that a cold-neutron

MXType.Localized
 Document Number Final Porposal
 Project Name CAMEA
 Date 05/05/2014

monochromator instrument would perform about equally well at ILL and ESS due to the similar time-averaged fluxes.

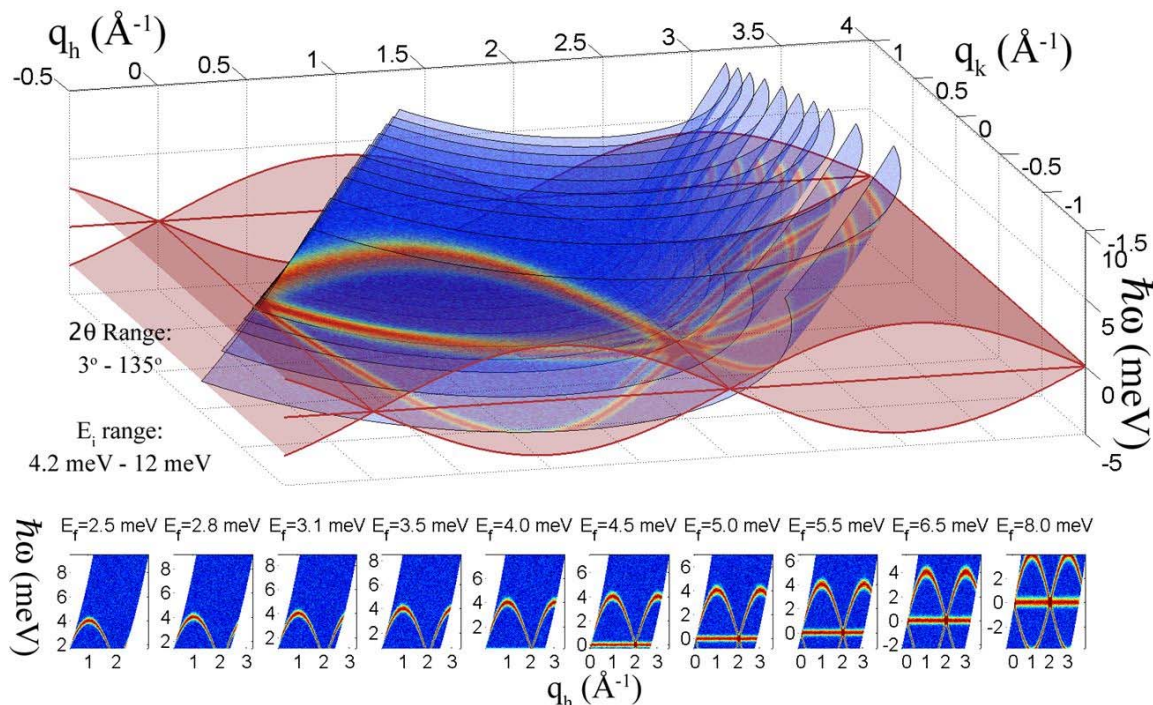


Figure 8: Simulation of data from a single CAMEA data acquisition, using a system with an elastic line and a magnon. The simulation is done for the high flux mode. For clarity we show only 10 surfaces, corresponding to 10 analyser-detector groups. When including the 3 energies from each analyser, the number would be as high as 30 (60 when including the order sorting chopper). The panel below shows the 10 individual datasets.

The graphite has a reflectivity of 60-70% and will cover a total solid angle of $0.13 \text{ steradians} \times 10 \text{ analysers}$. The neutron count rate in the detectors will of course depend on the scattering strength of the sample. For a single crystal Bragg peak, the signal in one single detector will be similar to that of a triple-axis spectrometer at ILL, e.g. IN12, but with the difference that the counts would come pulsed. Hence, the instantaneous count rate is potentially a factor 30 higher on CAMEA. Thus to protect the detectors special electronics will limit the current running through the illuminated detector.

The many angles and energies means that CAMEA will provide a selective mapping of a large part of the horizontal scattering plane in just one setting (See figure 8). In many cases this will be enough for parametric studies but it is possible to make a completely continuous map of most of the scattering plane by rotating the sample (See figure 9), or increase the energy and q range by changing the chopper settings.

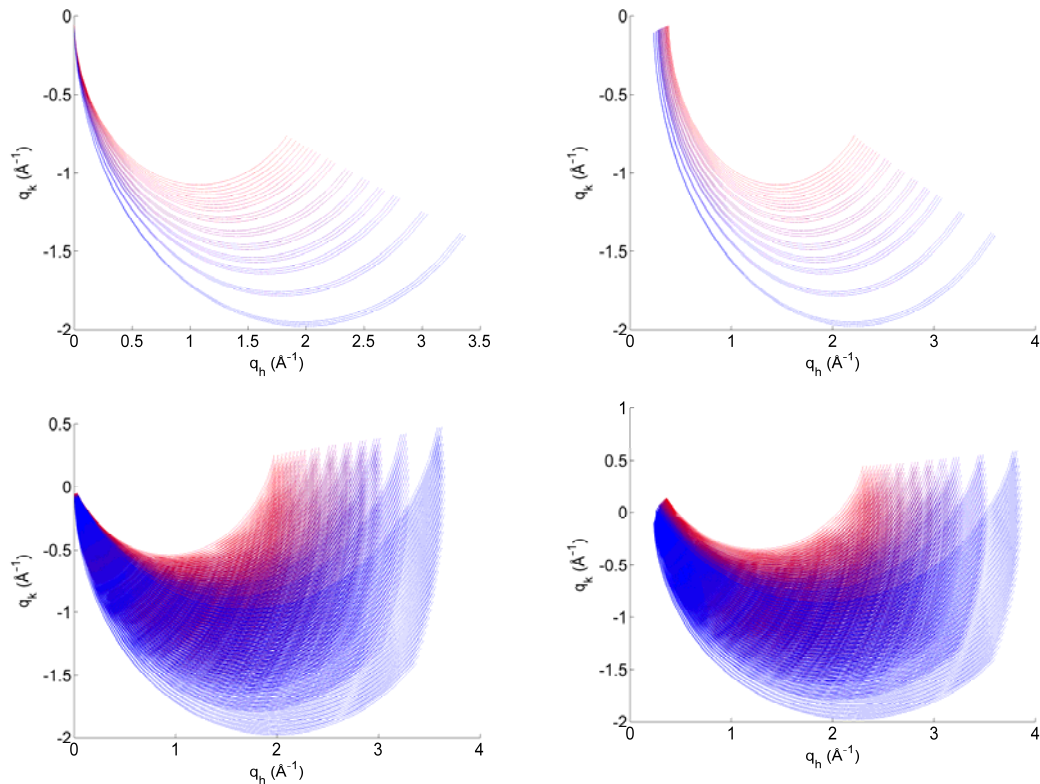


Figure 9: Schematic diagram of constant $\hbar\omega$ coverage with $\hbar\omega = 0$ at left and $\hbar\omega = 2$ meV at right. On the top a single scan step is shown and below 31 steps of 1° . The number of analysers, that are active for a given energy transfer will depend on the chosen incoming wavelength band.

1.2.2.3 Resolution

The contributions to the energy resolution are variable for the incoming neutrons and fixed for each analyser for the outgoing neutrons. The outgoing energy resolution is $\Delta E/E=1.1\%$ (FWHM) at $E=5$ meV. The incoming resolution at 5 meV can be varied between 3.0% and 0.1% by varying the opening time of the pulse shaping chopper, where the lower limit comes from the flight time uncertainties in the secondary spectrometer. Combining the two, one gets elastic resolutions between 4.2% and 1.1%. However, the instrument will perform best with 1.6% where primary and secondary resolutions are matched. The latter gives a vanadium linewidth of a $78 \mu\text{eV}$ at 5 meV, twice as good as a standard TAS at that energy (See figure 10).

The angular resolution of the secondary spectrometer at 5 meV is of the order of 0.6° outgoing (See figure 11). This resolution is as good as TAS with a 40 arc minutes outgoing collimator or about 4 times better than on a focusing TAS. The incoming resolution can be varied from 1.5° and downwards leading to a total angular resolution of an elastic powder scan of between 0.8° and 1.7° . The backmost analysers will have the best angular resolution due to the longer sample-analyser distance. This will somewhat compensate the better q resolution from

lower energies, as these come from the front analysers. This fact will make it easier to merge data from several analysers into one map.

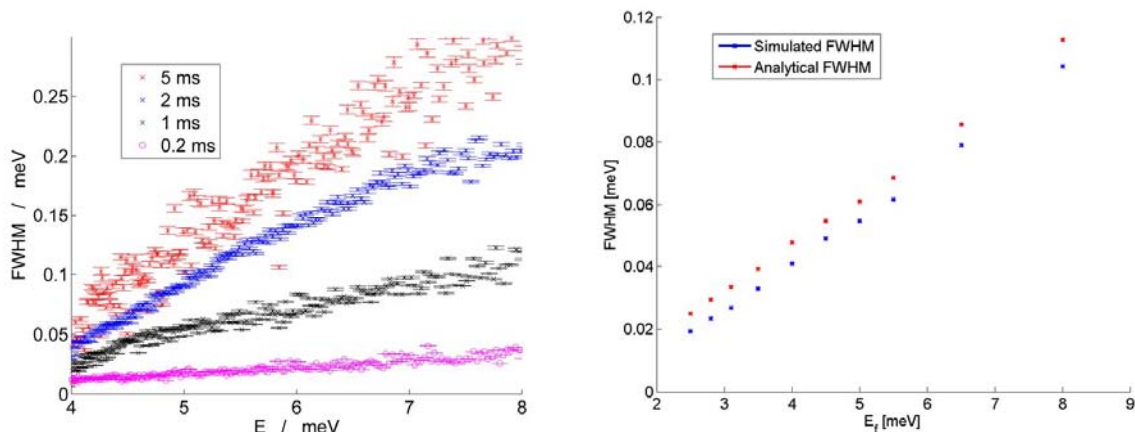


Figure 10: Left: Simulated incoming energy resolution with varying opening time of the pulse shaping choppers, running at up to 210 Hz. Right: Simulated and calculated outgoing energy resolutions for the 10 analysers.

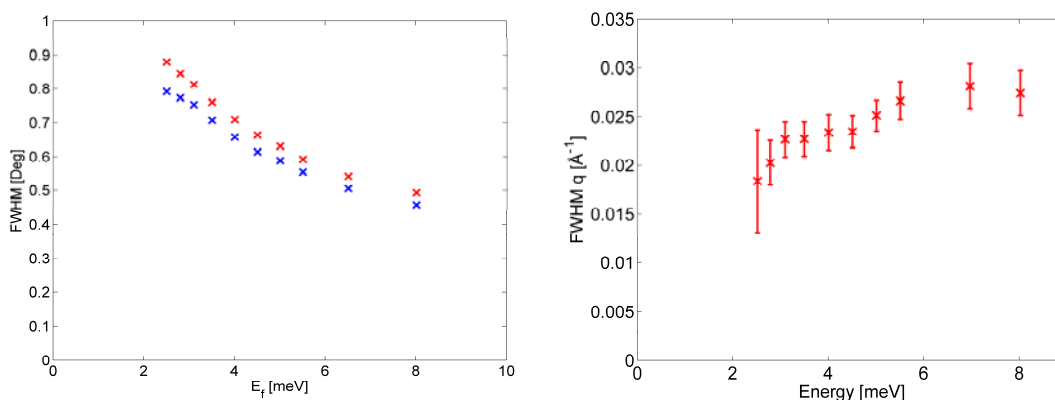


Figure 11: Left: Simulated (blue) and calculated (red) angular resolution of the secondary spectrometer. Right: momentum-resolution at the elastic line for 1 ms pulse shaping and $2\theta = 60^\circ$

For time resolved studies, we need to consider also the real-time resolution. It has two main components: Uncertainty in the flight-path and uncertainty in the final energy. The two main contributors change from analyser to analyser but they are generally well matched and for most analysers the total time uncertainty is between 20 and 30 μs as seen in table 1.

This is sufficiently low for CAMEA to be competitive with other neutron spectrometers for time resolved studies, and makes it possible to resolve the field changes from a pulsed magnet.

1.2.2.4 Fast-neutron background

The fast-neutron background is a cause for concern at ESS, in particular since the accelerator is being run with a very high proton energy, creating neutrons of very high energies. The intensity of these fast neutrons decay as $1/L^2$, where L is the distance from the target and even instruments as long as CAMEA cannot ignore this contribution (as seen from e.g. background counts on instruments at ISIS TS2, where the TS1 pulse is clearly seen). Hence, line-of-sight must be broken. In the case of CAMEA, we break line-of-sight by a kink in the guide. This leads to a contribution from secondary fast neutrons. Being once out of line-of-sight may be sufficient. However, later general studies at ESS will address this question in detail.

As an additional safeguard against background, we consider the option to place a tungsten beam stop to block line-of-sight between the pinhole and the kink point in the first guide. Essentially, this is equivalent to a stopped T-zero chopper, but without the mechanical complications. This will lower the guide transmission by around 10%, an acceptable price to pay for a reduced background. To investigate this plan B, a simulation of the fast-neutron background at the sample position was performed [filges13], resulting in the order of 100 fast n/sec/cm². The beam block reduction factor was around 10.

For an estimation of the background from this fast-neutron flux, we imagine an illuminated area of (conservatively) 10 cm² and an interaction rate with a thin sample environment of (conservatively) 10 %. These tertiary background neutrons will spread in 4π steradians, and there an estimated 2 % of these will fly towards the detectors. Assuming all of these are detected, this gives us 2 fast neutrons/second background over an area corresponding to 1000 single detectors, or 0.1 count/min/detector. Even this conservative estimate gives smaller background than typical electronic noise and our background-reducing scheme is thus adequate.

1.2.2.5 Background from sample surroundings

Traditionally time-of-flight instruments have challenges when handling multiple scattering from the sample surroundings (see figure 12 left). This is due to scattering events in the sample surroundings that changes the flight length and thereby the calculated energy of the neutrons, moving the elastic background of the sample surroundings into the inelastic region. Since CAMEA is an inverse time-of-flight spectrometer the change in flight path should be compared to the primary flight path of 165 m and not the approximately 4 m secondary flight path that is the source of the problem at direct time-of-flight instruments. The difference is discussed further in the supplementary reports and leads to a distribution in the maximal region that can potentially be covered by background as shown in figure 12 right. Even for 45 cm diameter sample surroundings the broadening of the elastic line is less than $\Delta E/E = 0.5\%$ on the most important positive energy transfer side for CAMEA, and is thus hidden by the instrument resolution.

MXType.Localized
 Document Number Final Porposal
 Project Name CAMEA
 Date 05/05/2014

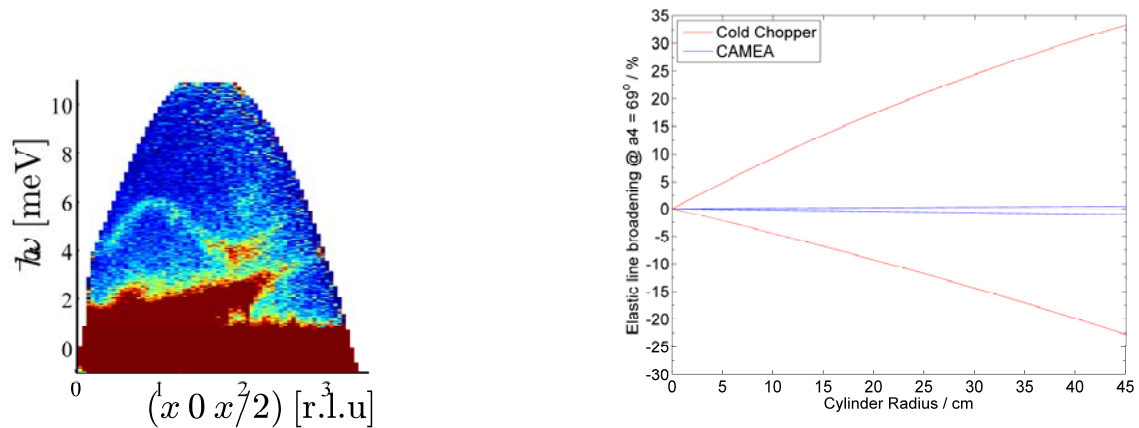


Figure 12: Examples of direct time-of-flight spectroscopy data polluted by sample surroundings. Left: CNCS, LNS data on $\text{CoCl}_2 \cdot \text{D}_2\text{O}$ taken with the 40.5 cm radius 16 T magnet Fat Sam. No inelastic data below 3.5 meV can be seen directly due to the noise from the magnet. Right: The maximal region that can be covered by neutrons performing two scatterings in a cylinder of a given radius as seen from the centre of the CAMEA detector.

Important progress has been made on this issue for direct time-of-flight and today instruments like CNCS can perform better than suggested on the figure using a new radial collimator. However the underlying problem is still there and will be a challenge when moving towards smaller samples or bigger sample environments such as 25 T split coil magnets or pressure cells. In both cases the primary flight path of CAMEA will contain the background within the elastic line, making inelastic experiments virtually untouched by the extra background.

1.2.2.6 The prototype and performance verification



Figure 13: The prototype before (left) and after (middle) installation in the MARS tank. In the right panel all of the shielding elements are mounted (side walls, walls between the banks, slits between analysers and detectors, and a slit between the sample and the first analyser).

We have built and tested the performance of a prototype of CAMEA [Prototype report]. The prototype was designed and built at DTU and was installed at PSI in the tank of the MARS inverse time-of-flight backscattering spectrometer.

MXType.Localized
 Document Number Final Porposal
 Project Name CAMEA
 Date 05/05/2014

During the prototyping the following results were achieved:

- We proved that the optical alignment of the analysers is sufficient in the given geometry.
- We confirmed that by using three detector tubes we can detect three different final energies selected by one analyser (see figure 14).
- We measured the energy resolutions and the resolution ellipsoids in several different configurations. We proved that the energy resolution is independent on the analyser mosaicity. The measurement results are in good agreement with the analytical calculations and simulations.
- We identified the sources of background, and reduced the background level in a Vanadium measurement to 5×10^{-5} compared to the elastic line.
- We made measurements on a single crystal of LiHoF_4 and compared with the same measurement obtained at FOCUS (direct TOF spectrometer at PSI).
- We measured magnon dispersions in a YMnO_3 single crystal.

Finally, we have proved that the CAMEA concept works and gathered experience in performing actual experiments on a CAMEA type instrument. The detailed description of the Prototype, and the descriptions of the measurements can be found in the [Prototype report].

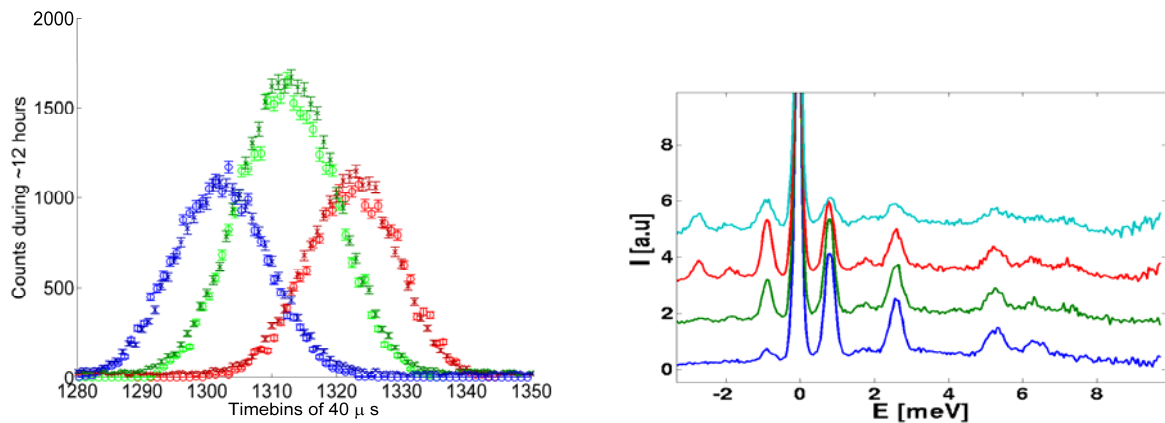


Figure 14: Left: Prototype results (crosses) and simulated data (circles) confirming that 3 detectors (blue, green and red) can detect 3 slightly different energies from one analyser and illustrating that the resolutions are well understood. Right: Inelastic prototype measurement on LiHo_4F sample at 4 K (blue), 10 K (green), 25 K (red), and 70 K (magenta). The base line of each data is shifted for the sake of visibility.

1.3 Technical Maturity

While the complete CAMEA instrument is highly innovative and goes beyond any previous similar multiplexing crystal analyser instrument, each of its technical solutions have already been implemented in different instruments. All technical solutions have been discussed with and agreed upon by ESS neutron technology staff. Below we detail the feasibility and technical maturity.

1.3.1 Guide

Since ESS is the first long pulsed source the guide will be longer than what have previously been constructed in other facilities and rely on modern guide geometries to transport the flux. The CAMEA guide will however be very similar to most other long cold neutron instruments at ESS, and also to e.g. the instrument Wish as ISIS. This means that we can rely on the huge work done by ESS and simulator teams to secure that these guides will indeed deliver as promised.

1.3.2 Choppers

The proposed chopper system consists of the following choppers: Two pulse shaping choppers at 6.5 m running at up to 210 Hz, at 8 and 13 m there are bandwidth and frame overlap choppers running at 14 Hz, a frame shaping chopper at 85 m running at 14 Hz and two order sorting choppers 3 m before the sample running at 180 Hz. The choppers will be standard solutions seen at many instruments today. The proposed 210 Hz limit is far below the 360 Hz that choppers at other instruments routinely reach.

The order sorting choppers run at 180 Hz with two symmetric openings, providing effective 360 Hz. They are placed relatively close to a strong magnetic field. While significant engineering work remains for constructing a 25 T magnetic the suppliers are confident in calculating the stray field such a magnet will have. They estimate that a 25 T vertical magnet with a 1 cm split will have a stray field of 1.04, 0.31 and 0.14 milli-Tesla at respectively 2, 3 and 4 metres from the sample. Running the choppers at 180 Hz in at 3 metres distance is therefore orders of magnitude below the 100 milli-Tesla typically quoted as maximum operating field of choppers.

The chopper system is designed with choppers with big opening angles making it more robust to phase uncertainties than many other chopper systems. We do not foresee any phase uncertainty problems using standard choppers [Simulations and Kinematic calculations].

1.3.3 Sample and Sample Environment

Large field magnet: Through dialogue with magnet manufacturers, it has been shown realistic to expect that a 25 T split-coil all-superconducting magnet can be purchased by the time ESS is built. This is therefore set as the aim of the instrument. The exact price and achievable field remain to be determined, but the field will undoubtedly be better than the 16 T, 1.5 M EUR split coil magnet built in Switzerland and based at SNS. Because CAMEA is a largely superior spectrometer for use with split coil magnets, new science in new materials and previously investigated systems will become possible at any field above 16 T.

MXType.Localized
Document Number Final Proposal
Project Name CAMEA
Date 05/05/2014

The magnet manufacturers are certain that the diameter of future magnets will not exceed the 90 cm reserved in the instruments design.

Pressure cells: The limited volume inside pressure cells means that science today is both limited by technology achievable maximum pressure and the working temperature range, as well as the restrictively small sample sizes. Even without any further development in the pressure cells the increased flux and coverage of the scattering plane at CAMEA will lead to new scientific possibilities using so-called Paris-Edinburgh cells. Ongoing research both in improving Paris-Edinburgh cells to higher temperatures, and in sintered-diamond cells for higher pressures with smaller sample volume will be directly applicable for CAMEA.

Sample activation: Both sample and sample environments will be exposed to strong radiation and will become active during and after the experiments. The ESS is performing calculations of the exact doses and decay times for activation of samples on CAMEA. ESS is considering using robotics for sample change. If that method is not used, we have designed a simple mechanical interlock solution for moving active samples and pressure vessels into a storage area for cooling. The sample removal device is awaiting calculations of sample activation for CAMEA, to determine the shielding required for its design. For the magnets only the Aluminium rings are exposed to high primary radiation so it will be possible to remove a magnet shortly after the experiment.

1.3.4 Analysers

CAMEA will have 10 rows of vertically focusing Pyrolytic Graphite analysers covering a large horizontal area. The Graphite crystals are mounted on 1 mm thick silicon (100) blades, which in turn are placed in aluminium holders accurately machined to provide the correct inclinations of the Rowland geometry, thereby eliminating the need for individual alignment, and the risk of losing that alignment through vibrations.

The silicon blades are cut 3° off the Si(100) orientation, which avoids any spurious Si Bragg scattering.

1.3.4.1 Alignment

Since CAMEA rely on distance collimation and relaxed mosaicity it is less sensitive to misalignment than standard crystal analyser spectrometers. Misalignment will not influence the measured wavelength only the intensity. With 1° FWHM mosaicity the intensity in the central detector will still be at 90% even at misalignments of 0.2° . During the building of the prototype of CAMEA we learned that the inclination of the normal of the crystal surfaces and the PG(002) direction are less than 0.1° (we used Panasonic PG). This means that if the graphite crystals and the silicon blades are clean, then there is no need for extra alignment after mounting the crystals. It also means that the alignment can be easily checked by optical methods [Prototype Report].

MXType.Localized
Document Number Final Porposal
Project Name CAMEA
Date 05/05/2014

1.3.4.2 Reduced phonon contamination

Following the literature [carlile92] and our measurements [PGreport], PG scatters the neutrons inelastically close to the Bragg peak due to the low energy phonons. This contamination has no intensity in the (00l) direction going through the PG(002) point [PGreport], but since the analysers of CAMEA will have a large mosaicity, the detectors may see inelastically scattered neutrons from the crystallites oriented out of the Bragg conditions. This phonon contamination is decreased significantly by cooling of the analyser crystals [PGreport]. Since the analysers sit in a vacuum tank, they can be relatively straightforward cooled via a base-plate on which all analyser segments are mounted by a series of pulse tube cryo-coolers. The mounting details for cooled PG has been designed and currently undergoes experimental testing at PSI. There will be no loss of alignment due to cooling.

1.3.4.3 Extinction at higher energies

The PG is polycrystalline around the c-direction, thus the (hkl) peaks (non-zero of h and/or k) will scatter out the part of the beam. This extinction appears only above 5 meV, and has a sharp edge at the lowest possible energy for a given peak at a given orientation [PGreport]. Analysers that work above 5 meV (the 8-10th analysers away from the sample position) work at energies that are chosen to avoid any energy for which the transmission of neutrons through PG mounted on Si support is low.

1.3.5 Detectors

The design work so far has focused on ³He tubes as detectors for CAMEA, but the instrument will work with any of the currently applied detector technologies. The choice of detector technology will be made together with the ESS detector group. Changing to solid state detectors will give almost the same count rates and background suppression but cause an increase in the detector thickness, which will have a small but tolerable influence the separation into several energies per analyser.

The detectors may saturate and potentially be damaged if exposed to high count rates from strong Bragg peaks in the sample. The solution that has been devised together with ESS detector group to eliminate this risk is a circuit which lowers the high-voltage supply and thereby the efficiency of detectors when too high count rates are recorded. This allows measurements to be performed more efficiently than by attenuating the incoming beam and the locally attenuated parts of a dataset can be corrected in the normalisation section of the analysis software. Since Bragg peaks move in and out of scattering condition on the ~seconds time scales of rotating the sample, voltage-controlling electronics can easily follow.

Should for any unforeseen reason this solution not be desired (e.g. in the unlikely case of a novel solid state detector technology, where it is not possible), a

MXType.Localized
Document Number Final Proposal
Project Name CAMEA
Date 05/05/2014

mechanical fall back option is a gallery of attenuating strips which lifts into the beam to block the angular range receiving Bragg scattered neutrons.

1.3.6 Electronics

The electronics have two major parts: detector electronics, and chopper driver electronics. These have no special requirements compared to the other instruments at ESS. However, the instrument is designed for extreme sample-environments, and the incoming flux will be high. All motors, encoders and other sensors at the secondary instrument should be designed to work in a high magnetic field and under high dose rates. For the fine movements (eg. driving of slits) piezo motors are recommended. For less fine movements (eg. for rotation of the omega-table or for rotation of the secondary instrument) pneumatic motors can be used. Close to the sample environment mechanical encoders are preferable due to their insensitivity to high magnetic fields and radiation. The challenges have been discussed with the ESS electronics group and they have found electronic solutions that can withstand both the radiation and magnetic field in question.

1.3.7 Shielding

The shielding around the detector tank will be built from tested materials and methods. Open geometry instruments can achieve low background levels by using similar techniques. For example at Rita-2 at PSI, we were able to suppress the background in the inelastic range down to 0.1 counts per minute for a 5 inch by 1 inch detector area [Lefmann 06]. Inside the detector tank shielding “chimneys” will ensure that detectors only “see” the relevant analysers. Slits and collimators will be constructed using standard solutions and materials. Further the prototyping have proven that we can achieve inelastic background levels of $5 \cdot 10^{-5}$ compared to the elastic line of cooled Vanadium, even without the use of radial collimators.

1.4 Costing

The costing of CAMEA is based on information from several sources as indicated in the table below. Costing was done conservatively in all cases. The largest uncertainties concerns the price of guide shielding, the price of shutters, which may be significantly lower if CAMEA does not need a heavy shutter, and finally the price of a 20+ Tesla split coil magnet based on high- T_c technology.

In the table below, the costing is divided into four categories: Guides and shielding, CAMEA spectrometer, sample environment for CAMEA, and manpower. For details, we refer to the CAMEA costing report [Costing Report].

MXType.Localized
 Document Number Final Porposal
 Project Name CAMEA
 Date 05/05/2014

Costing item	Price [M€]	Source of information and comments
Guides and shielding		
Guides	1,310	Swiss Neutronics.
Mechanics and installation	1,295	Swiss Neutronics.
Guide shielding	2,142	ESS. This assumes a ratio of guide cost to shielding cost of 1:2. The ratio is expected to be in the range 1:1 to 1:2.
Instrument cave and beam stop	1.000	ESS.
Shutters	0.790	ESS. MCNPX simulations are needed to decide on the need for a heavy shutter (0.75 M€)
Vacuum pumps for guides	0.056	CAMEA team.
Sum for guides and shielding	6.593	
CAMEA spectrometer		
Choppers	1.425	ESS.
Divergence jaws	0.123	ISIS.
Sample table	0.034	CAMEA team.
Vacuum tank	1.058	CAMEA team.
Vacuum pump	0.025	CAMEA team.
PG analyzer crystals and Si wafers	1.466	CAMEA team.
Cooling machines for analyzers	0.255	CAMEA team.
Detectors	0.897	ESS and CAMEA team.
Beryllium filter	0.222	ISIS.
Radial collimator	0.050	JJ X-ray.
Electronics	0.402	ESS.
Polarization analysis	2.100	Neutron optics Berlin, PSI and CAMEA team.
Sum for CAMEA spectrometer	8.057	
Sample environment for CAMEA		
Magnets	3.230	CAMEA team in communication with magnet suppliers. This includes a 20+ Tesla split coil magnet estimated at 2.5 M€
Pressure cell	0.580	Stefan Klotz. Université P. & M. Curie, France.
Sum for sample environment	3.810	
CAMEA cost excluding manpower	18.460	
Manpower		
Lead scientist (5 years) Lead engineer (5 years) Technical staff (11 years)	1.460	CAMEA team.
Sum for manpower	1.460	
Total cost of CAMEA	19.920	

MXType.Localized
Document Number Final Proposal
Project Name CAMEA
Date 05/05/2014

Schematic spending profile: We consider the following parts of the construction phase (1) Design and Planning; (2) Final Design; (3) Procurement and Installation; (4) Beam Testing and Cold Commissioning, and outline a rough spending profile. We assume a 5-year construction period starting from when the lead Scientist and lead engineers have been recruited. Costs related to the categories “Guides and Shielding” and “The CAMEA spectrometer” will be incurred mostly (~90%) in the Procurement and Installation phase, when the instrument is finally approved to go into physical construction. Some costs (~10%) from these categories can, however be expected during the “Beam Testing and Cold Commissioning” phase. The costs in the category “Sample environment” will be adjusted to match expected delivery times for the magnets, pressure cells and auxiliary equipment.

References

[bahl06] C.R.H. Bahl, K. Lefmann, A.B. Abrahamsen, H.M. Rønnow, F. Saxild, T.B.S. Jensen, L. Udby, N.H. Andersen, N. B. Christensen, H. S. Jacobsen, T. Larsen, P. Häfliger, S. Streule, and Ch. Niedermayer, *Inelastic neutron scattering experiments with the monochromatic imaging mode of the RITA-2 spectrometer*, Nucl. Instr. Meth. B, **246**, 452 (2006)

[bertelsen13] M. Bertelsen, H. Jacobsen, U.B. Hansen, H.H. Carlsen, K. Lefmann, *Exploring performance of neutron guide systems using pinhole beam extraction*, Nucl. Instr. Meth. A (2013)

[bertelsen14] M. Bertelsen and K. Lefmann, Optimizing neutron guides : the analytical minimalist concept and the program guide-bot, in preparation for J. Appl. Cryst. (2014)

[birk14] J.O. Birk et al, in preparation for Journal of Applied Crystallography (2014)

[carlile92] C.J. Carlile and M.A. Adams, The design of the IRIS inelastic neutron spectrometer and improvements to its analysers. Physica B 182 (1992) 431-440

[chapon11] L. C. Chapon, P. Manuel, P.G. Radaelli, C. Benson, L. Perrott, S. Ansell, N.J. Rhodes, D. Raspino, D. Duxbury, E. Spill, J. Norris, *Wish: the new powder and single crystal magnetic diffractometer on the second target station*, Neutron News 22:2, 22 (2011)

[cussen13] L.D. Cussen, D. Nekrassov, C. Zendler, K. Lieutenant, Multiple reflections in elliptic neutron guide tubes, Nucl. Instr. Meth. A 704, 121 (2013)

[D3] <http://www.ill.eu/instruments-support/instruments-groups/instruments/d3/characteristics/>

[ESS-SymposiumonSpinDynamics12] http://europenspallationsource.se/sites/default/files/spin_dynamics_of_correlated_electron_systems_2012.pdf

[filges13] U. Filges, unpublished MCNPX results (2012,2013)

MXType.Localized
Document Number Final Porposal
Project Name CAMEA
Date 05/05/2014

[jacobsen13] H. Jacobsen, K. Lieutenant, C. Zendler, and K. Lefmann, *Bi-spectral extraction through elliptic neutron guides*, Nucl. Instr. Meth. A **717**, 69 (2013)

[Hirschmann12] M. Hirschmann and D. Kohlstedt, *Physics Today* **65** (3), 40 (2012),

[Kempa06] M. Kempa, B. Janousova, J. Saroun, P. Flores, M. Boehm, F. Demmel, and J. Kulda, *Physica B-cond. Mat.* **385-86**, 1080 (2006).

[klenø12] K.H. Klenø, K. Lieutenant, K.H. Andersen, and K. Lefmann, *Systematic performance study of common neutron guide geometries*, Nucl. Instr. Meth. A, **696**, 75 (2012)

[lefmann06] K. Lefmann, Ch. Niedermayer, A.B. Abrahamsen, C.R.H. Bahl, N.B. Christensen, H.S. Jacobsen, T.L. Larsen, P. Häfliger, U. Filges, and H.M. Rønnow: *Realizing the full potential of a RITA-type spectrometer*, *Physica B* **385-386**, 1083-1085 (2006)

[lefmann13] K. Lefmann, K.H. Klenø, J.O. Birk, B. R. Hansen, S.L. Holm, E. Knudsen, K. Lieutenant, L. von Moos, M. Sales, P.K. Willendrup, K.H. Andersen, *Simulation of a suite of generic long-pulse neutron instruments to optimize the time structure of the ESS*, *Rev. Sci. Instr.* **84**, 055106 (2013)

[oxford13] Oxford Instruments, personal communication (2013)

[Rheinstädter04] M.C. Rheinstädter, C. Ollinger, G. Fragneto, F. Demmel, and T. Salditt, *Phys. Rev. Lett.* **93**, 108107 (2004)

[Rheinstädter12] M.C. Rheinstädter, Chapter 10 Lipid Membrane Dynamics, *Dynamics of Soft Matter. Neutron Applications, Neutron Scattering Applications and Techniques*, V. García Sakai, C. Alba-Simionesco, S.-H. Chen. (editors), Springer Science + Business Media, 2012.

[Rodriguez08] J A Rodriguez, D M Adler, P C Brand, C Broholm, J C Cook, C Brocker, R Hammond, Z Huang, P Hundertmark, J W Lynn, N C Maliszewskyj, J Moyer, J Orndorff, D Pierce, T D Pike, G Scharfstein, S A Smee and R Vilaseca, *Meas. Sci. Technol.* **19**, 034023 (2008)

[schober08] H. Schober, E. Farhi, F. Mezei, P. Allenspach, K. Andersen, P. Bentley, P. Christiansen, B. Cubitt, R. Heenan, J. Kulda, P. Langan, K. Lefmann, K. Lieutenant, M. Monkenbusch, P. Willendrup, J. Saroun, P. Tindemans, and G. Zsigmond, *Tailored Instrumentation to Long Pulse Neutron Spallation Sources*, *Nucl. Instr. Meth. A* **589**, 34 (2008)

[zendler12] C. Zendler, K. Lieutenant, D. Nekrassov, L.D. Cussen, M. Strobl, *Bi-spectral beam extraction in combination with a focusing feeder*, *Nucl. Instr. Meth. A* **704**, 68 (2012)

MXType.Localized
Document Number Final Porposal
Project Name CAMEA
Date 05/05/2014

CAMEA Reports Available Online:

[Bench marking]

<https://infoscience.epfl.ch/record/190012?ln=en>

[Guide Report]

<https://infoscience.epfl.ch/record/190503?ln=en>

[Comparison to Cold Chopper]

<https://infoscience.epfl.ch/record/190496?ln=en>

[Concept and science case]

<https://infoscience.epfl.ch/record/190010?ln=en>

[Scientific demand for CAMEA]

<https://infoscience.epfl.ch/record/190011?ln=en>

[Simulations and Kinematic Calculations]

<https://infoscience.epfl.ch/record/190505?ln=en>

[Technical Design]

<https://infoscience.epfl.ch/record/190506?ln=en>

[Costing Report]

<https://infoscience.epfl.ch/record/190502?ln=en>

[PGreport]

<https://infoscience.epfl.ch/record/190504?ln=en>

[Prototype Report]

<http://infoscience.epfl.ch/record/197952?ln=en>

[Resolution Calculations]

<https://infoscience.epfl.ch/record/190497?ln=en>

MXType.Localized
 Document Number Final Porposal
 Project Name CAMEA
 Date 05/05/2014

2. LIST OF ABBREVIATIONS

Abbreviation	Explanation of abbreviation
CAMEA	Continuous Angle Multiple Energy Analysis
CQS	Constant q Spectrometer
DTU	The Technical University of Denmark
EPFL	The École polytechnique fédérale de Lausanne
ESS	European Spallation Source
FWHM	Full Width Half Maximum
HZB	Helmholtz-Zentrum Berlin
ILL	Institut Laue-Langevin
KU	University of Copenhagen
INX	Inelastic X-ray Scattering
PG	Pyrolytic Graphite
PSI	Paul Scherrer Institute
QENS	Quasi-Elastic Neutron Scattering
RITA (II)	Re-Invented Triple Axis
RIXS	Resonant Inelastic X-ray Scattering
SNS	Spallation Neutron Source
TAS	Triple Axis Spectrometer

PROPOSAL HISTORY

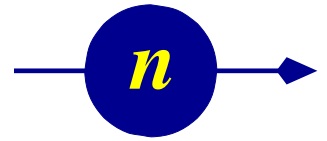
New proposal:	yes
Resubmission:	– no



Technical University of Denmark



McStas



CAMEA

Concept and Science Case

Author:

P. G. Freeman



PAUL SCHERRER INSTITUT



ÉCOLE POLYTECHNIQUE
FÉDÉRALE DE LAUSANNE

Danish-Swiss Work Package 1: CAMEA
Continuous Angular Multiple Energy Analysis Spectrometer
Report on Instrument Concept and Scientific Case

Authors: P. G. Freeman (EPFL)

Work Unit leader: H. M. Ronnow (EPFL)

Work Unit members:

Switzerland:

P. G. Freeman (EPFL), C. Niedermayer, F. Jurányi., M. Markó
(PSI)

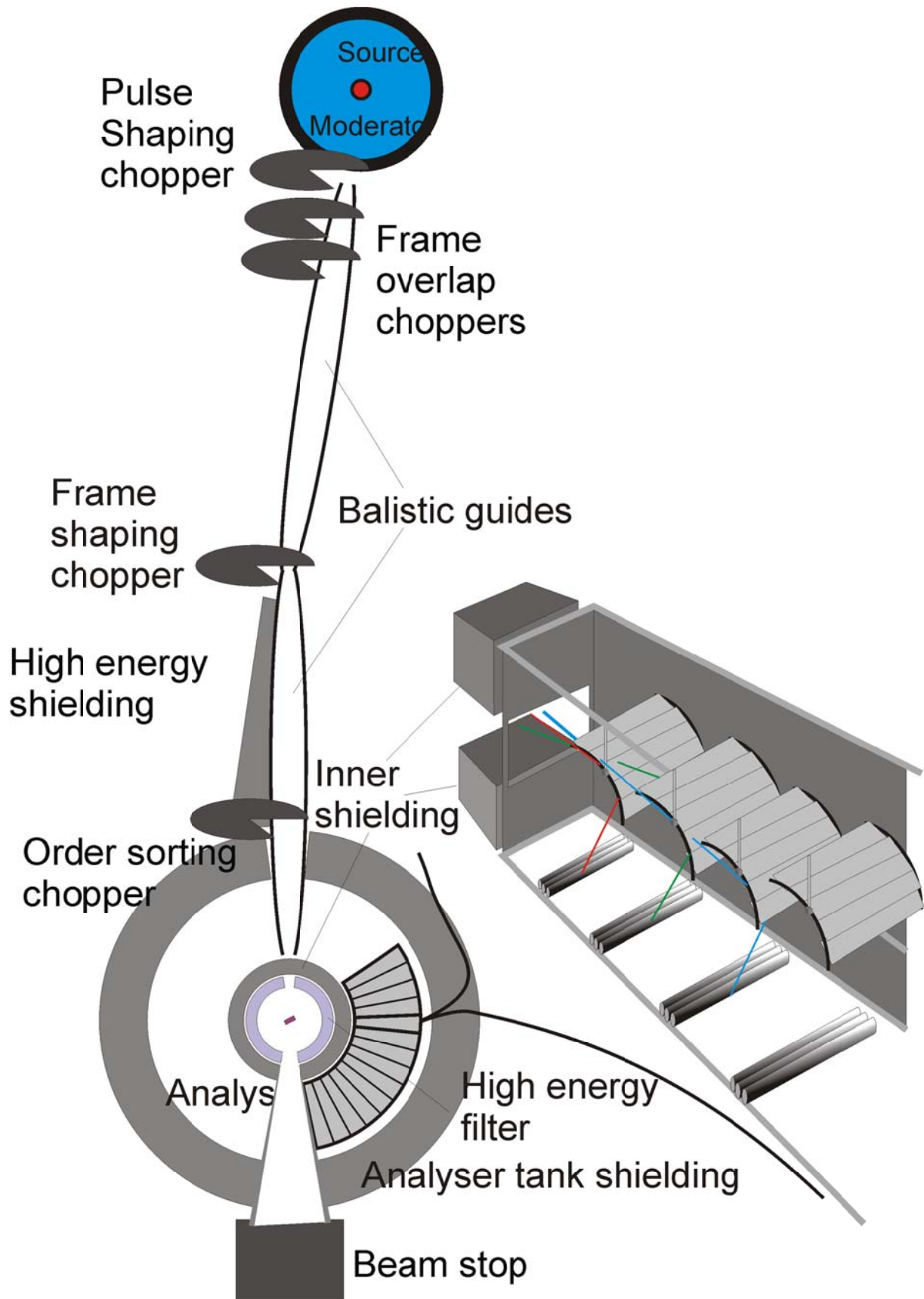
Denmark:

K. Lefmann, J. O. Birk, A. Hansen (KU), N. B. Christensen(DTU)

Abstract

This work unit proposes to construct a cold indirect geometry time of flight spectrometer for performing inelastic neutron scattering experiments optimized for optimal efficiency in the horizontal scattering plane at the European Spallation Source. A horizontal geometry is chosen for compatibility with performing neutron scattering experiments under extreme conditions. The instrument concept is called the Continuous Angular Multiple Energy Analysis Spectrometer, CAMEA. In this report we will outline the science case for CAMEA, highlighting the science that could be performed on CAMEA, the demand for an instrument of this type, as well as identifying the current and future technology in neutron scattering that can be utilized.

The basic concept of CAMEA is to maximize neutron count rates for scattering in the horizontal plane, with a quasi-continuous angular coverage of the scattered neutrons. High neutron detection efficiency will be obtained by using banks of concentric analysers placed behind each other, analysing different neutron energies of the scattered neutrons. Optimization of a horizontal scattering geometry has been chosen to be compatible with extreme sample environments and the ability to perform inelastic neutrons scattering studies. We will highlight how this provides a generation of advancement in inelastic neutron scattering under extreme environments, and what new possibilities for scientific studies CAMEA enables in inelastic neutron scattering.



Overview of the CAMEA instrument layout and the analyzer-detector concept, not to scale.

Contents

Motivation

1) Concept

- a) Motivation
- b) Existing Spectrometers
- c) CAMEA Concept
- d) Envisaged Instrument Parameters
- e) Advantages of Multi-Analyser System
- f) Polarization Analysis

2) Experimenting Capabilities of CAMEA

- a) Measurement types
 - i) Mapping
 - ii) Parametric Studies by Single Acquisition Scans
- b) Measurement Possibilities with CAMEA
 - i) Time Resolved Studies
 - ii) Small Sample Studies
 - iii) Rapid Identification
 - iv) In-situ Studies
 - v) Heavy Fermion Systems
- c) Extreme Conditions
 - i) Existing Neutron Extreme Sample Conditions
 - ii) User Community and Demand for CAMEA
 - iii) Future Developments

3) Science Case

- a) Magnetic Excitations in Applied Magnetic Fields
- b) Magnetic Excitations Under High Pressure
- c) Strongly Correlated Electron Systems
- d) Fundamental Understanding of Functional Strongly Correlated Electron Systems
- e) Unconventional Superconductivity
- f) Soft Matter in Applied Magnetic Fields
- g) Geoscience

4) Concluding Remarks

1) Concept

1a) Motivation

Neutron spectroscopy is a particularly powerful technique in condensed matter research, particularly in the fields of correlated electron materials and quantum magnetism. It is a unique tool in allowing momentum and energy resolved information on magnetic excitations and fluctuations in studied materials. Recent developments in resonant inelastic x-rays (RIXS) scattering complement inelastic neutron scattering. RIXS can study magnetic excitations in materials of 100 μm diameter to eV energies, but has several limitations in comparison to inelastic neutron scattering. The low energy x-rays required for RIXS have short penetration depths into materials, a problem for in-situ measurements. X-ray beam heating limits either the minimum achievable temperature to the order of several Kelvin or limits the maximum incident flux. Envisaged projects for the new RIXS spectrometers ERIXS at the ESRF (France), Centurion at NSLS-II (USA), spectrometers at the Diamond Light Source (UK), MAX IV (Sweden) and at other light sources, aim to achieve of the order of 5-10 meV energy resolution[1]. On the other hand cold neutron spectrometers can achieve energy resolutions below 50 μeV , reaching temperatures down to 50 mK, and neutrons can readily penetrate complex sample environments. The main limitation of inelastic neutron scattering is counting statistics due to low neutron flux and weak scattering cross-sections, meaning samples need to be orders of magnitude larger than those used in x-ray experiments.

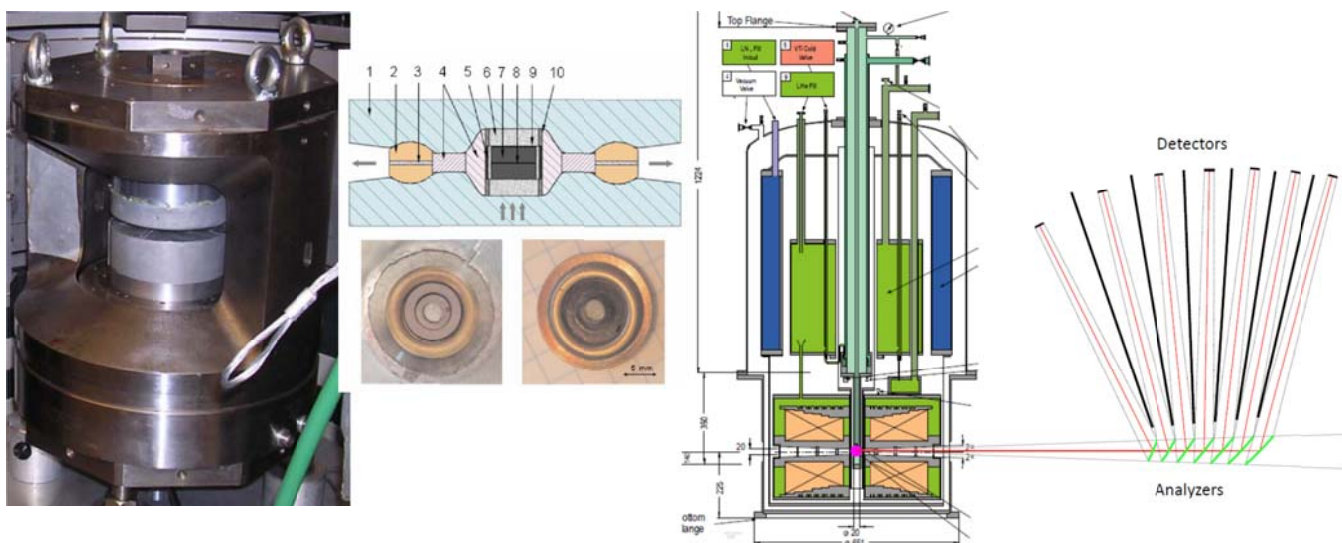


Figure 1: Left: A Paris-Edinburgh pressure cell that has a small vertical axis for neutrons. Centre: A diagram of a sample gasket inside a Paris-Edinburgh cell. Right: A diagram of a cryomagnet with restrictive vertical neutron access, alongside the main components of a CAMEA analyser setup. In this diagram the shielding tank around the analysers and detectors has been omitted for clarity, only neutrons that scattered into the solid angle of the analysers enter the shielding tank.

To understand the underlying physics of materials it is necessary to understand the different phases of these systems across the material's phase diagram. Studying the phase diagram of systems involve changing their properties by changing electronic doping level of the material, external or internal pressure, temperature, applying a magnetic or electric field on

the material, etc.. Changing a material's properties by changing doping level or changing the structure to introduce internal pressure necessarily alters the material being studied, opening up the question of whether effects are intrinsic to the underlying physics or extrinsic effects due to impurities in the material. Contrary to this, when an electronic phase diagram is studied by application of an external force, the sample quality is constant, and only intrinsic properties of the material vary. Examples of external forces that can be applied are high magnetic fields and high pressures. Furthermore the application of an external force can enable experimenters to tune systems into phases that cannot be found by sample growth, this allows experimenters to probe the emergent phenomena of new phases of matter. Using an applied external force therefore represents the cleanest way to study material phase diagrams, which in turn facilitates the realization of novel material states and investigating emergent phenomena.

The study of material phase diagrams by application of an external force in neutron scattering is limited by the achievable extreme sample environments, and the compatibility of these sample environments with neutron scattering instrumentation. The CAMEA concept is conceived as a neutron scattering instrument optimized to maximize counting efficiency in the horizontal scattering plane, a geometry that matches the performance required for performing inelastic neutron scattering under extreme conditions. To match the energy scale of the external forces that extreme environments can exert, plus the most desirable energy range and energy resolution for the science CAMEA can perform, CAMEA will be optimized for cold neutrons (2-25 meV). CAMEA's incident energy range will extend up to 80 meV to give access to the largest energy range that can be used by the CAMEA crystal analysers.

1b) Existing Spectrometers

The so-called triple-axis-spectrometer (TAS), the invention of which gave Bertram Brookhouse the 1994 Nobel Prize, continues to be a primary workhorse of neutron spectroscopy. Its force is flexibility in measuring a selected point in (q, ω) with high intensity. However, while focusing techniques allow many neutrons onto the sample, only a tiny fraction of the scattered neutrons are recorded.

The main development in neutron spectroscopy is a second type of neutron spectrometers: direct time-of-flight (TOF) spectrometer, with very large pixelated detector banks that have become the second standard instrument for single crystal neutron spectroscopy. They allow mapping large volumes of (q, ω) space, but require short incoming pulses which provide a low intensity of neutrons onto the sample. They therefore require large samples (up to 100g co-aligned single crystals) and hours to days of counting per setting, which is not suitable for parametric studies as function of temperature, magnetic field, pressure etc. They become particularly disadvantageous in combination with large split-coil magnets or large pressure cells (anvil type), which only offer a narrow horizontal plane of scattering, hence only illuminating a fraction of the detector bank.

An alternative approach to direct geometry ToF spectrometers is indirect geometry ToF spectrometers. Indirect ToF use crystal analysers to determine the final energy of neutron after scattering, like an analyser on a TAS. By recording the total flight path time and the

detector into which the neutron is scattered the wavevector and energy of the neutron can be determined. Whereas a direct ToF uses a fraction of the neutron incident beam using a monochromating chopper, an indirect ToF can use a broad bandwidth polychromatic neutron incident beam to have a very large flux advantage over direct ToF. A direct ToF makes up for the low incident flux by detecting as large a possible solid angle of scattered neutrons of all final neutron energies, whereas present indirect instruments detect only one final energy of neutrons for neutrons scattering near the horizontal plane.

At the ISIS facility the indirect ToF instrument PRISMA was the first spectrometer at ISIS to study the wavevector dependence of excitations in single crystals. The PRISMA concept underwent different development processes, identifying the difficulties of this type of instrument and the developments required to advance indirect ToF instrumentation. ISIS currently has two indirect ToF spectrometers in user operation working in backscattering geometry to achieve very high energy resolution, the ultra-high resolution Iris, and the high resolution Osiris instruments. Osiris has proven to be a very powerful spectrometer for studying magnetic excitations in single crystals[2].

To fill the gap between traditional TAS instruments and TOF instruments, novel instrument designs have evolved. These designs started with the RITA concept (Re-Invented Triple Axis spectrometer), which employed a large modular multi-analyser system compared to a single analyser of a traditional TAS[3]. Proposers in this work unit were active in the commissioning of the original RITA spectrometer at Risoe National Laboratory in Denmark, and in the design and commissioning of the RITA-2 spectrometer at PSI. A multi-analyser system works by recording neutron scattering simultaneously at a different wavevector for each analyser, unlike the point by point measurement of excitations by a traditional TAS. Several other multi-analyser TAS instruments covering an even larger number of angles with more analyser channels have been developed, and are in regular user operation[4-6]. The new multi-analyser TAS instruments measure typically 30 channels, but with each channel having less intensity than standard double focusing TAS analyser, with the analyser channels typically covering only 30-40° of scattering angle. This can be achieved by having 30 analysers arranged in a fan around the sample position, scattering the neutrons either in a horizontal sense like the MAD concept at the ILL, or scattering neutrons vertically like the Flatcone concept at the ILL. Scattering neutrons vertically has the advantage of being able to place the neutron detectors in a well shielded position, drastically reducing background neutrons scattering in to the detectors. The horizontal geometry can however use a double bounce analyser system to allow for the direct line of sight between the neutron detectors and the sample position to be heavily shielded from background neutrons, like the present version of the MACS spectrometer at NIST.

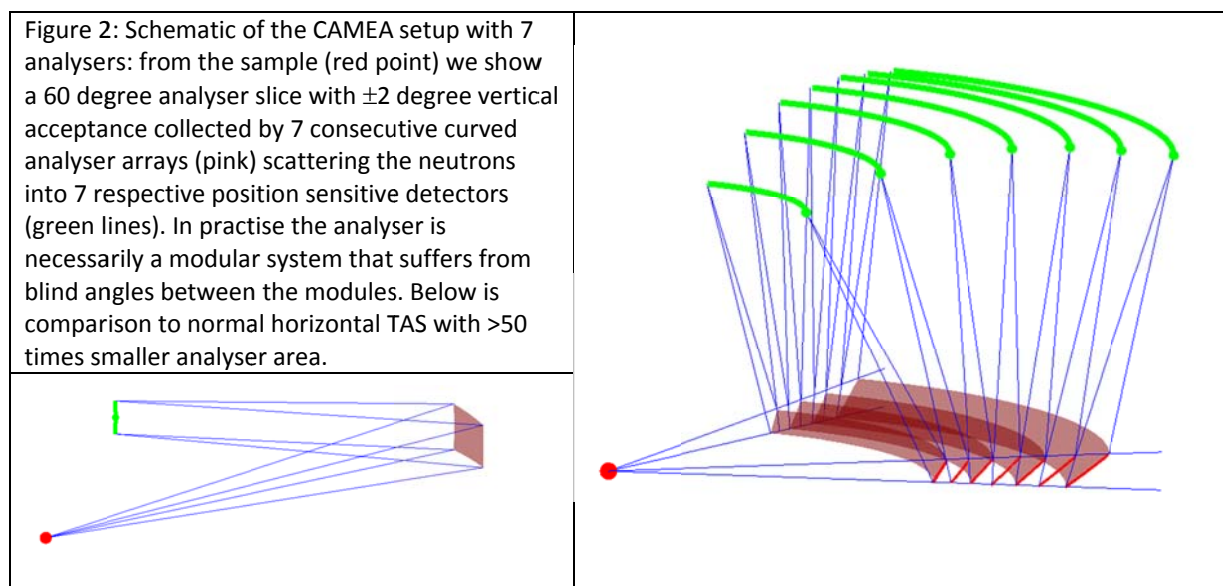
1c) CAMEA Instrument Concept

In a traditional TAS the back-end is a single analyser (flat or curved) that collects neutrons scattered into a certain solid angle element and with a certain final energy. The sample however scatters neutrons in many different directions and energies. Hence, tremendous gains in data collection rates can be achieved by collecting scattered neutrons over a larger solid angle and with differing energies. Direct geometry time-of-flight instruments detect neutrons scattered from sample over as wide a possible solid angle to increase neutron detection efficiency, but to be able to resolve the energy of neutron short pulses of

monochromatic neutrons must be cut from the incident neutron beam. Thus direct geometry spectrometers use only a small fraction of the available neutrons. To this end, we have developed the novel CAMEA indirect geometry spectrometer concept.

The novelty of the proposed CAMEA (Continuous Angle Multiple Energy Analysis) spectrometer is that it employs a series of 10 analyser arcs placed behind each other, where neutrons are scattered vertically into position sensitive detectors. The position the neutron is detected in the detectors determines the scattering angle of the neutron, while the analyser crystal determines the energy of the scattered neutron, which is combined with the time of flight to determine the energy transferred to the sample. Neutrons that are scattered to a different final energy by the sample will not fulfil the scattering condition at the first analyser, and hence continue straight through it. By placing subsequent analyser arcs, several different final energies of the scattered neutron can be measured simultaneously. Working as an indirect geometry time of flight instrument means that each analyser arc of CAMEA sweeps an energy range of excitations in the horizontal scattering plane, with different energy resolutions for each arc. The CAMEA concept arguably realises the most efficient in-plane spectrometer possible.

Transmission through the Pyrolytic Graphite analyser crystals is 98.5 % per mm - sufficiently high that more than 10 crystals of 1 mm thickness can be used, but the increasing analyser radius and increasing vertical size of the analyser renders arrays beyond 10 increasingly expensive for crystal material. We therefore aim for 10 analyser arcs, designed in a modular fashion. Prototype testing of CAMEA will enable calculation of the optimum number of analyser arrays to achieve maximum counting efficiency. Likewise, the spectrometer will employ analyser segments to cover as large as possible angular range that shielding of the neutron beam guide allows, potentially $\pm 150^\circ$.



CAMEA can be thought of as an evolution of the Prisma concept at ISIS. Prisma-II used one set of analysers with the scattered neutrons analysed at one energy for each scattering angle

covered, with analysers scattering the neutrons horizontally. With detectors in the horizontal scattering plane and little neutron absorbing material between the detectors and the sample position, PRISMA-II suffered from a high background count. The next generation PRISMA-III used a double bounce set of analysers to analyse the scattered neutrons energy, this allowed for heavy neutron shielding to be placed in the direct line of sight between the sample position and the detectors. The double bounce analyser system restricts the angular coverage, so although PRISMA-III had a good background, the large number of steps required to create a scan made this version of PRISMA inefficient. PRISMA-III is similar to the MACS multiplexed TAS concept developed and in user operation at NIST[4]. A new generation PRISMA-IV was envisaged to increase counting efficiency, in which a single set of analysers scatter the neutrons vertically into detectors. This geometry allows for heavy neutron shielding to be placed in between the sample position and detectors, without restricting the analyser coverage. The PRISMA-IV geometry has been realized and is in user operation in the Flatcone multiplexed TAS option at the ILL. CAMEA takes the PRISMA-IV concept an evolutionary step forward by using many analyser sets that simultaneously record excitations of differing energy ranges, with different energy resolutions, achieving a far higher efficiency of neutron detection in the horizontal scattering plane.

CAMEA removes additional shortcomings from which PRISMA suffered. PRISMA had a wider bandwidth of neutrons falling on the sample position than required, so that a neutron Laue diffractometer could be placed after PRISMA. The extra bandwidth of neutrons falling on the sample position of PRISMA increased the background counts. Computing capabilities to run PRISMA were limited, but advances in computing power have removed this problem. The success PRISMA experiments, like that of TAS experiments, relies on choosing the correct instrument resolution setup, whereas the CAMEA concept allows for excitations at the same energy to be simultaneously measured by different analyser arrays with differing energy resolution. CAMEA will also take into account the experience of instrument responsables working with the Flatcone option at the ILL, that have shown the importance of using radial collimation on spectrometers to remove the visibility of the sample environment for the secondary spectrometer.

1d) Instrument Parameters

In the following table we outline the starting parameters envisioned for the CAMEA spectrometer that are to be optimized during instrument development:

Parameter	Specification
Moderator	Cold
Pulse shaping chopper to sample distance	165 m
Guide System	Feeder into virtual source, followed by double elliptical guide with kink between ellipses to remove line-of-sight to the source.
Neutron incident wavelength	1-8 Å
Flux at sample position[8]	1.8×10^{10} neutrons per second per cm^2
Maximum Sample Size For Optimal Resolution	5 mm by 5 mm
Effective beam size at sample position	15 mm by 15 mm
Maximum beam divergence at Sample Position	$\pm 2^\circ$ vertical $\pm 1.5^\circ$ horizontal
Q- range	$0.04-7.1 \text{ \AA}^{-1}$
Final energies of PG002 analysers[9]	2.5, 2.8, 3.1, 3.5, 4, 4.5, 5, 5.5, 6.5, 8 meV
Fixed or variable final energies?	Fixed final energies
Angular coverage of Scattered neutrons	$3^\circ < 2\theta < 135^\circ$ for every analyser energy
Sample to Detector distance	1.8 to 3.25 m
Neutron Detectors	2.4 m^2 - ^3He or solid state detectors

The CAMEA instrument achieves significant gains from:

- 1) Using a medium bandwidth white neutron beam increases flux by more than an order of magnitude over the maximum triple axis spectrometer flux at high flux reactors. Optimized use of ESS long pulse will give a gain factor of over 200 compared to the flux of indirect geometry spectrometer Osiris at the ISIS facility[10]. And a flux advantage of more than 10000 over the direct time of flight chopper spectrometer IN5[11].
- 2) Increased efficiency in beam delivery using focusing neutron guides over using a crystal monochromator.
- 3) A fourfold or greater increased angular coverage of scattered neutrons for a single analyser array in comparison to the Flatcone and MACS multiplexed triple axis instrument concepts, or the PRISMA-III indirect geometry time of flight concept.
- 4) Advantages of a multi-analyser system

As CAMEA is being designed as a spectrometer that enables studies of small samples, we will investigate options such as the beam defining slit package of WISH to reduce the number of neutrons that reach the sample position but miss the sample, and cause an increase in the background[12]. Preliminary simulations indicate that instrument optimization for smaller beam size at the sample position does not increase flux density, but reduces the halo size of neutron beam at the sample position.

1e) Advantages of Multi-analyser System

Each analyser of CAMEA scans a specific wavevector and energy range. The analyser set to the smallest final neutron energy has the best resolution but covers the smallest region of reciprocal space, with the inverse being true for the analyser which reflect neutrons with the largest final energy. In this way data from different analyser arrays can provide a zoom for excitations measured at the same energy transfer.

For one measurement setup of CAMEA the analyser with the highest final neutron energy, will be measuring the excitations at the lowest energy transfers with the lowest energy resolution, the opposite to desirable situation. The converse is true for the analyser looking at neutrons with the lowest final neutron energy transfer, again opposite to the most desirable setup. In the general case not every analyser will provide equally important information. If, however, the experiment needs to determine accurately the dispersion at the zone boundary, for determining the strengths of weaker yet vitally important interactions, the scattering by different analysers of CAMEA matches the experimental needs.

The correct choice of energy resolution for an inelastic neutron scattering experiment can be vital for the success of an experiment. Estimates of the required resolution for an experiment can be wrong. If an experiment was being performed on a TAS with too low energy resolution, the measurements would have to be started from the beginning with a higher energy resolution. For CAMEA the instrument will be setup to perform an experiment with a specific energy resolution using a specific analyser, but the neighbouring analysers will be measuring excitations over similar overlapping energy ranges. Therefore, if the required resolution for the experiment is different to what was estimated, CAMEA will still be measuring excitations with the required resolution with a different analyser. This greatly reduces the potential of wasted neutron beamtime.

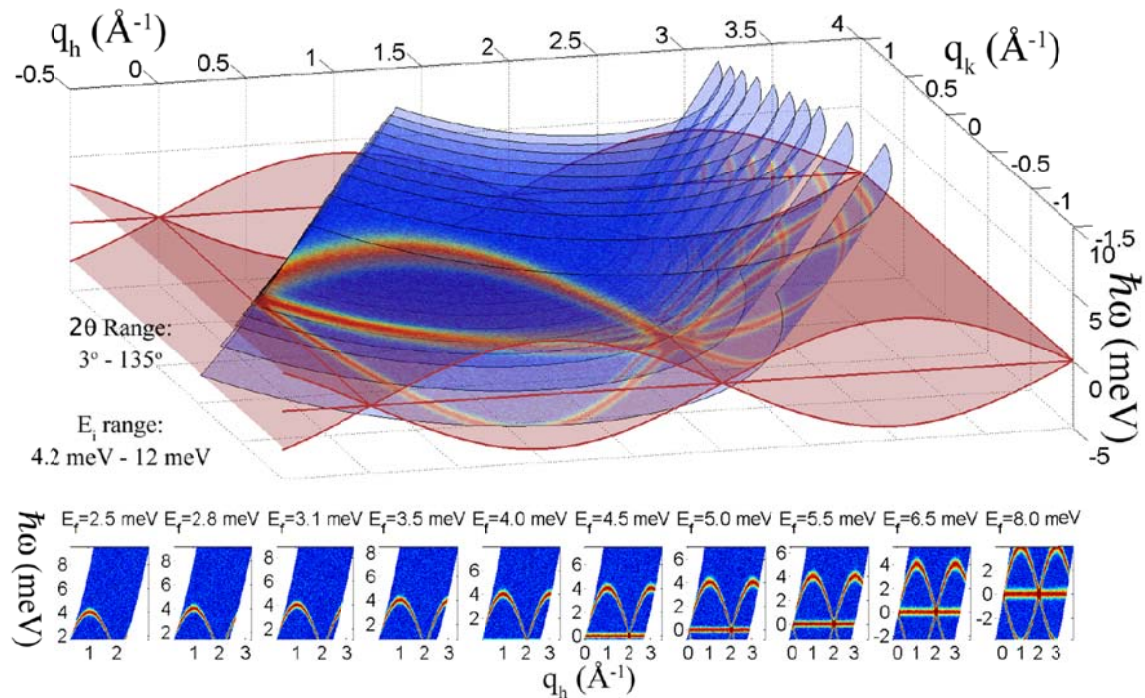


Figure 3: A diagram to represent the measuring capabilities of CAMEA measuring the magnon spin excitation spectrum of a one dimensional spin system, in one point scan. The main figure shows the surfaces in reciprocal space mapped by CAMEA, and the red surface represents the magnon dispersion. Below the main figure shows the projected excitation spectrum measured by the ten different analysers of CAMEA. No spinon continuum excitation is included, and dead angles between the analyser sections have been omitted.

As excitations will be measured at a specific wavevector and energy with differing energy resolution, simultaneous fits of the different data sets will increase the accuracy of mapping excitations in materials. Improvements in data fitting software will be required to maximise this potential.

In inelastic neutron scattering neutrons can scatter in an undesirable way from materials other than the sample in the neutron beam, or from multiple scattering events, and if these neutrons are detected they produce spurious additional counts. Techniques such as shielding, collimation, and filtering the neutron beam can reduce the number of spurious scattering events but not eliminate all spurious scattering. On CAMEA the same point in reciprocal space is measured with several analysers, so any remaining spurious scattering can readily be identified by comparison of data sets from different analysers and removed from the data.

A further advantage of the multi-analyser will be discussed in respect to CAMEA's capabilities in time resolved studies.

1f) Polarization analysis

Neutron polarization is a powerful tool in inelastic neutron scattering that user communities have requested as a day one priority for ESS instruments, see for example:

https://maiserxx.esss.lu.se/press/GetInvolved/SymposiaReports/ESS_report_Boothroyd.pdf

Hence, an option for polarization analysis on CAMEA must be considered. The D7 spectrometer at ILL is a working example of how polarization analysis can be successfully performed over a wide scattering angle in the horizontal scattering plane[13]. At present there are three proven techniques for producing polarized neutron and performing polarization analysis;- Heusler crystals, polarizing supermirrors, and He-3 spin cells. Here we outline the pros and cons of each polarizing technique for CAMEA. Our criteria for selection are as follows:

- 1) Wide angle analysis covering as large as possible scattering angle
- 2) Compatibility with extreme sample environments
- 3) Optimized for cold neutron spectroscopy
- 4) Ease of use, that requires rapid change setup from unpolarized to polarized neutron scattering

Incident polarization: Heusler crystals can only provide monochromatic neutron beams, which is not compatible with the CAMEA concept. Both He-3 spin cells and polarizing mirrors can be used to polarize the incident neutron beam over a bandwidth, and be an installed option using a guide changing section in the primary spectrometer. Ideally the incident polarizing option should be implemented without the need to access the neutron guide. The need to change He-3 cells during an experiment, or performing continuous re-filling of the He-3 spin cell, makes polarizing neutron supermirrors the preferable option. He-3 spin cells can however be used to polarize thermal neutrons, whereas supermirrors performance is poor for thermal neutrons.

Due to the time stability of a supermirror polarizer, we choose this option to produce polarized neutrons for CAMEA.

Polarization analysis: All three options for polarization analysis of the outgoing neutron beam can be used. Heusler analyzers are a proven technique but the reflectivity of heusler is significantly lower than Pyrolytic graphite or Si, and the required magnetic yoke would prohibit the possibility of using analyzers placed behind each other. A magnetic yoke greatly reduces the transmission of neutrons, and the yoke requires a large volume of space, so it is not possible to place Heusler analyzers with magnetic yokes behind each other. A wide angled He-3 spin cell could be used to analyse the scattered neutrons, the ISIS facility, ILL and Juelich have all been developing this concept which is commonly known as PASTIS. There are at least two large problems for using a PASTIS option on CAMEA. The sample space diameter of PASTIS options is typically ~6 cm, and this would need to be dramatically enlarged to be compatible with extreme sample environments, e.g. a 60 cm diameter cryomagnet, with the cost of He-3 cell approximately increasing with the cube of their diameter. Secondly the He-3 cell depolarizes in the presence of magnetic fields, therefore stray fields from cryomagnets would be a problem. This leaves a polarizing supermirror bender to analyse the scattered neutron polarization, which is a proven technique on D7 at

the ILL, and is compatible with using a series of analyser arrays placed afterwards. Stray magnetic fields from cryomagnets cause two problems that need to be addressed, induced stress on a supermirror bender, and the ability of neutron spin flippers to function.

The cost of supermirror polarization analyzer for CAMEA is of the order of 3 million Euros, estimation provided by Thomas Krist (HZB, Neutron Optics Berlin).

2) Experimenting Capabilities of CAMEA

2a) Measurement Techniques

2a.i) Mapping

The biggest break-through in inelastic neutron scattering of the last decade has been brought about by spectrometer innovations that enable full mapping of the reciprocal space, in wavevector and energy. After the success of using position sensitive detectors bank on HET, the MAPS spectrometer at ISIS was conceived as a direct geometry time of flight instrument utilizing 100% position sensitive detectors. MAPS lead directly to break throughs such as the observation of the universal hourglass excitation spectrum of cuprate superconductors[14], and to the planning of many new direct geometry time of flight spectrometers around the world. In comparison to this, the traditional work horse of inelastic neutron scattering the triple Axis Spectrometer (TAS,) has been advanced by multiplexing options such as Flatcone. Multiplexed TAS allows for fast mapping of a single scattering plane one energy at a time.

CAMEA provides a method for measuring the excitations of a single scattering plane in a manner similar to Flatcone; by performing a crystal rotation scan. Using Time of flight analysis means that CAMEA records the excitations over a range of energies similar to a direct ToF geometry spectrometer, or to a scan of k_i on a TAS. Compared to a multiplexed spectrometer, CAMEA mapping simultaneously different energies equates to an order of magnitude gain in measuring simultaneously excitations for each analyser array. Whereas CAMEA gains with respect to direct geometry ToF instruments by increasing the magnitude of the incoming flux by a factor of the order of 100-1000. The flux advantage of CAMEA over a direct ToF will enable CAMEA to map excitations in the horizontal scattering plan faster, but at the cost of not examining the out of plane neutron scattering recorded on a direct ToF. But with extreme sample environments that restrict coverage to the horizontal scattering plane, only inplane excitations can be measured anyway.

Mechanical issues, and the need for neutron shielding for the secondary spectrometer of CAMEA, results in blind spots in the angular coverage. A complete mapping of excitations by CAMEA in one sample rotation scan can be achieved by examining data taken by the different analyser arcs.

2a.ii) Parametric Studies by Single Acquisition Scans

In inelastic neutron scattering important information can be obtained by determining the development of excitations at specific (q,ω) points in reciprocal space with respect to an external parameter, i.e. an applied magnetic field, temperature etc.. It is therefore important to measure such excitations repeatedly at different values of the external control parameter. In this way we study the development of features such as resonances, gaps and crossings of excitation branches. The ability of TAS to focus on a specific energy and wavevector have made TAS the instrument of choice for performing parametric studies by measuring point by point scans. CAMEA can perform scans for parametric studies in a more efficient way than TAS, the quasi-continuous coverage of CAMEA in the horizontal plane allows multiple wavevectors along an arc in reciprocal space to be collected simultaneously, measuring the excitation over a limited energy range. In this way CAMEA can measure a specific excitation in a single spectrometer position or point, and this excitation can be studied parametrically without the need to move the spectrometer.

2b) Measurement Possibilities with CAMEA

2b.i) Time Resolved Studies

Inelastic neutron scattering studies the dynamics of the equilibrium states of materials, to fully understand materials we need to determine how systems that are pushed out of equilibrium relax back to their equilibrium state. Our present microscopic understanding of interactions of the out of equilibrium states is based mainly on our knowledge of the equilibrium state. An example of out of equilibrium studies that can presently be performed are studies using the pump probe technique. The experimental possibilities for the uses of neutron scattering in time resolved studies have been identified[15], yet the use of time resolved studies is limited by current instrument capabilities. The ESS provides an opportunity for inelastic neutron scattering to study out of equilibrium dynamics that potentially will lead to break through understandings and discoveries of the properties of materials. We envisage that such experiments will be limited by low neutron count rates, concentrating on focused studies of specific (q,ω) excitations in reciprocal space.

The CAMEA concept provides a powerful measuring tool for out of equilibrium studies, because of the instrument's good time resolution. For CAMEA the time uncertainty for when a neutron was in the sample is governed by the uncertainty in the flightpath of the neutron from scattering in the sample to its detection. The energy of the scattered neutron is determined by the crystal analysers. Estimates for the flight path uncertainty have been calculated to be $\sim 20 \mu\text{s}$ for every analyser arc, with the focusing geometry being the main source of uncertainty. An excitation at a specific energy can be studied at the same energy transfer for approximately 2.86 ms, the timewidth of the ESS source pulse, with a $\sim 20 \mu\text{s}$ time resolution. Furthermore each analyser arc will be looking at an excitation at a different

energy transfer during this time. In this way single point acquisition scans can be used to study excitations in polycrystalline and single crystals.

CAMEA therefore can provide the time dependence simultaneously of single acquisition scans from each analyser at a different energy, in one data collection setup. The CAMEA secondary spectrometer can be installed on a triple axis spectrometer at a continuous flux neutron source, but with the requirement to move around a monochromator the angular coverage would be restricted to one quarter of that possible for CAMEA at the ESS. For time resolved studies the peak flux is the important factor, which is a factor >10 larger at the ESS than for a continuous source. At a continuous source, however, there is no time limit to how long an excitation can be studied in time resolved studies.

Having identified the potential for time resolved studies with the CAMEA spectrometer it is important to identify what this ability can be used for. Magnetic fields can be used to tune the states of magnetic materials as will be discussed in section 3a). At present the number of systems and transitions that can be studied are limited by the maximum achievable steady state magnetic field in neutron scattering. Very recently in experiments performed at the ILL have shown that easily high magnetic fields of 30 T pulsed fields can be achieved to examine cyclic transitions with neutron scattering. The Full Width Half Maximum of the such a pulsed field is ~ 2 ms [16]. There is on-going work to increase the duty cycle of the magnets and hence counting time. It is also possible to increase the maximum magnetic field at the cost of the pulse width. Working with pulsed magnets the time resolution of CAMEA allows for highly accurate determination of the fields of transitions, to resolve the time/field evolution of both the ordering and decay of the field induced states, and the ability to resolve the highest magnetic fields from shorter pulse widths.

For a direct geometry TOF spectrometer the energy of the neutron and the time uncertainty of when that neutron was in the sample are determined from the time uncertainty of the neutron flight path from the monochromating chopper to neutron detection. That is, at each pulse one position in reciprocal space over one time interval will be measured. A 3 ms time decay of a specific location in reciprocal space with $40 \mu\text{s}$ time resolution would therefore take 75 scans. These 75 scans would however be mapping the excitations over other energies and wavevectors, containing potentially useful data.

Out of equilibrium time resolved studies require sample environments a level of complication greater than the simplest neutron sample environment, to push systems out of equilibrium. We have already highlighted the advantage CAMEA has in performing experiments with such sample environments, due to background reduction by radial collimation and the high incident neutron flux used by CAMEA.

2b.ii) Small Samples Studies

A present limitation of inelastic neutron scattering is the need for large samples to perform experiments on, typically 1 cm^3 in size. This limits inelastic neutron scattering to only materials that can have large samples grown, effecting:

i) Many materials cannot be grown in large volumes, due to stresses and strains in their structure. For example magnetic materials with high degrees of spin frustration are systems that are typically cannot be grown as large crystals. This limits studies of material classes and phenomena to a small number of materials that can be grown. The fact that only certain materials can be grown into large samples is suggestive that these materials are non-typical. In the case of copper based high temperature superconductors research with inelastic neutron scattering has been restricted mainly to La and Y based materials, leading to a fierce debate on the magnetic interactions of high temperature superconductivity in copper based materials[17]. By enabling inelastic neutron scattering to be performed on smaller crystals the number of materials available for experimentation drastically increases, allowing for identification of global behaviour over material specific properties.

ii) When new materials are discovered, inelastic neutron scattering has to wait a significant time until large samples can be grown to perform experiments. This limits the impact of inelastic neutron scattering, but more importantly allows for incorrect over interpretation of results from other techniques, on issues that inelastic neutron scattering can resolve. The lack of input from inelastic neutron scattering may lead to misdirection of experimental and theoretical studies of these materials.

iii) Neutron absorption by the sample material results in an optimum sample size, where increasing the sample size to increase neutron scattering rate is negated by neutron absorption. For samples with high neutron absorption, this size may be of the order of mm's. Here, the only improvement in inelastic scattering data therefore comes from instrument development.

iv) The crystalline quality of materials can bring into question whether the measured excitations display intrinsic or extrinsic characteristics of materials. Large 1 cm^3 sized crystals have a mosaic quality, a variation of composition, and are normally far from being perfect crystals. In general a small single crystal can be produced to a higher quality than a large single crystal of the same material. The higher quality crystals allow for the studying intrinsic behaviour closer to the ideal physical behaviour.

v) Extreme sample conditions can be used to manipulate the properties of materials into desirable phases, and across phase transitions. The greater extremes required, the smaller the sample volume becomes due to energy and mechanical restrictions, whereas the scientific possibilities increase with increasing extremes. To maximize the use of inelastic neutron scattering under extreme conditions requires an instrument optimized for small samples.

The optimization of CAMEA flux is for maximum intensity for 15 mm by 15 mm neutron beam cross-section at the sample position, with a neutron halo of double this size in both directions. A small beam size at the sample position will be achieved by the ability to tightly define the incident neutron beam with a series of jaws to reduce the number of neutrons not

reaching the sample position, this concept has been implemented on the WISH instrument at ISIS [19]. The beam definition jaws can define the beam size at the sample position and the vbeam divergence, thus reducing the halo of neutrons of background scattering from neutrons not hitting the sample position.

2b.iii) Rapid Identification

From material's structure and their bulk properties, materials are identified as being close to or an actually realization of theoretically predicted phases of matter. For magnetic systems inelastic neutron scattering provides a definite way to determine if the systems are model candidates for different magnetic states. Quick mapping of the excitation spectrum on CAMEA could be used to as a way to systematically identify if materials are realizations of model spin systems. For example the recent observation of an hourglass excitation spectrum in an iron based superconductor suggests that new classes of high temperature superconductors could be searched for by identifying materials in which hourglass magnetic excitation spectra occur[20]. Rapid mapping could readily be open to users in an express operation mode, such as Merlin EXPRESS at ISIS, enabling users to gain neutron beamtime in the short term.

2b.iv) In-situ Studies

A great advantage of direct geometry ToF spectrometers is the clean excitation spectra that can be measured when the amount of material in the neutron beam is kept to a minimum, such as a closed cycle refrigerator. Extreme sample environment however place lots of support material in the neutron beam, from which neutrons scatter off to produce structured background detector counts. The visibility of sample environment can be dramatically reduced by using collimators. This is a standard practise for performing neutron diffraction in extreme environments, but is not presently standard practise when using spectrometers due to the vast number of experimental configurations used on spectrometers. Spherical radial collimation required for a direct geometry time of flight spectrometer is hard to envisage in a flexible way for an instrument that is a general purpose spectrometer. As an instrument designed for extreme environments CAMEA can and will include radial collimation to reduce visibility of sample environment. Extreme sample environments are not the only sample environments that place large quantities of material in the beam, the same is true for in-situ studies of materials inside working components or reaction cells. CAMEA will therefore provide a clean way of performing measurement of excitations in in-situ experiments. The scientific drivers for in-situ experimentation for different field of research have been discussed in the ESS Technical Design Report, Chapter 2 Neutron Science.

2b.v) Actinide Heavy fermion Systems

Heavy fermion systems remain a major area of research in magnetism that has been under investigation for decades. The underlying physics of magnetic materials from the 4f and 5f elements is dramatically different to that of the transition metals in part due to the differing extent and orbital character of the systems electrons. Neutron scattering is an ideal probe of the magnetic interactions of these materials, but in many for many actinide elements neutron absorption activates the system leading to a decay that produces neutrons. The neutrons produced by the activated sample lead directly to background detector counts on direct geometry ToF instruments, rendering measurements of the excitation spectrums not possible. CAMEA shares two advantages with TAS that will enable it perform studies on the magnetic interactions of heavy fermion systems. 1) The neutron detectors have no direct line of sight view of the sample and significant neutron shielding is located between the sample and neutron detectors. 2) For any neutrons not absorbed by the shielding the solid angle of the detectors is small enough that the number of background neutrons that reach the detector is very low. These two points have been proven in a vast number of inelastic neutron scattering studies on heavy fermion systems using TAS.

2c) Extreme Conditions for Neutron Scattering

2c.i) Existing Neutron Extreme Sample Conditions

CAMEA is optimized for maximizing counting efficiency in the horizontal plane and to be compatible with extreme sample environments. An important question to answer is what we mean by extreme environments for performing inelastic neutron scattering. In this section we will identify what extreme sample environments are possible today that can be used on an instrument that is optimized for scattering in the horizontal plane.

In inelastic neutron scattering three extreme sample conditions are commonly employed for studying samples, namely temperature, magnetic field and pressure. It is often found that experiments require two extreme environments, typically low temperature combined with either high magnetic fields or high pressure. In the following table we list the extremes of sample environments that have been shown to be viable, or are in regular use, for inelastic neutron scattering.

Condition		Temperature Extreme (K)	Extreme Condition	Maximum Sample Size
Low Temperature	Dilution insert	50 mK		1 cm ³
High temperature	Levitation furnace	3000 K		
Vertical High Magnetic field	Nb based Superconducting cryomagnet	1.5 K	16 T (symmetric)	2 cm ³
	-With dilution fridge	50 mK	16 T	1 cm ³
	-With 2.0 T permanent magnet boosters*	1.5 K	18 T*	133 mm ³
Horizontal Magnetic field with horizontal access	Nb based Superconducting cryomagnet with 180° of dark angles	1.5 K	6.8 T	1 cm ³
High Pressure	Paris-Edinburgh cell	300 K	130 kbar	~50 mm ³ single crystal
	Paris-Edinburgh cell	3 K	50 kbar	
	Paris-Edinburgh cell ^Δ	2000 K	70 kbar	

⁺ Raffaele Gilardi¹ Journal of Neutron Research **16**, 93 (2008)

^{*} In practise the record is 17.9 T achieved in a nominal 15 T vertical cryomagnet at HZB, formerly HMI[21]. The 16 T maximum vertical field is a Bruker magnet named Fat Sam at ORNL.

^Δ Y. L. Godec, M. T. Dove, S. A. T. Redfern, M. G. Tucker, W. G. Marshall, G. Syfosse and S. Klotz, High Press. Res. **23**, 281 (2003).

We conclude that a wish list for extreme environments for CAMEA that are achievable with present technology is as follows:

- 1) Vertical split coil superconducting magnet with the highest possible available field
- 2) A dilution insert with a base temperature of 50 mK
- 3) High pressure cells that perform as good as or better than the currently available Paris-Edinburgh cells, one for low temperatures (<300 mK), and one for high temperatures (> 2000K).
- 4) A wide bore vertical split coil superconducting magnet (>10T) for a pressure cell (>3 GPa) that can be cooled to <1K.

In the next sections of this report we will highlight the needs for these different experimental extremes, and highlight the science that CAMEA can do beyond the capabilities of present day instrumentation without further development of extreme sample environments.

2c.ii) Present Neutron User Community for CAMEA, and User Demand for an Extreme Environment Spectrometer

An indicator of the size of the present user community is the demand for beamtime on available instruments. CAMEA will be an instrument optimized for extreme sample environments, a cold indirect time of flight spectrometer, with an energy resolution a factor of 1.5-2 better than a cold triple axis spectrometer. With this optimization criteria for CAMEA we have obtained information on the user demand for instruments in Europe that study predominately magnetic excitations, that is cold triple axis spectrometers, and time of flight spectrometers. Direct geometry time of flight spectrometers such as IN5 at the ILL. are not included as a large proportion of their beamtime is used for soft matter, experiments that do not require extreme sample environments. As ultra-high energy resolution is not required for the experiments envisaged on CAMEA, we do not include information on high resolution backscattering instruments.

The overload demand for instruments was determined from the ratio of days requested for in beamtime proposals, compared to the number of days available to perform experiments on those instruments. This information was obtained from instrument responsables of each instrument. In the table below we record those figures. Each type of sample environment is listed separately in the table even though there is a significant overlap between demands for different sample environments, i.e. for low temperature measurements in an applied magnetic field.

Instrument (Neutron Source/institution)	Overload [*]	Magnetic fields (%)	Pressure (%)	1 K < (%)	Polarized Neutrons (%)	Furnace (%)
RITA-II, TASP (PSI)	2.5	33.9	4.3	19.2	N/a	
PANDA (FRM-II)	2.7	30	5	20	N/a	
LET (ISIS) [#]					Commissioning	
IN14 (ILL)	2.5	30-40	< 5	60	20-25	
IN12 (JCNS@ILL)	2.6	23.5	-	27.5	9.8	3.9
Osiris (ISIS) ^{**}	2	40		40	Planned	
FLEX (HZB)	1.53	56.3		19.9	Commissioning	

^{*} The overload of an instrument is defined as the number of days applied for experiments divided by the total number of days available to perform experiments. [#] Requested ^{**} The data for OSIRIS is for before LET came into operation, stabilization of proposal demand between the two instruments is yet to occur. ⁺ No information has been provided

Table 1: The demand for European based cold spectrometers that concentrate on magnetic excitations, and the demand for extreme environments conditions on these instruments.

The user demand for the present spectrometers is strong with over load factors between 2 and 2.7 for all instruments. This high demand for beamtime has resulted in a large investment in cold spectroscopy instrumentation. In the last seven years the number of spectrometers has been increased by the addition of LET, PANDA and the inelastic setup of

OSIRIS, as well as augmented by upgrades to FLEX and IN12. Upgrades are planned for IN14, RITA-II and an additional polarized cold triple axis spectrometer instrument is planned for the FRM-II reactor. The large user base of these instruments is a well-established community of inelastic neutron scatterers studying magnetic excitations, whom are skilled at performing experiments, and performing detailed data analysis.

For the instruments of table 1 the demand for extreme conditions approximates to 40% of proposed experiments. With no dedicated extreme environment spectrometer existing, this represents a substantial demand for beamtime, especially when we consider that all systems studied under extreme conditions are first studied under nominal conditions. The beamtime demand for inelastic neutron scattering to study materials under extreme conditions shows that there exists a strong user base within the present user community of cold spectrometers in Europe. In the September 2011 ESS science symposium on Strongly Correlated Electron Systems, neutron users from this user community who study magnetic excitations stated that an extreme conditions spectrometer was one of their top three neutron instrument desires for the ESS.

We note that present demand for cold inelastic neutron spectrometers using a high pressure sample environment is low. We will highlight in examples of the science CAMEA will enable, and we will explain why pressure is low demand for inelastic neutron scattering. The main reason pressure cells are not regularly used is that the maximum samples dimensions that can be used with pressure cells is too limiting for feasible inelastic neutron scattering experiments with present neutron instrumentation.

CAMEA as an instrument that is optimized for inelastic neutron scattering in extreme environments the output of experiments in extreme environments on CAMEA will be higher than for a general instrument. In this way CAMEA would act as an ideal complement to a general purpose cold chopper spectrometer.

Demand for extreme spectrometer from ESS symposium:

http://europeanspallationsource.se/sites/default/files/spin_dynamics_of_correlated_electron_systems_2012.pdf

Recent Publication highlights of inelastic neutron scattering performed under extreme conditions at neutron facilities in Europe:

Quantum Criticality in an Ising Chain: Experimental Evidence for Emergent E_8 Symmetry. R Coldea, D. A. Tennant, E. M. Wheeler, E. Wawrzynska, D. Prabhakaran, M. T. F. Telling, K. Habicht, P. Smeibidl, and K. Kiefer, *Science* **327** 177-180 (2010).

Spin fluctuations in normal state CeCu₂Si₂ on approaching the quantum critical point. Arndt J., O. Stockert, K. Schmalzl, E. Faulhaber, H. Jeevan, C. Geibel, W. Schmidt, M. Loewenhaupt, F. Steglich, *Phys. Rev. Lett.* **106**, 246401-1-246401-4 (2011)

Magnetically driven superconductivity in CeCu₂Si₂. O. Stockert, J. Arndt, E. Faulhaber, C. Geibel, H. Jeevan, S. Kirchner, M. Loewenhaupt, K. Schmalzl, W. Schmidt, Q. Si, F. Steglich, *Nature Phys.* **7**, 119-124 (2011)

Resonant magnetic exciton mode in the heavy-fermion antiferromagnet CeB₆. G. Friemel, Y. Li, A. V. Dukhnenko, N. Y. Shitsevalova, N. E. Sluchanko, A. Ivanov, V. B. Filipov, B. Keimer, D. S. Inosov, *Nature Communications* **3**, 830 (2012).

Mixed acoustic phonons and phase modes in an aperiodic composite crystal. B. Toudic, R. Lefort, C. Ecolive, L. Guérin, R. Currat, P. Bourges, T. Brezowski, *Phys. Rev. Lett.* **107**, 205502 (2011).

Magnetic-field-induced soft-mode quantum phase transition in the high-temperature superconductor La_{1.855}Sr_{0.145}CuO₄: An inelastic neutron-scattering study. J. Chang, N. B. Christensen, C. Niedermayer, K. Lefmann, H. M. Rønnow, D. F. McMorrow, A. Schneidewind, P. Link, A. Hiess, M. Boehm, R. Mottl, S. Pailhès, N. Momono, M. Oda, M. Ido, J. Mesot, *Phys. Rev. Lett.* **102**, 177006 (2009).

Magnetic-field-enhanced incommensurate magnetic order in the underdoped high-temperature superconductor YBa₂Cu₃O_{6.45}. D. Haug, V. Hinkov, A. Suchaneck, D. S. Inosov, N. B. Christensen, C. Niedermayer, P. Bourge, Y. Sidis, J. T. Park, A. Ivanov, C. T. Lin, J. Mesot, B. Keimer, *Phys. Rev. Lett.* **103**, 017001 (2009).

Anomalous magnetic excitations of cooperative tetrahedral spin clusters. K. Prsa, H. M. Rønnow, O. Zaharko, N. B. Christensen, J. Jensen, J. Chang, S. Streule, M. Jiménez-Ruiz, H. Berger, M. Prester, J. Mesot, *Phys. Rev. Lett.* **102**, 177202 (2009).

Direct observation of magnon fractionalization in the quantum spin ladder. B. Thielemann, C. Rüegg, H. M. Rønnow, A. M. Läuchli, J. S. Caux, B. Normand, D. Biner, K. W. Krämer, H. U. Güdel, J. Stahn, K. Habicht, K. Kiefer, M. Boehm, D. F. McMorrow, J. Mesot, *Phys. Rev. Lett.* **102**, 107204 (2009).

Quantum effects in a weakly frustrated S=1/2 two-dimensional Heisenberg antiferromagnet in an applied magnetic field. N. Tsyrlin, T. Pardini, R. R. P. Singh, F. Xiao, P. Link, A. Schneidewind, A. Hiess, C. P. Landee, M. M. Turnbull, M. Kenzelmann, *Phys. Rev. Lett.* **102**, 197201 (2009).

Evidence of a Bond-Nematic Phase in LiCuVO₄. M. Mourigal, M. Enderle, B. Fak, B. K. Kremer, J. Law, A. Schneidewind, A. Hiess, and A. Prokofiev, *Phys. Rev. Lett.* **109**, 027203.

Normal-state hourglass dispersion of the spin excitations in FeSexTe(1-x). Shiliang Li, Chenglin Zhang, Meng Wang, Hui-qian Luo, Xingye Lu, Enrico Faulhaber, Astrid Schneidewind, Peter Link, Jiangping Hu, Tao Xiang, and Pengcheng Dai, *Phys. Rev. Lett.* **105**, 157002.

Normal-state spin dynamics and temperature-dependent spin-resonance energy in optimally doped BaFe_{1.85}Co_{0.15}As₂. D. S. Inosov, J. T. Park, P. Bourges, D. L. Sun, Y. Sidis, A. Schneidewind, K. Hradil, D. Haug, C. T. Lin, B. Keimer and V. Hinkov, *Nature Phys.* **6**, 178.

2c.iii) Future developments in Neutron Scattering for CAMEA

Focusing Optics for ultra-small samples

Neutron optics for focusing neutron beams down in size are continuing to be investigated at neutron scattering facilities such as the ILL and FRM-II. The neutron beam can be focused down by a focusing trumpet to gain neutron flux density at the cost of wavevector resolution and total neutron flux at the sample position. Providing CAMEA with an interchangeable end section to the neutron guide, will enable the installation of a neutron focusing device. This would provide the opportunity for CAMEA to study materials significantly smaller than the 5 by 5 mm beam size of the optimized instrument at the cost of significantly worsening wavevector resolution. Neutron focusing optics will be available to use before the start date of the ESS.

Cryomagnets

The maximum obtainable magnetic field from a vertical split pair magnet can be advanced by the use of copper oxide based high temperature superconducting (cuprate) materials. Advancement of the highest available magnetic fields would open up research into many new materials that have been already identified at high magnetic field laboratories around the world. This research would investigate the complex phases transition and phenomena such as magnetic plateau states identified in high magnetic field laboratories that have not been resolved due to the lack of wavevector resolved studies that inelastic neutron scattering provides.

We note that a conceptual design study is being carried out by another ESS work package, with an estimated 25 T maximum field for a split pair magnet with horizontal neutron access[22]. The present cost of the cuprate superconducting tape required to make this magnet is however prohibitive. The magnet would only become affordable if improvements were made to production of the superconducting tape that leads to a reduction in the sale price. The timescale for improvements in production technique of cuprate material is hard to predict. The National High Magnetic Field Laboratory, USA, are developing 20+ T high temperature superconductor magnets, which will resolve the technical feasibility problems of construct such magnets[23].

Electric Fields

The use of electric fields in neutron scattering is limited due to the size of electric fields in comparison to the typical neutron scattering sized sample. As the CAMEA concentrates on performing neutron scattering on smaller sized samples, studies of samples under applied electric field become increasingly feasible. We envisage that three dimensional control of the applied electric fields to investigate the single crystal polarization anisotropy to be desirable. Examples of present science that can be studied by applied magnetic fields are the manipulation of the magnetism of multiferroics, or the manipulation of skyrmion lattices.

Pressure Cells

There is continuing effort to increase the capabilities of pressure cells for neutron scattering studies. In the following section we will outline the need to increase pressure cell performance for the geoscience community, and how this will be to the advantage for material science. There is a clear difference in capabilities between Paris Edinburg cells used for neutron scattering experiments and the highest achievable pressures from diamond anvil cells at x-rays synchrotron sources[24]. The complimentary nature of the neutron and x-rays scattering technique ensure that the high pressure studies from x-ray experimentation will leave open questions in research. By increasing the available pressure range for neutron scattering, the high pressure user community of x-ray scatterers will have a new complementary experimental tool. One direction for advancing pressure cells will be discussed in the following geoscience section.

3) CAMEA for Science

3a) Magnetic Excitations in Applied Magnetic Fields

Magnetic states of a material are the result of competition between different interactions occurring in materials. Materials that can be grown do not necessarily have the most desirable or intriguing magnetic interactions leading to a physically desirable state. In certain systems the magnetism can be changed by doping to change the magnetic state, but the doping process introduces structural impurities into materials, bringing into question whether intrinsic effects are being studied or extrinsic impurity effects. The use of magnetic fields offers an alternative approach to tuning magnetic interactions in a material. An approach in which the same sample and hence sample quality is kept, and the intrinsic magnetic interactions of materials are studied. Here we wish to briefly outline some of the phenomena that can be studied by inelastic neutron scattering under applied fields and what CAMEA will offer in neutron experimentation to these studies beyond current capabilities. In the following two examples we take two different cases of quantum magnets to discuss first detailed mapping of excitations and then discuss parametric scanning of excitation spectra. We are restricting our discussion in this section to what is achievable with CAMEA using the presently available cryomagnets.

The new magnetic states that are found by tuning the magnetic interactions under an applied magnetic field often contain many different excitation modes. Of these often the continuum excitation modes from deconfined excitations that are of greatest interest with the purest quantum character. Continuum excitation modes by their nature cover large areas of reciprocal space in wavevector and energy but are weak in intensity, requiring high intensity instruments to study them. Therefore studies of continuum excitations ideal require the flux of TAS but the mapping capabilities of a time of flight spectrometer, which CAMEA offers in combination. In figure 4 we highlight the state of art in theory and capabilities of the world leading cold TAS IN14. Theoretical calculations have dramatically advanced with computing power, so that calculations of excitation spectra surpass the capabilities of experimental studies. Measurements on IN14 were restricted in what could be determined to the magnetic state of the material and the observance of fractional spin excitations, but the results could not test the theoretical calculations. The capability of neutron instrumentation needs to be advanced to re-establish the positive feedback between theory and experiments to advance our understanding of novel quantum magnetism. CAMEA provides this advancement, and will provide for inelastic neutron scattering under applied magnetic fields an option comparable to high resolution neutron diffraction, studies of magnetic excitations in detail.

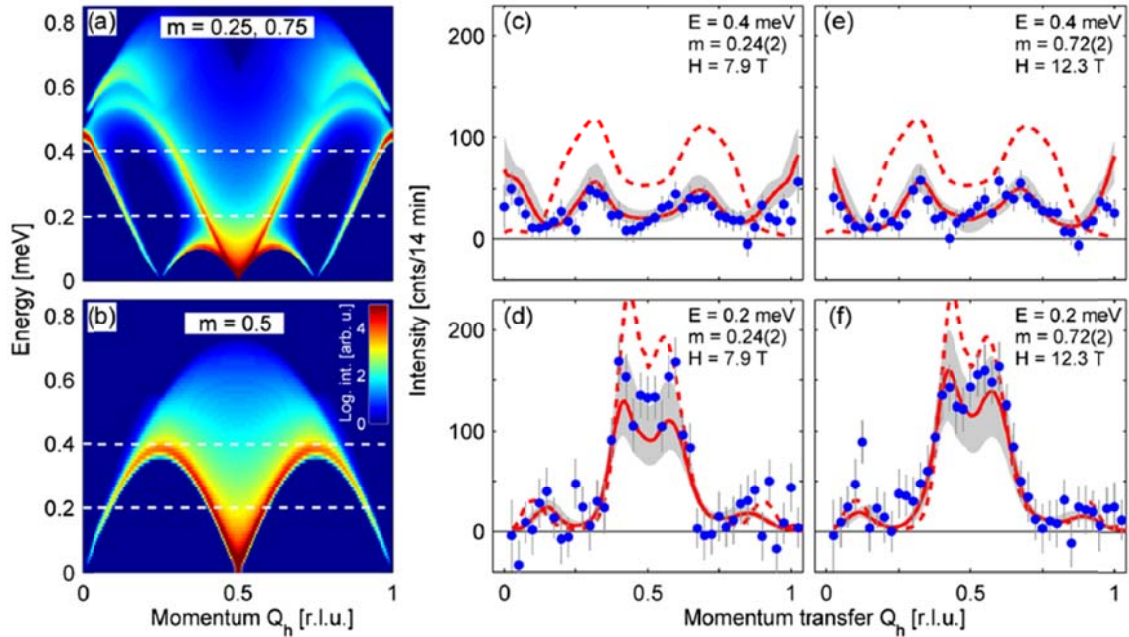


Figure 4: Inducing fractionalization of magnons in quantum spin ladder by application of a magnetic field. The spinon fractional spin excitations are observed as a weak excitation continuum between the sharp single magnon excitation modes. Left shows the theoretical calculation, and dashed lines indicated the scans that are shown in the centre and right panels on IN14. Theoretical calculations have surpassed the present measuring capabilities of inelastic neutron scattering. (Taken from Thielemann, Rüegg et. al. *Phys. Rev. Lett.* **102**, 107204 (2009).)

Quantum critical points (QCP) occur at a specific point in a phase diagram of certain materials, at this point quantum fluctuations dominate the material, and magnetic phase transitions are driven by quantum fluctuations. However a QCP has a very extended effect on the magnetic phase diagram. In figure 5 we show a typical QCP phase diagram, in YbRh_2Si_2 the material is driven from an antiferromagnetic state into a Landau Fermi liquid phase at low temperatures. The colours of the phase diagram indicate two types of behaviour, normal Fermi liquid type behaviour in purple, and non-Fermi liquid type behaviour in orange, the later driven by the QCP. At present inelastic neutron scattering can elucidate magnetic excitations at specific energy and momentum transfers around QCPs, but measurements are very limited in tracking across the phase diagrams to scans at specific wavevectors or energies. The rapid mapping of CAMEA will change studies of critical phase transitions such as QCPs. CAMEA can collect rapid maps of the excitations spectrum where the structure of the excitation spectrum can be identified, and rapid maps can be collected repeatedly across the critical transition in a stepwise approach. In this way critical exponents can be identified, and the exact location in field of the QCP identified for detailed studies. From the critical exponents universality classes of QCP can be identified, and the basic theories of QCP tested. Rapid mapping can be thought of as providing the similar equivalence to low resolution parameter ramping experiments in neutron diffraction.

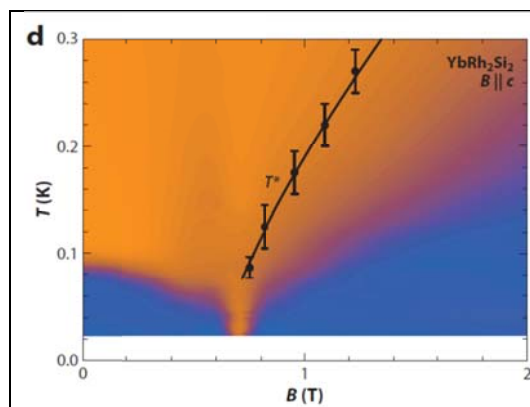


Figure 5: The magnetic phase diagram of YbRh_2Si_2 , taken from J. Custers, *et. al.*, Nature 424, 524 (2003). With a quantum critical point occurring at ~ 0.75 T at 0 K. The data points indicate Kondo breakdown as measured by resistivity. Purple indicates normal Fermi liquid type behaviour, whereas orange indicates non-Fermi liquid strongly correlated electronic behaviour

It is hard to predict what the future research into magnetism will be, but we would like to identify a couple of young fields of research that could prove to be as intriguing and rewarding as that of well-established phenomena such as high temperature superconductivity.

At present the research in magnetism is expanding beyond studies of materials based on transition metals from 3d row of the periodic table, to the 4d and 5d rows. For transition metals from the 4d and 5d elements of the periodic table the spin-orbit interaction strengthens from being quenched and near zero in the 3d transition metals. Theorists are studying the possibilities for new magnetic states within transition metal materials with spin-orbit interactions, and identifying theoretical possibilities of new phases of being, such as the quantum compass model[25]. The possibilities arising from the spin-orbit interaction for new magnetic states and studies of their potential use is a field of research in its infancy.

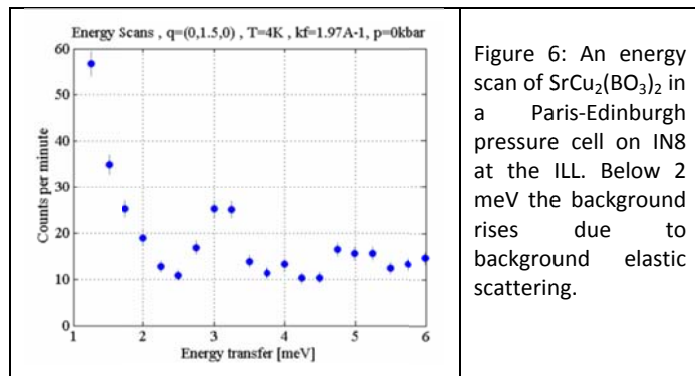
Research into 3d quantum magnets where electronic spin is a good quantum number are at an advanced stage for perfect model systems. The direction of research into the magnetism of 3d materials will therefore shift away from studying the perfect materials investigating the role of disorder, via impurity doping, bond disorder, and/or electronic doping. This research will be trying to identify protected states, phases of matter that are robust from disorder, surviving in imperfect materials, for example superconductivity is a protected state. Current interests in protected states revolve around topological materials, with a major recent finding being the discovery of magnetic monopoles in magnetic spin ices[26].

3b) Magnetic Excitations Under High Pressure

Pressure is an alternative tuning parameter of magnetic excitations, and pressure is distinctly differs from using applied magnetic fields. Pressure studies tune the magnetic interactions of the material by:

- 1) Altering bond angles, changing the magnetic path interactions and balance between different spin interactions in materials
- 2) Altering bond distances to alter spin interactions in materials
- 3) Pressure induced doping to study doping variation in a phase diagram

As applying pressure can simultaneously cause all of the above three effects, pressure can lead to tuning of the magnetic interactions in many different ways in phase space. Pressure can be used as a unique tool in this way to reach and go through phase transitions. In quantum magnetism, materials can be pushed through quantum critical points, and new quantum magnetic phases can be realized.



To reach the highest possible pressures we require the greatest possible force per unit volume. The maximum mechanical strength of pressure cells and the volume size of the sample are the two limiting factors of studying materials under high pressure. Paris-Edinburgh pressure cells have been proven an effective way to reach high pressures for

neutron diffraction, but the maximum volume for single crystals in a Paris-Edinburgh cell is $\sim 50 \text{ mm}^3$. It has been shown that magnetic excitations can be measured with a clean background in Paris-Edinburgh cells on the world's highest flux TAS, however the counting times prove to be prohibitive for performing inelastic neutron scattering studies. This limiting factor has restricted high pressure studies of excitations in inelastic neutron scattering to marginal use.

High pressure experiments on CAMEA would achieve two stages of advancement in spectroscopy under pressure. At present excitations at specific wavevectors can be studied under high pressure. The first advancement would enable determining the full dispersion of excitations along high symmetry directions, and the second stage would be that this is achieved by mapping the dispersion of excitations of an entire plane in reciprocal space. This advancement would enable phase diagram studies of excitations in materials under pressure that cannot be presently performed, revolutionizing the studies of excitations as direct geometry spectrometers with position sensitive detectors have previously advanced inelastic neutron scattering.

While this section has discussed high pressure studies with respect to magnetism, high pressure studies of phonon interactions are required to understand fundamental materials. As stated above pressure drives **changes** to the structure of materials, these structural changes alter the phonon modes of materials altering materials physical properties, and even lead to structural phase transitions, i.e. phases transitions driven by phonon softening. Phonon interactions under high pressure can be studied by inelastic x-ray scattering but the phonon excitation spectrum measured by x-rays is dominated by intensity of phonon modes arising from the heaviest elements. Therefore inelastic neutron scattering is needed to complement inelastic x-ray scattering, by determine the dispersion of phonon modes from light elements. For instance the different phases of water materials under high pressure continue to attract attention in high pressure neutron scattering[27]. With ability to perform phonon studies under extreme pressures and high temperatures having been already established [28].

3c) Strongly Correlated Electron Systems

Strongly correlated electron systems are systems in which the properties of the materials are governed by collective behaviour of the electrons away from the limiting Fermi liquid behaviour of simple metals, and the single particle exchange interaction. Collective correlations result in novel phenomena such as charge order, orbital order, density waves, colossal magneto-resistance, multiferroicity, and superconductivity, to name a few active fields of research. Inelastic neutron scattering has played a crucial role in study the magnetic excitations in these materials, determining the magnetic interactions that participate in the collective behaviour.

In many strongly correlated electron systems the magnetic structure results in different spin domains, leading to differing magnetic structure. To resolve the many different excitation modes in strongly correlated systems it is desirable to have mono-domain samples, especially in the case of incommensurate magnetic structures. In certain materials the use of applied magnetic fields or applied pressure can create mono-domain samples. The classic example is using a magnetic field to create a mono-domain magnetic order in Cr; this enables studies of the many possible excitation modes, and lead to the beautifully complex yet incomplete theoretical description of Cr[29]. A complete understanding Cr still eludes, but remains a prominent question as the spin density wave state of Cr is often compared to the magnetic excitation spectrum of hole doped cuprate high temperature superconductors. Alternatively temperature, magnetic field or pressure can be used in as a perturbative interaction on strongly correlated electron systems.

Strong correlations often occur in materials with reduced dimensionality, in which the interactions are no longer three dimensional. In materials with reduced dimensionality, parametric studies need only to concentrate on the excitations in the scattering plane with the dominant interactions. As CAMEA is optimized to maximize the count rates from the horizontal plane, CAMEA is ideally suited for studies of excitation spectra in a specific scattering plane.

3d) Fundamental Understanding of Functional Strongly Correlated Electron Systems

We have discussed ways in which CAMEA is suited to study strongly correlated electron systems, with a stress on understanding interactions in these materials. Several classes of strongly correlated electrons systems are of interest due to their physical properties, such as colossal magneto-resistance, multiferrocity, thermoelectrics and thermomagnetoeltrics materials. Colossal magneto-resistance and multiferrocity provide ways in which to manipulate magnetic memory, whereas thermoelectrics and thermomagnetoeltrics can be used in energy heat cycles. Inelastic neutron scattering provides a way to study the interactions of these materials to understand their fundamental behaviour, providing feedback into creating or discovering improved materials. CAMEA permits parametric mapping of the excitation spectra of these materials across their different phases, perform in-situ studies of these materials, and the possibility to study the time cycle of processes by time resolved studies not possible with present neutron instrumentation. Polarization

analysis on CAMEA enables the vital ability to disentangle magnon and phonon excitations, to understand the often important role of magnon-phonon coupling in these materials.

3e) Unconventional Superconductivity

Conventional superconductivity can be understood through the BCS theory of superconductivity, where phonon excitations mediate an attractive interaction between electrons enabling them to form Cooper pairs that can flow through materials without incurring an electrical resistance. Since the formulation of BSC theory there has been many discoveries of new classes of materials that superconduct but cannot be explained by BSC theory. These new classes of materials include heavy fermions, cuprates, cobaltates, ruthenates, pnictides, and chalcocinides. In these materials the formation of electron Cooper pairs and a superconducting condensate is not explained by BSC phonon mediation. Inelastic neutron scattering has provided a critical tool for identifying the magnetic origin of these new classes of superconductivity, discovering phenomena such as gapping of the magnetic excitation spectrum, and the occurrence of resonant spin excitations. While the origin and nature of these features in the magnetic excitation spectrums is unresolved, a magnetic origin for the superconductivity is commonly held belief.

Studies of unconventional superconductors typically require their excitation spectra to be studied at low energy transfers to study spin gaps, and resonance spin excitations, whereas to obtain the magnetic exchange interactions requires studies to large energy transfers. CAMEA will enable rapid mapping of the low energy excitation spectrum with high energy resolution. Rapid mapping can be used for identification of resonances, search for common characteristics of the magnetic excitations to identify unconventional superconductivity [16], and allow for parametric studies of the magnetic excitation spectrum evolution. An example of the limitations of present day inelastic neutron instrumentation is that it is still undetermined whether or not, resonance spin excitations in superconductors shift in energy with increasing temperature, and this is twenty years after the discovery in cuprates [30].

Recent publications on unconventional superconductors studies using inelastic neutron scattering performed on cold spectrometers at European neutron sources:

S. Raymond, K. Kaneko, A. Hiess, P. Steffens, and G. Lapertot *Phys. Rev. Lett.* **109**, 237210 (2012).

N. Tsyrlin, R. Viennois, E. Giannini, M. Boehm, M. Jimenez-Ruiz, A. Alahgholipour Omrani, B. Dalla Piazza, H. Rønnow, *New J. Phys.* **14**, 073025 (2012).

C. Stock, C. Broholm, F. Demmel, J. Van Duijn, J. W. Taylor, H. J. Kang, R. Hu, and C. Petrovic, *Phys. Rev. Lett* **109**, 127201 (2012)

C. Stock, C. Broholm, Y. Zhao, F. Demmel, H. J. Kang, K. C. Rule, and C. Petrovic, *Phys. Rev. Lett.* **109**, 167207 (2012)

J. Arndt, O. Stockert, K. Schmalzl, E. Faulhaber, H. Jeevan, C. Geibel, W. Schmidt, and M. Loewenhaupt, *Phys. Rev. Lett.* **106**, 246401 (2011).

- F. Bourdarot, N. Martin, S. Raymond, L. P. Regnault, D. Aoki, V. Taufour, and J. Flouquet, *Phys. Rev. B* **84**, 184430 (2011).
- D. S. Inosov, P. Bourges, A. Ivanov, A. Prokofiev, E. Bauer, and B. Keimer, *J. Phys. Cond. Matt.* **23**, 455704 (2011).
- S. Raymond, J. Panarin, G. Lapertot, and J. Flouquet. *J. Phys. Soc. Japan* **80**, SB023 (2011).
- J. Panarin, S. Raymond, G. Lapertot, J. Flouquet, and J. M. Mignot. *Phys. Rev. B* **84**, 052505 (2011).
- O. Stockert, J. Arndt, E. Faulhaber, C. Geibel, H. S. Jeevan, S. Kirchner, M. Loewenhaupt, K. Schmalzl, *Nat. Phys.* **7**, 119 (2011).
- R. Toft-Petersen, J. Jensen, T. B. S. Jensen, N. H. Andersen, N. B. Christensen, C. Niedermayer, M. Kenzelmann, M. Skoulatos, M. D. Le, K. Lefmann, S. R. Hansen, J. Li, J. L. Zarestky, and D. Vaknin, *Physical Review B* **84**, 054408 (2011).
- P. Babkevich, M. Bendekle, A. T. Boothroyd, K. Conder, S. N. Gvasaliva, R. Khasanov, E. Pomiakushina, and B. Roessli, *J. Phys.: Cond. Matt.* **22**, 142202 (2010).
- Shiliang Li, Chenglin Zhang, Meng Wang, Hui-qian Luo, Xingye Lu, Enrico Faulhaber, Astrid Schneidewind, Peter Link, Jiangping Hu, Tao Xiang, and Pengcheng Dai, *Phys. Rev. Lett.* **105**, 157002 (2010).
- J. T. Park, D. S. Inosov, A. Yaresko, S. Graser, D. L. Sun, P. Bourges, Y. Sidis, Yuan Li, J.-H. Kim, D. Haug, A. Ivanov, K. Hradil, A. Schneidewind, P. Link, E. Faulhaber, I. Glavatsky, C. T. Lin, B. Keimer, and V. Hinkov, *Phys. Rev. B* **82**, 134503 (2010)
- Miaoyin Wang, Huiqian Luo, Jun Zhao, Chenglin Zhang, Meng Wang, Karol Marty, Songxue Chi, Jeffrey W. Lynn, Astrid Schneidewind, Shiliang Li, and Pengcheng Dai, *Phys. Rev. B* **81**, 174524 (2010).
- D. S. Inosov, J. T. Park, P. Bourges, D. L. Sun, Y. Sidis, A. Schneidewind, K. Hradil, D. Haug, C. T. Lin, B. Keimer and V. Hinkov, *Nat. Phys.* **6**, 178 (2010).
- D. Haug, V. Hinkov, Y. Sidis, P. Bourges, N. B. Christensen, A. Ivanov, T. Keller, C.T. Lin, and B. Keimer, *New J. Phys.* **12**, 105006 (2010).
- F. Bourdarot, E. Hassinger, S. Raymond, D. Aoki, V. Taufour, and J. Flouquet, *J. Phys. Soc. Japan* **79** 094706 (2010).
- F. Bourdarot, E. Hassinger, S. Raymond, D. Aoki, V. Taufour, L. P. Regnault, and J. Flouquet, *J. Phys. Soc. Japan* **79**, 064719 (2010)

3f) Soft Matter in Applied Magnetic Fields

The potential for use of applied magnetic fields has been examined as a potential research field for high magnetic field neutron scattering instruments[31], from which we will outline here.

Many studies of biological molecules benefit from techniques that aid in orienting the molecules. It has already been known for decades that molecules exhibiting anisotropic diamagnetism, can be aligned with use of high magnetic fields, provided the magnetic anisotropy and/or the size of the molecules is sufficiently large.

Nevertheless, magnetic orientation has not been used systematically in the past, but rather occasionally for particular types of materials, partly because often high magnetic fields are necessary. On the other hand, the application of a magnetic field has several advantages over other, more frequently used, alignment methods, since it leads to a bulk, contact free, non-destructive force, which is homogeneous throughout the sample and thus can be used for producing highly oriented bulk samples as well as thin films.

Magnetic fields are especially useful for orienting fibrous structures such as fibrin and for filamentous viruses and membranes. This magnetic field orientation is due to the diamagnetic anisotropy of the peptide and ester bonds. It is emphasized that structure determination is not the only goal of studies using magnetic orientation. For membranes, changes of protein binding at the membrane surface are important aspects of signal transduction and issues of amplification associated with specific events can be addressed, as has been done with the rhodopsin and transducin system of visual processes.

The change in diamagnetic energy depends on the size of the molecular aggregate. Therefore the higher the magnetic field, the smaller the molecular entity that can be aligned at room temperature. A larger the maximum available field increases the possibilities for alignment of liquid crystals and macromolecules at room temperature. At present research at steady state high magnetic fields laboratories such as that of Radboud University Nijmegen are taking advantage of the use of high magnetic fields for studying soft materials[32]. The studies being performed at high magnetic field laboratories show that potential for this technique increases with the maximum available steady state field, these fields are provided by extreme environment cryomagnets that can take full advantage of the CAMEA optimization.

3g) Geoscience

i) Scientific Motivation for Neutron Spectroscopy of Molecular Systems Under Extreme Conditions

Simple hydrogenated systems, like water, methane, ammonia, and their mixtures are systems of paramount importance for many fields in science, ranging from applied and environmental science to condensed matter and planetary physics[33]. These systems are widespread in the extra-terrestrial space, both interstellar and on outer planets, moons (ice bodies), and comets, and due to their relatively simple stoichiometry and electronic structure they represent key system for the study of molecular systems.

In the last few years, a tremendous effort has been invested by several groups around the world in the determination of the phase diagram of these systems up to very high pressures (-30 GPa), a program in which several European teams been actively involved

With these data at hand, and with the information obtained from various spectacular space missions, the scientific community is currently trying to understand the interior of these bodies, the conditions of temperature and pressure, its chemistry (Figure 7).

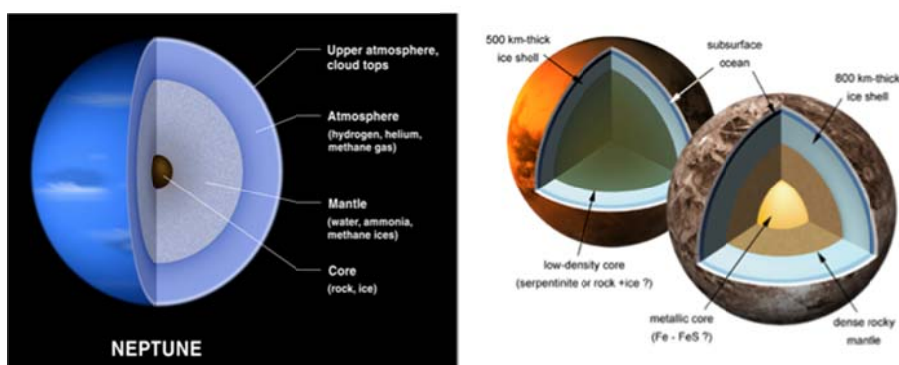


Figure 7: Models of the interior of Neptune and Jupiter's satellites Europa and Ganymede. Water, ammonia, methane and hydrogen under high pressure and temperature are major constituent.

(<http://ircamera.as.arizona.edu/NatSci102/NatSci102/lectures/jupmoon.htm>)

Present investigations of water and aqueous solution under extreme conditions, or in confined reveal the complex behaviour of water are limited by our experimental capabilities [27,34,35]. The study of picoseconds-dynamics, i.e. diffusion, fast relaxation effects, and vibrational dynamics in water and other simple molecular systems under extreme conditions is crucial for a variety of scientific issues spanning most of natural sciences. A few examples; The diffusion of water at pressures of a few GPa's and hundreds of K, typical of the transition zone of the Earth's mantle, has strong incidence on the processes governing volcanic eruptions and intermediate-depth seismicity. Hydrogen diffusion in porous systems and in metals under pressure is fundamental in problems relating to environment, hydrogen storage, and material functionality. Information on molecular re-orientation and hydrogen

delocalization and diffusion in solid water and ammonia under pressures of GPa's and thousands K is essential in order to interpret observations and develop models of planetary interiors and eventually characterize new exotic properties, as the predicted plasticity and superionicity of water and ammonia. The study of the dynamical destabilisation of high-pressure methane clathrates, largely found in the outer solar system (comets, satellites of the gas giant planets, Mars), could clarify methane punctual abundance detected by spatial probes on Titan or Mars.

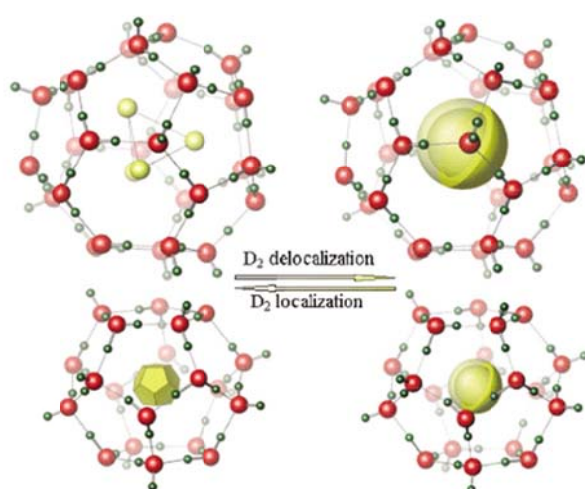


Figure 8 : Structural view of the thermal variation of the D₂ distribution in the large (64512 – hexakaidecahedron, top), and small (512–dodecahedron, bottom) cages in deuterium clathrate. Oxygen atoms are shown as red spheres, deuterium framework atoms–green, and guest D₂ molecules–yellow. Below 50 K, the guest D₂ molecules are localized: in the large cage four molecules are oriented to the centers of hexagons yielding a tetrahedral cluster; in the small cage one D₂ molecule is statistically distributed over 20 positions oriented towards the oxygen atoms forming the dodecahedron. With increasing temperature, the D₂ molecule can more freely rotate, yielding a nearly spherical density distribution inside the cages (right).

In this extent, there is a broad scientific community which will be interested in the possibility of extending INS studies at very high pressures, and both fundamental, and applied research in a wide field ranging from planetary interiors to the recovery to ambient conditions of non-equilibrium structures having novel functional properties, will be promoted.

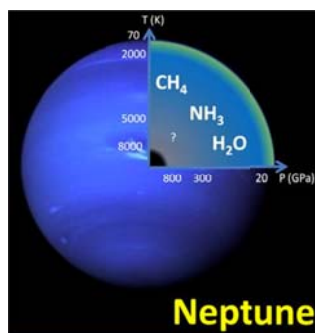


Figure 9: The composition of Neptune.



Figure 10: H-bonded water molecules.

ii) Experimental Realization of Extreme Pressures and Temperatures for Inelastic Neutron Scattering.

The Mbar pressures that can be achieved for inelastic x-ray scattering unrealistic for inelastic neutron scattering we need to identify a pressure range of interest that may be achievable for inelastic neutron scattering with a wide angular access. A target for high pressure and temperature studies is 30 GPa, the pressure by which all phase transitions in the Earth's upper mantle have occurred. Cambridge University and the Université P & M Curie have developed a Paris-Edinburgh cell with laser access from above and below to achieve high temperatures 2000 K with high pressures for a 65 mm³ sample space[36]. Increasing the maximum available pressure by a factor just over two would give neutron scattering access to all the structural transformations in the Earth's upper mantle.

An alternative approach to using Paris-Edinburgh cells is using diamond anvil cells. At present using diamond anvil cells for 100-300 K and 25 GPa is readily achieved for powder sample volumes of 20 mm³, and can be used for neutron scattering. The current record for successful neutron diffraction in diamond anvil cells now stands at >97 GPa in experiments performed on SNAP at the Spallation Neutron Source, Oak Ridge National Laboratory[37]. Due to thermal insulation, the furnace, electrical contacts etc., a high temperature version is plausible for 1-5 mm³ sample size for 30 GPa, but to achieve this would require a funded postdoctoral research project with access to neutron beamtime, preferably at a spallation source [38]. Diamond anvil cells for working at high temperature but for samples sizes an order of magnitude smaller are also being developed for use at the Joint Institute for Nuclear Research, with the aim of having a working pressure of 30 GPa[39]. With present development in pressure cells for neutron scattering, by 2020 the technology to produce the necessary high pressure and high temperature cell for CAMEA will exist.

Developing CAMEA for high pressure studies will necessitate that additional components are included into the design of the instrument. To determine the exact pressure that experiments are being carried out at, the lattice parameter of the pressure transferring

medium needs to be determined. To accurately determine the lattice parameter the chopper package needs a 1% high resolution ($\Delta\lambda/\lambda$) mode, a well collimated beam and a neutron diffraction detector. The well collimated beam can be obtained using the WISH beam definition package envisaged for CAMEA. There are two options for a diffraction detector, one is to place a pixelated diffraction detector behind the CAMEA analyzers, a second is to place the detector on the other side of the sample position.

iii) User Community

The geoscience community do not presently use inelastic neutron scattering for studying materials, although there are geoscientists who use neutron diffraction. Any inelastic neutron scattering experiments in geosciences would therefore be from a new user community. The potential for developing a geoscience user community would come from geoscientists with a neutron diffraction, Raman scattering, or x-ray scattering background, or from the experienced inelastic neutron scattering community collaborating with the geoscience community. For example, geoscience studies could be started in collaboration with neutron scatterers that presently study the different phases of types of water under extreme pressures [27,34]. The potential for proof of principal experiments should be investigated with state of the art neutron instrumentation; this would resolve the capabilities of CAMEA for geosciences.

One synergy of research with the geoscience community would be studying the in-situ growth of samples under high pressure and temperature. Geoscience studies under high pressure map out in detailed phase diagrams of materials, these phase diagrams can then be utilized by material scientists to obtain compounds with highly desirable structures, for instance magnetic systems. In-situ studies of the growth of these samples would provide information on the transition from the amorphous phase into single crystals. CAMEA's ability to study diffuse scattering facilitates detailed studies of synthesis phase transitions.

4) Concluding Remarks

We have argued the scientific case for CAMEA. In our report we have shown there is a strong existing using neutron scattering community for CAMEA, and that this community already has a strong demand for performing neutron scattering in extreme environments. We have provided a brief outline of how CAMEA advances neutron instrumentation, with the performance gains to be bench marked in neutron instrument simulations. Extreme sample environments presently available or that can be readily achieved have been identified for use with CAMEA. With the presently availability of technology we have outlined the experimental capabilities of CAMEA beyond present neutron instrumentation, and how these capabilities can be utilized for studying magnetism. We have also identified promising avenues for future developments in neutronics that CAMEA would embrace. There is a danger of labelling CAMEA as purely an extreme environment spectrometer but we have clearly identified other areas of research where CAMEA has an advantage, such as time resolved and in-situ studies. CAMEA is an instrument for which there is a clear demand. The capabilities of CAMEA at ESS will be unique in neutron scattering in the world, enabling science that cannot be performed on any other neutron instrumentation.

References

- [1] Diamond Instrument Proposal 057:
http://diamondlightsource.org/dms/Beamlines/phaseIII_proposals/IXSapplicationFinal-S.pdf
 Personal communication with Hasan Yavas (DESY).
- [2] R Coldea , D. A. Tennant, E. M. Wheeler, E. Wawrzynska, D. Prabhakaran, M. T. F. Telling, K. Habicht, P. Smeibidl, and K. Kiefer, *Science* **327** 177-180 (2010).
- [3] The RITA spectrometer at Riso - design considerations and recent results K. N. Clausen, et. al., *Physica B* **241**. 50(1997); Realizing the full potential of a RITA spectrometer. K. Lefmann, et. al., *Physica B-Cond. Mat.* **385-86**, 1083, (2006); Added flexibility in triple axis spectrometers: the two RITAs at Riso. K. Lefmann, et. al., *PHYSICA B* **283**, 343 (2000).
- [4] The performance of a multiplexing three-axis spectrometer. F. Demmel, N. Grach N, and H. M. Ronnow, *Nucl. Instrum. Methods Phys. Res.* **A530**, 404 (2004).
- [5] MACS-a new high intensity cold neutron spectrometer at NIST. J. A. Rodriguez, et. al., *Meas. Sci. Technol.* **19**, 034023 (2008).
- [6] The FlatCone multianalyzer setup for ILL's three-axis spectrometers. M. Kempa M. et al. *Physica B-cond. Mat.* **385-86**, 1080 (2006).
- [7] Neutrons down to 1 Å are required if the PG004 Bragg reflections are used to extend the useable energy range.
- [8] To be determined from neutron instrument simulation
- [9] Use of the PG004 Bragg reflections in the same scattering configuration as the PG002 reflections gives access to neutron finally energies 4 times larger.
- [10]<http://www.isis.stfc.ac.uk/instruments/osiris/technical/osiris-technical-information7523.html>
- [11]<http://www.ill.eu/instruments-support/instruments-groups/instruments/in5/characteristics/>
- [12] L. C. Chapon, P. Manuel et al, *Neutron News* **22** (2011) 22-25.
- [13] Disordered materials studied using neutron polarization analysis on the multi-detector spectrometer D7. J. R. Stewart, P. P. Deen, K. H. Andersen, H. Schober, J.-F. Barthélémy, J. M. Hillier, A. P. Murani, T. Hayes, B. Lindenau, *J. Appl. Cryst.* **42** (2009) 69.
- [14] S. M. Hayden *et. al.*, *Nature* **429**, 531 (2004) : J. M. Tranquada, *et. al.*, *Nature* **429**, 534 (2004)
- [15] G. Eckold, H. Schober, and S. E. Nagler. *Kinetics with Neutrons: Prospects for Time-Resolved Neutron Scattering: Springer Series in Solid-State Sciences 161*, (Springer, NewYork, 2009).

- [16] K. Kuwahara, S. Yoshii, H. Nojiri, D. Aoki, W. Knafo, F. Duc, X. Fabrèges, G. W. Scheerer, P. Frings, G. L. J. A. Rikken, F. Bourdarot, L. P. Regnault, and J. Flouquet Phys. Rev. Lett. **110**, 216406 (2013); M. Matsuda, K. Ohoyama, S. Yoshii, H. Nojiri, P. Frings, F. Duc, B. Vignolle, G. L. J. A. Rikken, L.-P. Regnault, S.-H. Lee, H. Ueda, and Y. Ueda Phys. Rev. Lett. **104**, 047201 (2010); S. Yoshii, K. Ohoyama, K. Kurosawa, H. Nojiri, M. Matsuda, P. Frings, F. Duc, B. Vignolle, G. L. J. A. Rikken, L.-P. Regnault, S. Michimura, and F. Iga Phys. Rev. Lett. **103**, 077203 (2009); <http://www.ill.eu/instruments-support/instruments-groups/instruments/in22/more/pulsed-magnetic-field/>
- [17] This debate has been active for two decades. An example of the contrast in approach to the problem from researchers into La based superconductors and those who research Y based superconductors can be seen in the differing interpretations in the following two papers: S. M. Hayden *et. al.*, Nature **429**, 531 (2004) ; J. M. Tranquada, *et. al.*, Nature **429**, 534 (2004)
- [18] A. Heiss, M. Boehm personal communication.
- [19] L. C. Chapon, P. Manuel, P.G. Radaelli, C. Benson, L. Perrott, S. Ansell, N.J. Rhodes, D. Raspino, D. Duxbury, E. Spill, J. Norris, *Wish: the new powder and single crystal magnetic diffractometer on the second target station*, Neutron News 22:2, 22 (2011)
- [20] N. Tsyrlin, R. Viennois, E. Giannini, M. Boehm, M. Jimenez-Ruiz, A. Alahgholipour Omrani, B. Dalla Piazza, H. Rønnow, New J. Phys. **14**, 073025 (2012).
- [21] K. Prokeš *et. al.* Physica B :condensed mat. **294–295**, 691–695 (2001)
- [22] Mark Bird (NHMFL), Oleksandr Prokhrenko (HZB) personal communication
- [23] <http://www.magnet.fsu.edu/usershub/scientificdivisions/highbt/index.html>
- [24] For example: Proton Disorder and Superionicity in Hot Dense Ammonia Ice. S. Ninet, F. Datchi and A.M. Saitta, Phys. Rev. Lett. **108**, 165702 (2012).
- [25] G. Jackeli, and G. Khaliullin, Phys. Rev. Lett **102**, 017205 (2009), A. Kitaev, Ann. Phys. (N.Y.) **321**, 2 (2006).
- [26] Two of the major works in neutron scattering on discovery of monopoles in spin ice can be found in: T. Fennell, *et. al.*, Science, **326**, 415 (2009) ,D. J. P. Morris, *et. al.*, Science **326**,411 (2009).
- [27] L. E. Bove, S. Klotz, J. Philippe, and A. M. Saitta, Phys. Rev. Lett. **106**, 125701 (2011).
L. E. Bove, S. Klotz, A. Paciaroni, and F. Sacchetti, Phys. Rev. Lett. **103**, 165901 (2009).
S. Klotz, L. E. Bove, T. Straessle, T. C. Hansen, and A. M. Saitta, NATURE MATERIALS **8**, 405 - 409 (2009).
- [28] The alpha-gamma-epsilon triple point of iron investigated by high pressure-high temperature neutron scattering. S. Klotz, Y. Le Godec, Th. Straessle, U. Stuhr., Appl. Phys. Let. **93**, 091904 (2008).
- [29] R.S. Fishman and S. H. Liu, Phys. Rev. B **54**, 7252 (1996)
- [30] J. Rossat-Mignod, L. P. Regnault, C. Vettier, P. Bourges, P. Burlet, J. Bossy, J. Y. Henry, G. Lapertot, Physica C **185-189**, 86 (1991).

[31] Mechthild Enderle (ILL) personal communication.

[32] M. Liebi, P. G. van Rhee, P.C.M. Christianen, J. Kohlbrecher, P. Fischer, P. Walde and E.J. Windhab, *Langmuir*, **29**, 3467 (2013); N. Micali, H. Engelkamp, P.G. van Rhee, P. C. M. Christianen, L. Monsù Scolaro and J. C. Maan, *Nature Chemistry*, **4**, 201 (2012); R. Herranz, A.I. Manzano, J.J.W.A. van Loon, P.C.M. Christianen and F.J. Medina, *Astrobiology*, **13**, 217 (2013); A.I. Manzano, J.J.W.A. van Loon, P. C. M. Christianen, J.M. Gonzalez-Rubio, F.J. Medina and R. Herranz, *BMC Genomics*, **13**, 2 (2012).

[33] M. Hirschmann and D. Kohlstedt, *Physics Today* **65(3)**, 40 (2012), and references within; O. Moussis et al., *Space Sci Rev* **174**, 213–250 and references therein.

[34] S. Fanetti, A. Lapini, M. Pagliai, M. Citroni, M. Di Donato, S. Scandolo, R. Righini, and R. Bini, *J. Phys. Chem. Lett.*, **5**, 235 (2014)

[35] D. Mantegazzi, C. Sanchez-Valle, and T. Driesner, *Gemchmica and Cosmochimica Acta* **121**, 203 (2013); M. Oguni, S. Maruyama, K. Wakabayashi, and A. Nagoe, *Cem. Asian J.* **2**, 514 (2007).

[36] S. Redfern (University of Cambridge, U. K.) personal communication.

[37] R. Boehler, M. Guthrie, J.J. Molaison, A.M. dos Santos, S. Sinogeikin, S. Machida, N. Pradhan, and C.A. Tulk, *High Pres. Res.* DOI: 10.1080/08957959.2013.823197

[38] S. Klotz (Universite P & M Curie, France) personal communication.

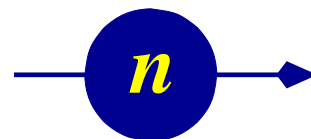
[39] S. Kichanov (Joint Institute For Nuclear Research, Russia) personal communication.



Technical University of Denmark



McStas



CAMEA

Scientific Demand for CAMEA

Author:

P. G. Freeman



PAUL SCHERRER INSTITUT



ÉCOLE POLYTECHNIQUE
FÉDÉRALE DE LAUSANNE

Scientific Demand for CAMEA

To document the enthusiasm for the CAMEA spectrometer, we provide in this document:

- i) Letters of support from leading scientists representing several of the fields of science that will be enabled by CAMEA.
- ii) A list of scientists who wished to be listed as supporters of CAMEA, because they are keen to see CAMEA built.
- iii) Statistics from a survey to identify the need for CAMEA, and the demand for each of the advanced measurement capabilities CAMEA will enable.

23 October 2013

To Whom It May Concern

I am writing to provide a letter of support for the CAMEA spectrometer which has been proposed as one of the instruments for the ESS.

My research interests encompass various aspects of the physics of novel superconductors and quantum magnets. For the last 25 years or so I have been interested in developing methods for studying the fluctuations that endow these materials with their unusual properties, most especially those based on neutron scattering. During this time I have developed an appreciation of the need to continually develop the sources and instrumentation in concert, as it is only by so doing that we can drive the science forward in the direction of addressing ever deeper questions on the nature of correlated electron states.

In my opinion, the CAMEA spectrometer at the ESS will open a new window on our understanding of the fundamental origin of the novel phases displayed by unconventional superconductors, quantum magnets, and other correlated systems. CAMEA, optimized as it is from the outset for extreme sample environment, and benefitting from the most intense neutron beams available, will allow radically new types of spectrometry to be performed. For example, studying the critical fluctuations at a pressure induced quantum critical point for pressures above 20 kbar. I therefore recommend selection of the CAMEA project in the highest possible terms.

Yours sincerely,

Des McMorrow

Professor of Physics
Deputy Director, London Centre for Nanotechnology
University College London

UNIVERSITY OF CALIFORNIA, SANTA BARBARA

BERKELEY • DAVIS • IRVINE • LOS ANGELES • RIVERSIDE • SAN DIEGO • SAN FRANCISCO



SANTA BARBARA • SANTA CRUZ

Professor Leon Balents
Ph: 805-893-6381
Fx: 805-893-3378
Em: balents@kitp.ucsb.edu

KAVLI INSTITUTE FOR THEORETICAL PHYSICS
UNIVERSITY OF CALIFORNIA
SANTA BARBARA, CALIFORNIA 93106-9530

Dear Colleagues:

I am writing in support of the proposed Continuous Angle Multi-Energy Analysis (CAMEA) spectrometer project. I am a theorist working broadly in correlated electronic systems and with a particular interest in complex magnetic materials, and would like to comment on the suitability and promise of this new instrument for that field.

Neutron spectroscopy has been and continues to be the pre-eminent tool for studying magnetism of solids. From elastic measurements of static order to inelastic studies of spin waves, it has formed the basis of our understanding of canonical ordered magnetic systems. In these situations, the order and excitations manifest as sharp peaks in line cuts of energy versus frequency, or versus wavevector. The sharpness of these peaks is a consequence of well-developed long-range order and of simple, particle-like spin-wave or magnon excitations. Seeing just the peaks really suffices to understand most of the physics in such cases.

However, there are many other system in which the physics does not manifest as sharp peaks, and indeed the information lies *entirely* in continuum scattering. There is a huge amount of information there, capable of describe subtle intermediate-scale or power-law correlations, and of revealing exotic excitations which are not particle-like. Such properties are the hallmarks of many long-sought states of matter, most notably quantum spin liquids, which have gone from a fringe idea of Phil Anderson to a hot – and hotly contested – field of research. New neutron spectrometers that can capture the continuum scattering with fine resolution are really the ideal tools to probe and discover these novel states. They will also be helpful much more generally with magnetic materials with complex interactions and large fluctuation regimes.

The proposed CAMEA spectrometer not only will provide broad maps of the diffuse scattering over large regions of momentum space in a single experiment, allowing the rapid identification of key features, and revealing these subtle fluctuations and excitations, it will do so with high resolution in the low to intermediate energy range relevant for the most interesting magnetic problems. I am also heartened by the promise of CAMEA to provide this information on considerably smaller samples than is possible at present. The need to produce large crystals is particularly onerous for the most interesting low-spin materials with small magnetic moments, and often in the discovery stage any crystals at all are hard to come by. Any steps to make that requirement less stringent will greatly speed scientific progress. In summary, I am excited at the scientific prospects of CAMEA, and strongly support its development at the ESS.

Sincerely,

Leon Balents
Permanent Member, KITP and
Professor of Physics

Department of Physics
Royal Holloway, University of London
Egham Surrey, TW20 0EX, UK
www.rhul.ac.uk

Dr Philipp Niklowitz
Tel: 01784-443499
Email: philipp.niklowitz@rhul.ac.uk



Dr Paul Freeman
EPFL SB ICMP LQM
PH D2 345 (Batiment PH)
Station 3
CH-1015 Lausanne
Switzerland

11 October 2013

Letter of support: CAMEA – the Continuous Angle Multiple Energy Analysis spectrometer

Dear Dr Freeman,

This is to express my strong support for your proposal for an instrument at the European Spallation Source.

The proposed CAMEA instrument will allow researchers to address a wide range of topics including our research area of strongly correlated electron systems. Tuning of strongly correlated electron systems can induce phase transitions and lead to the emergence of exciting material properties associated with quantum critical behaviour and with the formation of novel states of matter. At Royal Holloway we are for example interested in the formation of exotic and high-temperature superconductivity as found in iron-based compounds and the properties of magnetic quantum critical regimes in other d-electron systems.

In the past, hydrostatic pressure has proven to be a key tuning parameter in the exploration of strongly correlated electron systems as it provides highly controlled system tuning without externally induced symmetry breaking. Therefore, one of the particular attractive features of the proposed beamline is the envisaged high-pressure option and compatibility with Paris-Edinburgh large-volume high-pressure cells. This includes the design features of maximising count rates in the horizontal plane, having a well-defined flight path and sophisticated shielding, which will minimise background particularly from the pressure-cell sample environment. This will allow us to study the dynamics of tiny crystals down to 1 mm^3 in a wide parameter range and dramatically increases the number of accessible model systems.

At Royal Holloway, we have developed and are improving thermodynamic and transport techniques for high-pressure/low-temperature studies and we are now adding high-pressure/low-temperature X-ray diffraction experiments at the Extreme Conditions beamline I15 at Diamond Light Source. We would in the future greatly benefit from the possibilities CAMEA offers. Inelastic neutron scattering at high-pressures/low-temperature would complement our in-house capabilities and other experimental techniques available at large-scale facilities. CAMEA would allow us to study spin dynamics in a wide range of pressure-tuned compounds. We hope to be able to make ample use of the proposed facility.

Yours sincerely,
Philipp Niklowitz

A handwritten signature in blue ink, appearing to read "P. Niklowitz".

IOWA STATE UNIVERSITY

OF SCIENCE AND TECHNOLOGY

College of Liberal Arts and Sciences

Prof. Paul C. Canfield

Department of Physics and Astronomy

Iowa State University

Ames, Iowa 50011-3160

Telephone: (515) 294-6270

Email: canfield@ameslab.gov

May 5, 2014

Dear Henrik,

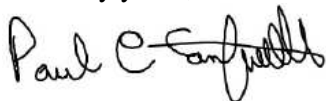
I am very excited about the CAMEA concept and proposal. I support it very strongly. As I understand it, Continuous Angle Multiple Energy Analysis (CAMEA) will allow for rapid data collection of inelastic neutron scattering data (i.e. dispersion curves) on relatively small samples as a function of temperature, pressure, and magnetic field. This would allow for the incorporation of inelastic neutron scattering into the materials / states discovery process. This would be a distinct change from neutron scattering's current role as a "high end" experiment that takes place as part of the detailed characterization of well characterized systems requiring very large samples and months if not years of sample preparation.

As an example CAMEA could aid in the identification of classes of compounds that might support new examples of high temperature superconductivity. Currently the feeling in the field is that some sort of "fragile" transition metal magnetism, that can be suppressed with either pressure or substitution, is key to finding new examples of the high T_c superconductivity found in the the CuO- as well as the FeAs-based systems. The problem is that in order to identify promising systems we need rapid feed back about the magnetic fluctuations in potential systems, often as they are doped or as pressure is applied. CAMEA can provide these data in a real time setting, studying samples on the 1 mm^3 scale. It would be my hope to have CAMEA run through scores of samples at ambient and high pressure and use these data to screen promising systems for further detailed synthesis and characterization. This would mark a turning point in the use of inelastic neutron scattering in terms of its use as an exploratory tool for new materials / states discovery.

Superconductivity is not the only example. Clearly CAMEA will be of great use for other pressure based systems, I can think of materials that we use pressure on to induce quantum criticality (by suppressing either anti- or ferromagnetic states) that would greatly benefit from that data that CAMEA could collect as well.

To repeat, I think CAMEA concept is GREAT and I strongly endorse it and hope to use it as well.

Sincerely yours,



Paul Canfield

Fellow of the American Physical Society

Distinguished Professor of Physics and Astronomy

Robert Allen Wright Endowed Chair in Physics

Senior Physicist, Ames Laboratory

Iowa State University

Princeton University

Department of Chemistry
Princeton New Jersey 08544 - 1009



Robert J. Cava

Russell Wellman Moore Professor of Chemistry

September 4, 2013

Prof. Henrik M. Rønnow
Head of Laboratory for Quantum Magnetism
École Polytechnique Fédérale de Lausanne
Lausanne, Switzerland
henrik.ronnow@epfl.ch

Dear Henrik,

Thank you very much for explaining to me your proposed instrument project for the future ESS when we spoke at the MaNEP workshop earlier this year. I understand that the instrument would be designed with the goal of characterizing the magnetic excitations in new materials, including at high magnetic fields, high pressures, and low temperatures.

In my view, this instrument would have an extremely high impact in the international materials physics community, and I would like to lend a strong voice in support of your proposal. As you know, new physics is often found when looking from a new perspective at the characteristics of new materials. My role in the research community over the past 30 years has been to try to find the new materials that form the basis for that new physics. I think that many possible discoveries in physics have unfortunately been missed because new materials have not been available in sufficient size to support the neutron scattering measurements that are needed to characterize their magnetic excitations. This type of research is at the forefront on quantum materials, as recent work for example in characterizing the magnetic excitations in cuprate superconductors and pyrochlore magnets, performed on very large samples, has shown.

Your proposed instrument, which would be designed specifically with an eye towards the study of much smaller samples than can currently be used, will dramatically expand the number of new materials that can be studied, and thus dramatically impact the discovery of new physics. This is because very often the materials that have the potential to display exotic new physics cannot be grown as large crystals or high volume samples. I have very often been asked to provide a crystal of a new material for neutron scattering studies, but have not been able to do so because it was impossible for me to provide a sample of sufficient size to allow the experiments to be done; it happens all the time, and is very frustrating. It would be great for the international materials physics and chemistry communities if your proposed instrument can be built; I am sure that it would change the kind of research that can be done for a large number of researchers, and would result in the discoveries of many new phenomena. I strongly support your proposal.

Sincerely yours,

Robert J. Cava



Université Pierre-et-Marie Curie (Paris VI)
IMPMC, CNRS UMR 7590
Case 115, 4 Place Jussieu, F-75252 Paris
tel. 33-1-4427-4454, fax 33-1-4427-3785

Dr S. Klotz
Tel. +33-(0)1 44 27 44 54
e-mail : Stefan.Klotz@impmc.jussieu.fr

Paris, Octobre, 2013

To whom it may concern.

Letter of support: CAMEA

This letter is to support funding and construction of the CAMEA spectrometer intended to be installed at the future European Spallation Source ESS.

My motivation for this support letter is the following: I have been involved during more than two decades in neutron scattering, in particular the development of novel high pressure methods for which I have an international reputation. Such experiments allow only small sample volumes in the order of mm^3 if pressures up to 100 kbar or higher are aimed for, i.e. pressures which are relevant for material and Earth sciences. Whereas synchrotron sources can nowadays routinely collect data under these conditions, the much weaker flux of neutron sources severely hampers the study of matter under pressure using neutron radiation.

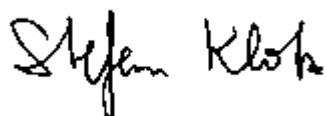
The CAMEA spectrometer is designed to overcome these limitations, thereby opening new directions in research under extreme conditions. CAMEA is optimized for the study of small samples in the mm^3 range. This is achieved by a clever combination of large detector coverage, a detector geometry allowing data collection at different final energies simultaneously, as well as a vastly improved signal-to-noise ratio. These are ideal conditions for high pressure measurements (potentially in combination with high temperatures) in the several 100 kbar range. This, in combination with the fact that ESS will have unprecedented neutron flux, will result in an instrument which will be unique in its kind. In addition, the horizontal scattering geometry of CAMEA is perfectly adapted to the geometry of high pressure cells which can reach 100 kbar and beyond.

In short: CAMEA has the potential of addressing fundamental questions on the dynamics and excitation of matter under extreme conditions, covering aspects of pure solid state physics (magnetism, highly correlated electron systems), material sciences (hydrogen in metals) and Earth sciences (diffusion and dynamics of hydrogen bearing rocks and minerals).

I strongly encourage funding and construction of this instrument. The team involved in the design of CAMEA are outstanding experts in neutron scattering with a strong interest in high pressure and extreme sample conditions in general. Having worked for decades in high pressure neutron scattering, I am delighted to see this team embarking in extending the frontiers of material research under extreme conditions.

Finally, I happen to be the current chairman of the European High Pressure Research Group (EHPRG, <http://www.ehprg.org/>), a more than 50 year-old organisation devoted to high pressure research and technology in Europe. In this function I wish to underline the importance of CAMEA for the European high pressure community. Most neutron activity worldwide is currently devoted to diffraction, in its own right. Probing dynamical properties under pressure using neutron has so far been neglected – for technical reasons – and CAMEA would fill a gap which is presently a ‘green field’. Funding agencies should realize that this is a unique chance to ensure the competitiveness of a large European science community covering very diverse research topics as listed above.

Sincerely,

A handwritten signature in black ink that reads "Stefan Klotz". The signature is written in a cursive, slightly slanted style.

Stefan KLOTZ
Head of the high pressure group
Chairman of the European High Pressure Group EHPRG
Editor in Chief of *High Pressure Research* (Taylor & Francis)

Adresse :
EPFL-SB – ICMP – EPSL
PH D2 435 (Bâtiment PH)
Station 3
CH – 1015 Lausanne
Tél. : +41 21 693 33 75
Fax : +41 21 693 46 66
URL : <http://epsl.epfl.ch>

To whom it may concern

N/réf. PG / cp

Ecublens, le 28 octobre 2013

Letter of support: CAMEA

This letter is to support construction of the CAMEA spectrometer intended to be installed at the future European Spallation Source ESS.

During my scientific carrier I have been involved in developing forefront methods for the investigation of systems of geophysical interest, and in particular I have, as first, developed the application of high-pressure methods (DAC) at synchrotron radiation facilities. Whereas synchrotron sources can nowadays routinely collect data under the extreme conditions relevant for Earth and Planetary Science, the much weaker flux of neutron sources still severely hampers this kind of studies. However neutrons are the ideal probe to investigate light elements which are scarcely visible to x-rays, and in particular hydrogen and hydrogen based systems, like water, methane, ammonia, which are basic constituents of earth and planets. In the last few years, a tremendous effort has been undertaken by several groups around the world to the determination of the structure of these systems up to very high pressures, a program in which my group has been actively involved. However, the knowledge of the dynamical counterpart lags far behind, due to the intrinsic technical difficulties linked to the necessity, for energy discrimination, of samples of large volume.

The CAMEA spectrometer is naturally designed to overcome this limitation as it is optimized for the study of small samples in the mm³ range, thus providing the unique opportunity to develop neutron spectroscopy under extreme conditions. In particular, the combination of large detector coverage, simultaneous data collection at different final energies, and excellent signal-to-noise ratio, provide ideal conditions for high pressure measurements in the several 100 kbar range. This, in combination with the fact that ESS will have unprecedented neutron flux, will result in an instrument which will be worldwide unique.

CAMEA is perfectly suited, due to its horizontal scattering plane, to the new generation of large volume presses recently developed for dynamics studies, and will thus provide the most versatile solution for a broad community of users interested in both fundamental, and applied research in a wide field ranging from planetary interiors to the recovery to ambient conditions of non-equilibrium structures having novel functional properties.

Therefore, the access to dynamical properties under extreme conditions guaranteed by the CAMEA specifics will open new exciting prospective in the field and will provide an a unique chance to ensure the competitiveness of a large European science community.

For all these reasons I strongly encourage construction of this instrument.



Philippe Gillet



Dr. Maikel C. Rheinstädter

Associate Professor
Department of Physics & Astronomy
1280 Main Street West
Hamilton, Ontario, Canada L8S 4M1
Tel: (905)-525-9140 Ext. 23134
Fax: (905)-546-1252
E-mail: rheinstadter@mcmaster.ca
<http://www.rheinstaedter.de/maikel>

Hamilton, October 30th, 2013

Prof. Henrik M. Rønnow
École Polytechnique Fédérale de Lausanne
Lausanne, Switzerland

Dr. Niels Bech Christensen
Technical University of Denmark
Department of Physics
Kgs. Lyngby, Denmark

Dear Henrik, Dear Niels,

I very enthusiastically support your proposal to build the novel Continuous Angle Multiple Energy Analyser spectrometer CAMEA at the future European Spallation Source ESS.

The determination of molecular dynamics in biological materials is certainly one of the greatest challenges in modern biology and biophysics. Few experimental techniques can access structural and dynamical properties on the nanometer scale. Advanced neutron scattering techniques have proven to be powerful tools to study dynamics and interactions in membranes and biomaterials down to nanometer length scales and up to the relevant picosecond and nanosecond times. However, sample sizes are typically small and the corresponding dynamical signals are further reduced by the intrinsic static and dynamic disorder in these materials, especially under physiological conditions.

Due to its design, CAMEA will be optimized for small samples and allow a fast data collection, thereby covering the relevant length and energy scales simultaneously. By aligning the materials, such as solid supported oriented membranes, spider silk or hag fish fibres, hair and chitin structures for instance, dynamics in the direction of interest can be measured fast, with a high resolution and a good signal to noise ratio. The high intensity of the machine should make it possible to study kinetics in these systems as well, which is very difficult to obtain with the current neutron instrumentation.

You and your project team, including Kim Lefmann, Christof Niedermayer, Fanni Juranyi , Marko Marton and Paul Freeman, have considerable experience in inelastic neutron instrumentation and are certainly in an outstanding position to tackle this challenge and successfully design and build CAMEA. I would envision that researchers who currently already use neutron diffraction in biomaterials will study dynamics in addition to structure using this novel instrument, especially in combination with dedicated sample environments that allow experiments under physiological conditions, such as body temperature and high humidity. The existing biophysical neutron community will welcome this new instrument as it opens up new possibilities and will enable exciting new science in the future.

I am very excited about this new instrument. Please do not hesitate to contact me if you have questions or need further information.

Sincerely,



Supporting Names for CAMEA

In addition to obtaining letters of support for CAMEA at the ESS we have asked known neutron scatterers if they wish CAMEA to be built.

The following names are a list of neutron scatterers who wish to see CAMEA built at the ESS:

Peter Svedlindh (Uppsalla University)
Alexander Komarek (Max Planck- Dresden)
Paolo Santini (University of Parma)
Andre Strydom (University of Johannesburg)
Andrew Boothroyd (University of Oxford)
Louis-Pierre Regnault (CEA, Grenoble)
Bella Lake (HZB)
Richard Mole (Bragg institute, ANSTO)
Toth Sandor (PSI)
Adroja Devishibhai (ISIS, STFC)
Tom Fennel (PSI)
Kirrily Rule (Bragg Institute, ANSTO)
Martin Boehm (ILL)
Oleg Petrenko (University of Warwick)
Simon Kimber (ESRF)
Markus Braden (university Of Cologne)
Pregelj Matej (Institut josef Stefan, Ljubljana)
Aziz Daoud-Aladine (ISIS, STFC)
Chris Stock (University of Edinburgh)
Tob Perring (ISIS, STFC)
Rob Bewley (ISIS, STFC)
Andrey Zheludev (ETHZ)
Takatsugu Masuda (University of Tokoyo)
Mogens Christensen (University of Aarhus)
Martin Rotter (Max Planck, Dresden)
Franz Demmel (ISIS, STFC)
Linda Udby (University of Copenhagen)
Collin Broholm (John Hopkins University)
Duc Manh Le (*Seoul* National University)
Oliver Stockert (MPG- Dresden)

Survey

Condensed matter neutron scatterers that may have an interest in CAMEA, were asked to complete a short survey. They were asked about what extreme environments they are interested in for neutron scattering, and what aspects of CAMEA are they particularly interested in.

Survey:

We wish to know if you are interested in performing neutron scattering experiments under:

- | | |
|---|--------|
| 1) High magnetic field (aim is 25 T assuming cuprate magnets become available)? | Yes/No |
| 2) High pressure (10 GPa range accessible with Paris-Edinburgh cells)? | Yes/No |
| 3) Simultaneously high pressure and high magnetic fields? | Yes/No |

What capabilities of CAMEA (see below for details) are you interested in:

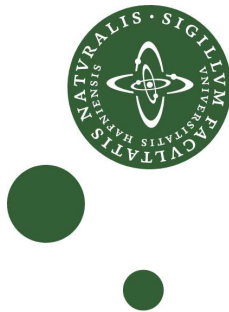
- | | |
|---|--------|
| A) Rapid mapping of excitations/parametric studies? | Yes/No |
| B) Studying small samples? | Yes/No |
| C) In-situ studies? | Yes/No |
| D) Time resolved studies? | Yes/No |

The results of the survey are:

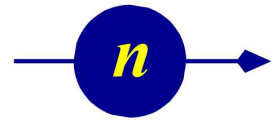
Question	Yes (%)	No(%)	Possibly
1) High Magnetic Fields?	91	9	0
2) High Pressures?	61	33	6
3) High Pressure and High Magnetic Fields?	39	58	3
A) Rapid Mapping?	97	3	0
B) Small Samples?	100	0	0
C) In-situ?	36	61	3
D) Time Resolved?	36	58	6

For performing neutron scattering under extreme conditions the highest demand is for performing experiments under high magnetic fields, the extreme condition that already has a significant user demand for inelastic neutron scattering. Despite the present strong limitations of performing inelastic neutron scattering under high pressures, there is a high demand for high pressure studies. As high pressure studies are severely limited with present neutron instrumentation it is of little surprise that going one step further for combining high magnetic fields and high pressures for experiments has a lower demand.

From the questions about what aspects of CAMEA are neutron scatterers most interested in we have a clear result. CAMEA's ability to perform rapid mapping, and CAMEA's ability to study small samples are the two most appealing aspects of the instrument.



Technical University of Denmark

*McStas***CAMEA**

Simulations & Kinematic Calculations

Author:

J. O. Birk



PAUL SCHERRER INSTITUT

ÉCOLE POLYTECHNIQUE
FÉDÉRALE DE LAUSANNE

Contents

1	Introduction	4
2	Working model	5
3	Coverage	5
3.1	Scanning k_f	5
3.2	Dark Angles	7
3.2.1	Discrete rotation of a_3	7
3.2.2	Contious rotation of a_3	8
3.2.3	Multiple energies from one analyser	10
3.2.4	Usefullnes of the a_3 scan mode.	10
4	The Chopper system	12
4.1	Pulse shaping choppers	12
4.2	Frame overlap choppers	13
4.3	Tail removal chopper	13
4.4	Order sorting chopper	13
4.5	Other possible choppers	14
4.6	Solutions with fewer choppers	14
4.7	Performance of Chopper system	14
4.8	Order sorting	15
4.8.1	Higher orders	16
4.9	Chopper phase uncertainties	16
4.9.1	Pulse shaping choppers	17
4.9.2	Frame overlap choppers	17
4.9.3	Frame shaping chopper	17
4.9.4	Order sorting chopper	17
5	Analysers	17
5.1	Analyser Materials	17
5.2	The asymmetric Rowland Geometry	18
5.3	Resolution	20
5.4	Angular coverage of a flat Rowland analyser	22
5.5	Rotation of Analysers	23
6	Detectors	23
7	Additional issues on Analyzer-Detector interaction	24
7.1	Mosaicity	24
7.2	Several Energies	28
7.2.1	The Principle	28
7.2.2	Simulations	28
7.2.3	Intensity and Resolution	29
7.2.4	Background	29
7.2.5	Energy tails	30

CONTENTS	3
<hr/>	
8 Time Resolved measurements	32
8.1 Flightpath uncertainty	32
8.2 Energy uncertainty	32
8.3 Uncertainty of scattering position	32
8.4 Uncertainty of detection position	32
8.5 Combined Result	32
9 The Prototype	33
10 Conclusion	33

1 Introduction

During the design of CAMEA extensive simulations and cinematic calculations were performed to explore the vast parameter space. These have led to a far better understanding of the instrument performance as well as new ideas to improve the instrument.

Many simulations of the backend were done using a simpler triple axis model of the instrument whereas some frontend simulations and calculations were done a version with a 3 % longer guide (and thus 3 % shorter wavelength band), than what is proposed.

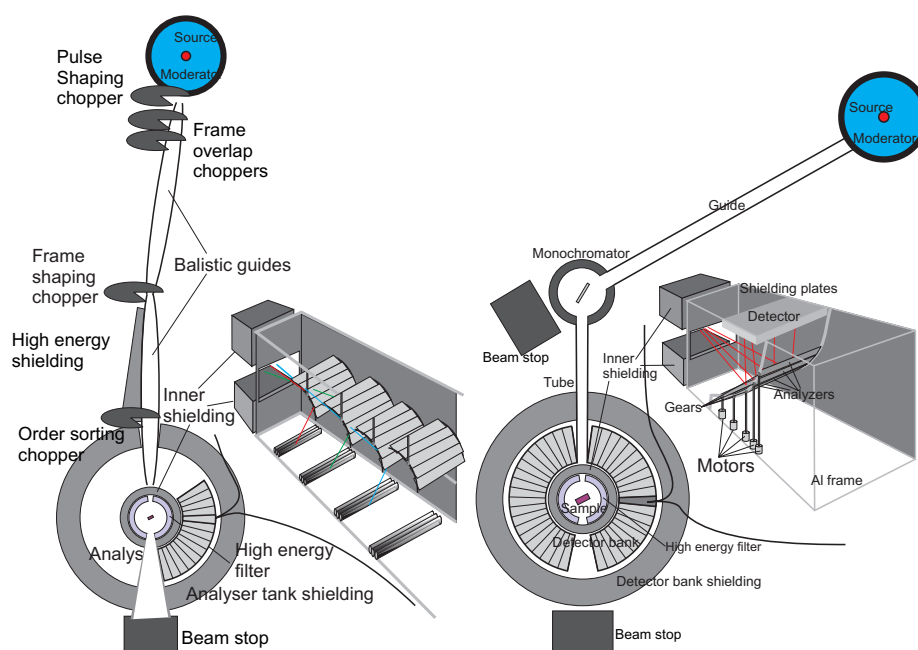


Figure 1: *Schematic drawings of CAMEA at ESS (left) and a reactor source (right).*

2 Working model

During the simulations and calculations a working model has been used. The model turned out to be so successful that most of it was reused as the final proposed instrument. Because of this almost all results can be transferred directly to the final proposed instrument, and simulations in different sections should be compatible. The newest working model have the following specifications:

- Analyser mosaicity: 60 arch minutes
- Detectors: 3 parallel H₃ tube with a 1/2 inch diameter per analyser *But in a few simulations 7 were used to understand the boundaries better.*
- Analysers crystals: 1 mm deep and 1 cm wide.
- Vertical covering angle: ± 2 deg
- Sample size: 0.5*0.5*0.5 cm³ to 1*1*1 cm³

Energies of analysers (meV)	2.5	2.8	3.1	3.5	4	4.5	5	5.5	6.5	8
Sample analyser distance (m)	1.00	1.06	1.13	1.20	1.28	1.37	1.46	1.56	1.67	1.79
Analyser detector distance (m)	0.8	0.9	1.0	1.1	1.15	1.25	1.35	1.4	1.45	1.5

3 Coverage

Kinematic calculations were performed to investigate the coverage of the instrument under certain settings, using $\mathbf{q} = \mathbf{k}_i - \mathbf{k}_f$ and $k\omega = \frac{\hbar^2}{2m}$ where ToF provides continous coverage of k_i for any k_f .

3.1 Scanning \mathbf{k}_f

Figure 2 shows examples of such coverages. It is shown that the optimal scan mode would often be a mode where the analysers were rotated and detectors moved to investigate different E_f values. Some of the displayed effect was found to be replaceable by the idea of getting several energies from one analyser. This together with a continuous sample rotation where data is recorded in event mode will make the performance gain from the E_f scanning mode far too small to justify the extra complexity and cost of such a solution.

To se how this coverage would map out an actual dispersion a magnon were simulated. This was done in the high flux mode where the full pulse length is used and the signal from all 3 detectors looking at a single analyser is integrated. The corresponding 4% energy resolution is the coarsest achievable at the instrument

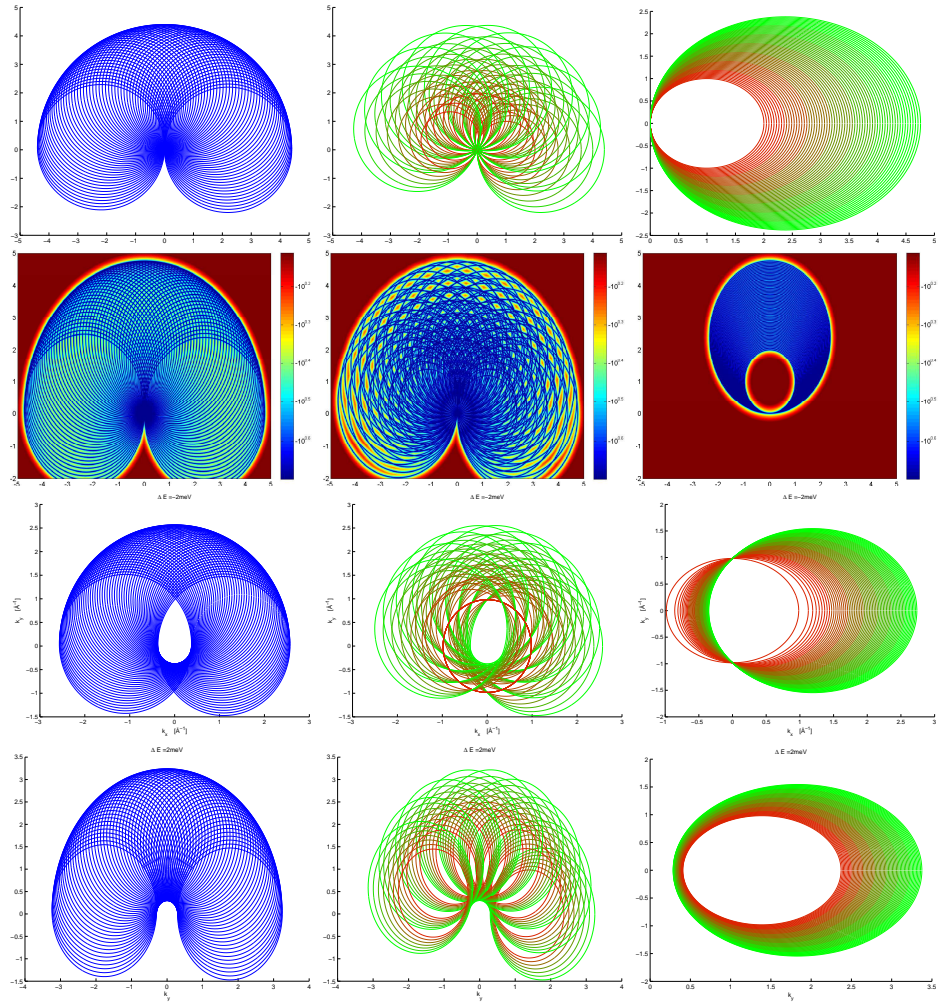


Figure 2: **Coverage illustrations** The figures shows idealised coverage of an ESS CAMEA module at different energy transfers ($\hbar\omega$). First row illustrates the signal at $\hbar\omega = 0$. Left shows a flat-cone-like instrument performing a sample rotation scan in 70 steps while the middle shows the same scan performed by a CAMEA system with 7 analysers but only in 10 steps. Finally the same 7 analysers scan E_f and keeps the sample still. As it can be seen the homogeneity is best for the E_f scan and worst for the CAMEA A3 scan. To further investigate this, a calculation of the distance to the closest measured point was done for all 3 setups. The results are displayed in the second row, again confirming that E_f scans are preferable. Finally the two bottom lines shows the inelastic coverage at $\Delta E = -2$ meV and $\Delta E = -2$ meV. The calculations were done before the work model were established with a different distribution of E_f values but the principle will also be true for the work model.

meaning that the count rate in each pixel will be comparable to that of a triple axis instrument with doubly focusing monochromator and focusing analyser. All energies and angles correspond to those of the work model. The energy band

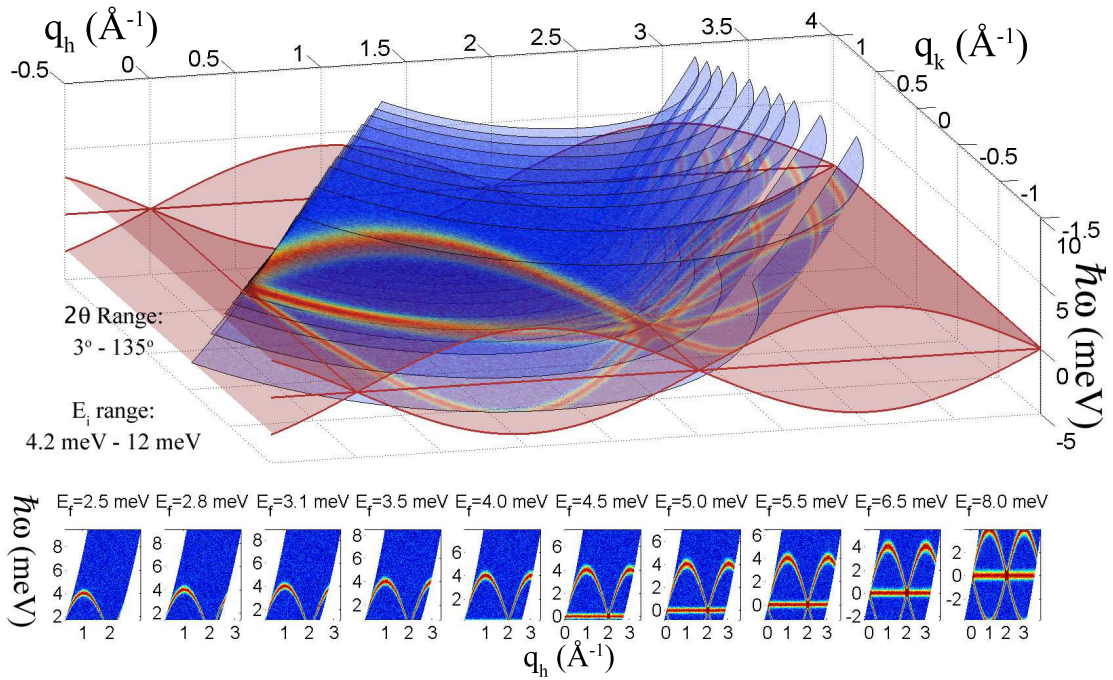


Figure 3: Simulated coverage of magnon dispersion. The signal corresponds to a single data accusation without dark angles and in high flux/low resolution mode.

has been decreased slightly when the pulse shaping chopper was moved to 6.5 m after this work was done.

3.2 Dark Angles

The CAMEA design has a quasi-continuous angular coverage of the horizontal scattering plane with gaps in the two theta coverage. The main contribution to these gaps comes from the flat analysers reflecting out of the plane, but even if curved analysers were chosen gaps for walls, analyser mountings and collimators would produce small dark angles. In order to cover these gaps the CAMEA analyser-detector module will be designed to be able to rotate a few degrees thus covering all two theta angles in its range by measuring two different settings or 2 times in 3 settings. There are however also possible to cover the plane by simply rotating the sample (a3) slowly around. This method will lead to a non-uniform statistical and resolution coverage but will still be useful for many experiments. Note that this work has been compiled before any technical drawings have been made. It is quite possible that we will get bigger or differently distributed dark angles in the final design but these will not change the principles described here.

3.2.1 Discrete rotation of a3

In many cases scans will be done with a series of discrete a3 steps. If that is the case the coverage will look as in figure 4. The covered area is without gaps, but

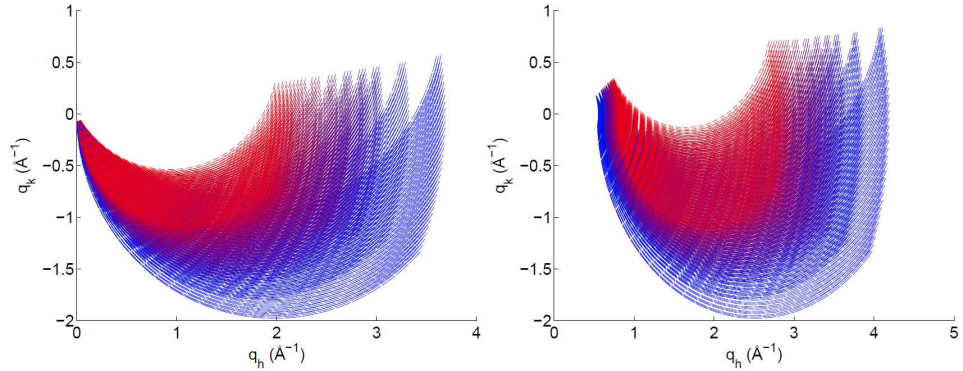


Figure 4: Examples of how the reciprocal space would be covered by a discrete sample rotation. Left: 0 meV energy transfer. Right 5 meV energy transfer. Each line represents the centre of the measurement from one specific analyser. The red lines are low E_f (fine resolution) and the blue high E_f (coarse resolution). The sample is rotated 30° in discrete steps of 1° .

some areas have gaps in the fine resolution data (red lines in the figure). It is however hard from the figure to quantify the gaps. Hence we will continue to the case of continuous a_3 scanning in section 3.2.2 as it makes it the coverage clearer and the results can be generalized to the discrete case. Note that the 1.7 \AA wavelength band accepted by CAMEA does not allow all analysers to display the elastic line at the same time, unless every second moderator pulse is removed by the chopper system. The exact number of analysers that can see the elastic line depends on the choice of wavelength band. On the other hand all analysers can see the 5 meV energy transfer line at the same time if the wavelength band is chosen with this in mind.

3.2.2 Continuous rotation of a_3

With the high flux and event mode data acquisition of ESS-CAMEA it is foreseen that many experiments will be done rotating the sample slowly around while counting. This will lead to a coverage as shown in figure 5. The gaps in the coverage from the first analysers are now clearly visible but it is also clear that all gaps are covered by analysers behind the front most ones. Only the small gaps in the regions exclusively covered by the backmost analyser are left open. It can be seen that the analyser overlap changes with both the scattering angle and energy transfer so it is impossible to design the dark angles and energies in a way so no gaps will be seen between the first two analysers for all energy transfers. This means that some areas will have lower statistical weight and a coarser resolution than others when the dark angles are only covered by a_3 rotation. Note that the 7th analyser is at 5 meV - the most used energy for cold triple axis spectroscopy. Hence if just one of the first 7 analysers covers the region, then the resolution will be better than in many cold triple axis experiments. In addition the distance collimation means that CAMEA has a q -resolution a well collimated triple axis

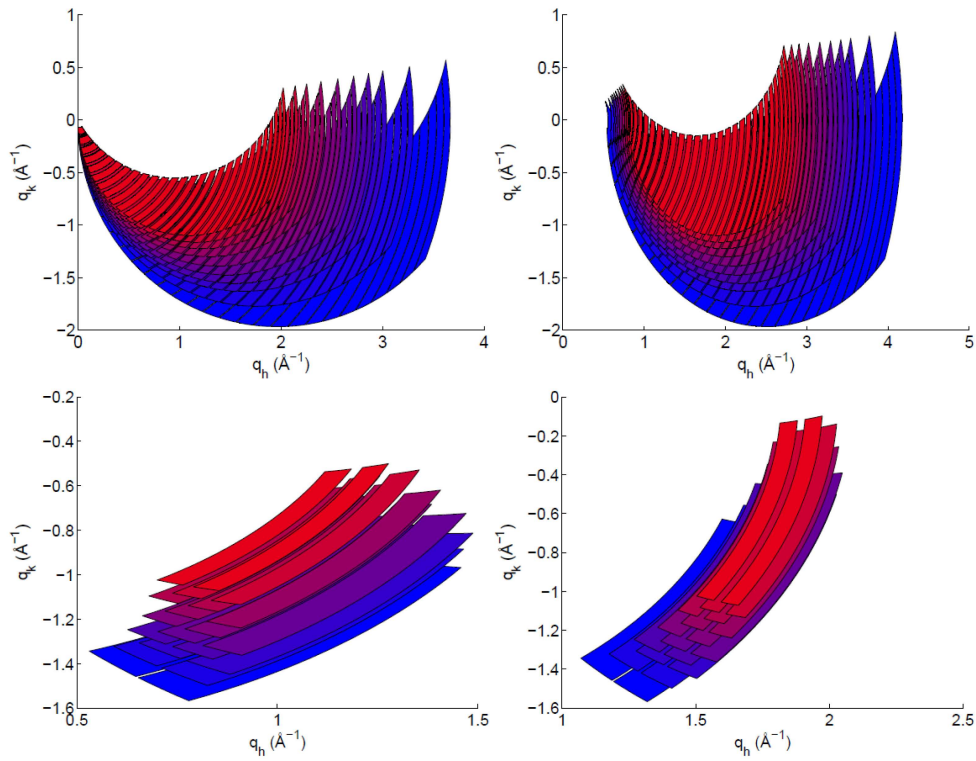


Figure 5: Examples of how the reciprocal space would be covered by a continuous sample rotation. Left: 0 meV energy transfer. Right: 5 meV energy transfer. Each coloured area represents the area covered by one analyser when the sample is rotated continuously through 30 degrees. The red lines are low E_f (fine resolution) and the blue high E_f (coarse resolution). The top row shows all analyser segments whereas the bottom row only shows two. As the coverage changes with energy the same segments are not displayed for all E_f values but instead segments covering approximately the same area in reciprocal space are chosen.

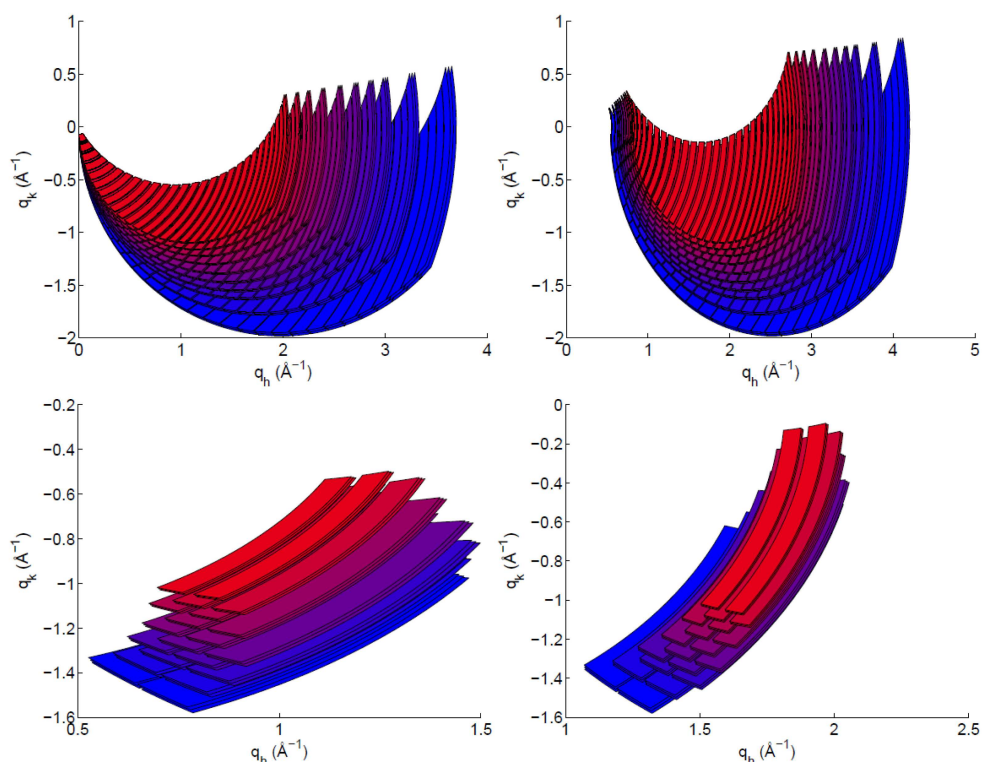


Figure 6: Examples of how the reciprocal space would be covered by a continuous sample rotation with 3 energies from one analyser. The same as in figure 5 but with 3 half-inch tube detectors 0.5 mm apart looking at the same analyser.

instrument and better Energy resolution.

3.2.3 Multiple energies from one analyser

As described in detail in section 7.2 it is planned to obtain 3 different energies from each analyser. If this is taken into account the gaps between the analysers becomes even smaller, though they are still there for the front most analysers (se figure 6). If one chose to collect 5 energies from each analyser the gaps would generally be covered (se figure 7) but there would still be a big difference in statistics. Partly because some areas are only covered by one energy per analyser and partly because the outermost energies from each analyser will have lower statistics due to the mosaicity of the analysers. This can be reduced by choosing analysers with a more relaxed mosaicity but the former will still be true.

3.2.4 Usefulness of the a3 scan mode.

Although the a3 scan mode does have its limitations in covering the dark regions of the scattering angles it will be useful for many experiments. If one needs the a3 scan anyway which most mapping experiments will then CAMEA will make

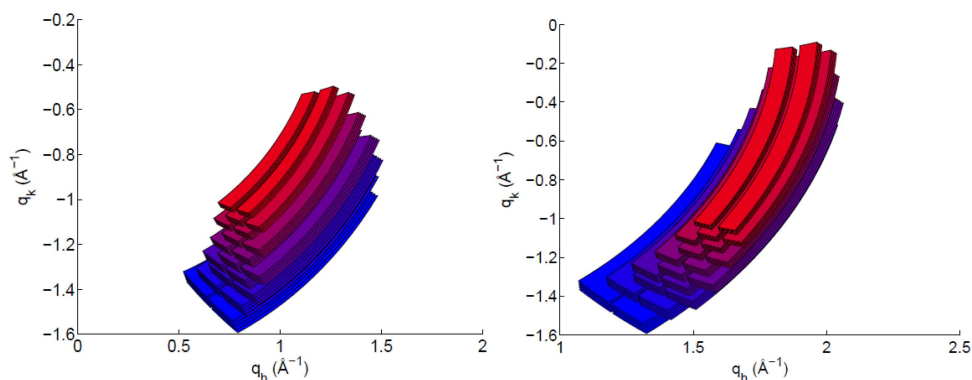


Figure 7: Examples of how the reciprocal space would be covered by a continuous sample rotation with 5 energies from one analyser. The same as in figure 5 bottom but with 5 half-inc tube detectors 0.5 mm apart looking at the same analyser.

a continuous coverage of the chosen part of reciprocal space, without rotation of the analyser tank. Not all areas will have the sample resolution or the same statistics but it should be possible to cover all areas with a resolution better than what is seen on typical triple axis experiments and statistics from at least half the analysers. Should the generated map show features in the regions where the resolution are limited the user can afterwards rotate the analyser-detector module and redo the scan.

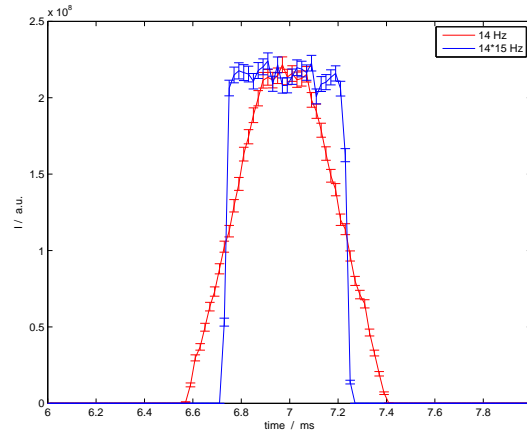


Figure 8: The pulse just after a pulse shaping chopper running at 14 Hz and 210 with 0.5 ms opening at a 1 cm pinhole. While the intensity is roughly the same the 210 Hz chopper has a much shorter opening/closing time.

4 The Chopper system

The instrument will ideally need 7 choppers, located at 6.5, 6.5, 8, 13, 78, 162, and 162 m. The reason for the choppers and their positions will be explained below.

4.1 Pulse shaping choppers

A pair of disc choppers placed 6.3 - 6.5 m from the moderator with a radius of 35 cm, an opening of 170° , and a variable frequency of up to 300 Hz

A pair of disc choppers should be placed as close to the source as possible to shape the pulse from the moderator (denoted "the main pulse"). The geometrical restrictions close to moderator are rather strong if not 100 % well defined, so we are limited to 35 cm disc choppers at maybe 6.5 m from the moderator.

These pulse shaping choppers define our instrument resolution so it is important that they open and close as fast as possible to minimize the energy tails. The geometrical restrictions make it impossible to achieve this with bigger choppers so we have to change the opening and closing in other ways:

We can design the guide with a needlepoint at the chopper position. This will help us get a better opening time but significant tails can still be observed at high resolution settings for 14 Hz frequency (see figure 8).

We can spin the pulse chapping choppers faster at $n_{pulse} * 14$ Hz and make the opening n_{pulse} times bigger also making the opening and closing n_{pulse} times faster. Exactly how fast we can run the choppers depends on the desired pulse width but for 2 ms the limit is $n_{pulse} = 15$ which is sufficient to give a well-defined pulse also for all relevant opening times. ESS has no problems with choppers so close to the moderator running at high frequencies as long as they are otherwise standard choppers.

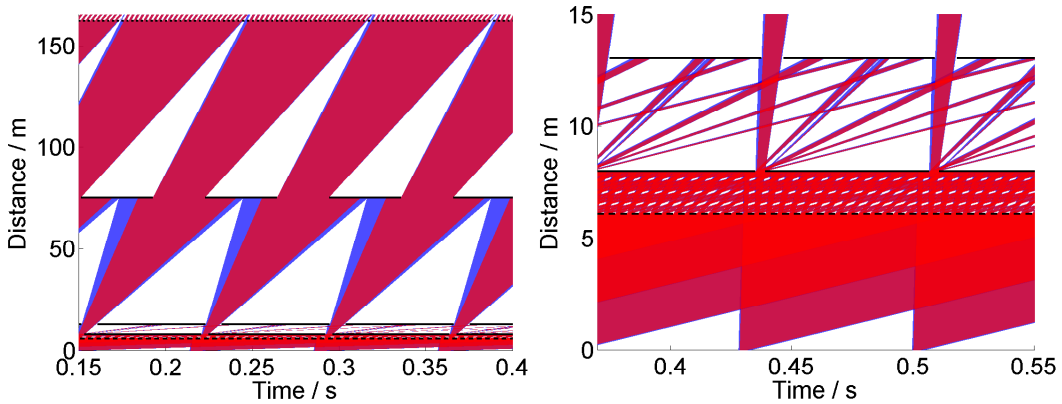


Figure 9: Left: Time of flight diagram for the proposed chopper system. The order sorting chopper system is not included for simplicity. Right: Details of the first 20 m's of the chopper system.

4.2 Frame overlap choppers

Two disc choppers placed 8 and 13 m from the moderator with a radius of 35 cm, frequency of 14 Hz, and an opening of $\sim 20^\circ$ and $\sim 45^\circ$

In order to remove $n_{pulse} - 1$ of the sup pulses from each main pulse and remove crosstalk between two different main pulses two extra choppers are needed: One as close to the pulse shaping choppers as possible to remove the sup pulses and one further away where second order pulses can be separated from first order pulses. The exact positioning can be modified but could for example be at 8 and 13 m, where 8 is chosen relatively close to the pulse shaping system and 13 far enough away to be outside the inner biological shielding for simpler maintenance.

4.3 Tail removal chopper

A single disc chopper placed 78 m from the moderator with a radius of 35 cm, an opening of 157.6° , and a frequency of 14 Hz

Though the tails of the moderator are removed from the resolution function by the pulse shaping choppers the tails do still have an effect on the width of the entire pulse at the sample position. It will severely limit the useful bandwidth if these tails are not removed. The chopper doing this should be as close to the sample as possible in order to remove as much tail as possible but far enough away that two neighbouring pulses can be separated. The limit turns out to be close to 78 m where our guide design is narrow due to the bending section.

4.4 Order sorting chopper

Two disc choppers placed 3 m before the sample of radius 35 cm, two openings of $\sim 80^\circ$, and a frequency of ~ 180 Hz

To distinguish first, second, (and possibly third) order scattering from the analysers a pair of choppers are installed as close to the sample as possible. The

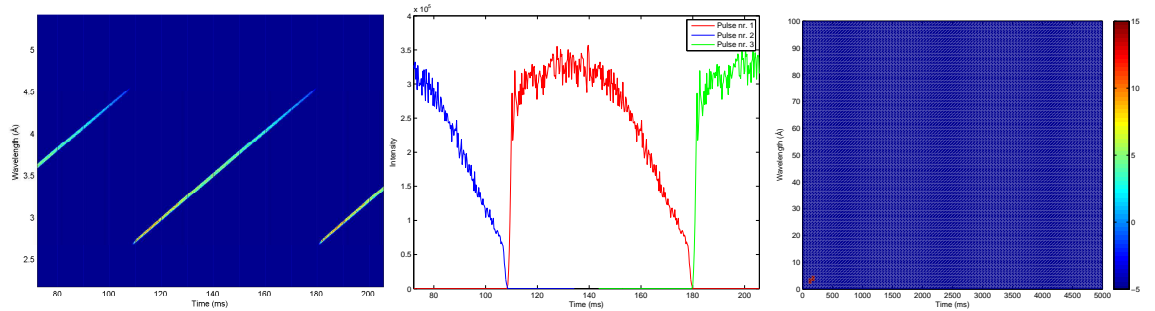


Figure 10: Left: McStas simulation of the pulse shape in a (t, λ) diagram. Middle: Collapsing the data to the time axis it is clear that two neighbouring pulses can be distinguished well. Right: Zoom out on log scale showing that no long wavelength neutrons (up to 100 Å) makes it through to the sample. Note that McStas as default only generates one pulse so in the first two figures this pulse have been repeated in Matlab with a frequency of 14 Hz while the last only show this single pulse. All simulations are done at 2ms chopper opening 14*15Hz pulse shaping chopper speed and a lowest transmitted energy of 4 meV (4.5 Å)

choppers will be running at close to 360 Hz slightly depending on the final geometry and while this is not a problem for normal choppers it is a question how well this will work close to a 25 T magnet. If we only want to distinguish first and second order scattering, while assuming higher orders to be insignificant, a single chopper is enough but if we want more freedom to also separate higher orders two choppers will be needed.

4.5 Other possible choppers

A t_0 chopper could be useful to remove the prompt pulse but may not be needed as we bend the guide out of line of sight.

4.6 Solutions with fewer choppers

It is possible to reduce the number of choppers but not without reducing the efficiency of the instrument significantly. Most obvious solutions would be to keep the pulse shaping choppers at 14 Hz and go for a single order sorting chopper, accepting the less desirable pulse shape, and removing the order sorting choppers to go for a filter solution instead.

4.7 Performance of Chopper system

The chopper system has been simulated and shown to block all unwanted neutrons in the range from 0.1 to 150 Å for a range of different wavelength bands, opening times and pulse shaping chopper speeds. An example of such a test can be seen in figure 10. Simulations of the energy resolution (see figure 11 shows that it is possible to vary it from 3% at 5 meV down to 0.3%. This makes it possible to tune it to give resolution matching anywhere in the entire dynamic

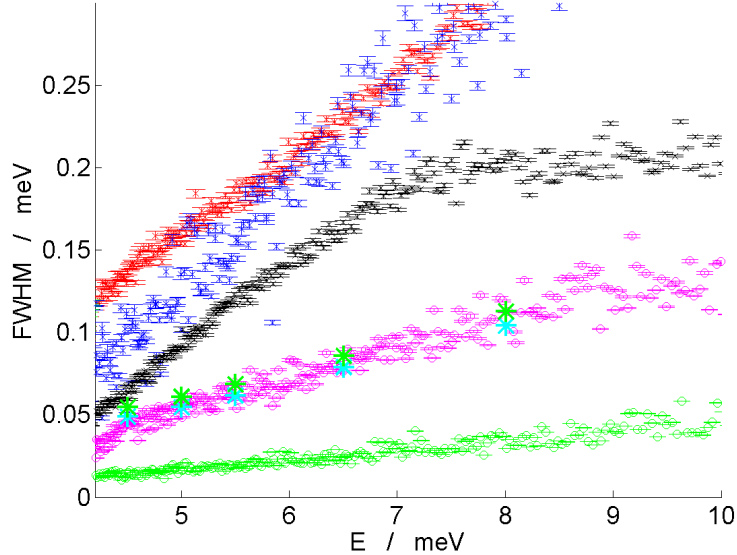


Figure 11: Energy resolution of the chopper system for varying opening times of the pulse shaping choppers. Red: full open, Blue: 5 ms, Black: 2.9 ms, Magenta: 1 ms, Green: 0.1 ms. The blue and green single asterisks are analytical and simulated resolutions of the secondary spectrometer for comparison.

range of the instrument and to unmatch the resolutions to push either flux or resolution above the standard operating numbers. The high possible resolution also enables precision measurements of powder lines e.g. needed to determine the pressure for high pressure experiments.

4.8 Order sorting

By placing a chopper a few meters before the sample it is possible to distinguish first and second order scattering on the analysers from the flight time. In principle one can have a chopper opening time of 50% but with flight time uncertainties, chopper opening and closing times and the fact that placing all detectors from the different analysers at the same optimized distance means that opening times of about 40 % is more likely. Of course this leads to a flux on sample reduction of 60 % but at the same time the coverage is doubled and the Be filter removed together with its beam attenuation so the number of neutrons counted on the detector will not suffer as much.

The system would perform best with the choppers running at 360 Hz just before the sample but as a chopper with a single opening of $\sim 50\%$ is unbalanced and hard to run at these frequencies and it is foreseen to mount 25 T magnet on the instrument leading to strong stray fields the performance at different number of openings and distances to the sample was done (see figure 13). Based on the results two openings and 180 Hz was chosen as it makes the chopper far more stable and it was moved back to 3 m from the sample. Here the stray field

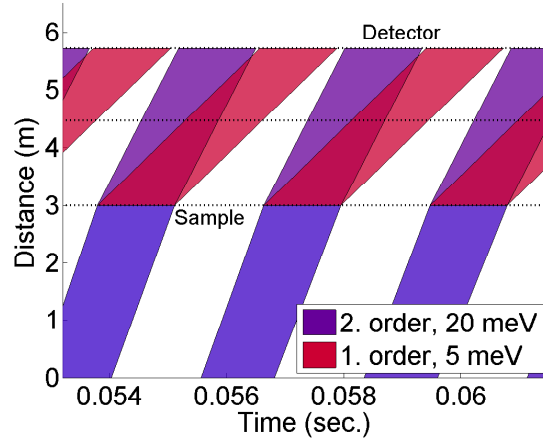


Figure 12: *Order sorting for one analyser.* The graph only shows a limited part of the wavelength band as it would otherwise become extremely messy.

is expected to be 300 times lower than the limit given by chopper producers making the chopper more reliable.

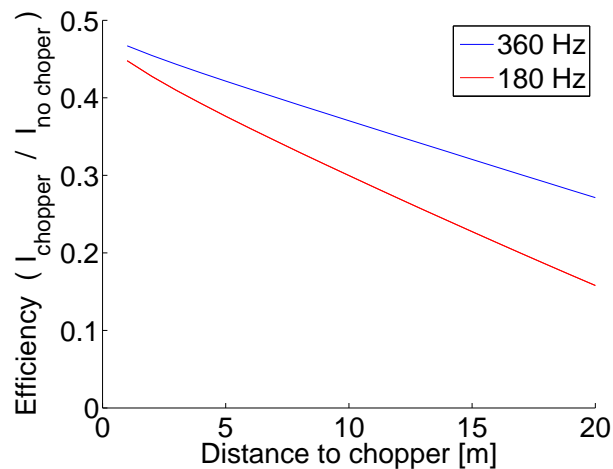


Figure 13: *Performance of order sorting chopper.* The 180 Hz chopper has two symmetric openings while the 360 Hz chopper has a single large opening.

4.8.1 Higher orders

It is in principle possible to use choppers to distinguish higher orders by closing the order sorting choppers more but the loss factor will be higher.

4.9 Chopper phase uncertainties

The long pulse of ESS and corresponding long primary flight path makes the instrument more resilient to phase uncertainties than many other instruments.

Since the radius of the choppers are not scaled together with the timeframes and instrument lengths one can either relax the frequency or produce choppers with bigger openings. The choppers most sensitive to phase uncertainties are for CAMEA chosen with very big openings, and that reduces the phase uncertainty problem significantly. Below is a description of how phase uncertainties in each chopper will influence the performance of the chopper system.

4.9.1 Pulse shaping choppers

Phase uncertainties in the pulse shaping choppers can in principle both lead to a lower intensity and a wrong determination of λ_i . Both effects will be very small due to the big opening of the choppers. A phase uncertainty of 1° leads to a drop in flux of less than one percent and a wrong determination of λ_i of the order 0.01%.

4.9.2 Frame overlap choppers

The frame overlap choppers are independent of phase uncertainties up to about 5 degrees, since they are not shaping the actual beam but only removing unwanted pulses.

4.9.3 Frame shaping chopper

The frame shaping chopper will shift the wavelength band if out of phase. The shift can however be determined and will not influence the resolution and intensity at a given wavelength. A shift of 1° on the chopper and will lead to a shift of the wavelength band of about 0.5 % of the lowest selected wavelength. In principle the width of the wavelength band can be reduced but for the proposed chopper system this will only happen if the chopper is more than 10° out of phase and can thus be ignored.

4.9.4 Order sorting chopper

Phase shift in the order sorting choppers will shift each pulse and can in principle lead so a loss of flux of 1.5% for 1° if the phase shift is unknown but since phase shifts can be determined by both direct measurements and data analysis the effect becomes negligible.

5 Analysers

5.1 Analyser Materials

Different materials were considered for analysers. Pyrolytic Graphite is commonly used for cold monochromators/analysers and has several nice characteristics:

- The peak reflectivity is very high.

Material	Attenuation though 1 blade at 45° (%)	Reflectivity (%)	Thickness (mm)
PG	0.01	75	1.0
Si	5.34	40	20.0
Ge	17.5	40	6.0

Table 1: **Analyser materials.** Attenuation calculated from data from [1] at 0K. At room temperature 2mm PG has been measured to have an attenuation of 2% at 5 meV. Above this energy, the attenuation increases strongly.

- The attenuation is low, even more so when considering the low thickness needed.
- No other Bragg peaks will be a serious issue even with a relatively open geometry.

It does however also show a number of drawbacks:

- Crystals are relatively small so a wafer material is needed.
- PG is expensive, especially considering the huge analyser area needed.
- Phonon scattering is a real issue and leads to Lorentzian energy tails. It is thus not ideal for quasi elastic and near elastic studies.

As the drawbacks are considerable, other materials were investigated as well. Si, Ge and Cu are all harder and thus decrease the phonon scattering issue. But unfortunately they have a higher attenuation at sufficient thicknesses and coupled with their lower reflectivity would lead to much lower total count rates. The attenuations at 0 K can be seen in table 1. Although the difference is small for room temperature analysers it is clear that PG is superior for transmission geometries.

For the prototype PG mounted on Si wafers are thus used. Since the cost of PG is proportional to its volume we have gone with 1 mm thickness. It displays almost as good reflectivity for cold neutrons as 2mm but comes at half the cost and with lower attenuation. It is mounted on 1 mm of Si (4,0,0) wafer. The orientation means that $k_{Si} = 2.3 * k_{PG}$ so the Si reflection lies at energies ~ 5 times higher than PG and thus does not even interfere with the second order reflection. Besides the extremely low mosaicity of Si means that the reflection is weak.

5.2 The asymmetric Rowland Geometry

The analysers will be mounted in an monochromatically focusing Rowland geometry. Since constraints in space, dark angles, order sorting chopper geometry and price makes it difficult to have equal sample-analyser and analyser-detector distances we will need to use the asymmetric Rowland geometry for at least some of the analysers. This means that we cannot use bent analysers and there will be

5.2 The asymmetric Rowland Geometry

19

a small difference in flight time from different parts of the analyser (Se 8.1). The first can however be solved satisfyingly by the use of a piecewise curved analyser, whereas the time broadening has a small influence for time resolved studies but can be neglected for the energy resolution because of the long primary flight path.

In the plain it is possible to curve the analysers, but that would be expensive, limit transmission and severely limit the q -resolution. So instead a piecewise linear setup is suggested.

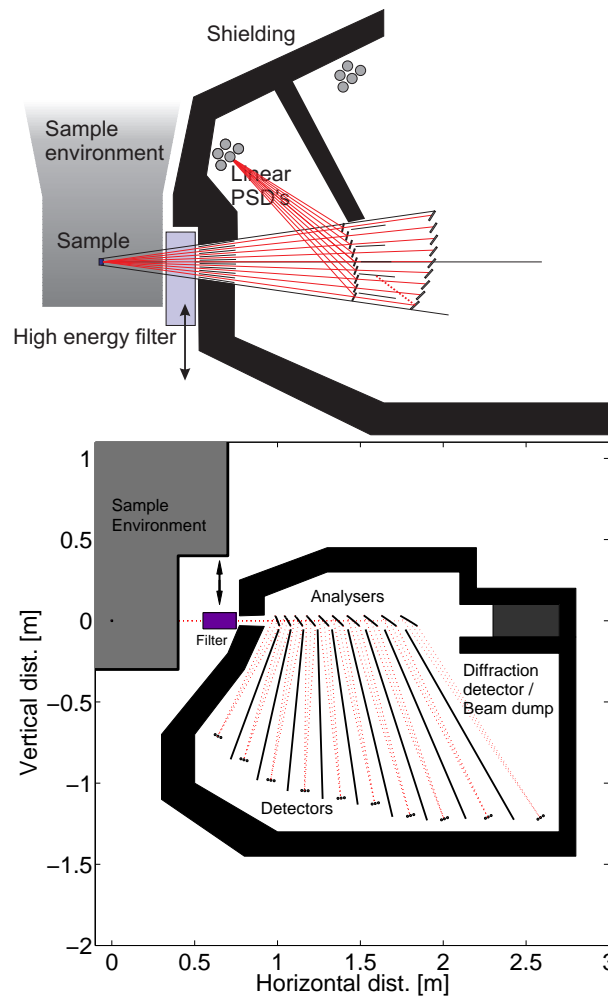


Figure 14: *Top: Illustration of the Asymmetric Rowland Geometry. Bottom: Example of an entire analyser setup with work model numbers.*

5.3 Resolution

The simulated and calculated resolutions can be seen in figure 15. The angular resolution decreases with analyser energy due to the longer distances to the backmost analysers. The angular resolution worsens with higher mosaicity and analyser-detector distances so either one have to limit those, accept a limited q-resolution, or insert collimators. Limiting the mosaicity is expensive and will reduce the flux in the outer detectors, whereas limiting the analyser-detector distance costs energy resolution, time resolution, and increases the phonon tails of the graphite. The chosen numbers will guarantee a good angular resolution while matching different time resolution contributions and giving a very good energy resolution.

The energy resolution can be extremely good in this setup. This is due to the

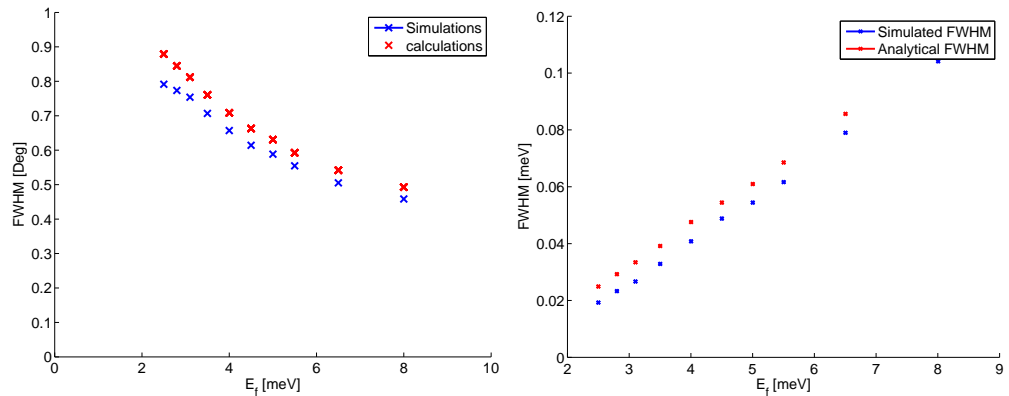


Figure 15: **Angular and E resolutions.** Simulated and theoretical resolutions of the backend. Left: Angular resolution, right: Energy resolution. for all 10 analysers in the work model.

small sample (1x1 cm), small analyser and detector sizes, and the long distances. Note that one can always worsen resolution by combining data from several detectors. This will indeed often be done as it fits with the incoming resolution of the high flux mode. The good resolution will however still be a key feature of the instrument, and will also be important for time resolved experiments and when the order sorting choppers are running.

Since distance collimation is the main contributor to the energy resolution, and the flight paths to the high energy detectors are longer than to the low energy detectors, the energy resolution changes less with energy than on a normal triple axis instrument. The change is however still more than a factor 5 so it is not possible to combine all data together without advanced data analysis, but the change will be smaller than it would be if a corresponding energy scan were made on a normal triple axis spectrometer.

The q resolution is dependent on E_i , E_f , pulse width, scattering angle, and direction through the ellipsoid. It is not possible to these settings to a single meaning full figure, but the powder resolution at the elastic line for 1 ms opening time of the pulse shaping chopper system can be seen in figure 15

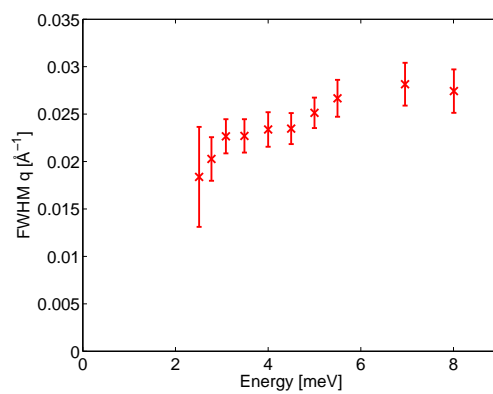


Figure 16: ***q resolution.*** Simulated q resolution for the full instrument at 1 ms neutron pulse and elastic scattering.

5.4 Angular coverage of a flat Rowland analyser

Figure 17 describes how the resolution and intensity changes when the analyser is no longer perpendicular to the incoming beam. As it can be seen the geometry works well out till an angular coverage of $\pm 10^\circ$ whereas the final setup only covers $\pm 3^\circ$ for each analyser segment.

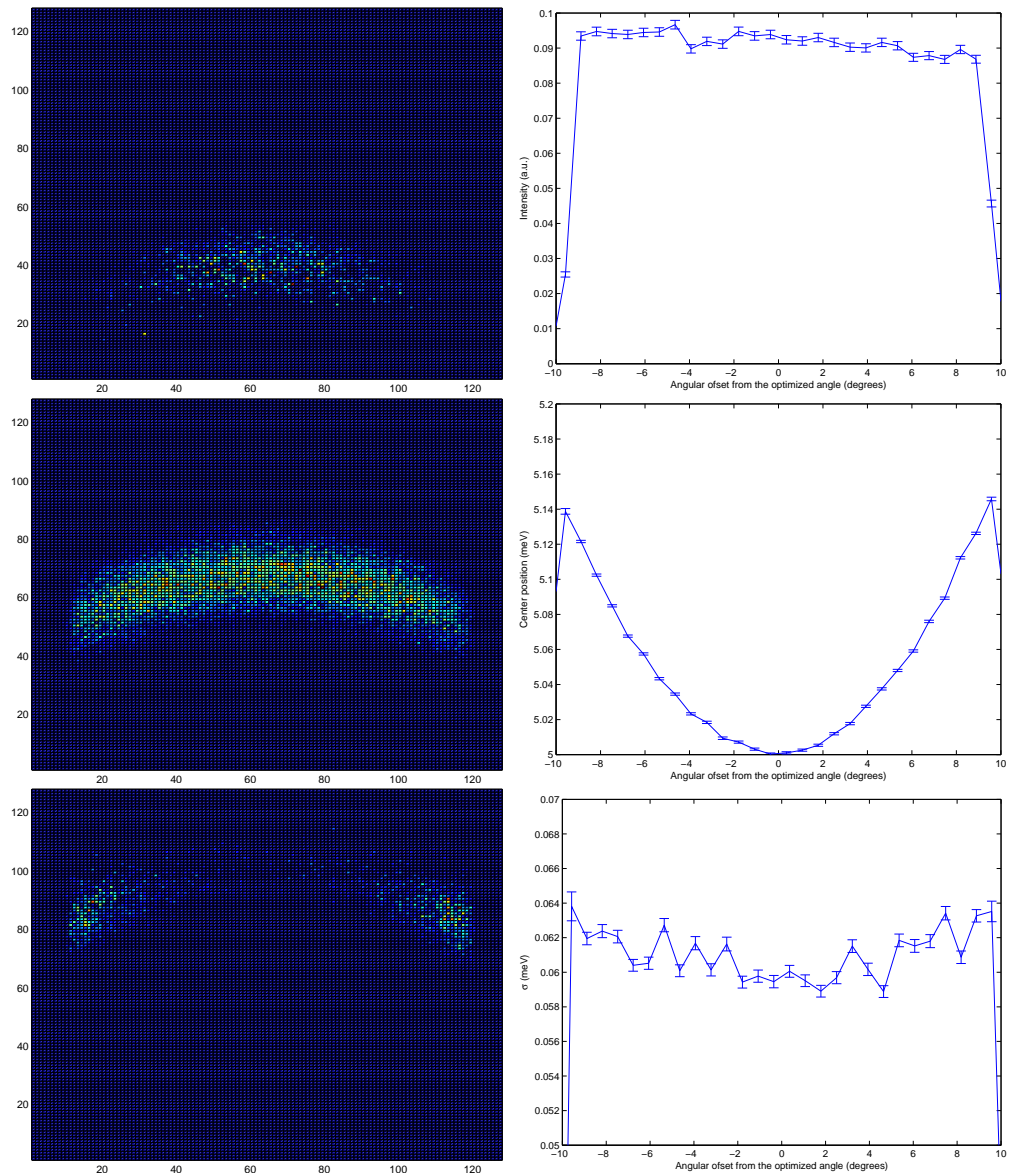


Figure 17: **Width of detector.** Left: PSD view of beam reflected from the analyser for energies below (top), at (middle), and above (bottom) the analyser energy. Right: The Intensity (top), centre point (middle), and width (bottom) as a function of angle. The small change in resolution corresponds to the change in measured energy.

5.5 Rotation of Analysers

The Asymmetric Rowland Geometry was also tested with respect to a θ , 2θ rotation of the analysers and detectors. The result shows that it is indeed possible to scan k_f without a big drop in performance but it was decided that the gain from having this option would not out weight the additional cost and technical complications of such an instrument.

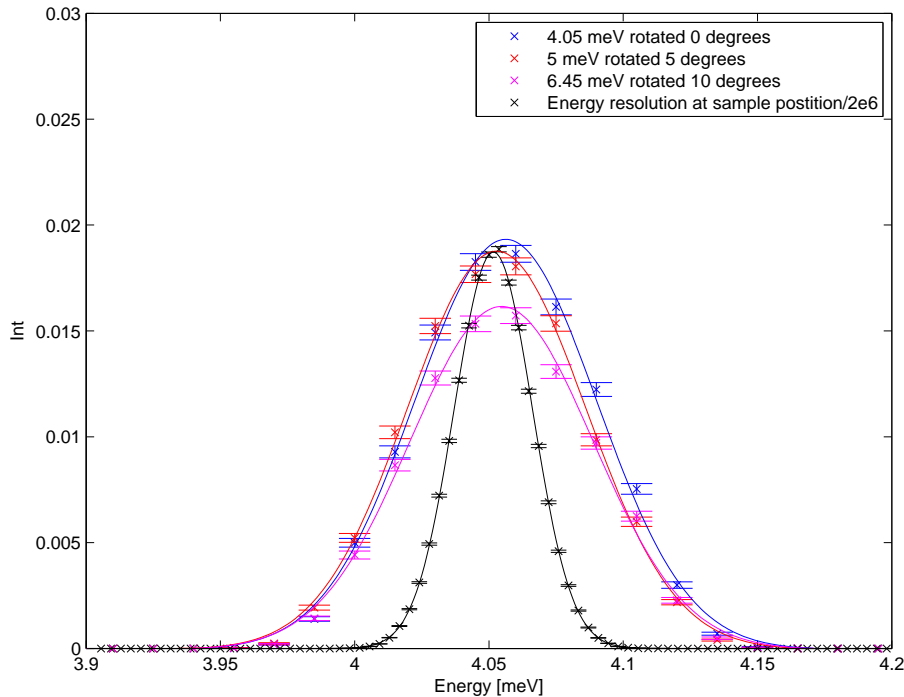


Figure 18: *Rotating Analysers.* A Rowland analyser works fine if rotated 5° . The simulations were done for the full resolution of a triple axis instrument but the (artificially low) incoming resolution (displayed in black) does not dominate the full resolution.

6 Detectors

All simulations were done assuming He^3 detector tubes, since this is what the prototype has and the technical details of the solid state detectors are still rather uncertain. At the initial simulations a psd was used and the relevant regions were cut out to simulate actual detectors. Later a special detector component was developed for McStas in order to make precise simulations of the instrument performance. This 1d psd with time resolution incorporates time delays and position uncertainty due to the unknown detection depth of the neutron and calculates realistic absorption strengths depending on whether the centre or edges of the detector was hit. The detector has been used for many of the performance studies.

It was also considered if a lower than usual gas pressure would be beneficial in suppressing the thermal background compared to the cold signal. Figure 19 shows how it is possible to dampen the thermal background a factor 2 for 5 meV neutrons using very inefficient detectors. This does however not outweigh the loss in detector efficiency and would make the option of recording second order neutrons by using the order sorting inefficient due to the low detection rate at the second order wavelength.

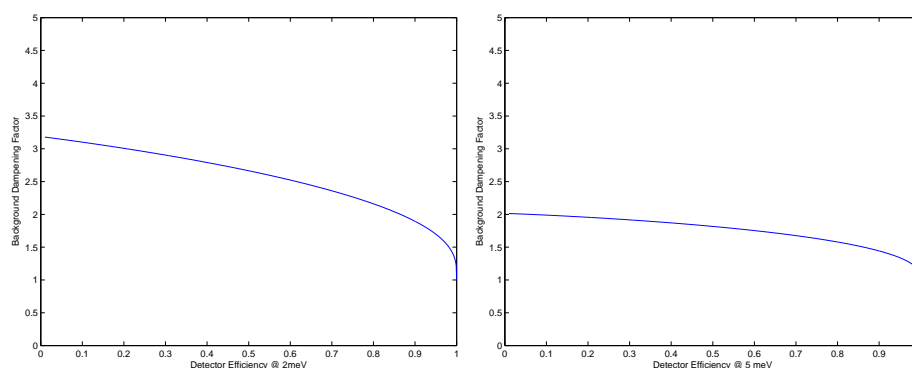


Figure 19: *He* pressure.

7 Additional issues on Analyzer-Detector interaction

7.1 Mosaicity

The influence of analyser mosaicity on the energy resolution and intensity was simulated. The result can be seen in figure 20. It can be seen that the resolution for a single tube does not depend on the mosaicity. This is because the distance collimation dominates the resolution. For the 3 tubes the distance collimation is less strong and the mosaicity do influence the total resolution.

The intensity does not take the lower peak reflectivity of the graphite into account. In order to investigate this a simple Monte Carlo routine was written to estimate the influence of analyser thickness and mosaicity on the peak reflectivity. The result are shown in figure 21 and shows a limited influence of reducing the mosaicity. The model is very rough but the main findings were later confirmed with prototype data.

Simulations of how the q resolution of the spectrometer depends on the analyser mosaicity can be seen in figure 22. Since the long analysers makes the distance collimation extremely rough in the angular direction the angular resolution does depend on the mosaicity.

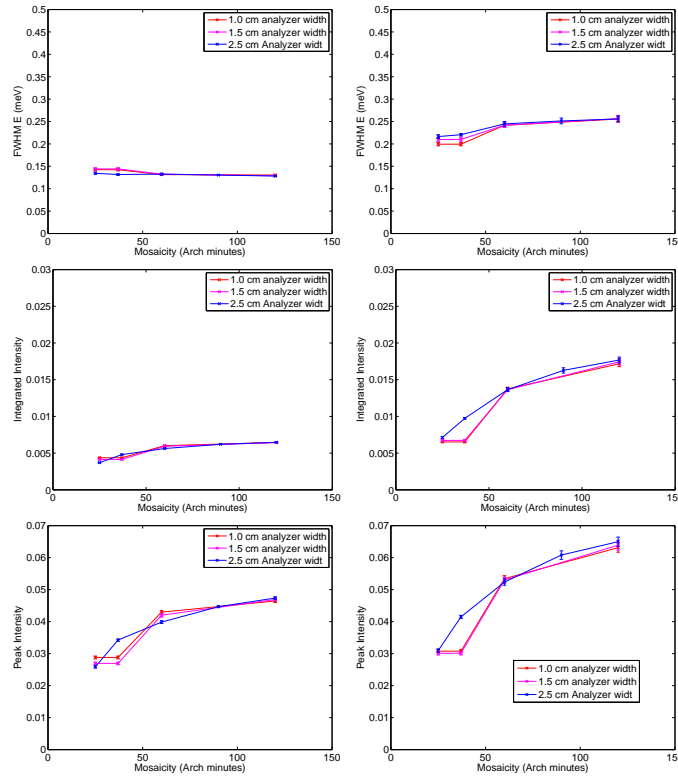


Figure 20: ***E** resolution and Intensity for different mosaicities* Top: Energy resolution (left), Integrated intensity (middle) and Peak intensity (left) for one $\frac{1}{2}$ inc detector tube, Bottom: the same simulations for integrated intensity in 3 three tubes. For one tube higher mosaicity simply gives better resolution and higher intensity. For wider detectors it is a trade-off between resolution and intensity. The work was done with $E_f = 5$ meV, 1 cm sample and 1.2 m sample to analyser and analyser to detector distances. Note that a slight decrease in peak reflectivity with higher mosaicity was not included in the model.

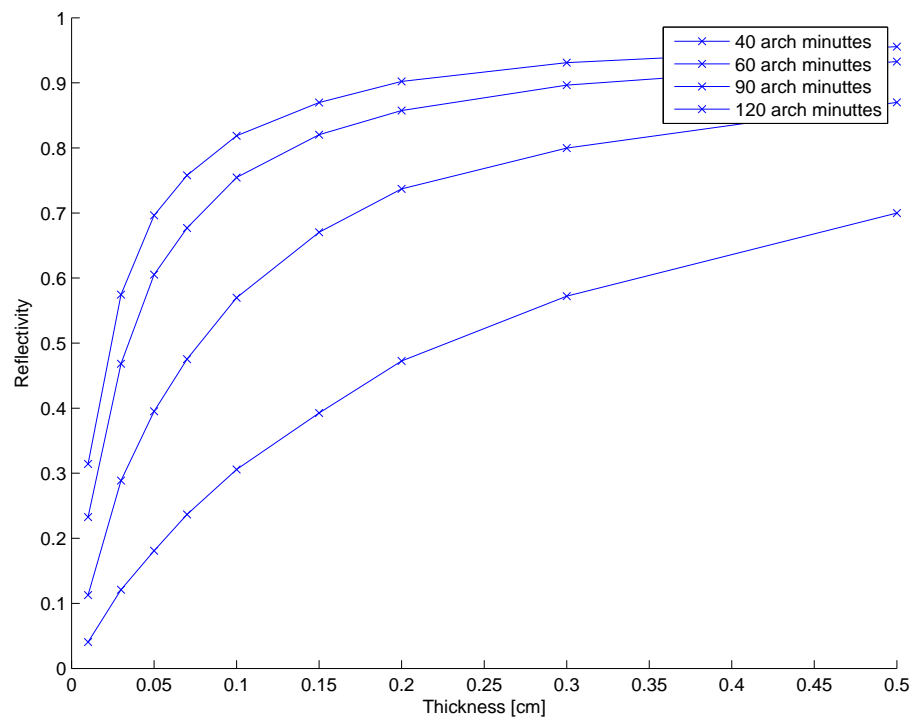


Figure 21: *Approximate reflectivity of PG as a function of mosaicity & thickness.* The reflectivities are found through a simple Monte Carlo model described in 7.1

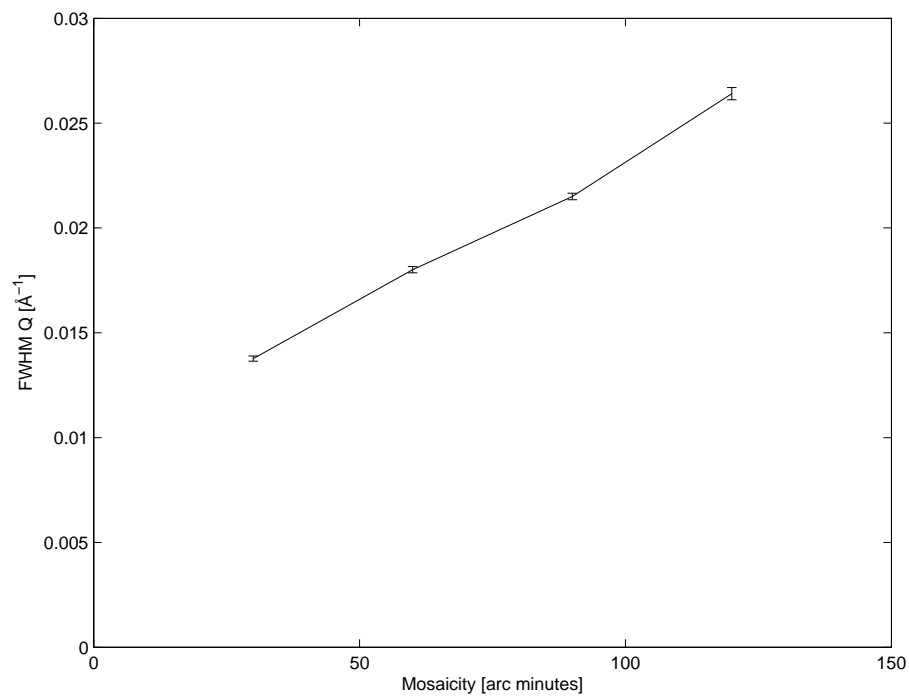


Figure 22: *Q resolution of CAMEA on a TAS* The resolution is a constant contribution from incoming divergence, sample size and detector resolution plus a varying effect from the different divergences. Same settings as in figure 20 was used except for that the energy was 3.5 meV.

7.2 Several Energies

In our coarse-mosaic analyser set up neutrons with slightly wrong energies are also scattered and will reach the detector surroundings. It is thus possible to detect these in other detectors and thereby increase the total number of counted neutrons without suffering worse energy resolution. This section looks into how well this works in a Rowland geometry and how intensity, resolution and number of detectable energies varies with different mosaicities.

7.2.1 The Principle

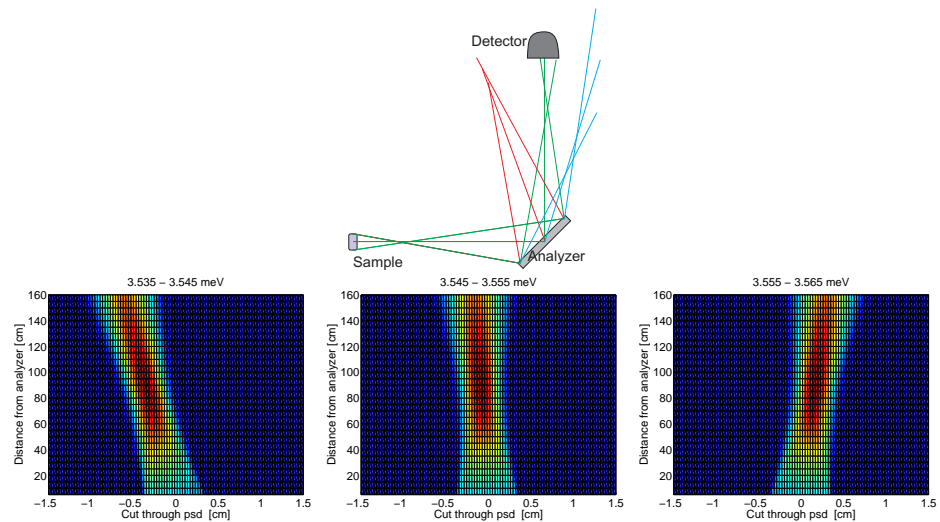


Figure 23: *Principle of energy selection.* Top: Schematics of how an analyser reflects different energies at different angles and focus them at a certain distance. Bottom: McStas simulations the beam profile from a single reflecting analyser for 3 narrow energy bands when the analyser is optimized for the central energy band. The vertical axis is the distance from the analyser and the horizontal axis is transverse to the main beam as in the top panel

The geometry of a Bragg reflection from a flat analyser slab with a finite width and mosaicity ensures that the desired energy is focused towards one spot whereas other reflected energies are reflected in other directions. (See figure 23). By the right use of distance collimation the energy resolution becomes almost mosaicity independent for relevant mosaicities while the intensities increase with mosaicity before reduced reflectivity and extra q -collimation is taken into account. Another promising use of this effect is to separate different energies reflected from each analyser and thus measure several energies from each analyser.

7.2.2 Simulations

To investigate this effect by simulations a Rowland analyser was placed on a triple axis instrument, reflecting part of the beam up at a PSD and the incoming

7.2 Several Energies

29

energy was scanned. 7 parallel $\frac{1}{2}$ inch tubes 14 mm apart (far within the possible space of CAMEA) was then cut out of the PSD (and a correction for the different sensitivity at different part of the tube applied).(Se figure 24).

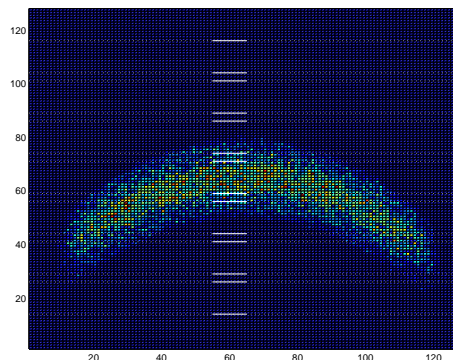


Figure 24: *Example of psd from simulations.* The dotted lines marks the boundaries of the 7 tubes and the solid part the part of the tubes used in the following analysis.

Figure 25 shows this energy scan for the centre of the tubes for different analyser mosaicities. As it can be seen the tubes sees a well defined Gaussian shaped energy, although each energy overlaps with the one at the neighbour tubes. Unsurprisingly, higher mosaicity means signal in more tubes.

7.2.3 Intensity and Resolution

Figure 26 shows the fitted peak intensity and FWHM from the different tubes and mosaicities. There is no major difference in the width at the different tubes except the expected increase with higher energy. The intensity does of course decrease width the distance from the central tube but for high mosaicities the intensity is quite high in several tubes. Of course one should include the reflectivity of the different analyser crystals in order to get an absolute comparison. So far my simple model suggest that the reflectivity of 90 minutes PG is 0.7 times that of 25 minutes PG if the analysers are 1 mm thick. As a compromise we chose 60' mosaicity and 3 detectors to both increase countrate and improve E and q resolution.

7.2.4 Background

Experience from Rita II shows that a rough collimator in front of the detector, to distinguish different windows, reduce the background a lot. This will be difficult in a set-up where several analysers focus different energies on different detectors. It should, however, not be as important here since all analysers are placed to reflect the same energy at the same q to the detectors. Anyway, in the results above, the tubes are placed 14 mm apart and not the minumum possible 13 mm since this leaves space for a short rough collimation in front of the detectors if necessary.

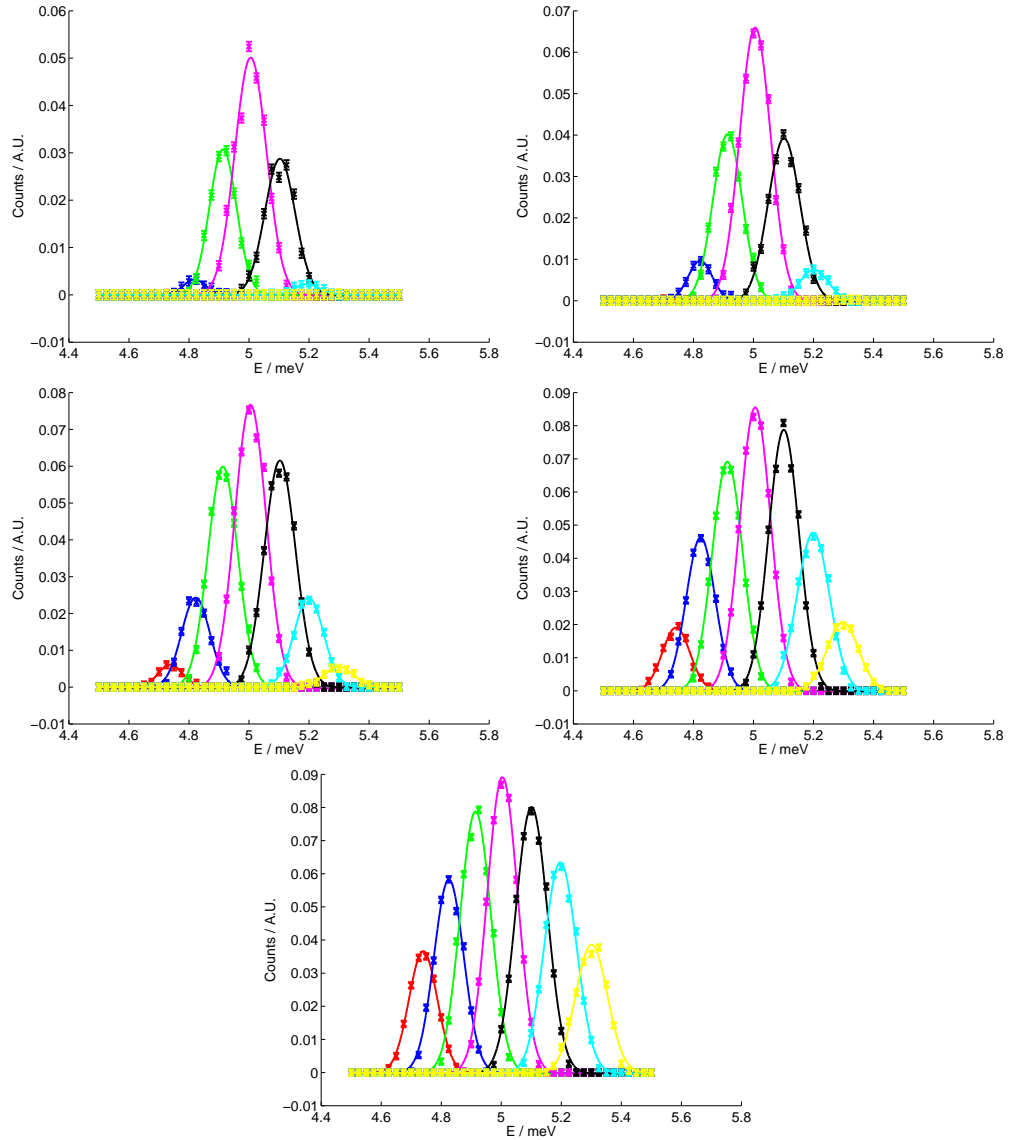


Figure 25: *Simulated Intensity on detector.* The figures shows the simulated intensity in 7 parallel tubes as the incoming energy is scanned for 25, 37, 60, 90, and 120 arch minutes of mosaicity.

7.2.5 Energy tails

The phonon tails of the strong central reflection as seen on RITA-2 will be relatively stronger compared to the lower flux of the reflections towards the outer tubes. It is thus even more important to reduce the tails in this set-up.

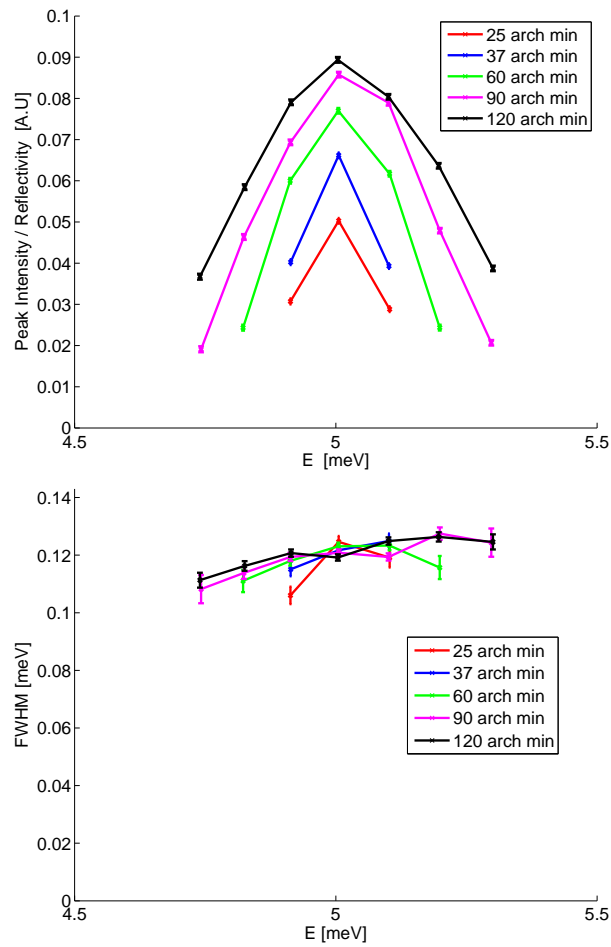


Figure 26: *Intensity and resolution of the different tubes.* The higher the mosaicity the more energies can be measured and the higher the intensity/mosaicity. The FWHM does as expected increase with energy but is almost independent of mosaicity. For both graphs, tubes with sufficiently low statistics were removed since the fitted parameters were too uncertain for any useful conclusions.

8 Time Resolved measurements

The possibility to do time-resolved neutron scattering on CAMEA was investigated and the time resolution was found to be between 20 μs and 30 μs for most analysers. The main contributions to the resolution is:

8.1 Flightpath uncertainty

The analysers are placed in an asymmetric Rowland Geometry and thus the flight length will vary depending on the neutron scattering position. The effect is bigger the more asymmetric the Rowland geometry. For most analysers an effect of about 10 μs is foreseen whereas the effect for the innermost analysers will be considerably bigger. Both due to more asymmetric setup and lower neutron speed.

For analysers with a high mosaicity and without collimation an uncertainty in the transverse length will also occur but since this is much smaller than the longitudinal travel length it can be neglected.

8.2 Energy uncertainty

The uncertainty in E_f will correspond to an uncertainty in time. If one wants to use time resolution it is therefore advantageous to use the increased energy resolution from the many detectors. If this is used flight time uncertainties become in the order of 10 to 20 μs .

8.3 Uncertainty of scattering position

Since sample has a finite size there is an uncertainty in the exact scattering position. This effect is sample size and energy dependent but in general below 2 μs and thus negligible.

8.4 Uncertainty of detection position

The exact detection position for He^3 tubes is slightly less uncertain than the diameter of the tube as most neutrons are detected in the first part of the detector. On the other hand the round shape of the tubes gives a broadening. Altogether the effect becomes: 3 μs .

8.5 Combined Result

Combining the effect and assuming they are independent leads to a total flight time uncertainty of 20-30 μs as described in table 2. Better results can only be obtained by increasing energy resolution and/or decreasing the asymmetry. The uncertainty on the first analysers is mainly due to the asymmetric Rowland Geometry while the uncertainty in at the last analysers mainly arises from energy uncertainty. Generally they are however well matched. The dependency of the energy resolution makes it crucial to use the high resolution mode in time

Analyzer #	1	2	3	4	5	6	7	8	9	10
Energies of analysers (meV)	2.5	2.8	3.1	3.5	4	4.5	5	5.5	6.5	8
Time Resolution (μ s)	37	28	23	22	22	22	21	22	21	19

Table 2

resolved studies, but this is anyway foreseen to be the standard operation mode of CAMEA anyway.

9 The Prototype

The main findings in the report were tested against prototype data as the described in the prototype report. The results show a very good agreement between simulations and experiments, strengthening the credibility of the findings. The details are described in the Prototype Report.

10 Conclusion

The use of cheaper coarse mosaic graphite, the possibility to obtain several energies from a single analyser, and the possibility to cover dark angles with sample rotations are direct consequences of simulation results. Together this has led to a cheaper instrument with much better E-resolution and higher coverage but slightly worse q -resolution than originally planned.

Throughout the design process of CAMEA extensive simulations and calculations were performed. The simulations confirms that the instrument will deliver a very high performance, making it possible to investigate a substantial part of the huge parameter space available to the instrument and was key in the design process revealing new possibilities.

[1] ILL Neutron Data Booklet, ed. A.-J. Dianoux and G. Lander, 2003



Technical University of Denmark



McStas



CAMEA

Analytical calculations for CAMEA

Author:

M. Markó



Contents

1	Introduction	3
1.1	Goal of calculating the analytical model of the instrument	3
1.2	Basic method	3
1.3	Parameters out of optimization	3
2	Primary resolution	3
2.1	Resolution of the pulse shaping chopper	4
2.2	Pulse shaping chopper and instrument length	4
2.3	Calculation of the divergence of front end	6
3	Resolution of the secondary instrument	6
3.1	Energy resolution of the analysers	6
3.2	Tangential k_f resolution of the secondary instrument	7
3.3	Time resolution of the secondary instrument	8
4	Resolution ellipsoid	8
5	Conclusions	10

1 Introduction

1.1 Goal of calculating the analytical model of the instrument

CAMEA is a totally new instrument concept, thus its performance is not explored. Furthermore it is a complex instrument using many different analyser arrays in a wide angular range. For studying the performance of the instrument we use three approaches: McStas simulations, analytical calculations, and prototyping. Due to the complexity of the instrument all of the previously mentioned methods can have faults misleading us during the instrument development. We use Monte Carlo and analytical modeling to calculate and optimize the instrument, while the measurements on the prototype validate the model calculations, give informations about the background and reveals the problems arising in the treatment of data obtained in real inelastic measurements. The main goal of the analytical calculation is to reveal the effects of the different instrument parameters on the resolution and on the intensity of the instrument. For this, I calculate and analyze the basic resolutions, then I calculate the resolution ellipsoid.

1.2 Basic method

The resolution is locally a convolution. Since the total convolution function of CAMEA has many different contributions, the final resolution function will be close to a Gaussian. I use Gaussian functions to describe each of the partial resolution functions. These Gaussian functions have the same variance (second moment) as the functions describing properly parts of the instrument. i.e. a cylindrical sample can be described as a box function with H width vertically, and a sphere with d diameter horizontally in the calculation I use the Gaussians with the variances of $H^2/12$ and $d^2/16$ respectively. Since during the convolution of two functions the variances are additive, this simplification causes just a small error. The difference between the calculated and the real resolution function has two main contributions: there are parts of the instrument I can not calculate analytically (i.e. the divergence of the incident beam at the sample position), and that the final resolution function is not exactly Gaussian.

I investigate the effects of the following parts of the instrument:

- Pulse duration, and the effect of the pulse shaping chopper
- Lengths: source-sample, sample-analyser and analyser-detector distances
- Divergence at the sample position (as a parameter of the instrument)
- Sample size (height and width)
- Size of the analyser elements
- Resolutions (radial and tangential) of the detector system

1.3 Parameters out of optimization

There are some parameters of the instrument we cannot choose, or optimize. The pulse duration of the ESS is 2.86ms, the frequency of the source is 14Hz. The pulse shaping chopper is minimum 6.5m away from the moderator, and the first analyser array cannot be closer to the sample than 100 cm. Due to the flexibility of the instrument the pulse shaping chopper should be close to the source, and due to the cost of the pyrolytic graphite analysers, the analysers should be as close to the sample as it is possible, thus I use the above mentioned values as fix parameters.

The analyser arrays select final energies between 2.5 meV and 8 meV (5.7 Å and 3.2 Å), and we want to see also the higher orders up to 32 meV (1.6Å).

2 Primary resolution

The duration of the pulse is τ . The length of the primary instrument is L . The wavelength of the neutrons starting at $t=0s$ and arriving to the sample at t is: $\lambda = (h/m_n)\tau/L = 3.956\tau/l$ where λ is the wavelength in Å,

t is in ms, L is in meter. Thus assuming constant τ (independent on the wavelength), the wavelength resolution of the front end is constant (the time resolution is constant). Thus the relative wavelength resolution is inversely proportional to the wavelength. Since there is just a second order difference between the relative wavelength and relative k resolution, the absolute k resolution is proportional to the square of k. The relative energy resolution is two times larger than the relative k resolution thus the absolute energy resolution is proportional to $E^{1.5} \sim 1/\lambda^3$.

2.1 Resolution of the pulse shaping chopper

The transmission of a chopper at a given time is the non-covered area of the guide opening divided by the total area of the guide. In general the transmission function of a chopper after a given guide can be described by a zeroth order spline (only the values of the polynoms are equal at the meeting points) containing maximum second order polynoms. From the time dependent transmission one can calculate the variance of the transmission distribution. I use a Gaussian function with similar variance can in the further calculations. There is a more simple way to calculate the time resolution: Neglecting the height of the guide, we can calculate an effective angle (ϕ_e) for the guide which is equal to the rotation angle of the chopper needed for full opening or closing: $\phi_e = 2 * \arctan(w/(2h))$ where d is the width of the guide, and R is the distance between the middle of the guide opening and the rotation axis of the chopper. The transmission of the chopper is a convolution of two box function with the width of ϕ_e and ϕ (the opening angle of the slit). Using the corresponding Gaussian approximation, the FWHM of the transmission function in time is:

$$FWHM_{ch} = \frac{1}{f} \sqrt{\frac{\phi^2 + \phi_e^2}{2\pi} \frac{8 \ln 2}{12}} \quad (1)$$

Where f is the frequency of the chopper in Hz, and $\sqrt{\frac{8 \ln 2}{12}}$ is the change factor between a box function with unit width and the FWHM of the Gaussian having the same variance as the box function. The time resolution of the instrument is a bit larger since the pulse duration (seen by the sample) is the projected transmission in the flight time - flight path diagram (TOF diagram) from the sample to the source: the correction factor is: $L_p/(L_p - l_{ch})$ where L_p is the primary instrument length, and l_{ch} is the source - chopper distance. In other words we see a virtual source at the position of the pulse shaping chopper at 6.5 m. The total transmitted intensity is proportional to the minimum of ϕ and ϕ_e and inversely proportional to the frequency of the chopper (in the case of pulsed source). This calculation describes well the resolution and the transmission of the choppers as long as the neutron intensity is constant in time and in wavelength. Later I show that near the end of the wavelength band the finite pulse duration causes a decreasing of the intensity and also the resolution width.

2.2 Pulse shaping chopper and instrument length

The pulse shaping chopper can be used to decrease τ thus to improve the resolution. In the TOF diagram looking back from the sample position to the source the pulse shaping chopper will make a "shadow" covering parts of the source. In other words we see an effective source. The position of the pulse shaping chopper is 6.5m. This means, that the effective source will move as we change the wavelength (time at the sample). At two different times (difference is Δt) at the sample position the middle of the effective source will move by $-6.5/(L - 6.5)\Delta t$. This means that if L is smaller than 169m, the effective source will move more than the pulse duration, thus applying strict pulse shaping, there will be no incident neutrons at the ends of the wavelength band since the effective source is outside of the real pulse (in time). So (without wavelength-multiplication method), the minimum length of the front end (the 'natural length') is 169m [4, 5]. In reality the duration of the neutron pulse is larger than the duration of the proton pulse (due to the asymmetric response function of the moderator) causing a bit smaller natural length. The maximal primary instrument length at ESS is 165m, thus we choose this value for our instrument. In this case the wavelength band is roughly 1.7Å, the absolute wavelength resolution (without using PSC) is roughly 0.048 Å and the energy resolution at 4 Å (5 meV) is 0.12 meV.

In reality the real resolution is a bit more difficult: The time resolution is constant only if there is no pulse shaping chopper applied, or if we use very narrow (almost totally closed) pulse shaping chopper. In other case the time resolution will be better at the ends of the wavelength band where one end of the pulse will be defined

by the real pulse duration not by the chopper (i.e. the shadow of the chopper is out of the pulse). This has to be taken into account in the calculations. The effect of a moderate pulse shaping is seen on the figure 2. The given parameters with infinitely long pulse duration would give constant 1.343 ms time resolution.

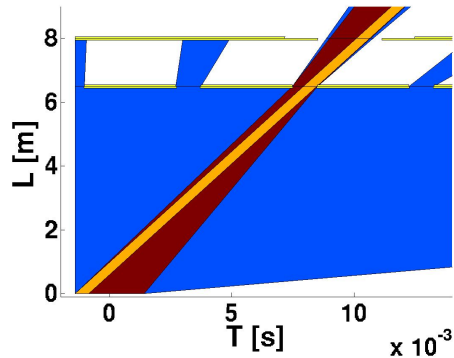


Figure 1: Effect of pulse shaping chopper at the end of the wavelength band: TOF diagram till the first two choppers of ESS CAMEA. The blue area shows the possible trajectories of the neutrons, the yellow lines show the choppers (double line is the fully closed, single line is the partially closed), the brown area shows the neutrons reaching the sample, and the orange area shows the neutrons arriving to the sample in one time at the end of the wavelength band. The time resolution in this case is much smaller than the opening of the pulse shaping chopper.

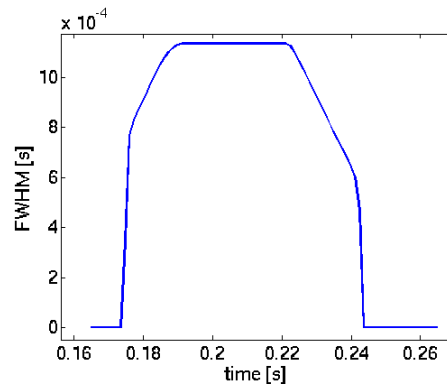


Figure 2: Effective FWHM of time-resolution for ESS-CAMEA: mean wavelength is 5\AA PSC frequency is 210Hz, position is 6.5 m, opening angle is 150° . The time resolution with infinitely long pulse would be 1.343 ms, the total chopper opening is 1.85 ms

By increasing the instrument length the resolution without PSC will be better and the energy band will be smaller. A two times longer instrument needs two separate measurement to cover the same (q or energy) range, but due to the longer length the PSC opening can be two times larger, so the intensity at the same resolution is larger (two times larger if the pulse duration is large enough). It has other advantages like smaller background and larger flexibility to use the PSC. However, the maximum total intensity (without using PSC) will be two times smaller due to the smaller wavelength band. As a consequence, the instrument length should be defined by the worst resolution (highest intensity) is still useful for measurements. In our case the worst resolution (0.17 meV at 165m without PSC) is useful, so the optimal length remains 170m. The same calculation is true for a two-times shorter instrument with frame multiplication. In this case the reachable highest intensity corresponds to a very bad resolution the flexibility of the instrument is worse, and the design is more difficult. **Finally the maximal length (165 m) is also the optimal length for CAMEA.**

2.3 Calculation of the divergence of front end

There are two possibilities: Assuming constant intensity distribution one can calculate the minimum of the maximal divergence allowed by the guide opening or the last slit, and the maximum divergence transmitted by the guide system. The other possibility to use the results of McStas simulation. Note that the divergence is wavelength dependent. According to the experiences the first method frequently gives false data (if the collimation after the guide is not too strict), thus we checked the primary divergence by using MonteCarlo simulations.

3 Resolution of the secondary instrument

3.1 Energy resolution of the analysers

Assuming negligible variation of the lattice spacing, the derivation of the Bragg-law ($\lambda = 2d \sin(\theta)$) gives the relative resolution of one analyser crystal: $\frac{\Delta\lambda}{\lambda} = \Delta\Theta_a \cot \Theta_a$, where Θ_a is the scattering angle of the analyser and $\Delta\Theta_a$ is the angular resolution. Furthermore I calculate for focusing crystals in Rowland geometry. In Rowland geometry each crystal blade scatters the neutrons with the same energy, if the neutrons are coming from a point source (sample) and it focuses them to an other point (detector). Looking one crystal, the deviation from the scattering angle for a given path is half of the difference of the angular deviations before and after the analyser comparing to the nominal path (the path going through the center of sample, analyser and detector). Thus the change of the scattering angle is:

$$(\Theta_a - \Theta_{a0}) = \frac{1}{2} \left(\frac{x_s}{l_{sa}} + \frac{x_a(l_{sa} - l_{ad})}{l_{sa}l_{ad}} + \frac{x_d}{l_{ad}} \right) \quad (2)$$

where x_s , x_d are the positions perpendicular to the beam at the sample and detector respectively x_a is the position of on the analyser corrected with $\sin \theta_a$, l_{sa} and l_{ad} are the sample analyser and the analyser detector distances. For the same path (assuming elastic scattering) the angular deviation from the nominal q-direction is the half of the sum of divergences before and after the analyser:

$$\phi - \phi_0 = \frac{1}{2} \left(\frac{x_s}{l_{sa}} - \frac{x_a(l_{sa} + l_{ad})}{l_{sa}l_{ad}} - \frac{x_d}{l_{ad}} \right) \quad (3)$$

The analyser reflectivity, detector efficiency (as the function of the distance from the nominal beam) and mosaicity have the variances of s^2, a^2, d^2, m respectively. We can write the intensity of all of the paths corresponding to a given $(\Theta_a - \Theta_{a0})$ as a double integral (there are three parameters, but one is fixed by the equation 2. After calculating the integral we got also Gaussian intensity distribution in the function of $(\Theta - \Theta_0)$. The variance of the scattering angle distribution becomes:

$$\sigma_{\Theta_a}^2 = \frac{m^2 (s^2 l_{ad}^2 + d^2 l_{sa}^2 + a^2 (l_{sa} + l_{ad})^2) + a^2 d^2 + s^2 d^2 + s^2 a^2}{4m^2 l_{sa}^2 l_{ad}^2 + s^2 l_{ad}^2 + d^2 l_{sa}^2 + a^2 (l_{sa} + l_{ad})^2} \quad (4)$$

If we take a large mosaicity value, then we get back the Rowland resolution:

$$\sigma_{\Theta_a}^2 = \frac{s^2}{4l_{sa}^2} + \frac{a^2 (l_{sa} + l_{ad})^2}{4l_{sa}^2 l_{ad}^2} + \frac{d^2}{4l_{ad}^2} \quad (5)$$

Large mosaicity value means, that $\phi - \phi_0$ in the equation 3 is always smaller than the mosaicity (the distances are large enough, and the sample and detectors are small enough). In this case we are speaking about geometry limited resolution. At CAMEA the secondary resolution is geometry limited due to the large distances. The high resolution due to the large distances and good detector resolution does not affect the detected intensity: applying many detectors next to each others we cover the whole angular range of the neutrons scattered by the analyser, thus we analyse many different energies simultaneously [1]

Using the eq.5 the energy and radial k_f resolution due to the geometry is:

$$\sigma_{E_f}^2 = E_f^2 \cot^2(\Theta_a) \left(\frac{s^2}{l_{sa}^2} + \frac{a^2 (l_{sa} - l_{ad})^2}{l_{sa}^2 l_{ad}^2} + \frac{d^2}{l_{ad}^2} \right) \quad (6)$$

$$\sigma_{k_{fr}}^2 = k_f^2 \frac{\cot^2(\Theta_a)}{4} \left(\frac{s^2}{l_{sa}^2} + \frac{a^2 (l_{sa} - l_{ad})^2}{l_{sa}^2 l_{ad}^2} + \frac{d^2}{l_{ad}^2} \right) \quad (7)$$

So in the case of asymmetric Rowland geometry, the size of the crystals has a small effect on the energy resolution, while in symmetric case this is just a second order effect. As the equations show in optimal case $s/l_{sa} > 2d/l_{ad}$ meaning that the secondary resolution is defined mainly by the sample size thus the detected intensity is near proportional to the secondary resolution. As an example in symmetrical Rowland geometry the detector width (or resolution in the case of position sensitive detector) should be smaller than the sample. In the case of CAMEA at ESS this is possible but extremely expensive. The generally used tubes with the diameter of 1/2" will mostly define the resolution if the sample is smaller than 1 cm.

There is another second order effect on the resolution which is not taken into account. The analysers are straight. This means that the angle between the beam coming from the sample and the scattering plane depends on the position where the neutron reaches the crystal (the crystal is in tangential direction but it is not curved). That means that the scattering angle changes slightly but the effect of it is much smaller than the resolution of the analyser. Also the sample - analyser and the analyser - detector distances are changing, but the differences in the resolution are smaller than the accuracy of the analytical calculation.

It is important to note, that we use distance collimation meaning that the mosaicity of the analyser crystals does not effect the resolution. To detect every neutrons scattered by the analyser, we use more detectors next to each other looking the analyser from a slightly different angle. With this solution we can analyse many different energies using one analyser [1]. This also means, that the detected intensity depends only on the angular coverage of the analysers, and on the integrated reflectivity but not depends on the resolution of the secondary instrument.

3.2 Tangential k_f resolution of the secondary instrument

This part of the resolution is produced by the width of the sample, the resolution of the detector (in tangential direction), the take-of angle of the detector, and the mosaicity.

The analyser banks contain flat analyser crystals. This means that after Bragg-reflection the horizontal divergence remains the same. The scattering angle (a_4) can be calculated (in first order) using the total secondary flight path and the position of a count in the detector. Let us sign a_{4_0} the scattering angle in which direction the plane of the secondary flight path is vertical. In this case l_0 is the secondary flight path, and $x_0 = 0$ is the position on the detector. Then the scattering angle of the neutron arrived to the detector at x position is: $a_4 = a_{4_0} + \arctan((x)/l_0)$. If the analyser width is not too large then we can simplify this function: $a_4 = a_{4_0} + x/l_0$. In the case of resolution calculation the differences between the positions are small, so we use this last function.

The variance of the sample (S^2) and the resolution of the detector (D^2) has the same effect on the resolution, so resolution due to the geometry is:

$$(\sigma_{a_4,g})^2 = \left(\frac{D}{L_s}\right)^2 + \left(\frac{S}{L_s}\right)^2 \quad (8)$$

Where $L_s = l_{sa} + l_{ad}$ is the total secondary flight path. The mosaicity has different effect: The mosaicity in the direction lying in the scattering plane of analyser has no effect on the tangential k_f -resolution. On the other direction (perpendicular to the scattering plane) it changes the direction of the scattered beam in the plane defined by the analyser and the detector. If an ideally collimated beam reaches the analyser then the reflected beam will be divergent: m mosaicity cause $\sigma_\phi = m2 \sin \Theta_a$. This divergence causes a spot on the detector with the width of $\Delta x = \Delta\phi l_{ad}$ where l_{ad} is the analyser-detector distance. The tangential k_f resolution caused by the analyser is:

$$\sigma_{k_f,ta} = \frac{k\Delta x}{L_s} = q_a m \frac{l_{ad}}{L_s} \quad (9)$$

where q_a is the length of reciprocal lattice vector of the analyser. The total tangential k_f resolution is:

$$\sigma_{k_f}^2 = \left(\frac{q_a m l_{ad}}{L_s}\right)^2 + k_f^2 \left(\frac{D}{L_s}\right)^2 + k_f^2 \left(\frac{S}{L_s}\right)^2 \quad (10)$$

Equation 10 shows a unique property of the ESS CAMEA: the first part is independent of k_f , and implicitly the second and third parts are independent: k_f/L_s is inversely proportional to the secondary flight time what should be the same for each analyser due to the effective working of the order sorting choppers. As a result, the

tangential resolution of k_f is independent on the analysed energy, it is defined only by the ratio of the analyser-detector distance and the total secondary flight path. Moreover, if the primary divergence is proportional to the wavelength (since the critical angle of the mirror is proportional to it) then the final two dimensional q-resolution ellipsoid of the instrument caused by the angular resolution depends only on the scattering angle.

3.3 Time resolution of the secondary instrument

The time resolution consists two parts: the secondary flight path distribution, and the secondary energy resolution.

The secondary length distribution gives a part of the secondary TOF distribution. The sample size has two effects: the size in the direction of the primary beam causes a time distribution depending on the initial speed (energy), and the size in the scattered direction causes a time distribution depending on the analysed speed. The detection position distribution in the detector depends on the total cross section of the detector material, the detector width, shape and also on the speed of the analysed neutrons. These effects are smaller than 1 cm causing a maximum of some tens of μs time distribution calculating with the smallest incident and final speed. The last effect is the path distribution caused by the Rowland geometry. In figure 3 the radius of the Rowland circle divide the SAD angle to ϕ_1 and ϕ_2 . Then the difference between the longest and shortest paths in first order is $d(\sin \phi_1 - \sin \phi_2)$ where d is the total width of the analyser. It is in extreme case $2d$. Since we do not plan to use extremely asymmetric Rowland geometry, the flight path differences will be around some centimeters.

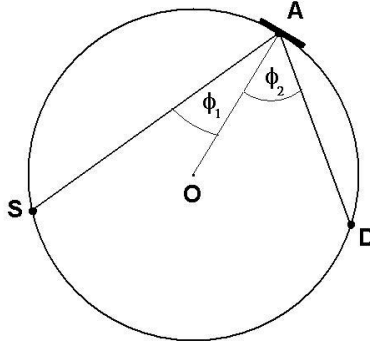


Figure 3: Rowland geometry: S: sample, A: analyser, D: detector, O: center of the rowland circle

The total time resolution (Δt_s) is calculated as:

$$\Delta t_s^2 = t_s^2 \left(\left(\frac{\Delta l_s}{l_s} \right)^2 + \left(\frac{\Delta E_f}{4E_f} \right)^2 \right) \quad (11)$$

where l_s and t_s are the secondary flight path, and flight time respectively.

4 Resolution ellipsoid

The calculation of the total resolution is based on the works of Cooper and Nathan [6], and Popovici [7]. The modifications I made are similar to the calculations of Ionita [9] and Violini[8]. The starting variables are the starting time, and the horizontal and vertical position at the end of guide, sample, analyser crystal and detector. An extra variable is the number of the crystals in one focusing analyser. I calculated the transformation from these variables to the $q-\omega$ space, and made the integration. I used the matrix formalism proposed by Popovici with a small change: Instead of using the transformations from step to step (from positions to divergences, from divergences the the six dimensional space of k_i and k_f , and to the $q-\omega$ space, I calculate the resolution matrix and then the covariance matrix (inverse of the resolution matrix) in the space spanned by the starting

parameters, and then I applied the coordinate transformation on the covariance matrix, getting the covariance matrix in the q - ω space. The final resolution matrix is the inverse of the covariance matrix.

The steps of calculation are:

- I describe the trajectory of the neutron by a 10 dimensional, vector (\mathbf{x} : starting time, position at the end of the guide, position of scattering on the sample, position of scattering on the analyser crystal, number of the analyser crystal, and the horizontal and vertical position of detection. (the number of analysers is also used as a continuous variable, it causes not significant error also in the original Popovici method).
- The first part of the resolution matrix is a diagonal matrix (R_0) containing the inverse of the variances of the starting parameters in the main axis.
- I calculate the divergence matrix D containing the divergence vectors (column vector): \mathbf{d}_i . \mathbf{d}_i gives the angular deviation ($\Delta\phi_i = \mathbf{x}^T \mathbf{d}_i$) of the trajectories between two neutron optical elements. Before and after the analyser I calculate two kind of divergence: caused by one single analyser crystal, and the other is due to the focusing geometry. $\mathbf{x}^T D$ is a row vector containing all of the angular deviations. \mathbf{d}_0 is not a divergence it contains only the time (i.e. this vector is a unit vector, the first element is 1, and the others are zeros).
- The deviation of the scattering vectors on the analyser can be calculated as a linear combination of the divergences: M_i and M_o column vectors describe these linear transformations to get the angular deviation of the scattering vectors from the nominal one in the scattering plane and perpendicular to them. So, for a given trajectory these deviations are: $\mathbf{x}^T D M_i$ and $\mathbf{x}^T D M_o$.
- The intensity distribution due to the divergencies and due to the mosaicities gives the second part of the resolution matrix: $R_d = \sum_j \mathbf{d}_j \mathbf{d}_j^T / \sigma_{dj}^2 + D M_i M_i^T D^T / \sigma_{mi}^2 + D M_o M_o^T D^T / \sigma_{mo}^2$ where σ_j^2 is the variance of the j -th divergence (where there is no extra restriction on the divergence (e.g. collimator), there σ_j is infinite, thus it does not count in the resolution matrix), σ_{mi}^2 and σ_{mo}^2 are the the mosaicities of the analyser in the scattering plane and perpendicular to it (variance, not FWHM).
- The total resolution matrix in the starting parameter space is: $R_p = R_0 + R_d$. The correlation matrix of the starting parameters is $C_p = R_p^{-1}$.
- The deviation of q -and E is also a linear combination of the divergences (and in our case also the starting time), I use the Q -matrix to describe this transformation, so for a trajectory given by \mathbf{x} gives the $[\mathbf{q}; E]$ vector: $[\mathbf{q}; E] = \mathbf{x}^T D Q$. So, the transformation from the positions to the q - E space is described by the $F = D Q$.
- The resulting resolution matrix and correlation matrix in the q - E space are: $C = F^T C_p F$ and $R = C^{-1}$

The total q and E resolutions are the square root of the diagonal elements of the covariance matrix. The ‘‘Bragg resolutions’’ are the square root of the inverse of the diagonal elements of the resolution matrix. Bragg resolution shows the width of a curve we can get using a q or E scan over a Dirac-like scattering function (e.g. Bragg peak). The elastic resolution R_e is the 3X3 submatrix of R (not containing the 4th row and column), and the elastic covariance matrix C_e is the inverse of R_e .

This modified Popovici method calculated for TAS is mathematically equivalent with the original method, however it has some advantages:

- It is a bit more general, gives an easier procedure to calculate the resolutions for every kind of instrument
- The method gives the covariance matrix of the starting parameters. One can check whether a given optical element is too large or too small: if the given diagonal element of C_p is much smaller than the variance of the given parameter, then the corresponding optical element is larger than it should be. i.e. if the width of the guide end is 3cm, the variance of this parameter is 2, if the corresponding diagonal element of the covariance matrix is smaller than 4, then the guide is too large or the divergence transported by the guide is too small. In this case all of the neutrons exiting near the wall of the guide are useless, and they just increase the background. A smaller slit at the guide end does not effect the detected intensity nor the resolution, but decreases the background. Note that this effect can also be due to the intrinsic inaccuracy of the method (see below).

- Other kind of resolutions can be easily calculated like the time resolution of the secondary instrument for pulsed probe experiments. In this case the time resolution is also a linear combination of the starting parameters, the secondary flight time difference is $dt = \mathbf{x}^T \mathbf{t}$, thus the variance of the secondary flight time is: $\sigma_t^2 = \mathbf{t}^T C_p \mathbf{t}$.

Since this method differs from the original Popovici method only in the formalism, it has the same limitations. The most important ones are:

- The result is as correct as the input parameters are correct. The spatial and divergence distribution at the end of the guide (and the wavelength dependences of them) should be carefully investigated by McStas simulations.
- If there is one dominating part of the resolution (e.g. long pulse length), then the shape of the resolution function will be defined by the given partial resolution function, and it can be far from the Gaussian function.
- At some instruments (like backscattering spectrometer) the precise knowledge of the resolution function is needed in four order of dynamic range. In this case this method is good to predict the resolution during the instrument design, but the result cannot use as a convolution function at the actual data treatment.
- In some cases the Gaussian assumption gives better resolution than in the reality. e.g. at TAS if the guide end is close to the monochromator having the same size as the guide (and the divergence is small), the calculation shows a reduced useful area of the monochromator (like the monochromator of RITA II at PSI). In this case the artificially increased monochromator size in the calculation can result more realistic result. The small covariance matrix element (much smaller than the variance of the corresponding input parameter) can be due to the calculation method, or it can be due to real physical (or geometrical) cause. If the slight increasing of the input parameter does not effect the covariance matrix, then the given resolution is realistic. In other case the slight increasing of the input parameter causes half times large relative increasing of the corresponding diagonal element of the covariance matrix.

The projections of calculated and measured resolution ellipsoids for the prototype of CAMEA (built by DTU and installed in Mars instrument at PSI) can be found in [2] as an example three projection of the ellipsoid is shown in Figure 4. The basic resolutions are shown in the instrument proposal.

The projections of calculated resolution ellipsoids for the prototype of CAMEA (built by DTU and installed in Mars instrument at PSI) are seen in figure 4.

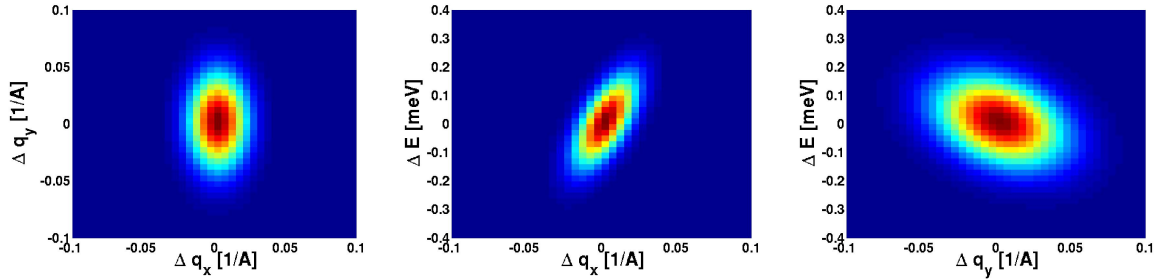


Figure 4: Projections of the resolution ellipsoid of one analyser-detector bank of the Prototype of CAMEA (elastic scattering, $E_i = 7$ meV $a_4 = 60^\circ$)

5 Conclusions

The calculation method for the total resolution of CAMEA is presented. The calculations are validated by measurement on the prototype of CAMEA [2], and are in good agreement with McStas simulations [3]. We wrote a CAMEA object (in Matlab) containing all of the resolution calculations to help the final optimization of CAMEA. The secondary resolution can be calculated analytically, the primary divergence needs McStas

simulation, and the primary energy resolution needs numerical calculations due to the changing τ_{eff} . Altogether, with a given primary divergence the calculations are fast, and precise enough for the total optimization.

References

- [1] J.O. Birk et al, in preparation for Nucl. Instr. Meth. A (2013)
- [2] M. Marko, J. O. Birk Building and testing Prototype for CAMEA
- [3] H. Ronnow et al. ESS Instrument Construction Proposal CAMEA
- [4] K. Lefmann et al. Rev. Sci. Instr. 84, 055106 (2013)
- [5] H. Schober et al., Nucl. Instr. Meth. A 589, 34 (2008)
- [6] M.J. Cooper and R. Nathans, Acta Cryst. A29, 160-169.
- [7] M. Popovici, Acta Cryst. A31, 507 (1975)
- [8] N. Violini et al., Nucl. Instr. Meth. A. 736, 3139 (2014)
- [9] I. Ionita Nucl. Instr. Meth. A. 513, 511523 (2013)



Technical University of Denmark



150
McStas



CAMEA

Guide Report

Author:

J. O. Birk



PAUL SCHERRER INSTITUT



1 Guide for CAMEA proposal

The CAMEA guide was made by extensive use of the optimizer `guide_bot`. The `guide_bot` tool generates the McStas instrument and iFit files necessary for guide optimization, making it easy to investigate a large number of possibilities. The baseline requirements for the CAMEA guide is a $15 \times 15 \text{ mm}^2$ sample 0.6 m from the end of the guide, with a divergence requirement of $\pm 0.75^\circ$ in the horizontal direction and $\pm 1.0^\circ$ in the vertical direction. The distance between moderator and sample is 165 m. The guide does provide flux in a larger area than the requirement and at larger divergences, but the phasespace illumination is only uniform within the requirement. The guide is intended to be used for the wavelength range 1.65 Å to 6.4 Å, but was optimized for a wavelength range of 1.0 Å to 3.6 Å, because experience with the optimizer shows that the results are better when optimizing for a slightly lower wavelength range than needed.

1.1 Guide description

The guide geometry can be seen on figure 3 for the horizontal and vertical plane respectively. The overall guide geometry is a parabolic feeder which starts 2.16 m from the moderator followed by a 10 cm gap at 6.5 m to accommodate a pulse shaping chopper. The width at 6.6 m has been fixed to 30 mm. Widths of 25 mm and 35 mm were also investigated, but the smaller pinhole reduced performance by almost 15% and the larger did not show any improvement. The height at 6.6 m was not restricted, the optimal solution had a height of 8.8 cm. In the horizontal direction the feeder works as a funnel, but in the vertical direction it seems to be an extension of the ellipse which follows the gap. The rest of the guide is a double ellipse with a kink to escape line of sight. The kink is designed to loose line of sight 25 m before the end of the guide. On either side of the kink there is a straight section, the total length of this is 13.9 m. They effectively makes the guide narrower at the centre which means the kink angle can be made smaller while still escaping line of sight. In the horizontal direction the maximum width of the ellipses is 11.4 cm and 12.4 cm respectively. In the vertical direction the first ellipse is 17.8 cm high and the second is 20.8 cm high.

1.2 Guide geometry

As `guide_bot` allows for fast automatic optimization of many guide geometries about 150 different geometries were tested. The best performing guides with respect to brilliance transfer were then further manually investigated for the spacial and divergence distribution and robustness to degradation of the mirrors. The chosen guide performs well in all categories.

1.3 Phase space on sample

Both the illuminated sample area and the divergence on sample were scanned and it was found that the chosen numbers do almost not influence the maximal brilliance transfer while keeping a homogenous illumination of the sample area and a smooth divergence distribution. The $1.5 \times 1.5 \text{ cm}^2$ sample space was thus chosen even though the instrument is optimized for maximum $1 \times 1 \text{ cm}^2$ samples to allow some freedom of sample rotation. Likewise the divergence limits were chosen as to be $\pm 0.75^\circ$ horizontally and $\pm 1^\circ$ vertically. Note however that this is not the maximal possible divergences but the maximum divergences that contributed to the optimisation. Hence divergences above these will hit the sample though they will decrease fast above the limits. Divergence jaws will enable users to choose a small divergence if they desire.

1.4 Moderator height

As the design of the instrument neared its end the moderator division at ESS released data showing how the brilliance of the moderators could be increased by reducing the moderator height. As a part of the ESS investigation of this effect the 4 most promising guide geometries were tested for other moderator heights. It was found that the chosen geometry would also be preferable at lower heights and that a gain factor of 1.8 can be achieved by going from 10 to 2 cm moderator height (see figure 1). Note that even at 10 cm the flux is the double of what it was at 12 cm. This is both due to the new better moderator model provided by the

moderator group and the fact that the flux here is not displayed in a 1.7 \AA wavelength band but for the entire band of interest. However since the official ESS policy that the instrument proposals should use the old 12 cm high moderator this is also done here.

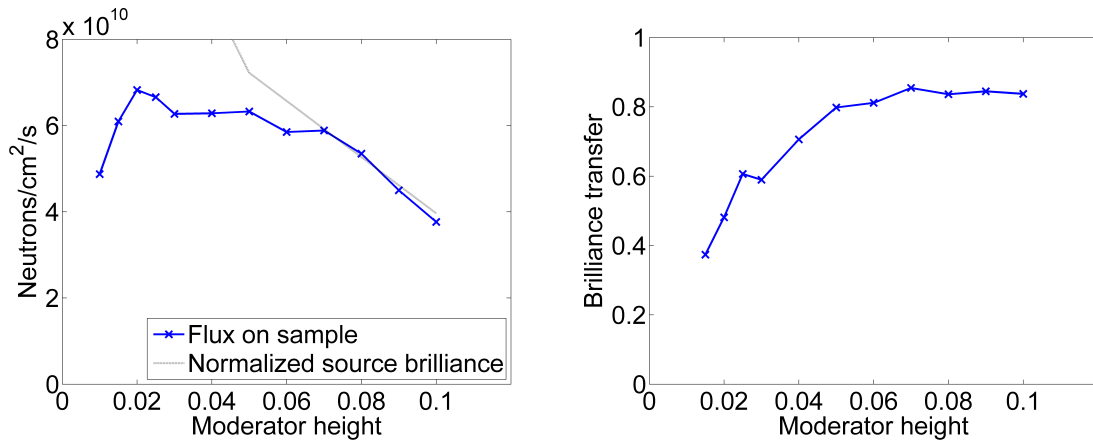


Figure 1: Simulation of the influence on the instrument performance if the new ESS moderator geometries are chosen.

1.5 Line-of-sight

guide_bot includes a ray tracer that makes it possible to do automatic optimization for any guide geometry. A scan of optimal solutions were performed for line-of-sight losses at different points in the guide (see figure 2). The guide were found to be quite resilient to more demanding line of sight requirements and in the end it was decided that losing line-of-sight to the moderator 25 m before the guide end provided a good compromise between guide background dampening and brilliance transfer. Note that most of the fast neutron background will leave the guide at the kink, but the last direct source of fast neutron background is 25 m before the end.

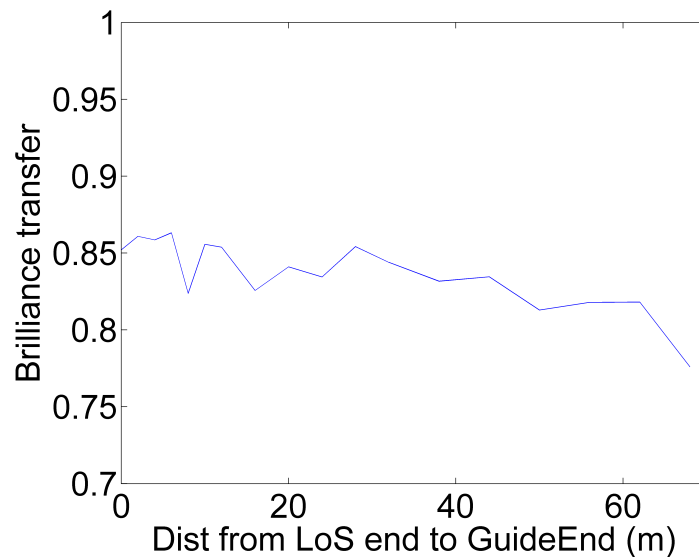


Figure 2: Simulation of the influence on the guide performance when the point where line-of-sight to the moderator is broken is moved from the end of the guide and closer to the guide start.

1.6 Coating

The optimizations were done with a coating with $m=3.5$ everywhere in the guide system and perfect ellipses. The resulting optimal guide geometry is used, but afterwards the guide was divided into 25 segments that were

Component	length of coating segment	coating value	position relative to moderator
Feeder	1.74 m	3	2.16 m - 3.90 m
Feeder	1.74 m	3.5	3.90 m - 5.63 m
Feeder	0.87 m	3	5.63 m - 6.5 m
Ellipse	6.52 m	3.5	6.6 m - 13.12 m
Ellipse	6.52 m	2	13.12 m - 19.64 m
Ellipse	39.12 m	1.5	19.64 m - 58.78 m
Ellipse	6.52 m	2	58.78 m - 65.28 m
Ellipse	6.52 m	3	65.28 m - 71.80 m
Straight	13.94 m	2	71.80 m - 85.74 m
Ellipse	15.73 m	2	85.74 m - 101.47 m
Ellipse	47.20 m	1	101.47 m - 148.67 m
Ellipse	7.87 m	2	148.67 m - 156.53 m
Ellipse	7.87 m	3.5	156.53 m - 164.4 m

Table 1: Overview of the guide coating and position of each guide element measured from the surface of the moderator.

individually scanned to investigate what m values were needed in that part of the guide. It was found that the coatings in table 1 were sufficient and that the ellipses could be segmented into 75 pieces each, and still maintain above 90% of the performance. It is expected that these coatings can be reduced further by allowing different coatings in the left and right side of the guide as it is asymmetrical after the kink.

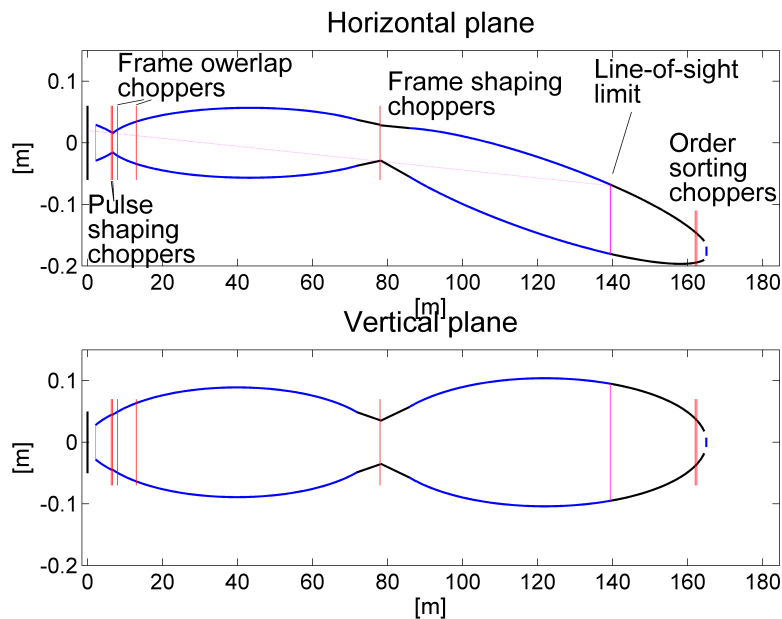


Figure 3: The guide geometry. The pink lines illustrate the line-of-sight and the red lines choppers.

1.7 Performance - Brilliance transfer

In this section the performance of the guide is investigated in terms of brilliance transfer. The source used is uniform in space, divergence and wavelength distribution. All figures have wavelength snapshots, which are simulations done using a very narrow wavelength band. The snapshots shown are for 1.0 Å, 1.7 Å, 2.3 Å, 3.0 Å and 3.6 Å.

Performance for the proposed guide is shown in figures 4, 5 and 6. Brilliance transfer is about 55% at the lowest used wavelength 1.65 Å, going to the maximum value of around 85% at approximately 3.0 Å. The divergence profile does show slight horizontal asymmetry caused by the kink at the lower wavelengths. The spatial distribution is also affected, but to a smaller extent. The vertical distributions are well behaved apart from small dips in the divergence for the lowest used wavelength. Though gravity was included, the simulations

show almost no signs of gravity affecting the vertical distributions. It does however cause a slight decrease in brilliance transfer at the very longest wavelengths.

The red line in the plot showing brilliance transfer as a function of wavelength on figure 4 show the performance in the case of a 20% reduction of the m value and a 40% increase in the slope of the reflectivity. This can be used to gauge how resistant the guide is to mirror degradation. It can be seen that such a loss in mirror quality would only be relevant below 2.5 Å, and would cut the brilliance transfer roughly to half at 1.7 Å.

1.8 Performance - Absolute units

In this section the proposed guide is investigated in terms of absolute flux. The guide have been simulated with the newest McStas 2.0 ESS source. The resulting performance is shown on figures 7, 8 and 9. The guide was placed at the center beamport and pointed directly at the center of the cold moderator. The flux is above 8×10^9 n/s/cm²/Å from 2.5 Å to 3.3 Å. The flux on sample declines below 2.5 Å. Even though the brilliance transfer at 1.7 Å is above half, the total flux is below 20% of the peak flux because of the source spectrum. Figure 10 shows the flux integrated over the natural 1.7 Å wide wavelength band, as a function of the center of the wavelength band.

Notice that when calculating brilliance transfer, the intensity is summed only over the figure of merit box, and thus adding for example divergence limits on the position monitor. On the figures in this section all neutrons are counted regardless of their divergence. This makes the spatial positions sharper, which can be a problematic characteristic, and will be addressed in future iterations of the guide design.

Proposed guide

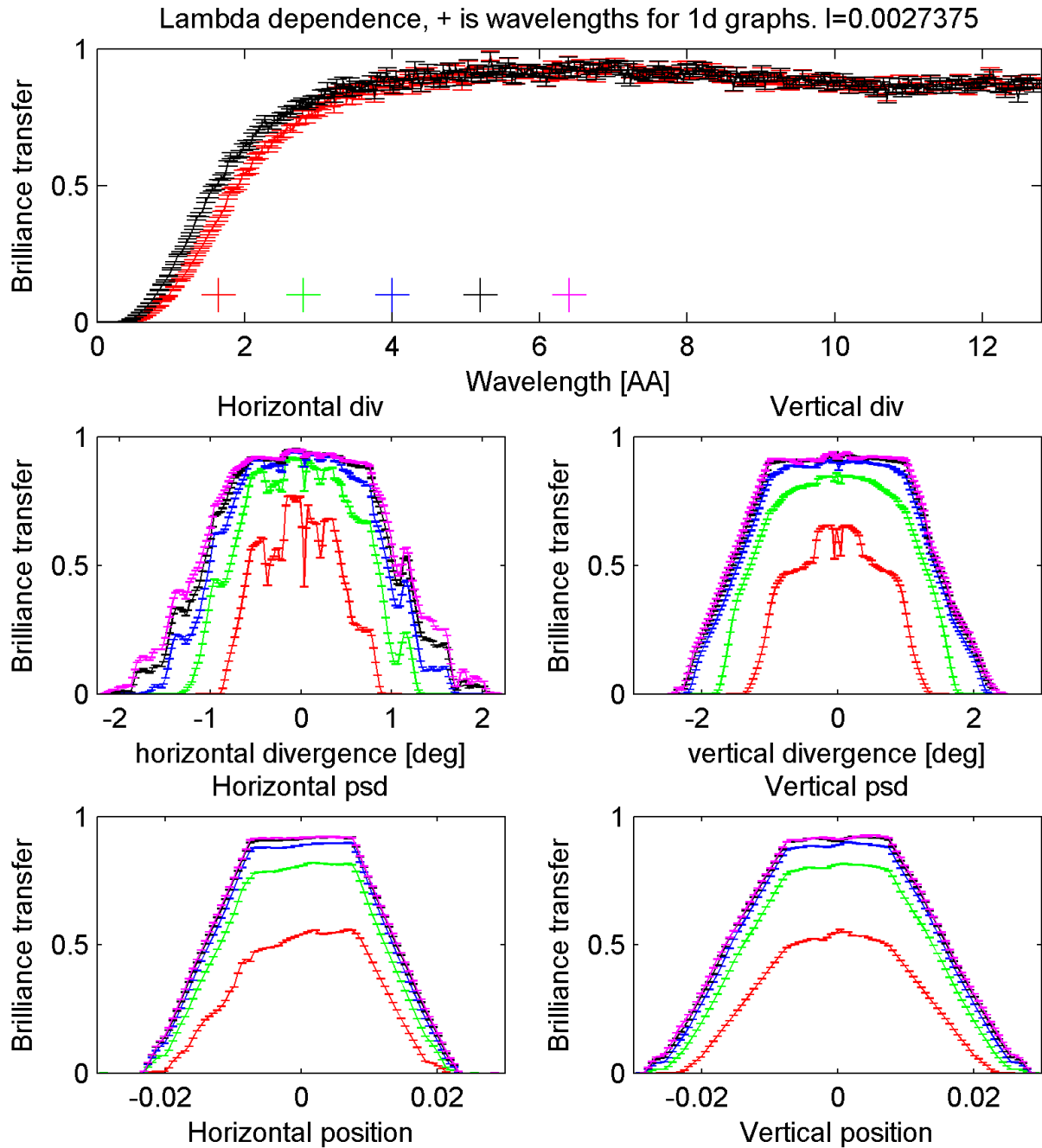


Figure 4: Summary of the overall results showing brilliance transfer as function of wavelength, spatial distribution and divergence distribution in terms of brilliance transfer. The red line in the brilliance transfer as function of wavelength plot shows the performance of the guide in case of a reduction mirror quality. The wavelength snapshots are at 1.0 Å 1.7 Å, 2.3 Å, 3.0 Å and 3.6 Å.

Proposed guide

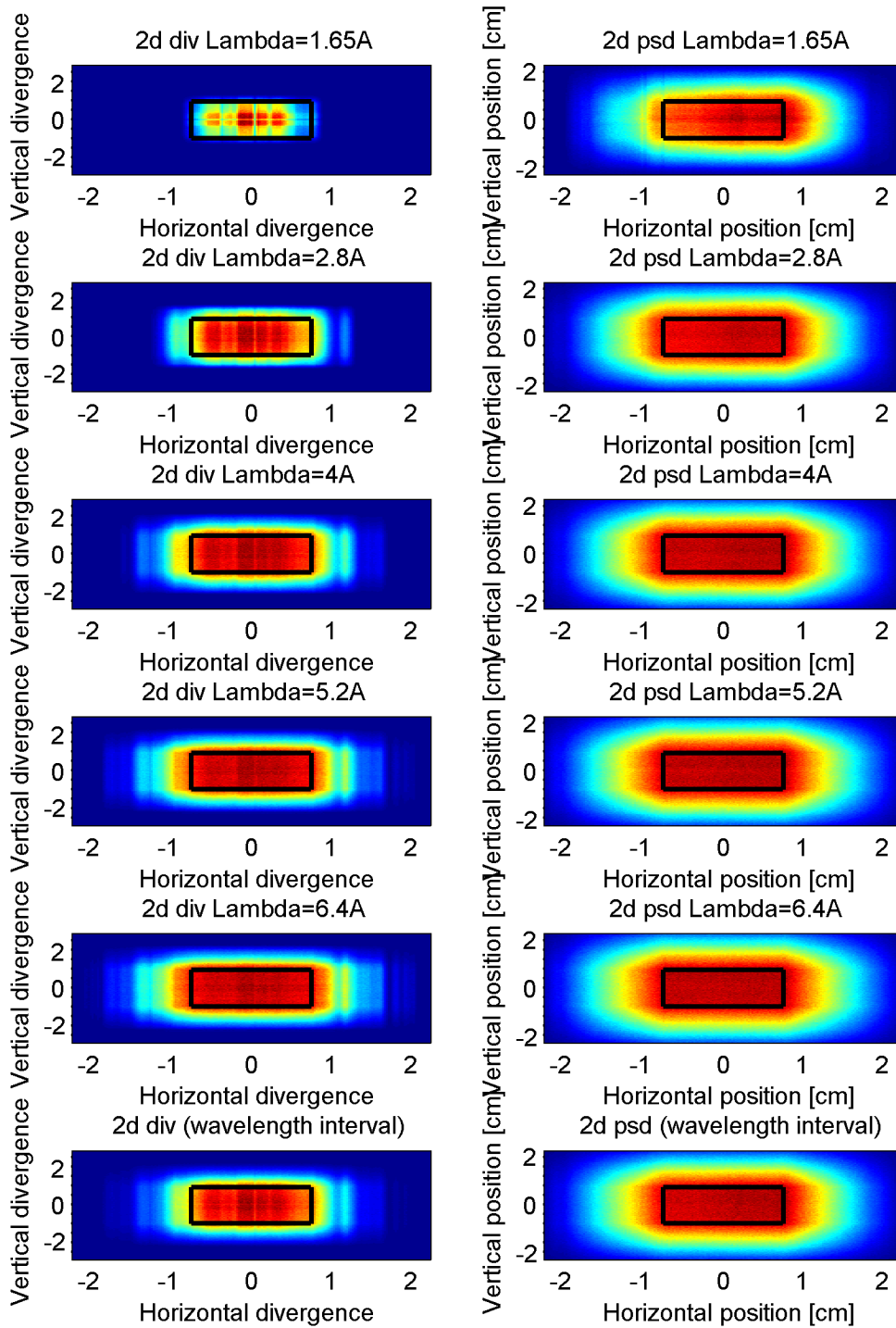


Figure 5: The two dimensional spatial and divergence distributions for wavelength snapshots and for the entire wavelength range. The box indicates the figure of merit.

Proposed guide

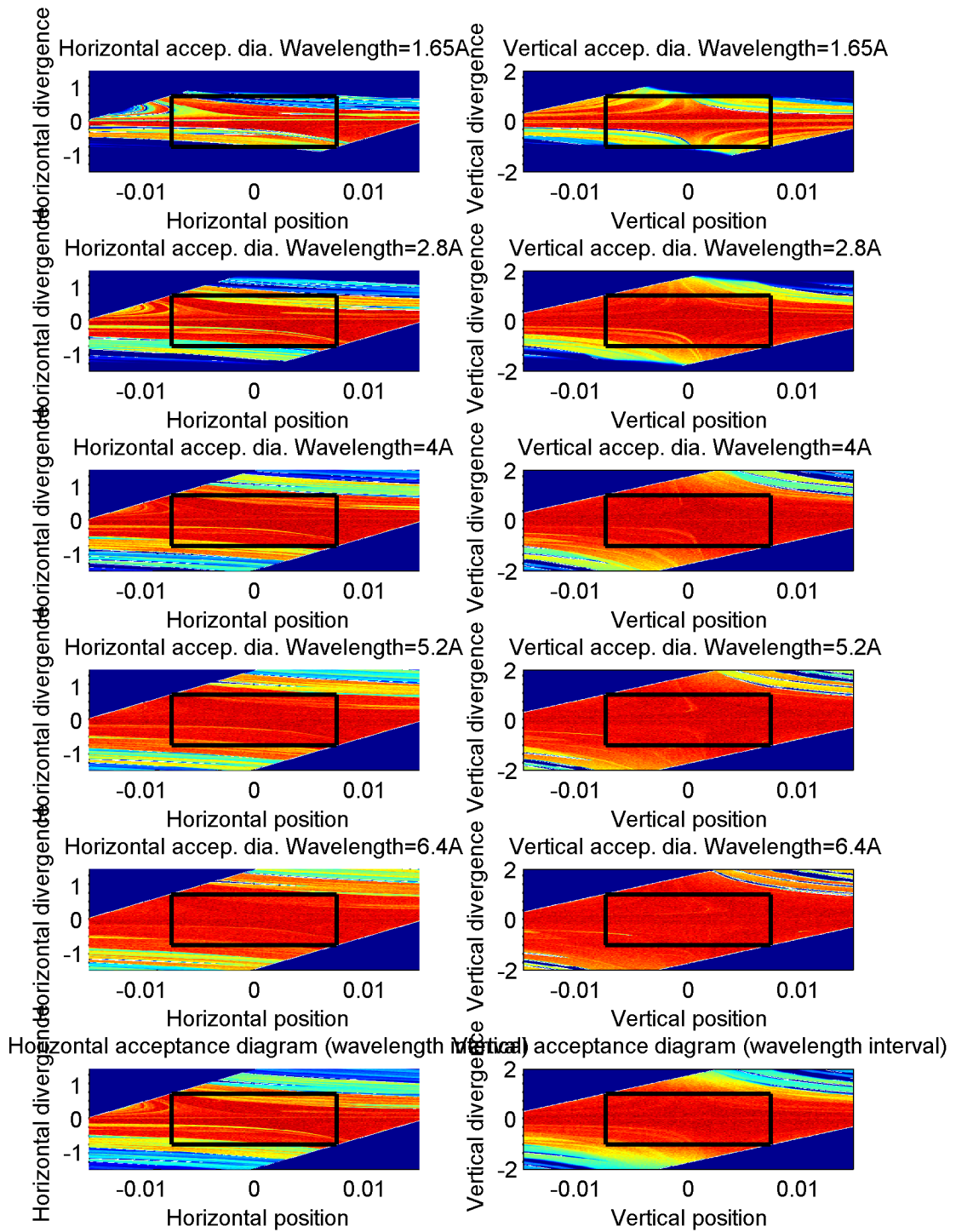


Figure 6: Acceptance diagrams for the horizontal and vertical directions for different wavelength snapshots and for the entire wavelength range. The box indicates the figure of merit limits.

Proposed guide

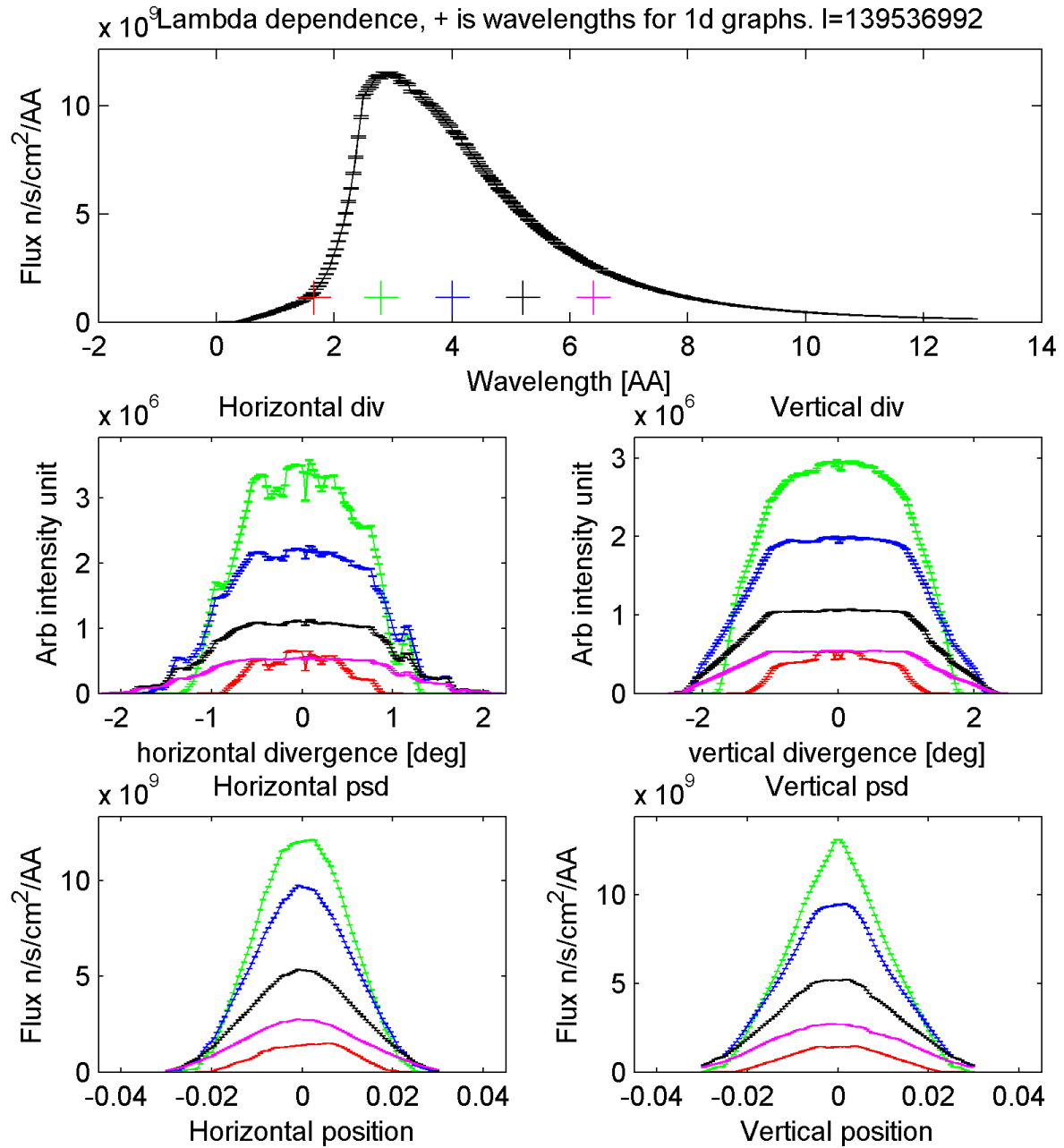


Figure 7: Summary of the overall results showing absolute flux on sample when using the ESS cold moderator. Shown as function of wavelength, spatial distribution and divergence distribution. The wavelength snapshots are at 1.0 Å 1.7 Å, 2.3 Å, 3.0 Å and 3.6 Å, the colors correspond to the markers in the plot showing wavelength dependence.

Proposed guide

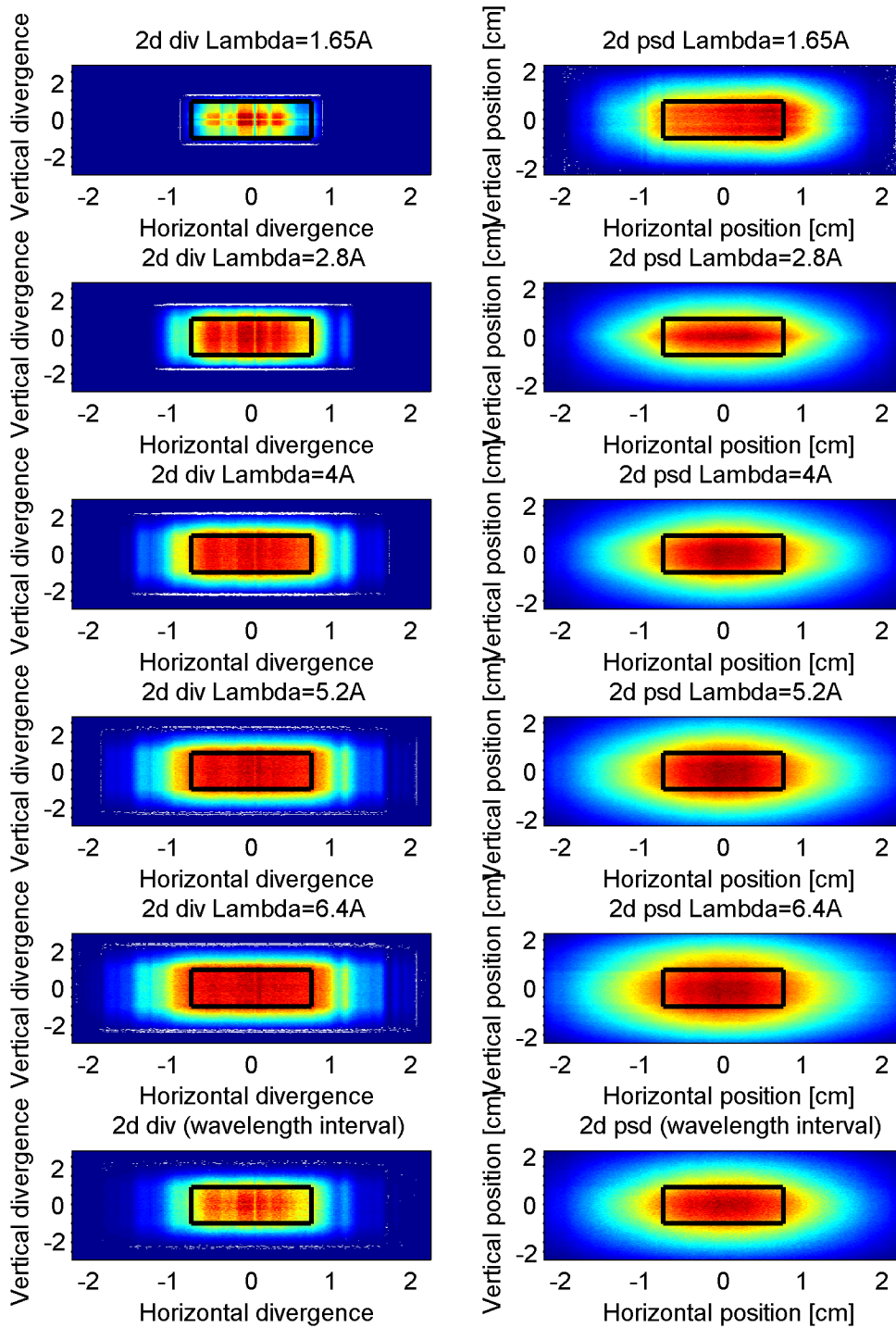


Figure 8: The two dimensional spatial and divergence distributions for wavelength snapshots and for the entire wavelength range. The box indicates the figure of merit limits. Simulated using the ESS cold moderator.

Proposed guide

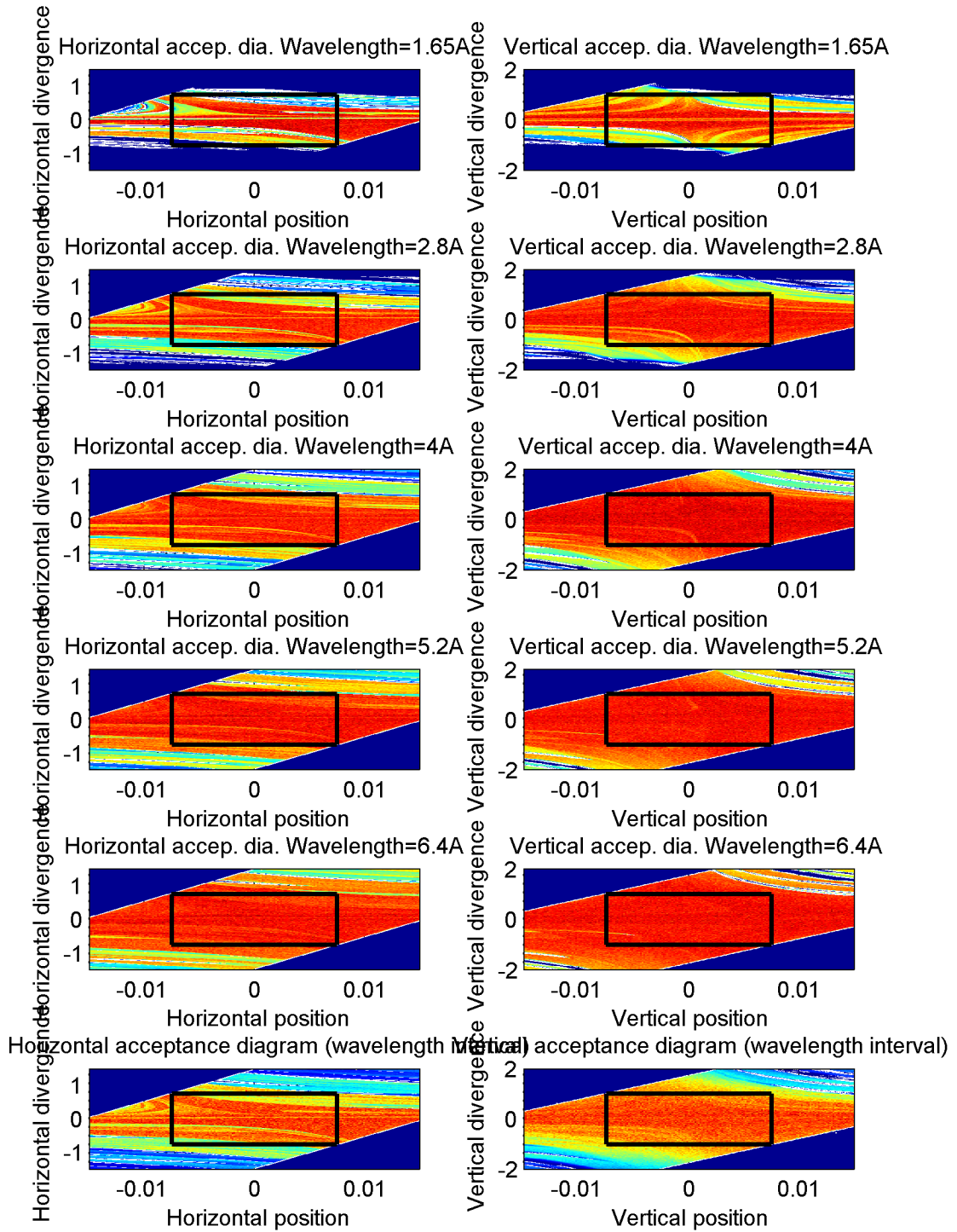


Figure 9: Acceptance diagrams for the horizontal and vertical directions for different wavelength snapshots and for the entire wavelength range. The box indicates the figure of merit limits. Simulated using the ESS cold moderators

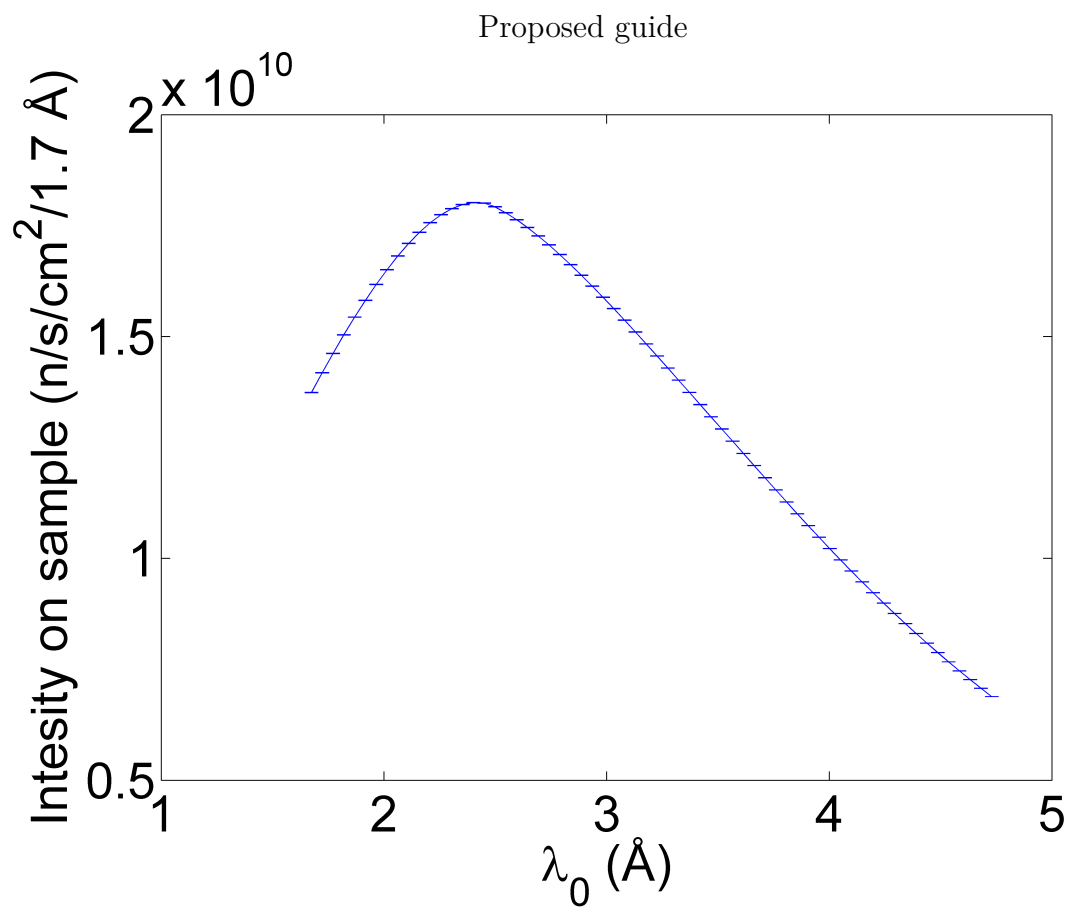


Figure 10: Absolute flux as a function of the lowest wavelength in the 1.7 Å wide wavelength band. For 3 Å the integrated flux is $1.8 \times 10^{10} \text{ n/s/cm}^2$.

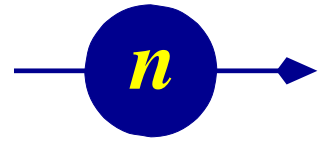


Technical University of Denmark

DTU



McStas



CAMEA

Bench Marking

Author:

P. G. Freeman



PAUL SCHERRER INSTITUT



ÉCOLE POLYTECHNIQUE
FÉDÉRALE DE LAUSANNE

Benching Mark CAMEA Against Present Inelastic Neutron Spectrometers

The CAMEA concept will be compared to the world leading spectrometers to grade performance. The exact performance of CAMEA will be detailed in the instrument proposal, whereas here we will compare two key areas where CAMEA has a clear gain factor. Additional gain factors from improved resolution, and background suppression are not considered here. Furthermore a comparison to a direct geometry time-of-flight spectrometry will be made by instrument simulations.

As CAMEA is an indirect time-of-flight spectrometer we will compare it to other indirect time-of-flight spectrometers capable of performing similar science. CAMEA's performance can also be compared to the performance of multiplexed triple axis spectrometers (TAS), and the flux of world leading TAS. The two gain factors for CAMEA that we will consider are neutron flux, and solid angle of analysis of the scattered neutrons.

In table one we outline a comparison of the neutron fluxes of triple-axis Spectrometers (TAS) and indirect geometry spectrometers with respect to CAMEA. The optimization of the CAMEA guide was for a vertical divergence of $\pm 1.5^\circ$ vertically and $\pm 0.75^\circ$ horizontally. As of March 2014 neutron simulations of the CAMEA guide were indicating a neutron flux of $1.8 \times 10^{10} \text{ ncm}^{-2}\text{s}^{-1}$ for 1.7 Å wavelength band centred at 3.25 Å in the maximum flux mode. In the resolution matching mode the incident resolution is matched to the resolution of the secondary spectrometer for a specific energy transfer and neutron final energy, for this mode the flux is approximately a factor of 3 lower. We compare the maximum flux mode for a flux gain factor of CAMEA in table one. We note that TAS have a monochromatic incident beam, so the comparison in table one should not be taken as an absolute gain factor for every possible experiment. As far as we are aware there is no published data on the neutron flux of the indirect geometry spectrometer PRISMA, which could operate at similar final neutron energies as CAMEA. From consideration of source brightness and >80% brilliance transfer for CAMEA's guide, a highly conservative estimate of the flux gain factor of CAMEA over PRISMA is >20. As can be seen in the values quoted in the table, for cold neutron spectrometers CAMEA has a gain factor that is between 100-1000 times that of present neutron instruments with cold neutron energy resolution. The THALES upgrade to IN14 will reduce this gain factor to 50, but for a larger beam divergence that will lower the resolution of the instrument, particularly the wavevector resolution. The low gain factor in comparison to MACS is due to MACS' flux being quoted for thermal neutrons, i.e. a ~0.9 meV energy resolution.

Table 1:

Instrument	Facility	Instrument Type	Flux	CAMEA Gain	Final Neutron Energy	Energy Range	Resolution at E = 0 for stated Final Energy
			n per cm ² per s		(meV)	(meV)	(meV)
IN14 [§]	ILL	TAS - PG(002)	1.7x 10 ⁸	105	5	0.1-17*	0.120
PANDA [§]	FRM-II	TAS - PG(002)	1.9 x 10 ⁷	947	5	0.1-20*	0.120
MACS ⁺	NIST	TAS - PG(002)	5x10 ⁸	36	14.7	2.3-14 [#]	0.85
THALES [§]	ILL	TAS - PG(002)	3.5x10 ⁸ @ k _i = 2.0 Å ⁻¹	51	5	0.1-20*	0.060
OSIRIS	ISIS	Time-of-Flight	3.24x10 ⁷ @ 180uA	554	1.84	-3 to 4	0.0254
IRIS	ISIS	Time-of-Flight	1.2x10 ⁷ @180uA	1500	1.84	-3.5 to 4	0.0175
IN20 (Polarized)	ILL	TAS - Heusler	1.05 x 10 ⁷	>20 [≡]	14.7 [^]	2-90*	0.85

[§] The values given for THALES and IN14 are from instrument simulations. With the measured flux of IN14 being 50% of this value: M. Boehm, *et. al.*, Meas. Sci. Technol. **19**, 034024 (2008), M. Boehm, *et. al.*, unpublished.

*A range of negative energies below 0 meV can be reached on TASs.

[§] The quoted flux of PANDA is for a vertically focused and horizontally flat monochromator.

Employing that uses both vertical and horizontally focusing would increase PANDA's flux by a factor of 3.

⁺ The flux quoted for MACS is for thermal neutrons of 12 meV energy.

[#] This energy range is only accessible for lower final neutron energies.

[^] In practise a final neutron energy of 14.7 meV is rarely used above 30 meV for studies of magnetic excitations. Higher energies are reached by using a final neutron energy of 34.8 meV.

[≡] This value represents a first estimate, and is variable depending on beam divergence at the supermirror polarizer's position on CAMEA and the m value that is used.

The flux gain alone gives CAMEA the ability to out-perform other spectrometers, but an additional gain comes from efficient detection of the scattered neutrons. In table two we compare the solid angle of analysers to represent detection efficiency. The back scattering instruments IRIS and Osiris use a large vertical divergence of analyser coverage to achieve high count rates at the cost of poor out of horizontal plane resolution. We therefore compare the solid angles of existing instruments to that of the typical solid angle of a single CAMEA analyser arc, covering $\pm 1.4^\circ$ vertical divergence. Within a $\pm 1.4^\circ$ vertical divergence CAMEA gains a factor of 2.4 or greater for existing multiplexed spectrometers, this is because of either the need of the instrument to move around the monochromator restricting size, or the use of a double bounce analyser system introducing large dead angles. For the indirect geometry spectrometers CAMEA has slight gains on the ISIS backscattering

spectrometers, but has a large gain on the double bounce analyser setup of PRISMA. On top of the larger solid angle for a single analyser, CAMEA also has the advantage of using analyser arcs sat behind each other, each detecting a different final energy of the scattered neutrons. The multiple analyser arcs will therefore provide an additional gain factor, which will be dependent on the needs of each experiment.

Table 2:

Instrument	Facility	Analyzer Bragg Reflection	Solid Angle (steradians)	$\pm 1.4^\circ$ Solid Angle (steradians)	CAMEA Gain $\pm 1.4^\circ$ single analyzer	CAMEA Gain for All Analysers ⁺
CAMEA		PG (002) or (004)	0.13 x 10	0.13 x10	-	-
OSIRIS	ISIS	PG (002) or (004)	1.09	0.12	1.08	7.7
Iris	ISIS	PG (002) or (004)	0.36	0.11	1.18	8.4
IN14/THALES	ILL	PG(002) double focusing analyser	0.016	0.0051	25.5	181
PRISMA	ISIS	PG (002)	0.021 @ 5 meV	0.0112	11.6	82.4
MACS	NIST	PG (002)	0.15	0.0525	2.5	17.8
Flatcone	ILL	Si(111)*	0.066	~0.033	3.9	27.7

* The Si(111) Bragg reflection has an approximately 2 times lower reflectance than PG(002), but Si(111) on TAS gains an advantage in not having contamination from second order Bragg reflections. We do not include a reflectance gain factor for using PG(002) over Si (111), this is because Flatcone could be constructed using PG(002) analysers.

⁺ This number represents the total analyser coverage of CAMEA corrected for transmission efficiency of the CAMEA analysers, a total gain factor of 7.1.

In table 3 we summarise the combined gain factor CAMEA can achieve in neutron flux and analyser solid angle.

Table 3:

Instrument	CAMEA Flux Gain	CAMEA Analyser $\pm 1.4^\circ$ Solid Angle Gain [§]	CAMEA Gain Factor
IN14 with Flatcone	105	27.7	2910
PANDA with Flatcone*	947	27.7	26200
THALES with Flatcone [#]	51	27.7	1410
MACS ⁺	36	17.8	640
OSIRIS	554	7.7	4270
IRIS	1500	8.4	12600
PRISMA	>20	82.4	>1650

[§]The full multiplied gain factor is only applicable for cases where the entire coverage of $S(q, \varpi)$ is scientifically relevant.

*Flatcone is not available at FRM-II for PANDA. The CAMEA flux gain is in comparison to PANDA using a monochromator with vertical focusing only.

[#] This gain factor is reduced to 199 for THALES using a CAMEA type secondary spectrometer.

⁺ Flux gain compares CAMEA to the low energy resolution, high flux thermal setup of MACS.

Conclusions

To summarize, in terms of both incident neutron flux and neutron detection efficiency, CAMEA offers clear gain factors on present cold inelastic neutron spectrometers. In comparison to presently built TAS combined with available multiplexing analysis the gain factor of a single CAMEA analyser is of the order of 400-3700, which can be reduced to 199 for THALES using Flatcone with PG(002) analysers installed. In comparison to the nearest equivalent indirect geometry spectrometer to CAMEA, namely PRISMA, a gain factor >230 can be expected for a single CAMEA analyser. For the resolution matching mode of CAMEA a higher resolution than that of TAS can be achieved, with an incident flux a factor of three lower, see [Guide Report]. The gain factor for CAMEA is 7.1 times larger when all analyser arcs of CAMEA are taken into consideration.

References:

The information for this report was obtained from the following sources:

IN14:

<http://www.ill.eu/instruments-support/instruments-groups/instruments/in14/characteristics/>

PANDA:

<http://www.mlz-garching.de/panda>

MACS:

http://www.ncnr.nist.gov/instruments/macs/Instrument_details.html

M. Mourigal (John Hopkins University) personal communication

THALES:

M. Boehm, *et. al.*, Meas. Sci. Technol. **19**, 034024 (2008); M. Boehm (I.L.L.) personal communication

OSIRIS:

<http://www.isis.stfc.ac.uk/instruments/osiris/technical/osiris-technical-information7523.html>

M. T. F. Telling and K. H. Andersen, Phys. Chem. Chem. Phys. **7**, 1255-1261(2004)

Iris:

<http://www.isis.stfc.ac.uk/instruments/iris/technical/iris-technical-information7247.html>

M. T. F. Telling and K. H. Andersen, Phys. Chem. Chem. Phys. **7**, 1255-1261(2004)

IN20:

<http://www.ill.eu/instruments-support/instruments-groups/instruments/in20/characteristics/>

PRISMA:

<http://www.isis.stfc.ac.uk/instruments/prisma/documents/prisma-document6428.html>

F. Demmel (ISIS, STFC) and B. Fåk (CEA, Grenoble) personal communications.

Flatcone:

<http://www.ill.eu/instruments-support/instruments-groups/instruments/flatcone/characteristics/>

J. Kulda, Nuc. Eng. and Tech., **38**, 433 2006;

P. Steffens (I.L.L.) personal communications.

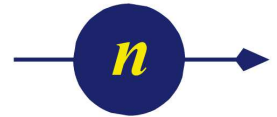
[Guide Report] http://www.psi.nbi.dk/~jonaso/ess/CAMEAProposal/Guide_report.pdf



Technical University of Denmark



McStas



CAMEA

Comparison to the Cold Chopper Spectrometer

Author:

J. O. Birk



PAUL SCHERRER INSTITUT



ÉCOLE POLYTECHNIQUE
FÉDÉRALE DE LAUSANNE

Contents

1	Introduction	2
2	Kinematic flux calculations	2
3	Flux simulations	3
3.1	Results	4
4	Background	4
4.1	Single scattering events.	4
4.2	Multiple scattering events	5
5	Other experimental issues	8
5.1	Coverage	8
5.2	High Resolution	8
5.3	Time Resolution	9
5.4	Thermal Measurements	9
5.5	Bragg peaks	9
6	Conclusion	9

1 Introduction

The cold chopper and CAMEA spectrometers are in many ways equivalent. One uses several incoming energies combined with a continuous outgoing energy band while the other use a continuous incoming band and several outgoing energies, and both have big angular coverage. They do however also have some key differences. CAMEA have a higher flux in each channel while the cold chopper have a bigger angular coverage, bigger resolution flexibility, and more freedom in choosing its energy range. Since CAMEA cannot compete with the cold chopper at very high resolutions it is important to investigate how the CAMEA compares to the cold chopper spectrometer in the primary operational region of CAMEA. For this comparison we have thus concentrated on settings where CAMEA excels (1.4% energy resolution, in plane scattering). We choose to consider only low temperature scattering i.e. where downscattering is dominating and a wavelength band of 3.1 Å to 4.76 Å.¹

2 Kinematic flux calculations

It is possible to get an idea of how the two instruments will compare from simple kinematic considerations:

¹When the flux simulations were done the natural length of long instruments at ESS was 170 m corresponding to a wavelengthband of 1.66 Å. In the meantime the numbers have been changed to 165 m and 1.7 Å. The results are however still valid for the new settings.

- CAMEA uses the full 71 ms pulse while the cold chopper can for similar resolution use 8 pulses of approximately $25 \mu\text{s}$ (in Rep Rate Multiplication mode). This gives CAMEA a factor ~ 360 .
- The reflectivity of the CAMEA analysers are on average about 50% if all 30 detectors are counted and beam attenuation is included. This gives the Cold Chopper a factor 2.
- Camea has 33% dark angles giving the cold chopper a factor 1.5.
- Camea have 30 detectors with a 1.4% resolution giving a total covered EF bandwidth of about 2 meV. The cold Chopper goes from $0.2 E_i$ to E_i giving on average a 4 meV energy band. This gives a factor 2 to the cold chopper.
- We have so far only disregarded upscattered neutrons from the cold chopper. Approximately half information from the sample lies in the upscattering giving the cold chopper a factor 2.
- As we only regard downscattering CAMEA will get almost no signal from the analysers with the coarsest resolution (highest count rate) whereas the cold chopper will get the highest signal from the shortest wavelength. The exact effect of this needs simulation but a factor 2 is estimated.

Combining these factors one find that CAMEA will win with a factor 15 if only in-plane scattering is considered. But if out of plane scattering is also included The $\pm 30^\circ$ coverage of the cold chopper will mean that the two instruments are comparable. However this is just an approximate calculation that amongst others does not take into account that

- the flux varies with the wavelength
- or there are small gaps between the analyser crystals.

Here, in order to reach a more accurate number, simulations have been performed.

3 Flux simulations

In order to compare the flux and coverage of the two instruments we performed a simulation with as equal settings as possible.

Both instruments used the same source, guide, chopper settings before the monochromating chopper, and same sample. The incoming and outgoing energy resolutions were chosen to match the outgoing resolution of CAMEA, and the bandwidth chosen were 3.1 to 4.76 Å. This resulted in a factor 380 in favour of CAMEA at the incoming flux.

For simplicity the secondary spectrometers were simulated individually. The ESS source was set to focus directly on the sample. A sample with a scattering cross section of $\frac{d\sigma^2}{d\Omega dE} = \frac{k_f}{k_i} s(q, \omega)$ with constant $s(q, \omega)$ was chosen as to not

favour one instrument that eg. happened to match a certain excitation curve. The signal just before the analysers was compared to the signal in the detectors to measure the fraction of the beam from the sample that each detector records. Afterwards the data was corrected for beam attenuation through the analysers and an average graphite reflectivity of 70% was chosen. Finally dark angles and the smaller vertical coverage of the backmost analysers of CAMEA were included. Only down scattering was considered.

3.1 Results

Comparing the two instruments gives a factor 22 to the CAMEA instrument if a $\pm 2^\circ$ opening angle is considered. If one considers the full $\pm 30^\circ$ detector coverage, the two instruments are almost equal CAMEA having 50 % more counts. It is thus clear that CAMEA in its key performance is more powerful than the cold chopper. This is however not a full and fair comparison as other experimental considerations leads to the cold chopper being the best choice in many cases.

4 Background

The two instruments deal with background in very different ways. The cold chopper will almost only allow useful neutrons on the sample but is not able to distinguish neutrons coming from the sample region from each other. CAMEA will have a much higher flux on the sample and relies on shielding and analyser crystals to sort away background neutrons. If a sample is placed completely alone in vacuum the cold chopper will probably be able to reach a lower background level since there will not be any background from the analysers. On the other hand it is easier to install vertical collimation on CAMEA so if there is a strongly scattering sample environment around the sample the cold chopper suffers far more than CAMEA.

Another important issue is the distribution of the background. Any neutron scattered from the sample surroundings of the cold chopper will get additional flight path and thus appear as inelastic background. On CAMEA the tens of cm difference in flight path will be small compared to the 165 m primary flight path so the extra background will fall within the elastic line. This is not the case for direct time-of-flight.

Heavy sample surroundings will cause an increased background in neutron scattering experiments. Two examples of such problems can be seen in figure 1 and shows how scattering from sample surroundings on time-of-flight spectrometers can pollute the inelastic region. We will in the following treat the background in two groups: Single and multiple scattering events.

4.1 Single scattering events.

These can be reduced by applying collimation however, if the sample environment has strong scatterers close to the sample it is impossible to shield it entirely,

4.2 Multiple scattering events

5

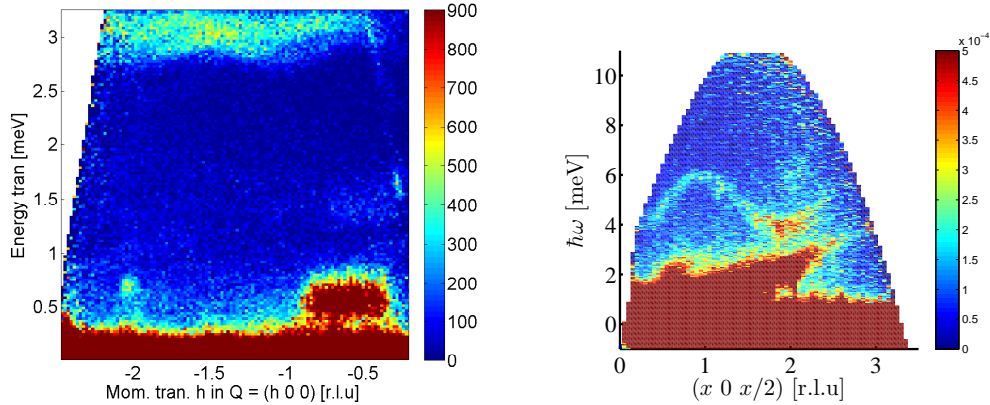


Figure 1: Examples of background from sample surroundings. Left: LET data of $\text{SrCu}_2(\text{BO}_3)_2$ in an orange cryostat ($E_i=12$ meV). Right: CNCS data on $\text{CoCl}_2 \cdot 2\text{D}_2\text{O}$ with the 16 T magnet 'Fat Sam' that has a radius of 40.5 cm ($E_i=12$ meV). The signals close to the elastic line are from the sample surroundings and stronger than the inelastic signal from the sample. In both cases the background can be reduced by the right choice of collimation/cryostat.

although the limited opening angle of CAMEA can help shielding material above or below the sample. The signal will however look sample like - i.e. Bragg peaks, Debye Scherrer cones and phonon dispersions and these can be mapped out by measuring without a sample.

4.2 Multiple scattering events

Although the cross section for multiple scattering is low, sufficient amounts of material in the sample surroundings can cause the elastic signal from these events to shadow inelastic scattering. Collimation can limit the problem but there is no way to shield for example the events shown in figure 2 by external collimation. The exact distribution of such background will depend on the precise layout of the sample surroundings but it is possible to calculate limits on the background distribution. Assuming that the multiple scattering respectively adds or subtract a distance Δl from the flight path the recorded of the neutron energy (E') will be:

$$E' = E \left(\frac{l}{l \pm \Delta l} \right)^2 \quad (1)$$

where l is the flight path used for time-of-flight measurements and E is the actual energy of the neutron. Since CAMEA uses analysers to determine E_f the distance in question will be the 165m primary flight path while it for direct time-of-flight will be the ~ 4 m secondary flight path. This leads to the distribution seen in figure 3 left.

The extreme values for Δl that will make it through a radial collimator can be found from figure 2. The minimum will be $\Delta l = R(\sqrt{2(1 - \cos(2\theta))} - 2)$, where R

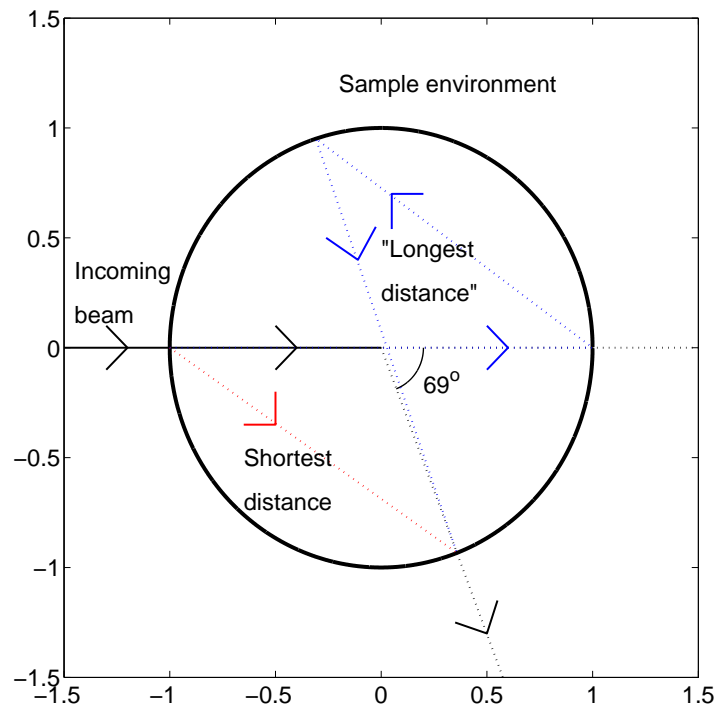


Figure 2: The longest (blue) and shortest (red) paths a neutron can travel to a detector at 2θ with maximum 2 scattering events if radial collimation removes neutrons that do not come from the sample direction.

4.2 Multiple scattering events

7

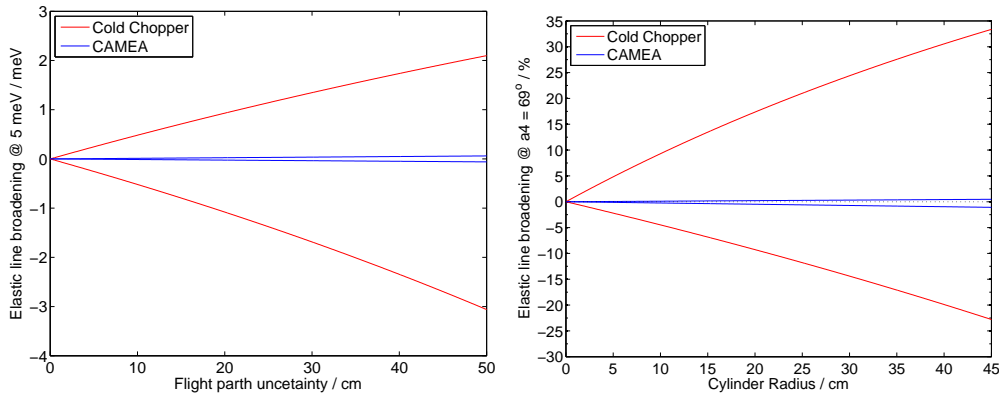


Figure 3: Boundaries for multiple scattering in the sample surroundings with maximum two scattering events pr. neutron. Left: calculated from a the travel path uncertainties. Right: Calculated from the longest Δl possible withing a cylinder of a given radius, as described in figure 2.

is the radius of the sample environments and 2θ is the recorded scattering angle. The maximum is in principle infinite but discarding events with more than two scatterings as higher order we reach a limit of: $\Delta l = R * (\sqrt{2(1 - \cos(2\theta))} + 2)$. At CAMEA the minimum path will be recorded as down scattering, while the maximum will appears as up scattering, while it is opposite for direct time-of-flight. These boundaries for multiple scattering from sample surroundings are displayed in figure 3 right for the centre of the CAMEA detector ($2\theta = 69^\circ$). It can be seen that in the down scattering region where CAMEA is designed to deliver its optimal performance the extend of the scattering is less than $\Delta E/E \approx 0.5\%$. So multiple scattering will be contained in the elastic line, while it for direct time-of-flight can cause problems for low lying excitations and quasi elastic scattering with $\Delta E/E \approx 30\%$. On the up scattering side the maximum deviation can get close to 1% so in the most extreme cases it might cause a small widening of the elastic line on CAMEA while it can again ruin inelastic data on direct time-of-flight machines with $\Delta E/E \approx 25\%$.

It is important to note that the above equation do not predict that big inelastic regions will be overshadowed by multiple scattering events. It merely places a limit on what region can potentially be overshadowed by double scattering. Figure 1 does however confirm that the effect can be a real issue on direct time-of-flight spectrometers.

For direct time-of-flight one can obtain better results than shown in figure 1 by applying radial collimation outside the sample environment, reduce the sample environment in the beam, or incorporate radial collimation in the sample environments. This makes measurements with specialised light and medium level environments achievable but the bigger the amount of material the harder it becomes. For certain kinds of environments such as very strong magnets or pressure cells it is impossible to reduce the environments at beam height enough, or to add a radial collimator in the presure cell case. In these cases it will be easier to measure low lying excitations and quasi-elastic scattering on CAMEA.

Especially if the inelastic signal is weak, for example because a small sample is used.

It is possible to subtract parts of this background by measuring without the sample but if the multiple scattering event involved the sample, subtraction will be inaccurate. This can however only happen for $\Delta l > 0$ so it is possible to map out all contribution from multiple scatterings without the sample on the down scattering side on CAMEA and up scattering side on direct ToF. Note that in the examples from figure 1 the background is much stronger than the inelastic signal from the sample so even if it is mapped out it might not be possible to reliably retrieve any actual data hidden below it.

We have assumed elastic scattering background events. Multiple scattering from sample surroundings including inelastic scattering can of course also occur but the cross section is substantially smaller and the events cannot be given the same meaningful limits as in the elastic case.

This further emphasises that CAMEA is an extremely strong instrument in the presence of complex sample environments but it will not be able to compete with the cold chopper at all settings.

5 Other experimental issues

5.1 Coverage

The cold chopper spectrometer looks at the elastic line with all RRM frames whereas the amount of analysers looking at it in CAMEA will be different. Usually only the high E_f frames will be recording the elastic line; the others will be concentrating on the down scattering region. This means that CAMEA will have a worse resolution at the elastic line but a much higher coverage in the inelastic than the elastics while the cold Chopper will have the highest coverage at the elastic line and lowest in the deep inelastics. (It is possible for CAMEA to have high coverage and good resolution at the elastic line too. By choosing a wavelength band that will enable the 2.5 meV analyser to record elastic scattering a resolution of 20 μeV can be achieved but in that case the covered area will shift towards the upscattering region.) This difference makes the cold chopper even better at quasi elastics and emphasises the CAMEA strength in low temperature inelastic measurements.

5.2 High Resolution

CAMEA can reach a $\frac{\Delta E}{E}$ resolution of just above 1.1% at 5 meV by using unmatched primary and secondary resolutions but will lose a substantial part of its flux doing so (the matched value is $\frac{\Delta E}{E} = 1.4\%$). The cold chopper can not only reach these levels with a smaller loss by matching the resolutions. It will also be able to surpass it, making far more accurate measurements.

5.3 Time Resolution

Both CAMEA and the cold chopper can in principle have good time-resolution for time dependent experiments. However the monochromating chopper of the cold chopper means that the time where a certain energy transfer is recorded will be comparable to the time resolution of $30 \mu\text{s}$ while it will be 100 times longer (3 ms) than the time resolution on CAMEA. This means that CAMEA will be able to resolve many processes with constant experimental settings while this can only be reached by running a stroboscopic measurement with a different frequency than the ESS pulse at a cold chopper instrument. The later will make for much longer experiments and together with the lower count rates makes many experiments unrealistically long on a cold chopper instrument while manageable on CAMEA.

5.4 Thermal Measurements

If we consider up-scattering the cold chopper will at first glance win a lot since the outgoing bands can be increased to any energy for almost no cost in time and it will thus be possible to reach any energy coverage. Of course much of this gain is insubstantial since the resolution will worsen considerably. None the less the Cold Chopper Spectrometer will gain compared to CAMEA in conditions where up-scattering is relevant.

5.5 Bragg peaks

The high intensity of CAMEA means that some Bragg peaks will be strong enough to harm the detectors if they are not protected for example by reducing the efficiency of the detectors that are illuminated by a Bragg peak. The problem will be much smaller at the cold chopper spectrometer. The primary focus of a spectrometer is however not to measure high intensity Bragg peaks so the problem will be small for practical measurements.

6 Conclusion

The Cold chopper spectrometer has an impressively large achievable parameter space compared to most other spectrometers and will be an excellent flexible spectrometer that can handle most challenges but will not be able to compete with more specialised instruments within their optimal field of operation.

CAMEA will have 22 times higher count rates and lower inelastic background when cold samples and extreme environments are needed. Both instruments thus have a clear role in an instrument suite.



Technical University of Denmark



McStas



CAMEA

Building and testing Prototype for CAMEA

Author:

M. Markó



PAUL SCHERRER INSTITUT



ÉCOLE POLYTECHNIQUE
FÉDÉRALE DE LAUSANNE

Contents

1	CAMEA	3
2	Description	3
2.1	Primary spectrometer	3
2.2	Secondary spectrometer: Prototype	4
2.2.1	Detectors	6
3	Aligning and calibrating the prototype	6
3.1	Aligning of the frame	6
3.2	Mounting of the analysers	6
3.3	Optical alignment I	6
3.4	Measurement of the quality and orientations of the graphite sheets at POLDI	7
3.5	Limits of the information from POLDI	9
3.6	Measurements at Morpheus	9
3.7	Optical alignment II.	9
3.8	Calibration procedure	10
4	Measurements	10
4.1	Energy resolution measurements	10
4.2	resolution ellipsoids	11
4.3	Background and spurions on the prototype	12
4.4	Inelastic measurement on $LiHoF_4$	15
4.5	Inelastic measurement on $YMnO_3$	16
5	Conclusions	16

1 CAMEA

CAMEA (Continuous Angle Multiple Energy Analyser) is a new concept for analysing inelastically scattered neutrons with high efficiency. It contains many (up to 10) vertically focusing analyser arrays behind each other, analysing the scattered neutrons with a given energy by scattering them vertically. Each array analyses different energies (Multiple Energy Analyser). The vertical scattering planes of analysers enable to cover large angular range in the scattering plane (Continuous Angle). Thus CAMEA gives a fast mapping possibilities in the three-dimensional q - ω space spanned by the horizontal q -plane and the energy transfer.

The large sample-analyser and analyser-detector distances provide clearly geometry limited energy resolution. This geometry combined with analyser crystals with relaxed mosaicity enable to use several detectors next to each other, seeing slightly different take-off angles, thus detecting neutrons with slightly different energies. Thus this concept has the advantages both of geometry limited resolution (high resolution) and mosaicity limited resolution (high analysing efficiency).

CAMEA, as a secondary spectrometer can be optimally combined with a time of flight primary spectrometer resulting in an inverse geometry TOF spectrometer. ESS CAMEA is such an instrument proposed to be built at ESS.

2 Description

The prototype of ESS CAMEA was designed to achieve a number of goals:

1. **Confirm concepts:** CAMEA includes a number of elements that have not been used before together. Both the overall concept of several focusing analysers behind each other simultaneously analysing different energies and the concept of getting several energies from one analyser. Though they work on paper some concerns have been raised about their implementation in the real world.
2. **Measure resolutions and intensities:** Both simulations and analytical calculations need actual measurements to confirm the results. The investigated parameter space is far too big for us to measure everything so the measurements will be used to validate the simulations.
3. **Measure background:** While simulations and calculations give a lot of insight into the resolutions, intensities and coverage it struggles to give realistic numbers for the background. The best way to get actual numbers is prototyping.
4. **Gain experimental experience:** By doing real experiments one can often learn things about how the instrument and data analysis should work, that is not apparent in simple idealised cases such as resolution measurements.

To meet these challenges the prototype was designed with a lot of flexibility so resolutions can be measured in a lot of different settings, and shielding and collimation can be installed at different places. The prototype was planned and built at KU and DTU and installed at the backscattering spectrometer MARS at PSI. It consist of an Aluminum frame that contains three analyzer banks and three detector banks. Four different type of pyrolytic graphite analyser crystals have been used having 24', 30', 60' and 90' mosaic width. To maximize the flexibility both analysers and detectors can be moved and the Al frame allows one to mount shielding and collimators where they are needed. Furthermore the chopper system of MARS was modified to adopt the rotating frequency of the choppers to the frequency of the ESS (14Hz).

2.1 Primary spectrometer

MARS is an indirect TOF spectrometer having five choppers, with a base frequency of 50 Hz. For improving the resolution, the second (master) chopper can run at $n \cdot 50$ Hz (up to $n=7$). The flight path from the master chopper to the sample is $L=38.47$ m. In the original concept the second chopper shapes the pulse, the first and third choppers avoid the overlap between the pulses, and the last two, close to the sample position, are the higher order selection choppers (the names positions, opening angles, and frequencies of the five choppers are given in the table 1).

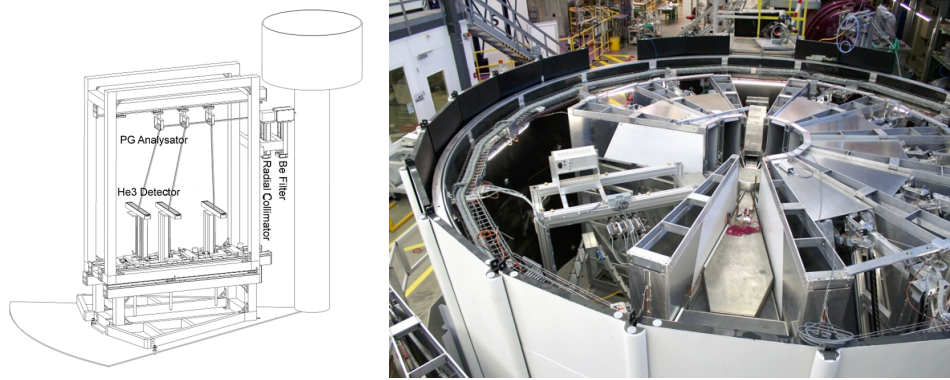


Figure 1: left: drawing of the prototype, right: Prototype in the MARS tank

#	name	position [m]	opening angle [$^{\circ}$]	f [Hz]
1	snail	-0.308	4.05	50
2	master	0	3.053	$50 * n$ n=1..7
3	rabbit	15.601	54.27	50
4	energy window	34.439	121.02	50
5	energy window	34.494	121.02	50

Table 1: Choppers of front end of MARS

Since MARS was optimized for using mica analysers close to backscattering geometry (lattice spacing is 10.2 Å), the order selecting choppers (and also the third chopper) enable to see only the 1/3 part of the time window (thus also the wavelength band) would be enabled by the repetition time. In this way the second and higher order reflections from the mica analyzer do not overlap with the first order reflection at the given base frequency, secondary flight path (3.5 m), and 20.37 Å final wavelength (197 μeV final energy).

We modified the base frequency to be capable for working between 10 and 20 Hz also. During the measurements we used 14Hz base frequency. This resulted in 0.605 ms pulse duration, and 71.4 ms repetition time i.e. the initial wavelength band was 2.45 Å (taking into account the order sorting choppers). The low base frequency and also the planned higher final energies (between 2.5 and 8 meV) would need to close the order selecting choppers leaving less than 5° opening, thus we did not planned to use the order selection.

The pulse duration can be decreased by a slight dephasing of the first chopper (right part of Figure 2) causing shorter but wavelength dependent pulse duration with a small (also wavelength dependent) time shift. We applied -3° shift on the phase of the first chopper. Furthermore we call this mode high resolution mode, while the original mode with no dephasing is the low resolution mode. Thus in high resolution mode the first chopper also takes part in the pulse shaping.

Before the first chopper a strongly curved guide suppresses the high energy neutrons. Before and after the first two choppers the guide is converging diverging respectively to increase the time resolution of the primary spectrometer without increasing of the divergence. The last section of the guide is also convergent causing high intensity at the sample (see left part of Figure 2). There are two monitors, one before the sample, and an other after the sample.

2.2 Secondary spectrometer: Prototype

The secondary spectrometer is the prototype of CAMEA. To install it, we have removed three inelastic units and two diffraction detectors from the MARS tank (see figure 1). The scattering angle (a_4) at the middle of the prototype is 60°. The prototype has a bottom frame fixed to the floor, and an upper frame holding the detectors, analysers and shieldings. This upper frame is movable in the direction of the scattered beam to ensure easy access to every part of prototype. To improve the flexibility analysers can be moved in one direction, and the detectors can be moved in two directions.

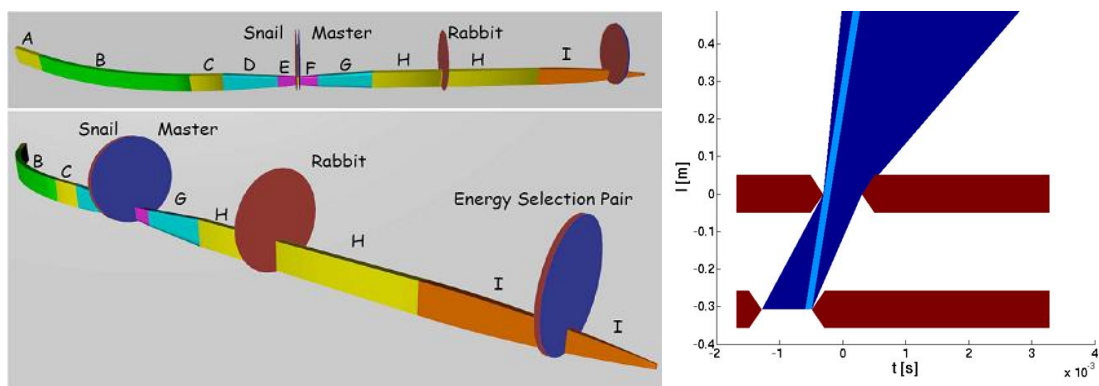


Figure 2: left: Front end of MARS right: Effect of dephasing of the first chopper: time-flight path diagram at the first two chopper. The deep blue area shows the possible trajectories of the neutrons passing through the choppers, while the light blue line shows the trajectories of neutrons arriving to the sample in one time (and shows also the effective pulse duration at a given energy)

Analysers

The sample-analyser distance can be varied manually from 1 to 2.3 m. The analysers can be rotated slightly around the vertical axis by hand. Each analyzer bank has a frame rotated by motors around the horizontal axis perpendicular to the beam direction. Each frame can hold up to 7 Si (100) wafers. Each wafer can hold 15 cm² of Pyrolytic Graphite (PG) crystals (002) - see figure 3. The wafers can be individually rotated by hand to generate different focusing geometries. A number of different PG batches was bought from Panasonic (see table 2). This system allows us to test different final neutron energies, sample analyser and analyser detector

Batch #	Mosaicity (arc minutes)	# of pieces	Length (mm)	Width (mm)	Thickness (mm)
1	40	15	50	10	1
2	40	15	50	10	1
3	60	10	75	10	1
4	90	10	75	10	1
5	30	15	50	10	1

Table 2: Overview of PG batches. Most of badge 1 and 2 can be combined to make a single large analyser for experiments where this is needed.

distances and graphite qualities.

Firstly it was ensured that the wafers were uniformly oriented and the PG was approximately adjusted to that orientation by the use of a reflected laser. Before mounting the quality and uniformity of the graphite had to be tested and the different pieces oriented together.

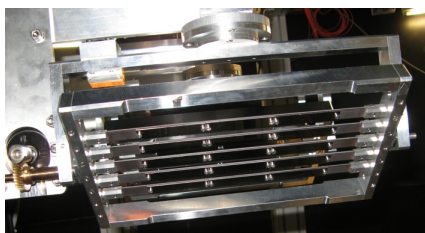


Figure 3: Analyzer bank

2.2.1 Detectors

In each detector bank facing to one analyzer there are three position sensitive ^3He detector tubes with the diameter of 1.26 cm (0.5"), the length of 50 cm and the position resolution of 0.5 cm. The tubes were perpendicular to the scattering plane of the analyzers, so the position along the tube can be converted into scattering angle (a4). The three tubes were next to each other, so each tube saw neutrons with a slightly different energy [1]. The plane of the tubes is horizontal, but it can be tilted around the direction of the tubes by 10° to increase the covered scattering angle range of the analysers. The energy distributions of the neutrons detected by the different tubes are seen in the figure 4

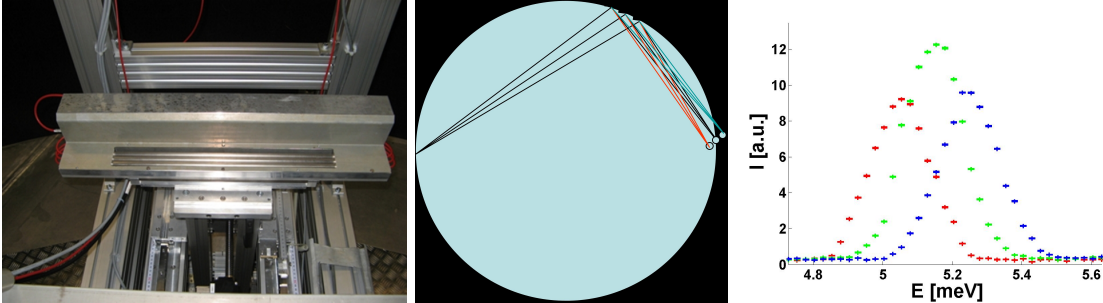


Figure 4: Left: photo of detector bank, middle: Rowland geometry with three different detectors, the different colors show different wavelengths, right: energy distributions in the different tubes simulated by McStas

3 Aligning and calibrating the prototype

3.1 Aligning of the frame

The horizontal position, orientation and height of the frame was set by using high resolution theodolite.

3.2 Mounting of the analysers

The sizes of the crystals are $5 \times 1 \text{ cm}^2$ or $7.5 \times 1 \text{ cm}^2$ depending on their quality (see table 2). This means that a small particle between the crystals with the size of $10 \mu\text{m}$ causes 0.06° tilting in the vertical distance if it is at the edge of the crystal. If it is closer to the middle, then the tilting is larger. To avoid these problems, before mounting we have carefully cleaned the whole frame, the silicon holders, the silicons, and the pyrographite crystals using ethanol and cotton wool. We have found that even at very careful cleaning the crystals are slightly misaligned (less than 0.2°) with respect to each other. Moreover, the mounting of PG crystals on the silicon, and also the mounting of silicons on the aluminium holder caused a bending of the silicon blades. The directions of the bending was the same at every mounting, thus we defined the direction of the graphite, that they are facing to the same direction as the fix part of the holders. In this way, the silicons remained bent close to the holder but systematic misorientation of the PG crystals disappeared. At the beginning we did not realize that a small force during fixation of the silicon holders cause a hole on them (where the fixing screw touched them). Later we have applied small cotton wool spheres as a soft spacer between the screws and the silicon holders, but often it was not useful (either they were too small, or the existing holes were in the wrong place). The holes caused large movement during fixation of the silicon holders making the precise alignment difficult. The complete change of silicon holders solved the problem and reduced the time of alignment below 15 min per analyser. At ESS CAMEA the holders will be fixed (precisely cut from an Al mono block) so there will not be such a problem.

3.3 Optical alignment I

After mounting of the PG crystals each blade was set to flat due to the easy checking by neutrons. For this first alignment we used an optical method. We used a laser which had a double lens system. The first lens

produced a large elongated spot, the second one was movable and focused the light into one spot. The focusing distance can be moved by moving the second lens. We put the laser close (30 cm) to the frame, and focused the laser reflected by the polished silicon holder to a screen 2.5 m far from the frame. Then we shifted the frame to see the reflected spot from each PG crystal. In this way the laser illuminated a large spot on the PG crystal, and the reflected spot on the screen showed the average surface normal of the PG. Checking each PG on the frame and also the silicon holders we got the relative orientations of the PG sheets. After this prealignment we checked the frames with neutrons. We found that this optical alignment is in agreement with the neutron measurements within the accuracy of 0.1° .

3.4 Measurement of the quality and orientations of the graphite sheets at POLDI

Poldi is designed as a strain scanner (see figure 2) but is also very powerful as a 1D Laue camera for characterization of graphite. the instrument has direct line of sight from a thermal moderator to the sample position so the sample is strongly illuminated. The scattered neutrons are detected by a 1d PSD, measuring the entire peak and tail at once through the different channels, thanks to the white beam.

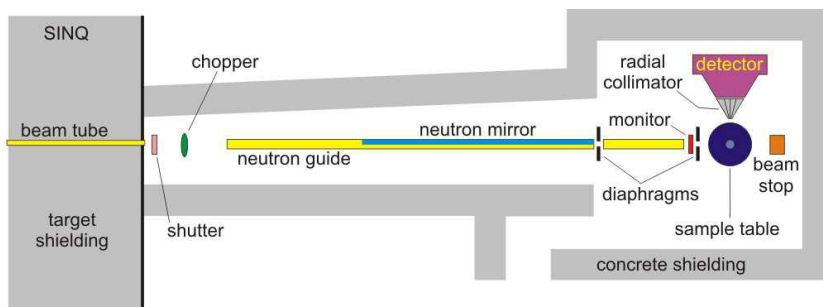


Figure 5: Layout of POLDI.

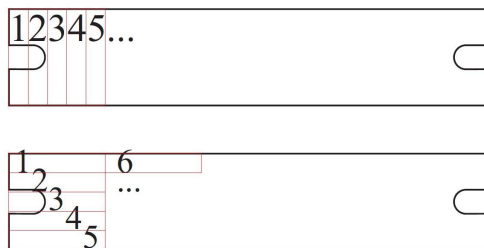


Figure 6: Scanning of the PG Schematic illustration of how the PG was scanned in the horizontal (Top) and vertical (bottom) direction.

For a strong scatterer like PG the measurements become very fast and it is possible to measure the reflection through a 20mm^2 slit opening in 5 seconds with plenty of statistics. This made it possible to scan across the graphite and measure the quality and homogeneity of each piece of graphite in a short time. 3 batches of graphite was investigated through 2250 individual measurements and the results for the first frame (mosaicity is $30'$) are plotted in figure 7

The measured intensities from one frame have variations below 5% if one disregards the points were holes or edges reduce the total PG volume.

The position variation is a combination of two things: The crystals are not perfectly aligned with each other and thus a jump is often seen between crystals. Within each crystal the center point increases systematically with higher scan points for the horizontal scan and show a systematic behavior with a periodic change corresponding to the PG sheets for the vertical case. This is because the frame has not been perfectly aligned with the robotic translation system and so the positions of the different graphite sheets next to each other are slightly shifted changing also the angles.

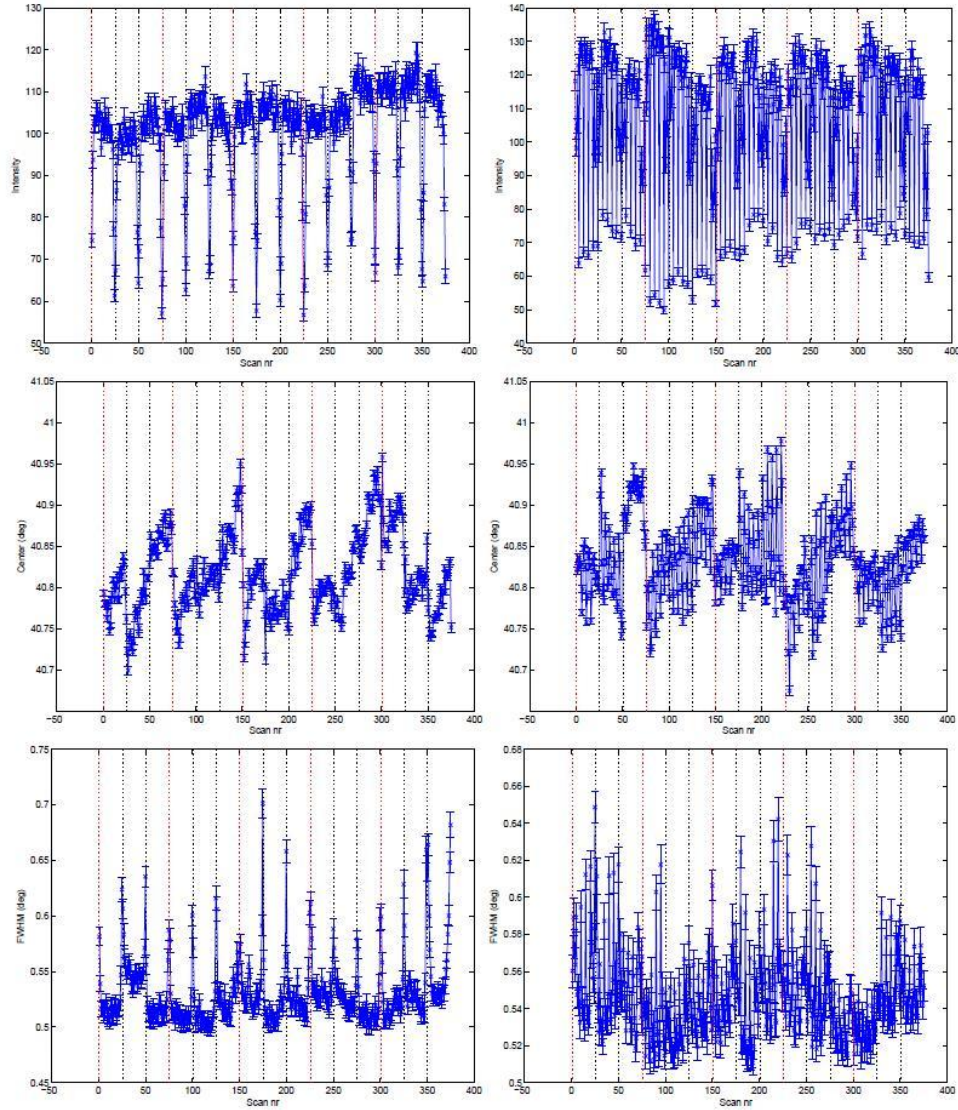


Figure 7: Summary of Poldi measurements The intensity(top), position(middle) and width(bottom) of the measured $(0\ 0\ 2n)$ reflections of one batch Panasonic PG with nominal mosaicity of $40'$ scanned horizontally (left) and vertically (right) The black dotted lines indicate a new crystal and the red dotted lines a new wafer. The chopper of Poldi was stopped in open position

Both intensity and position variations are mainly due to non-perfect calibration of crystal positions and should not raise any concerns in a study of the crystal quality, but when we look at the width of the reflection some effects can be seen. It is clear that some crystals are a few percent coarser than others but also that the FWHM increases close to the edges of the crystals. This is believed to be an artifact of the way the holes for mounting the crystals were drilled. While it does not pose a serious risk to the prototype performance it is worth considering other ways to produce these holes in the future. For example using lasers or acids instead of drilling, or fix the graphite with thin aluminum straps. Two other batches with $40'$ and $60'$ mosaicity were also investigated. The general behavior is comparable to the first batch but reflectivity of the $60'$ mosaicity is seen to be about 10% lower. The number is however not completely accurate (see chp. 3.5).

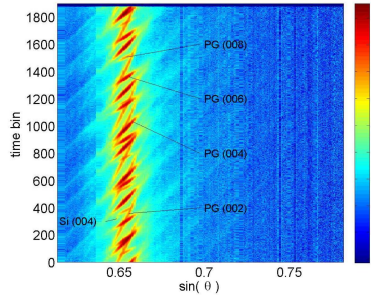


Figure 8: Poldi measurement running the chopper at 8000 RPM.

3.5 Limits of the information from POLDI

Despite the fact that Poldi gives an excellent fast overview of the graphite performance it is not designed for single crystal orientation or characterisation. The angular resolution is only 5% of the typical width of the measured PG peak, but the white thermal beam means that all of the (002), (004), (006) and (008) reflections are seen on top of each other. This should not influence on the position or the width of the peaks but it can make differences in intensity bigger than what is observed only for the (002) reflection since warmer neutrons have a higher penetration depth and thus will be more influenced by a lower reflectivity than cold neutrons where reflectivity saturation is almost reached. So while we can trust the behavior of the intensity graph we should not trust the actual numbers. We have made a measurement with chopper running at 8000 RPM also (see Figure 8). In this case the neutrons start from pulses, and the neutrons scattered slightly smaller or larger 2θ than the nominal value, thus they arrive sooner or later to the detector resulting in a tilted ellipsoid on the t - 2θ map. This tilting strongly depends on the wavelength of the neutrons, thus by checking the tilting angles of the peaks one can distinguish the different order reflections but the instrument loses the advantage of being fast, so other instruments designed for scanning a single reflections become more advantageous.

3.6 Measurements at Morpheus

For the alignment of the different pieces of graphite the two-axis diffractometer Morpheus at PSI was used. One frame at a time was mounted and rocking curves (rotations of the sample around the vertical axis) recorded for the different blades. The wavelength was $\lambda = 5.05 \text{ \AA}$. The horizontal and vertical orientation of all crystals was recorded with a combination of automated and manual movement of the frame, and small pieces of aluminum foil was inserted to coaligning the graphites. Unfortunately this also caused the Silicon wafer to bend, making alignment an iterative process. The measured orientations were compared with laser optic measurements and it was found to agree quite well. Since optical alignment is cheaper and faster this was afterwards used for prealignment before the final alignment on Morpheus.

3.7 Optical alignment II.

Since for the different measurement geometries the corresponding Rowland geometries were also different, after every change in geometry we had to realign the analysers. We pushed backward the upper frame of the prototype and, using a holder, we placed the laser at the sample position. We rotated the analyzer frame in the calculated position (to fulfill the Rowland condition) then we shoot one blade with the laser, and rotated the blade until the reflected laser beam reached the middle detector tube (see figure 9). We made it for all of the blades of the frame. We applied the same method for every frame starting from the back (the farthest from the sample selecting the largest final energy). After alignment, we have removed the laser, pushed every analyzer and detector 10 cm forward to the calculated position, and pushed the upper frame of the prototype to its original place.

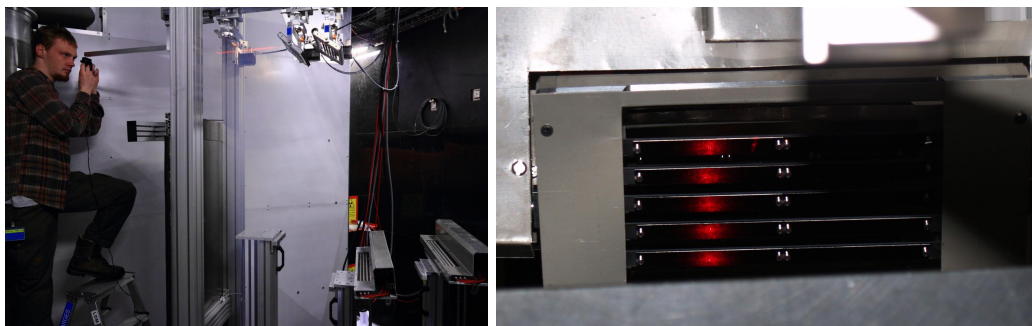


Figure 9: Left: optical alignment of Rowland geometry, right: well aligned analyser, the laser beam from the sample position is reflected down by one analyser crystal, the middle detector tube reflects it back, and all of the blades focuses the laser back just next to the sample position. The camera is next to the laser.

3.8 Calibration procedure

The calibration has two parts. At first the elastic line of vanadium shows the energy of the analysed neutrons. Both the primary and the secondary flight path is known, thus the energy can be calculated from the flight time. If there is a difference between the calculated (from the scattering angle of the analyser) and the measured energies, then the sample is not well centered vertically. The second step is the calibration of the scattering angle. This is done by using polycrystalline sample. For the correct calibration at least two Bragg-peak is needed in each detector bank.

The relative efficiency calibration is time consuming. Long vanadium measurement should give a locally flat signal (it shows a shape dependent slow decreasing as the scattering angle increases but it can be calculated). The sharp changes in the intensity are due to the gaps between the neighbouring analyser crystals, the holes (for the screws) and due to a non perfect electronics.

4 Measurements

4.1 Energy resolution measurements

To check the energy resolution we have carried out several measurements at different setups.

We made an energy resolution measurement using vanadium cylinder sample, and checked the energy distribution of the neutrons arriving to the three detector tubes facing to one analyzer. The sample height was 3 cm, the measurement was done in low resolution mode. Since we measured the elastic line, the speed and the energy was calculated simply from the total flight time. In the figure 10 we show the time resolutions in the three tubes facing to one analyser batch. Each tube is at slightly different take-off angle with respect to the others, thus the neutrons scattered to the different tubes have different energies. The flight path differences at the different tubes are less than the total mean flight path differences of the instrument, thus the time distributions can be directly converted to energy distributions. The three different energies (even at this low resolution) are clearly discernible. The McStas simulation and the measurement fit well.

At the beginning we used two analyzer banks, two vanadium cylinders in different size, and two different primary resolutions. We have set the analyzers to select 5 and 7 meV. The sample-analyser distances were 1.2m and 1.35 m respectively, the analyzer-detector distances were 1m. We analyzed separately the three tubes of each analyzer. In the figure 11 the different primary resolutions (left and right side), and the effect of different sample sizes are shown.

We have made measurements with three different analyzers also. The data was obtained at high primary resolution, using V sample with the height of 1 cm. The energies were 4 meV, 5 meV and 7 meV at the different analyzers. The sample-analyser distances were 1.28 m, 1.45 m, and 1.57 m, while the analyzer- detector distances were 1.23 m 1.35 m and 1.42 m respectively. We used three kind of different analyzers with 0.65° , 1° and 1.3° mosaicity. As it is seen in the figure, the mosaicity has no effect on the resolution, confirming our simulations [2] that the energy resolution is due to distance collimation.

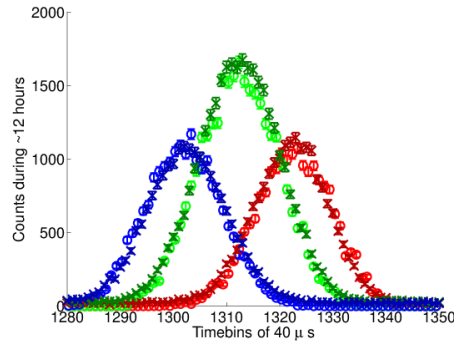


Figure 10: Time distributions in the different tubes facing to one analyzer. Circles: measurement, X: McStas simulation

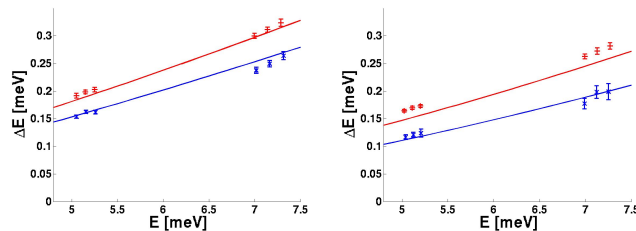


Figure 11: Elastic energy resolution (symbols) and the calculated energy resolution (solid lines) at different primary resolutions (blue: high resolution, red: low resolution) and sample heights (left 3 cm, right 1 cm).

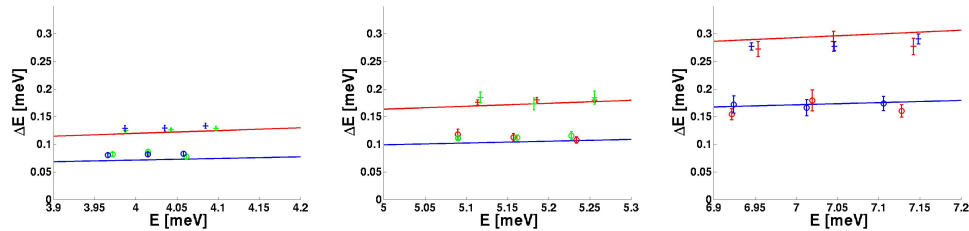


Figure 12: Elastic energy resolution (symbols) and the calculated energy resolution (solid lines) applying different primary resolutions and analyzers with different mosaicities (red: blue: green:).

4.2 resolution ellipsoids

We measured the resolution ellipsoids of the prototype at different setups. We used the 002 reflection of the pyrographite sample. At the given q -value the Bragg-peak can be reached only in one analyzer selecting 7meV final energy. In each measurement we made an omega (ω) scan around the Bragg position of the sample. One measurement of the scan gave three parabolic surfaces close to each other in the q - ω space (taking into account that the three tubes looking to the analyser collect neutrons with slightly different final energies). We chose the q_x -direction parallel to the corresponding reciprocal lattice vector, q_y is perpendicular to it. We summed up the data in the three dimensional $q - \omega$ space, and in the figures below we show the data projected to the planes ($E=0$, $q_x=0$ and $q_y=0$).

The figures 13 - 14 shows the measured and calculated ([2]) resolution ellipsoids. In the Figure 13 - 17 the resolution ellipsoids measured under different conditions are seen. Each figure is normalized to its maximum intensity, so the color bars are the same for each figure. In the figure 13 and 14 the difference between the measurements made using a sample with high and low mosaicity (0.5 and 1.5 degree) is clearly seen. (The finite mosaicity of the sample causes a smearing in the q_y direction). In the figures 15 and 16 the effect of the mosaicity of the analyser (0.6 and 1.3 degree respectively) is seen. The tangential resolution is increasing with the mosaicity, while the energy resolution does not change. The last (17) figure the worse q -resolution is

the effect of the high mosaicity of the analyzer, while the energy resolution get worse due to the low primary resolution. We fitted the measured resolution ellipsoids with three-dimensional Gaussians. The calculated and fitted parameters of the resolution ellipsoids are shown in the table 3. The reduced χ^2 values of each fitting shows that the 3D resolution is not exactly Gaussian, the large differences (mainly at the first two measurements) need more careful investigations.

measurement #	σ_x	σ_y	σ_z	χ	ϕ	ω	χ^2
1-c (Fig. 13)	1.37	3.16	8.83	26.2	168.0	49.7	
1-m	1.26	4.18	9.02	26.7	148.2	64.8	71.1
2-c (Fig. 14)	1.92	4.69	8.94	29.9	139.1	57.0	
2-m	1.79	7.17	9.59	42.1	116.5	81.7	180.2
3-c (Fig. 15)	1.87	4.43	6.12	39.8	129.2	68.6	
3-m	2.09	3.94	5.61	52.2	111.4	86.3	6.7
4-c (Fig. 16)	1.88	4.56	6.18	42.5	126.5	71.2	
4-m	1.65	4.19	6.07	65.8	110.8	93.0	2.3
5-c (Fig. 17)	1.93	4.84	8.49	34.0	129.6	64.7	
5-m	1.72	6.00	8.13	43.0	117.5	81.7	7.0

Table 3: Parameters of the resolution ellipsoids calculated values: c, measured values: m, the main axes of the ellipsoid are: s_x, s_y, s_z , the orientation is given by the Eulerian angles, like in a diffractometer: $\omega \chi \phi$. The last column is the reduced chi-square of the fitting. The calculated errors of the fitted parameters are always below 1%

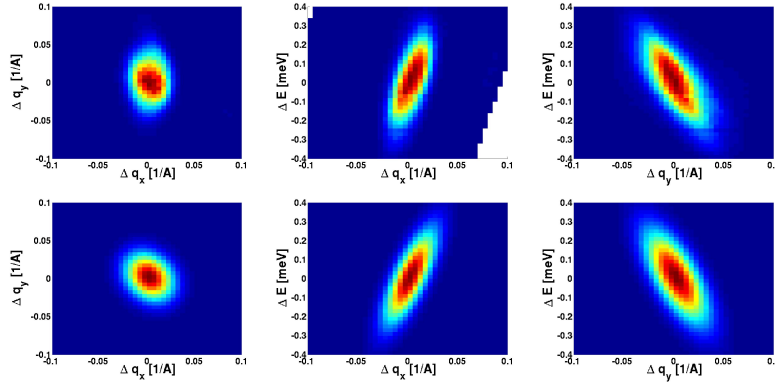


Figure 13: Resolution ellipsoid using high quality (mosaicity is 0.5°) graphite as a sample. The sample height is 1 cm. We used low primary resolution.

4.3 Background and spurions on the prototype

In the Figure 18 the time structure of the detected intensity coming from vanadium sample is shown. During the measurement we did not use any kind of shielding except a boronated plastic sheet to block the direct view of the sample from the detectors. Around the elastic peak a roughly flat background is visible. This background is roughly 1% of the peak height, and the total intensity is 1/3 part of the intensity of the elastic peak. Outside of the opening time of the order sorting chopper there is only a negligible background. This means that the background comes from the sample vicinity and from the MARS tank. The intensity of the inelastic scattering of the vanadium is smaller and more structured, however it can give a small part of the signal over the elastic incoherent intensity. There are two other sources of the background: the inelastic scattering on the air around the sample, and the secondary scattering of the scattered beam in the MARS tank (on the air and on the other structural elements of the prototype). The air scattering in the MARS tank is large (20-25% depending on the actual flight path and on the humidity), but it is not enough to give the whole measured intensity.

Later we improved the shielding by applying Cd walls separating the different analyser-detector units, side walls (figure 19), vacuum-box around the sample, kadmium around the vacuum box defining the vertical

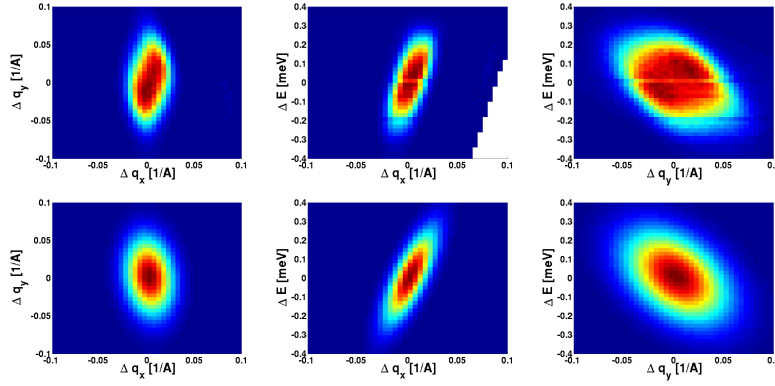


Figure 14: Resolution ellipsoid using low quality (mosaicity is 1°) graphite as a sample. The sample height is 1 cm. We used low primary resolution.

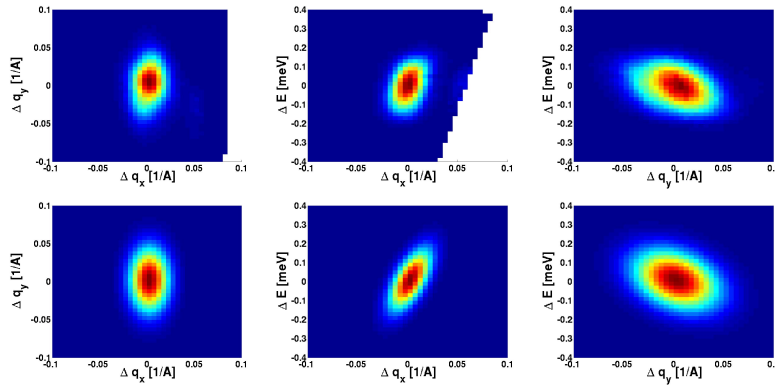


Figure 15: Resolution ellipsoid using low quality (mosaicity is 1°) graphite as a sample. The sample height is 1 cm. We used high primary resolution.

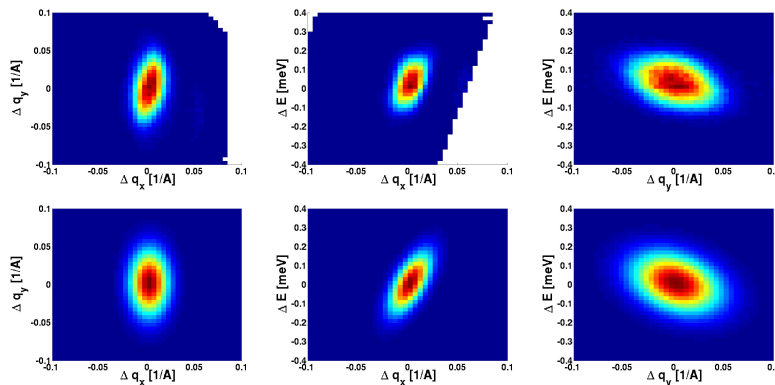


Figure 16: **Resolution ellipsoid** using low quality (mosaicity is 1°) graphite as a sample. The sample height is 1 cm. We used high primary resolution. Analyser mosaicity is 1° .

divergence, and also cd beam stop to absorb the neutrons passing the three analyser. Finally the background elastic peak ratio went below 10^{-4} , and the inelastic signal coming from the vanadium sample (and/or from the analysers) appeared as a decreasing background (Figure 20). We made measurements under argon atmosphere in the MARS tank, at good shielding Ar caused a slight decreasing of the background level.

The other source of background is the strong Bragg-peak coming from the sample. It is partly scattered

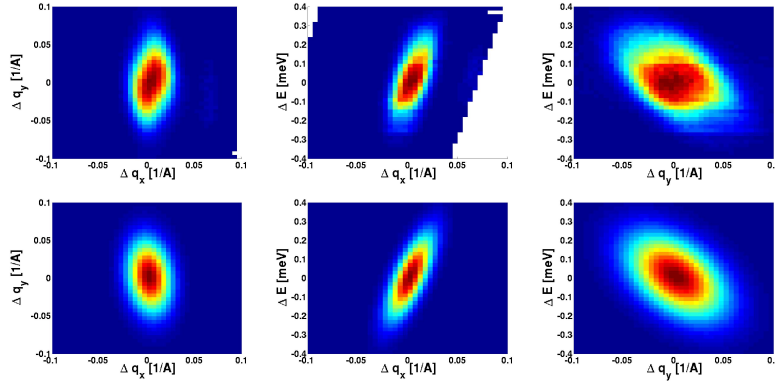


Figure 17: **Resolution ellipsoid** using low quality (mosaicity is 1°) graphite as a sample. The sample height is 3 cm. We used low primary resolution. Analyser mosaicity is 1.3°

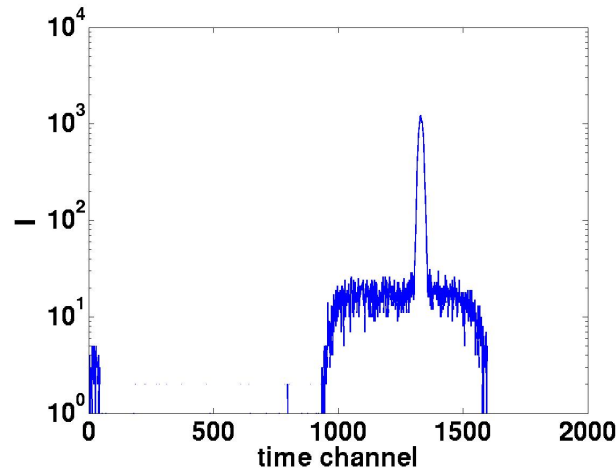


Figure 18: Time dependent signal from V sample (measurement without shielding)



Figure 19: Different shielding parts of prototype

by the air, causing an orientation dependent background, and it can be scattered inelastically by the analyser. In the two video attached to this report the intensity distribution is seen in the q - ω space measured near the (002) reflection of a pyrographite sample. The first measurement (PG2_XE.avi) was done at room temperature while the second one (PG6_XE.avi) was done at 5K. The data was collected to check the resolution ellipsoid but some part of the low energy phonon surface is seen on the first video which disappears at 5K. However, a strong spurion appears in both measurement caused by the Bragg peak appearing in the direction of the prototype. Other investigations on the pyrographite show that this spurion is due to the phonon scattering, and it can be

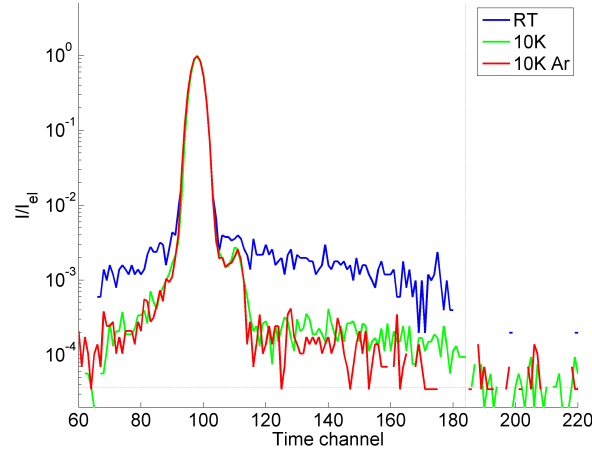


Figure 20: Time dependent signal from room temperature and cooled V sample, and the effect of the Ar atmosphere. On the right side the electronic background is shown.

reduced by cooling the crystals [3].

4.4 Inelastic measurement on $LiHoF_4$

We have made an inelastic measurement on $LiHoF_4$ sample at four different temperatures. $LiHoF_4$ has strong crystal field excitations at low temperature. The sample consist many plate-like large single crystal stacked together. The data obtained at 14Hz base frequency, with low primary resolution within ca 3h at each temperature. In the left part of Figure 21 the measurements at four different temperatures are seen. We made the same measurement at Focus (direct TOF instrument). After correcting with difference of the detected angular area, we get similar intensity but much better resolution (right part of Figure 21. To compare the two measurements, the only data treatment was the summing up on energy channels, normalizing for the time, and applying the correction factor for the detected angular area. The green line shows the summed data on the 9 tubes, while the red line shows the data normalized to the number of tubes also. With the angular coverage of the ESS CAMEA at the prototype we could get roughly three times more detected intensity than at FOCUS.

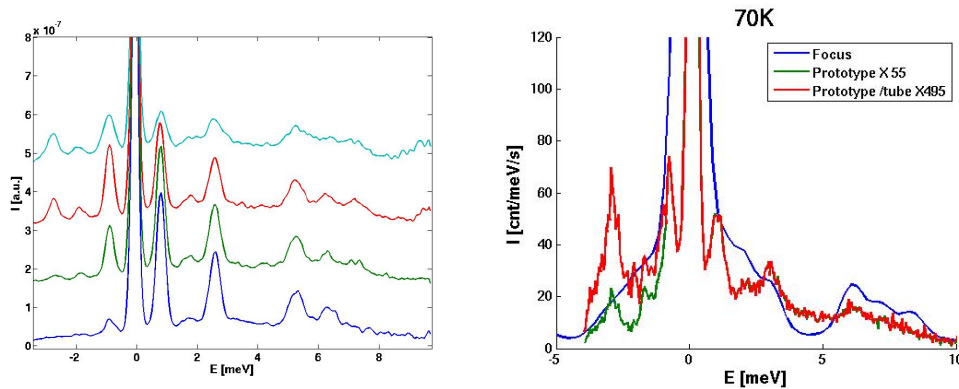


Figure 21: Inelastic measurement on $LiHoF_4$ sample. Left: measurement in the prototype at 4K (blue), 25K (green), 25K (red), and 70K (magenta). The base line of each data is shifted for the sake of visibility. Right: Comparison of measurements at the prototype and at Focus. The counts summed in energy bin and normalized to monitor.

4.5 Inelastic measurement on $YMnO_3$

We made inelastic measurement on $YMnO_3$ single crystal also. To reach the Bragg peaks of the crystal at the given scattering angle (around 60°) we used higher final energies (4.8 meV, 6.1 meV, 7.5 meV). The sample was cooled to 40 K. The data collection took roughly one day. In the Figure 22 the magnon dispersions are visible at 8meV (left) and at $q_y = 2.35 \text{ \AA}^{-1}$ (right). The data obtained during one day in the given q, ω volume is equivalent to 2% of ESS CAMEA's coverage counting for 8s, at the same resolution.

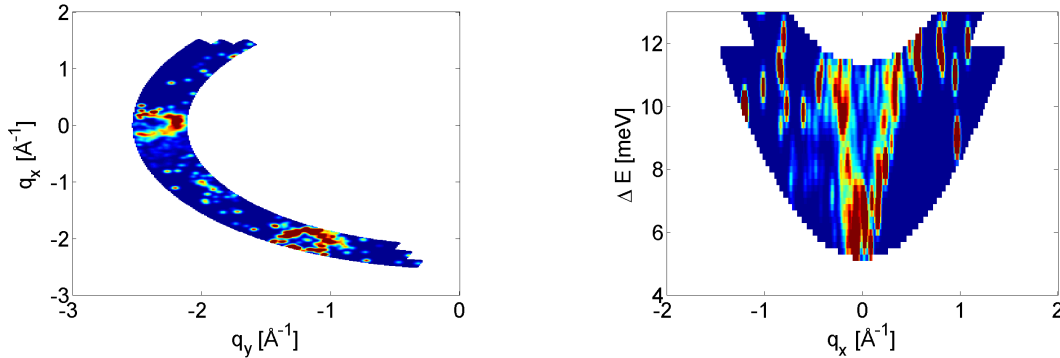


Figure 22: Magnon dispersion on $YMnO_3$ single crystal at 40K. Left: q -plane at $E=8$ meV, right: q_x - E plane at $q_y = -2.35 \text{ \AA}^{-1}$.

5 Conclusions

During the installation of the prototype, the alignment and the measurements were obtained, we got answer to several important questions.

The most important result is that the CAMEA concept is working, and the idea to analyse several energies using one analyser is also working. We have validated the analytical calculations. The analytical model of the instrument is precise enough to use it for the optimization of the instrument and to check the consequences of using different geometries. We found a possible source of a very strong spurion appears when a Bragg peak coming from the sample goes through the analyser. It can be strongly reduced by the cooling of the analysers. The the background is less than 10^{-4} times the elastic line of cooled vanadium. We proved also that a slight phase shift applied on the second chopper change the resolution of the front end without changing the base frequency. We learned what are the drawbacks of the method i.e wavelength dependent effective pulse duration. We found also that at the ESS, due to the large source - first chopper distance, we will see similar effects when using not too strict pulse shaping however it can be used to decrease the general $E^{1.5}$ dependence of the incident energy resolution.

From the practical side, we worked out how to mount the graphite sheets onto the silicon to achieve the less differences between the different crystals. We have proved that the optical alignment of the PG crystals is precise enough for preorientation.

References

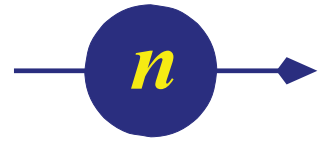
- [1] J.O. Birk et al, in preparation for Nucl. Instr. Meth. A (2013)
- [2] M. Marko Analytical calculations for CAMEA
- [3] J. Larsen Pyrolytic Graphite Experimental Results



Technical University of Denmark



McStas



CAMEA

Pyrolytic Graphite Experimental Results

Author:

J. Larsen



PAUL SCHERRER INSTITUT



ÉCOLE POLYTECHNIQUE
FÉDÉRALE DE LAUSANNE

Content

1 Introduction	2
2 PG Alignments	2
2.1 Tails	2
2.2 Lorentzian Tails and Mosaicity	3
2.3 Further Investigations on RITA II	3
3 Reflectivity and Transmissions Measurement	5
4 Cooled PG Experiments	7
4.1 Experimental Results from DMC	8
4.2 Experimental Results from RITA II	10
5 Outlook	12

1 Introduction

The ultimate goal of the CAMEA concept is to reach a high analysing efficiency. This can be achieved in two ways. An analyzer crystal with medium mosaicity will scatter neutrons with slightly different energies in different directions. Given a sample which is small enough i.e. geometrically limited resolution, then using several detectors next to each other will produce slightly different energy distributions in the different detectors. With one such analyzer bank it is possible to measure several energies. The second way in the CAMEA concept is, many analyzers are placed behind each other selecting different energies. This report deals with the different aspects of the Pyrolytic Graphite (PG) analyzers for CAMEA. In section 2 of this report we present our finding on aligning such a setup of crystals.

With CAMEA, we make use of the finite mosaicity of the analyzer crystals. The broader the mosaicity of the analyzer, the wider the energy band one can measure. However the reflectivity of the analyzer crystal generally decreases as the mosaicity increases. To be able to optimize the reflectivity/mosaicity for the CAMEA concept we checked the peak reflectivities and the integrated reflectivities of 1mm thick PG sheets with different mosaicities. Putting many analyzer crystals behind each other requires that the transmission of the crystals is high for the energies analysed by the others. PG has negligible absorption and low incoherent scattering. However, it is powder-like in the (a,b) -plane. Thus, due to the (hkl) scattering where h or k is non-zero PG has a different orientation and energy dependent extinction. To select the optimal energies for CAMEA, we have measured the transmission of PG in different orientations and for different energies. These measurements are presented in section 3 of this report.

PG is a soft material and it has low energy phonon branches in a large q-range that can cause undesirable phonon contamination of the analysed beam. This phonon contamination can degrade the resolution [1] or produce spurious around strong Bragg peaks from the sample. In section 4 of this report we measured the diffraction map of PG at different temperatures and present our first measurement of the energy width of PG(002) as function of temperature. PG is a hexagonal crystal which is a powder in the (a,b) -plane and a single crystal in the c -direction. The lattice parameters are $a=2.46 \text{ \AA}$ and $c=6.71 \text{ \AA}$.

2 PG Alignments

For the alignment of the different pieces of graphite the two-axis diffractometer Morpheus at PSI was used. One frame at a time was mounted and rocking curves (rotations of the sample around the vertical axis) recorded for the different blades. The wavelength used was $\lambda = 5.05 \text{ \AA}$. The horizontal and vertical orientation of all crystals was recorded with a combination of automated and manual movement of the frame, and small pieces of aluminum foil was inserted to co-align the graphite crystals. Unfortunately this also caused the Silicon wafer to bend, making alignment an iterative process.

The measured orientations were compared with laser optic measurements and it was found to agree within 0.1° . Since optical alignment is cheaper and faster the optical method was generally used afterwards for pre-alignment, with the final alignment achieved on Morpheus.

2.1 Tails

During the Morpheus measurements different tails were observed around the PG(002) reflection (see figure 1). Since Morpheus is a diffractometer it was impossible to determine whether these were phonons, spurions or some crystalline tails, though if it was crystallites it would need to be a systematic variation in both orientation and d-spacing. These tails were afterwards explained in detail using RITA II (see section 2.3).

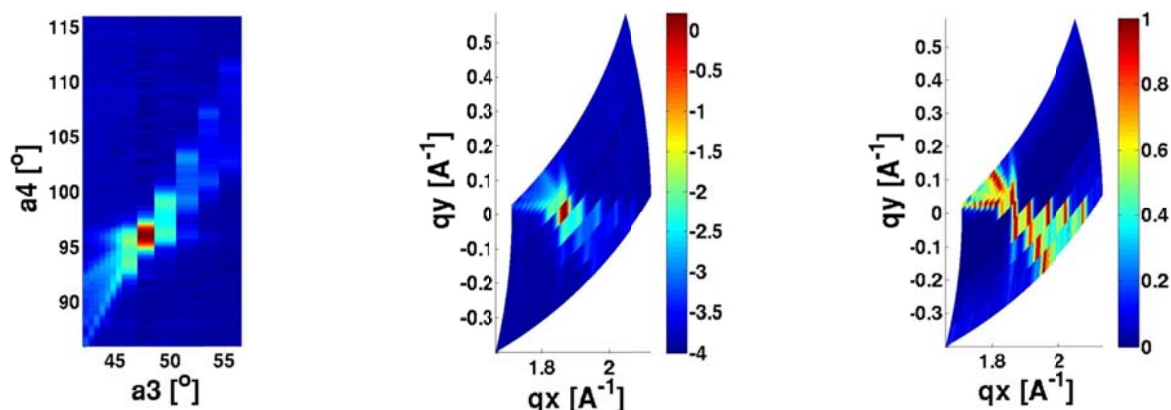


Figure 1: Inelastic stripes around the Bragg peak measured on Morpheus. Left: data in the A3-A4 map in logarithmic scale, middle: data in the q -space (assuming elastic scattering) in logarithmic scale, right: data in the q -space, each A4-scan is normalized to their maximum for the better visibility.

2.2 Lorentzian Tails and Mosaicity

The (002) peak shape of PG is not a perfect Gaussian but has Lorentzian tails. The tails are often 2-3 orders of magnitude below the main peak but they still limit the performance. However, during the measurements of the different crystals it was seen that a sample dependence exists, so that PG with coarser mosaicity also had stronger Lorentzian tails (see Figure 2), suggesting a structural effect.

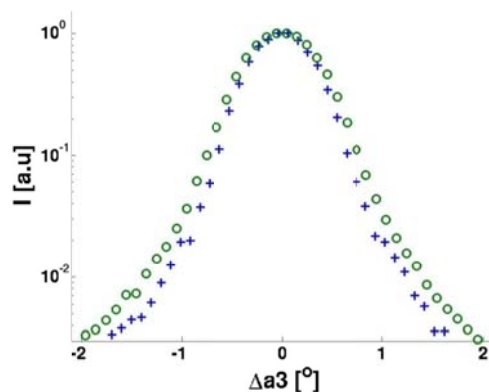


Figure 2: Lorentzian tails of PG (002) measured on Morpheus. The mosaicities are: 0.5° (blue crosses), 0.6° (green circles). The measured intensities are normalized to the peak height.

2.3 Further Investigations on RITA II

To investigate the tails seen on Morpheus, the cold multiplex triple axis spectrometer RITA II at PSI was used. At the beginning we repeated the measurement performed at Morpheus. RITA II was used in diffraction mode without analyzer, thus, the two-dimensional detector gave the intensities at different scattering angles. Figure 3 shows that the signal out of the Bragg peak is also clearly seen on Rita. Then we made a k_f scan in imaging TAS-mode (each analyzer blade analyses the same energy at different A4 values and reflects the neutrons to different places of the 2D PSD) to check whether the signal we get is inelastic.

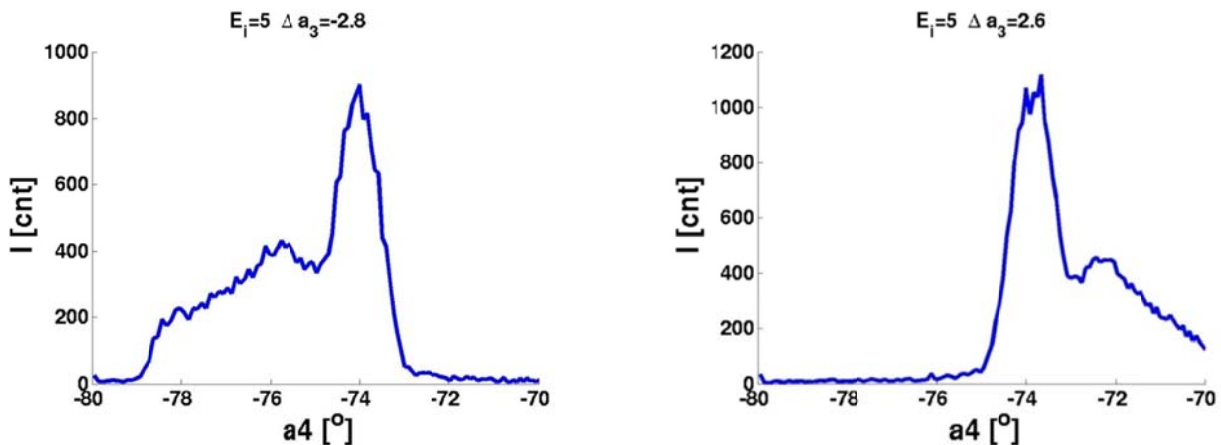


Figure 3: Diffraction measurements at Rita. ΔA_3 means the offset from the Bragg position. The high intensity peak at 74° is the tail of the Bragg peak.

In the figure 4 the result is seen in the three-dimensional (\mathbf{q}, ω) space. The scan shows that at the left side of the Bragg peak the trajectories of the scans at different A4 values are touching the dispersion surface of the graphite phonons. At larger A4 offset the trajectory meshes the surface, while on the other side of the Bragg peak the trajectories go to too low energies, so they do not show any signal.

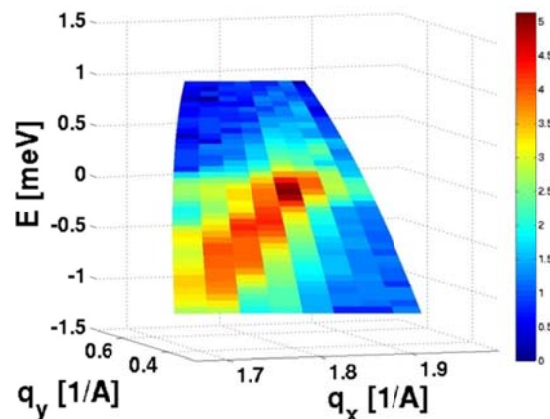


Figure 4: k_f -scan on PG sample near the Bragg peak. The nine different A4-values are given by the nine different analyzer blades of RITA II.

Pyrolytic Graphite, an experimental report for the ESS CAMEA

This result proves that the stripes seen in the Morpheus measurement are inelastic signals. For diffraction measurements there is no analyzer, so one sees the integrated intensities of these k_f -scans at different A3/A4 values causing strong signals. Thus, these spurious need further investigations.

We have also checked the mosaicities of the different PG crystals (in TAS imaging mode). In the figure 5 these measurements are seen at 300K, while in the figure 6 the comparisons are seen between the measured rocking curves at 300 K and 5 K. The results show that the Lorentzian tail of the Bragg peak is stronger if the mosaicity of the graphite has higher value, and also show that the Lorentzian tail of the Bragg peak is elastic and temperature independent.

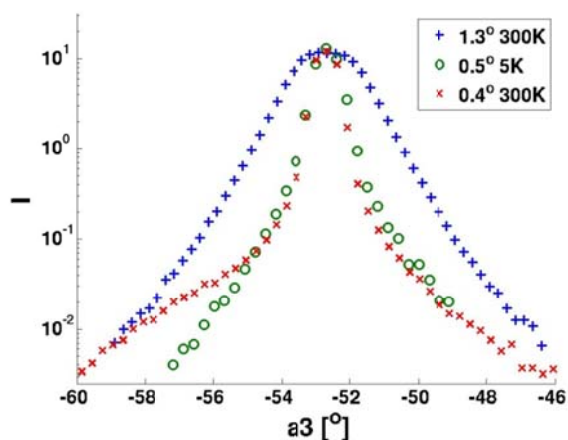


Figure 5: Rocking curves of the different PG analysers. On the left side of the third dataset (mosaicity is 0.4°) shows increasing background because that sample was measured without cryostat.

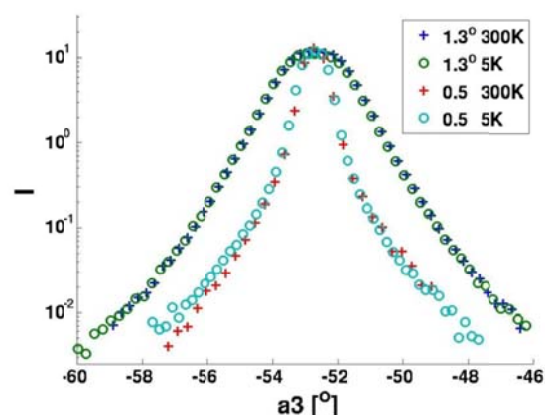


Figure 6: Temperature dependence of the tails of Bragg peaks.

3 Reflectivity and Transmission Measurement

We have made reflectivity measurement on the PG sheets of the prototype at Morpheus. We used a silicon monochromator, a very well collimated incident beam and practically no collimation on the reflected beam. The wavelength was 4.67 \AA and the scattering angle was 44.17° .

mosaicity from Xray measurement	0.4	0.5	0.7	1.3
Peak reflectivity	0.70	0.68	0.63	0.48
Relative integrated reflectivity	1.00	1.11	1.30	2.01
fit result: A	0.74	0.70	0.63	0.48
fit result: FWHM	0.65	0.75	1.01	2.06

Pyrolytic Graphite, an experimental report for the ESS CAMEA

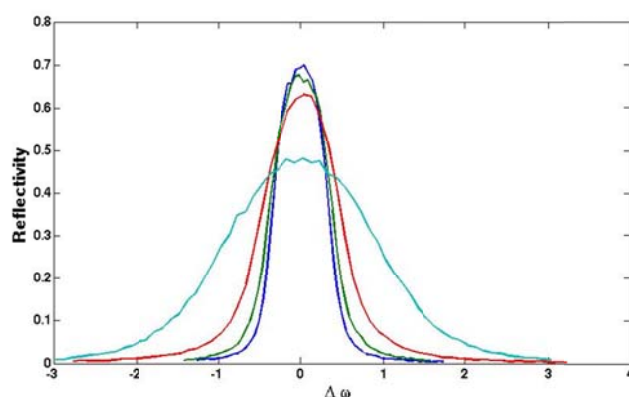


Figure 7: Measured rocking curves of the PG sheets with different mosaicities.

The difference between the measured maximum reflectivity and the fitted value indicates that there is a saturation effect at high reflectivity values.

We made a transmission measurement of the PG with the mosaicity of 0.7° at the MARS instrument at PSI. We used the monitor placed after the sample position, and a 2 mm slit just before the sample. We collected the data in two parts, between 2.6 and 9 meV and between 5.11 and 35 meV. In each chopper setup we rotated the sample between 30° and 75° .

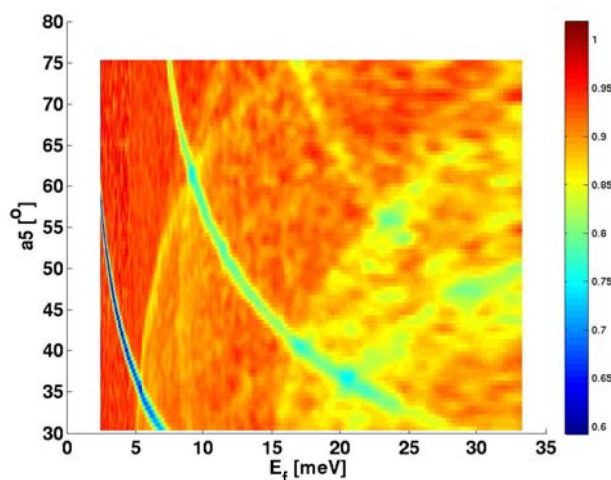


Figure 8: Measured orientation and energy dependent transmission of a 1mm thick PG sheet.

This measurement shows the energy and orientation dependent transmission of the PG. At the designing of the prototype we can calculate the reduction of intensity at a given energy after the analyzers. This helps to define the optimal set of analyzed energies for CAMEA.

4 Cooled PG Experiments

In Refs. [1-3], it was shown that cooling of pyrolytic graphite (PG) analyzer crystals to cryo-temperature greatly improved the signal-to-background ratio (SBR), on the indirect time of flight spectrometers IRIS and OSIRIS at the ISIS facility, see

Pyrolytic Graphite, an experimental report for the ESS CAMEA

Figure 9 and Table 1. The SBR ratios quoted in Table 1 were evaluated by first integrating the area around the elastic line (“the signal”) from the PG(002) reflection in the raw time spectra. Subsequently the background was found from a similar calculation sufficiently far away from the elastic line (“the background”).

For comparison with the geometry of CAMEA, note that the OSIRIS analyzer bank, located 0.7m in front of the detector, consists of 9040 $10 \times 1 \times 1$ mm³ PG crystals with a mosaic spread of 0.8° . The instrument operates with a scattering angle, $2\theta \approx 170$ degrees. The OSIRIS and the IRIS analyzer banks are cooled using three 1.5 W Sumitomo closed cycle refrigerators (CCR’s) [2].

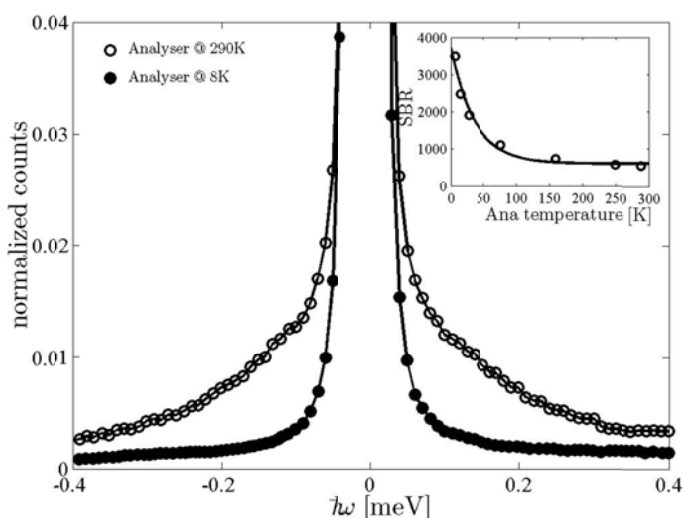


Figure 9: Suppression of the phonon-induced diffuse scattering on the OSIRIS spectrometer. The data was collected with Vanadium at 290K on the sample position. The insert shows the dependence of the SBR on the analyzer temperature. The line shows a fit to an exponential function. Figure adapted from Ref. [1].

	$T_{\text{sample}} = 300\text{K}$	$T_{\text{sample}} = 10\text{K}$
	$T_{\text{analyzer}} = 300\text{K}$	$T_{\text{analyzer}} = 10\text{K}$
OSIRIS	500:1	3350:1
IRIS	350:1	3250:1

Table 1: Signal-to-background ratios for various combinations of sample (vanadium) and analyzer temperatures. Adapted from Refs. [1,2].

Our previous work, see sections 2 and 3, indicates that PG has strong scattering from phonons (1% close to the Bragg peak). In order to assess if this will be a problem for the proposed CAMEA on ESS, which does not operate as close to the backscattering condition as do OSIRIS and IRIS, we have studied the scattering from a PG sample using the cold powder diffractometer DMC (SINQ, Switzerland). We use the data from this experiment to gain insight into the different contributors to the scattering from PG, and mainly around the PG(002) reflection. The results of this experiment are described in section 4.1.

To evaluate the temperature dependence of the signal-to-background ratio for a non-backscattering instrument, we performed initial inelastic neutron scattering experiments on a standard vanadium sample at the RITA II triple axis spectrometer (SINQ, Switzerland), which was operated with a cooled PG crystal at the analyzer position. The preliminary results of this experiment are described in section 4.2.

4.1 Experimental Results from DMC

DMC has a "Banana" type multi-detector, which consists of 400 BF₃ counters and covers scattering angles from 13° to 93°. The instrument is equipped with a focusing monochromator made from 5 PG crystals. A PG filter is installed in the incident neutron beam path. Rotating a single crystal sample on a powder diffraction instrument like DMC yields a reciprocal space map of the horizontal scattering plane integrated over the final neutron energy.

In our experiments the incident neutron wavelength was 2.45 Å. The sample was a single 50x10x1 mm³ PG crystal of mosaicity 0.5°. It was mounted in vertical position on a thin Aluminium sheet (thickness ~1mm) and inserted into a cryostat. Subsequently, the sample was rotated through an angular range of 180 degrees and the scattering recorded as a function of sample rotation angle, θ , and scattering angle, 2θ .

We performed measurements at 10K and 290K. The data are shown in figure 10 and 11, respectively, where they are plotted versus Q_x and Q_y . Here Q_x is parallel to the crystallographic c-axis of pyrolytic graphite and Q_y is an in-plane direction. The data have been symmetrized to cover 360 degrees in sample rotation angle, θ , and are shown on a logarithmic color scale (\log_{10}) for clarity.

Before turning to the scattering related to phonons in graphite, let us first describe the qualitative features of the remaining data starting with sharp Bragg peaks that can be attributed to PG: (i) The PG(002) reflection is clearly visible at $(Q_x, Q_y) = (2, 0)$ and $(-2, 0)$. (ii) Also seen are reflections with $(Q_x, Q_y) = (2, 1)$, $(1, 1)$ and $(0, 1)$. (iii) Second order reflections are suppressed by the filter and we observe only faint contributions at $(-3, 0)$ and $(-1, 0)$. (iv) Further, we observed four peaks of unknown origin around $(\pm 3, \pm 0.73)$, with intensities similar to the second order PG(002) reflections. (v) Curved lines going through the PG(002) reflections in the $A_4/2\theta$ direction can be observed at both temperatures. These are due to overloading of the detectors when the intense PG(002) peak is in the reflection condition. (vi) A powder ring is visible at the same scattering angle 2θ as the PG(002) reflection. The intensity of the ring is roughly five orders of magnitude smaller than the PG(002) reflection. We believe that this feature comes from powder remaining on the crystal surface from the production or from the process of drilling holes in the PG piece for mounting purposes. (vii) In addition, the maps in Figures 10 and 11 show lines of scattering in the (00l)-direction connecting the Bragg peaks. These lines do not have any detectable temperature dependence. While we don't at present have a clear understanding of the origin of these lines, we speculate that they may be caused by incoherent inelastic scattering from the monochromator followed by Bragg scattering from PG(002).

Finally, we turn to the diffuse scattering contributions around the PG(002) reflections. These are very clearly visible in the 290K data set (Fig. 11), where one also sees the tails of similar diffuse contribution centered at PG(004). At 10K (Fig. 10), however, the part of this diffuse scattering contribution on one side of the PG(002) reflection (e.g. at negative values of Q_y with respect to the $(Q_x, Q_y) = (-2, 0)$ reflection) has completely disappeared while the part on the opposite side (at positive values of Q_y with respect to the $(Q_x, Q_y) = (-2, 0)$ reflection) still carries spectral weight. If the diffuse scattering is due to phonons, we would associate the former with neutron energy gain processes, which are suppressed to zero at low temperature due to the Bose occupation factor in the phonon cross-section, and the latter with neutron energy loss processes, which are suppressed too, but not fully. Figures 12 and 13 illustrate how the intensity suppression of the diffuse scattering is anisotropic in angular (and therefore in momentum) space.

Pyrolytic Graphite, an experimental report for the ESS CAMEA

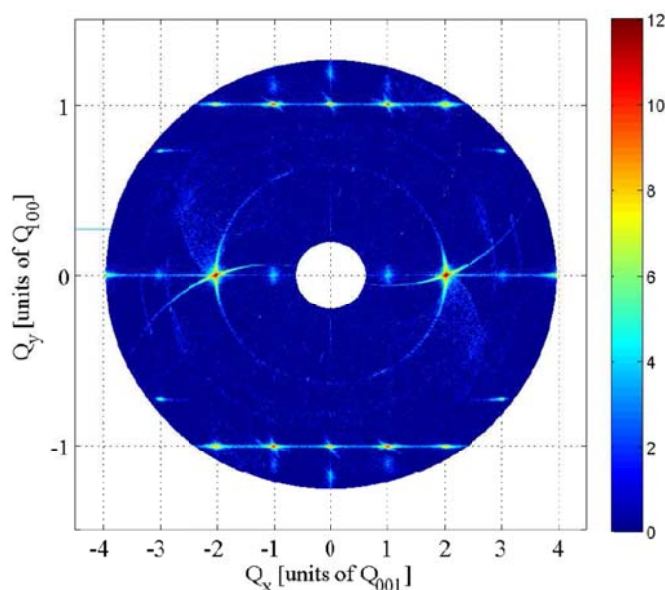


Figure 10: Reciprocal map of PG at 10K. The color scale is logarithmic (\log_{10}).

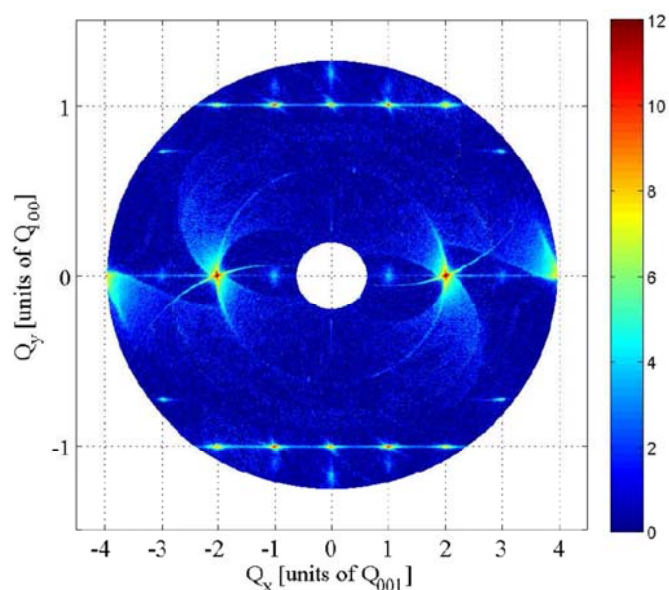


Figure 11: Reciprocal map of PG at 290K. The color scale is logarithmic (\log_{10}).

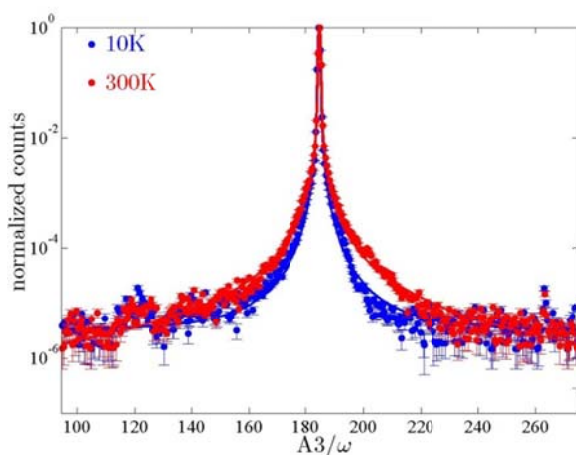


Figure 12: Constant-A4 scans at 10 K and 290 K, integrated over $\pm 1^\circ$ around PG(002). Towards higher angles significantly more scattering is observed at 290K.

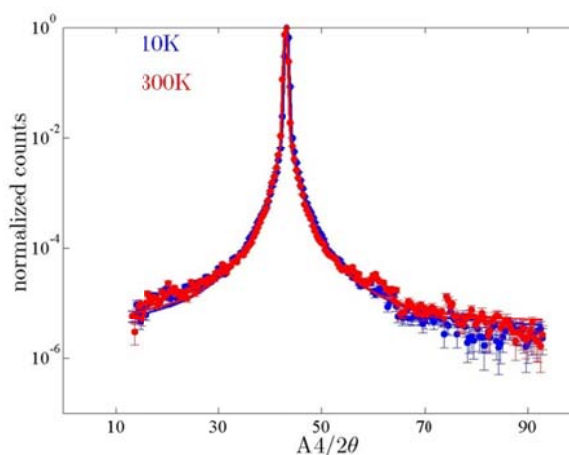


Figure 13: Constant-A3 scans at 10 K and 290 K, integrated over $\pm 1^\circ$ around PG(002). Almost no difference is observed.

To prove that the observed diffuse scattering is indeed due to phonons, we performed McStas simulations. DMC was modelled using the built-in McStas instrument PSI_DMC (version: May 7th 2008). At present a dedicated McStas component for phonons in pyrolytic graphite does not exist. Instead we used the Phonon_simple component, which

Pyrolytic Graphite, an experimental report for the ESS CAMEA

models acoustic phonons in FCC crystals and takes (among other parameters) temperature and the velocity of sound as entries. Since graphite is hexagonal, such a model will clearly not give an exhaustive account of all the observed scattering in PG (Figs. 10 and 11). However, for our purposes a qualitative comparison is sufficient. We chose a lattice spacing of $a_{\text{FCC}}=6.71 \text{ \AA}$, corresponding to the c-axis lattice constant of PG, and a velocity of sound $c_{\text{FCC}}\approx 26 \text{ meV \AA}$, which is a reasonable value for phonons travelling along the c-axis. The results of our simulations are shown in Figure 14.

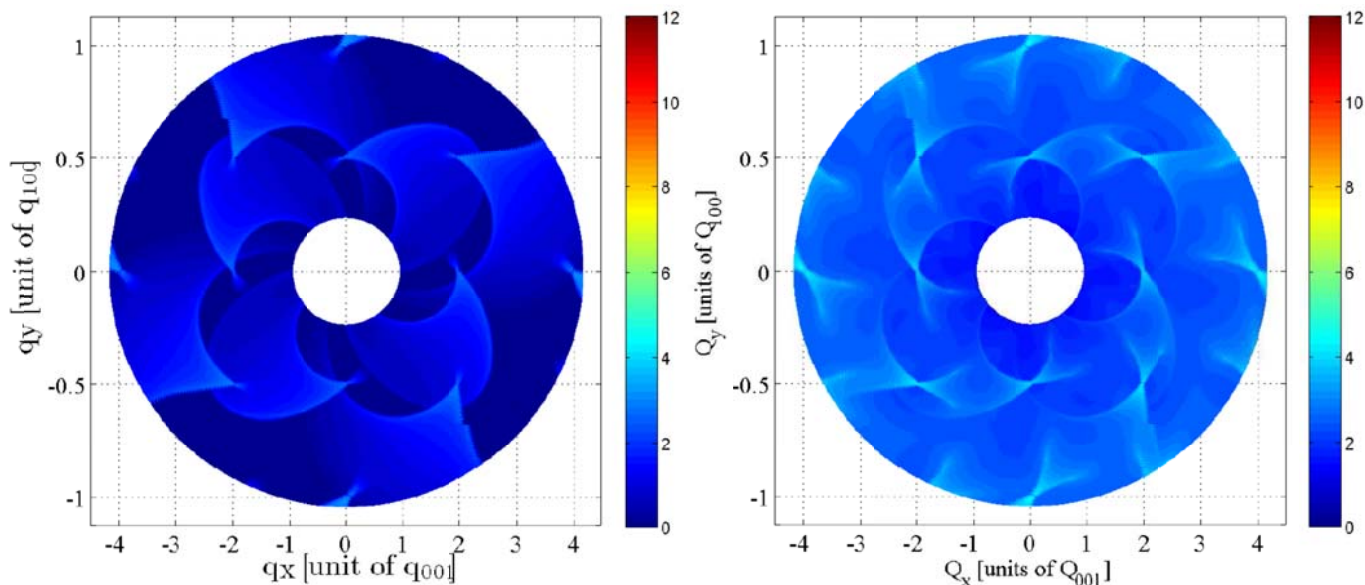


Figure 14: McStas simulations of the scattering from an FCC crystal at 10K (left) and 290K (right). The lattice constant and phonon velocity of sound have been set to the c-axis lattice parameter of PG and the phonon velocity of sound for phonons propagating along c, respectively.

Given that the FCC model does not include elastic scattering at all, there are no Bragg peaks in the maps. Further, we re-emphasize that the model uses an incorrect crystal structure for PG. We therefore limit ourselves to looking at the scattering in the immediate vicinity of $(Q_x, Q_y)=(-2, 0)$.

At 290K the diffuse phonon tails extending from $(-2, 0)$ are roughly equally intense at positive and negative values of Q_y . By contrast, at 10K, there is a pronounced asymmetry, with the diffuse intensity at negative Q_y being suppressed more strongly than the diffuse intensity at positive Q_x . Even with the significant limitations of the McStas model for the sample, a comparison between figures 10, 11 and 14 clearly shows that the observed diffuse scattering is due to phonons, and strongly suggests that a McStas simulation using a sample that more accurately reflects the structure of PG will successfully capture all the diffuse intensity in the data maps.

4.2 Experimental Results from RITA II

The aim of this experiment was to measure the energy width and any possible tails directly, by taking data similar to those shown in Figure 9. The low background and large volume of its detector tank makes RITA II ideally suited to this experiment. The analyzer of the triple axis spectrometer RITA II was modified from a 9 blade multiplexed PG analyzer to a single cooled PG blade analyzer mounted inside a CTI cryo device. The CTI was mounted directly on the existing analyzer motor and was fully rotatable, see figure 15. To avoid background from the surrounding instruments and guides

Pyrolytic Graphite, an experimental report for the ESS CAMEA

boron enriched plastic blocks were used to shield the front of the setup, see figure 16. For practical reasons the blocks limit the rotation of the CTI, meaning that any optimization of this motor was done prior to the shielding.

The detector of the RITA II instrument is a position sensitive detector (PSD). In front of the detector there is a collimator normally used to avoid cross talk between the 9 blades of the multiplexed analyzer. This collimator is seen just behind the CTI in figure 15 and was kept in our setup, where it serves to minimize background. The total distance between the analyzer and the PSD was roughly 350 mm.

To emulate the experiments at IRIS and OSIRIS as closely as possible, we also used a vanadium sample, which was mounted inside a standard cryostat on the sample position of RITA II. We chose a fixed $k_f = 1.57 \text{ \AA}^{-1}$ corresponding to $E_f = 5 \text{ meV}$. This is a commonly used energy in cold-neutron triple axis experiments due to the possibility of cleaning away higher-order contamination of the scattered beam using a cooled Be-filter. In our experiment we also used such a filter, placed directly before the entrance into the analyzer tank (the trumpet visible on the left in Figure 15 is where the beam enters the analyzer tank after having passed through the Be filter). The incoming energy was tuned by a PG monochromator and collimated by an 80' collimator. Finally the doors of the RITA II analyzer tank were partially closed and the small opening needed for the CTI tubes and wires was covered with cadmium. The PG analyzer blade, inside the CTI, was mounted on an aluminum plate which was 1mm thick. For this experiment we chose a $50 \times 10 \times 1 \text{ mm}^3$ PG piece of mosaicity 0.5° , which was thoroughly cleaned before it was inserted in the CTI.

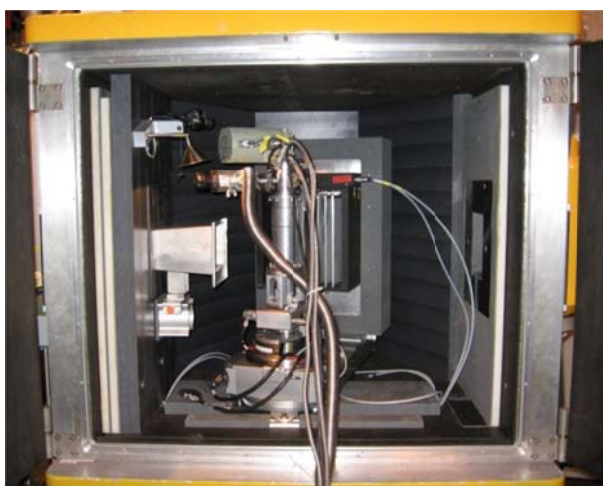


Figure 15: A sideways view into the detector tank of RITA II. On this picture the doors are open. The CTI was mounted on the analyzer motor with a custom-made adapter which brings the PG blade inside the CTI into the right height relative to the neutron beam.



Figure 16: The final shielding of the detector tank, (before closing the doors of the analyzer housing as much as possible) leaving only a necessary hole for the CTI tubes and wires.

Unfortunately, the outcome of the experiment was severely limited due to the unscheduled 2½ week shutdown of SINQ. We were able to set up and acquire only two complete datasets - both with the vanadium sample at 10K. We performed constant two Q-scans between -1 meV and +1 meV in 41 points at an analyzer temperature of 10 K and 290 K (See Figures 17 and 18). We observe that the width of the elastic peak is slightly larger at 290 K than at 10 K, see figure 8. Using a simple fit to a single Gaussian peak profile we find $\text{FWHM}(T=290 \text{ K}) = (0.1945 \pm 0.0016) \text{ meV}$ and $\text{FWHM}(T=10 \text{ K}) = (0.1700 \pm 0.0021) \text{ meV}$.

Pyrolytic Graphite, an experimental report for the ESS CAMEA

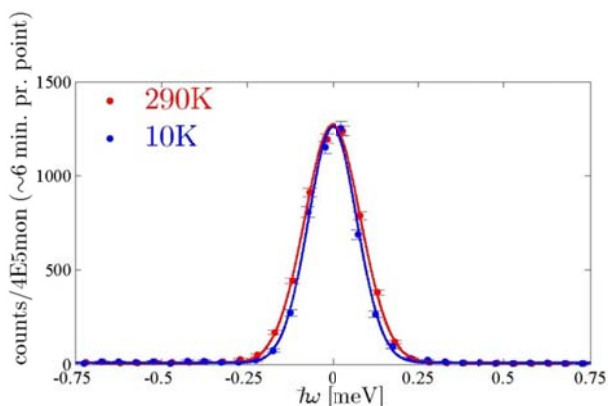


Figure 17: The constant-Q scans of the elastic line from vanadium. The blue and red lines represent fits at 10K and 300K, respectively, as described in the main text.

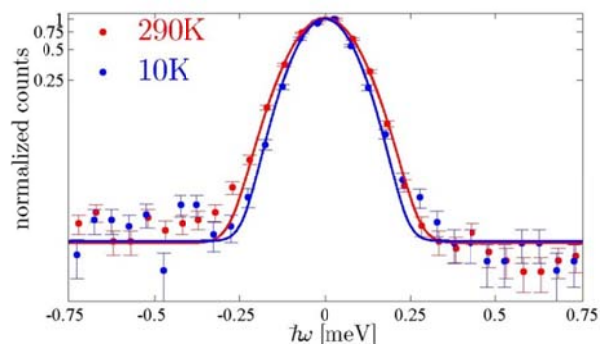


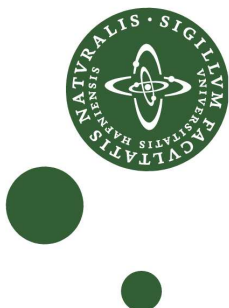
Figure 18: The constant-Q scans normalized to their maximum shown on a logarithmic scale. If any tails are present on either side of the main peak, they are generally easily identified on this scale.

No clear tails/shoulders are observed on either flank of the main peak, see figure 17 (or 18 on a logarithmic scale), indicating only very little contamination from thermal diffuse scattering at the selected value of E_f and with the high-quality 0.5° mosaicity PG piece chosen. A more complicated peak profile consisting of one Gaussian, describing the main peak, plus one Lorentzian, describing any tails, was tried. However, this did not produce stable fits.

5 Outlook

Our original plan for the RITA-II experiments included studying the temperature dependence of the thermal diffuse scattering at different values of A_4 and E_f as well as several values of the PG mosaicity. This was not possible due to the unscheduled shutdown mentioned above. Our results are therefore preliminary and will be followed by another test experiment in May 2014. The results of this experiment will feed into the eventual decision process regarding whether to cool the CAMEA analyzers or not.

- [1] C.J. Carlile and M.A. Adams, *The design of the IRIS inelastic neutron spectrometer and improvements to its analysers*, Physica B, 182, 431-440 (1992)
- [2] M.T.F. Telling et al., *Performance of the cooled pyrolytic graphite analyser bank on the OSIRIS spectrometer at ISIS*, ISIS facility reports (2004)
- [3] M.T.F. Telling and K. H. Andersen, *Spectroscopic characteristics of the OSIRIS near-backscattering crystal analyser spectrometer on the ISIS pulsed neutron source*, Phys. Chem. Chem. Phys., 7, 1255-1261 (2005)



Technical University of Denmark



McStas



CAMEA

Technical Solutions

Author:

J. O. Birk



PAUL SCHERRER INSTITUT



ÉCOLE POLYTECHNIQUE
FÉDÉRALE DE LAUSANNE

Contents

1	Introduction	2
2	Sample area	2
2.1	Sample Changing	2
3	The Analyser-detector tank	3
4	Analysers	6
4.1	Aligning	6
5	Beam vanes	6
6	Detectors	6
7	Magnetic materials	7

1 Introduction

CAMEA is a new instrument concept so it is possible that the construction could or maintenance of the instrument would be hampered by technical details. In order to prevent this a technical pre-design have been performed. This is not a final technical solution with bolts and nuts but a 3d drawing where the important elements were put into place to confirm that it could be constructed in reality and that it would be possible to get access to the key areas for maintenance. Further the design has been used as a basis for the cost estimate. Since the primary instrument will not be unique the design has concentrated on the secondary instrument.

2 Sample area

The sample will be placed on a commercial sample table, compatible with the extreme sample environments planned for CAMEA. It is hoped that certain sample environments can be bought especially for CAMEA and can contain a radial collimator plus shielding hiding everything above and below the scattering plane from the analysers. There will further be space for an external radial collimator and filter outside the sample environments. These can be rotated away when not needed.

2.1 Sample Changing

With the unprecedented high flux on the sample of CAMEA certain samples will become too active for human handling after the experiment. Waiting for them to cool down will delay experiments considerably so a solution where samples can get changed without close human contact will be needed. The best solution will be a robotic sample changer but as a fall back we will here describe a simple

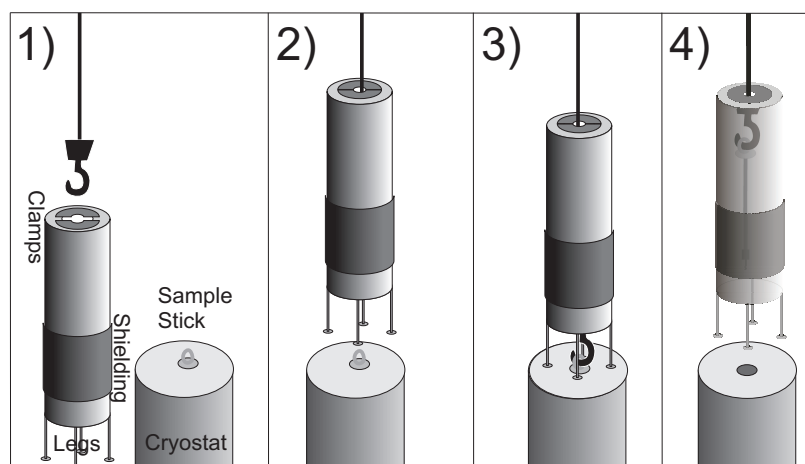


Figure 1: Illustration of simple sample changer. 1) The crane is lowered down through the sample changer tube and the clamps are closed. 2) The crane lifts the tube on top of the cryostat. 3) The crane is connected to the sample stick and it is disconnected from the cryostat. 4) The crane lifts samplestick with active sample and the tube with shielding away from the cryostat to a storage area.

mechanical solution that will work with any cryostat.

The fall back solution is a tube that is lifted onto the cryostat with a crane, then the sample stick is raised into it and lifted away with the sample on it to a safe storage facility where it can cool down. (See figure 1)

3 The Analyser-detector tank

The entire analyser-detector module will be encapsuled in an Al vacuum tank (se figure 2). To sustain the outside pressure 5 cm Al is generally needed giving a tank mass of 6 tons in total. Since the tank will remain stationary once installed the weight will not be problematic. A thin window for the incoming beam will be incorporated and will not compromise the structure. It will be possible to remove the lid of the tank to allow access to the analysers and hatches in the side will allow access below the detectors. The tank will be covered on the outside in a thick layer of plastic and Boron plastic and on the inside with a thin layer of Cd.

Inside the tank the analyser-detector module will be standing on the floor in a way designed to make it independent of any pressure deformations of the tank. This module will have a rail allowing the entire module to shift up to 9 degrees in order to cover dark angles.

The module itself consists of 15 segments each covering 9 degrees and with a 6 degrees active area covered by 10 analyser-detector setups behind each other.

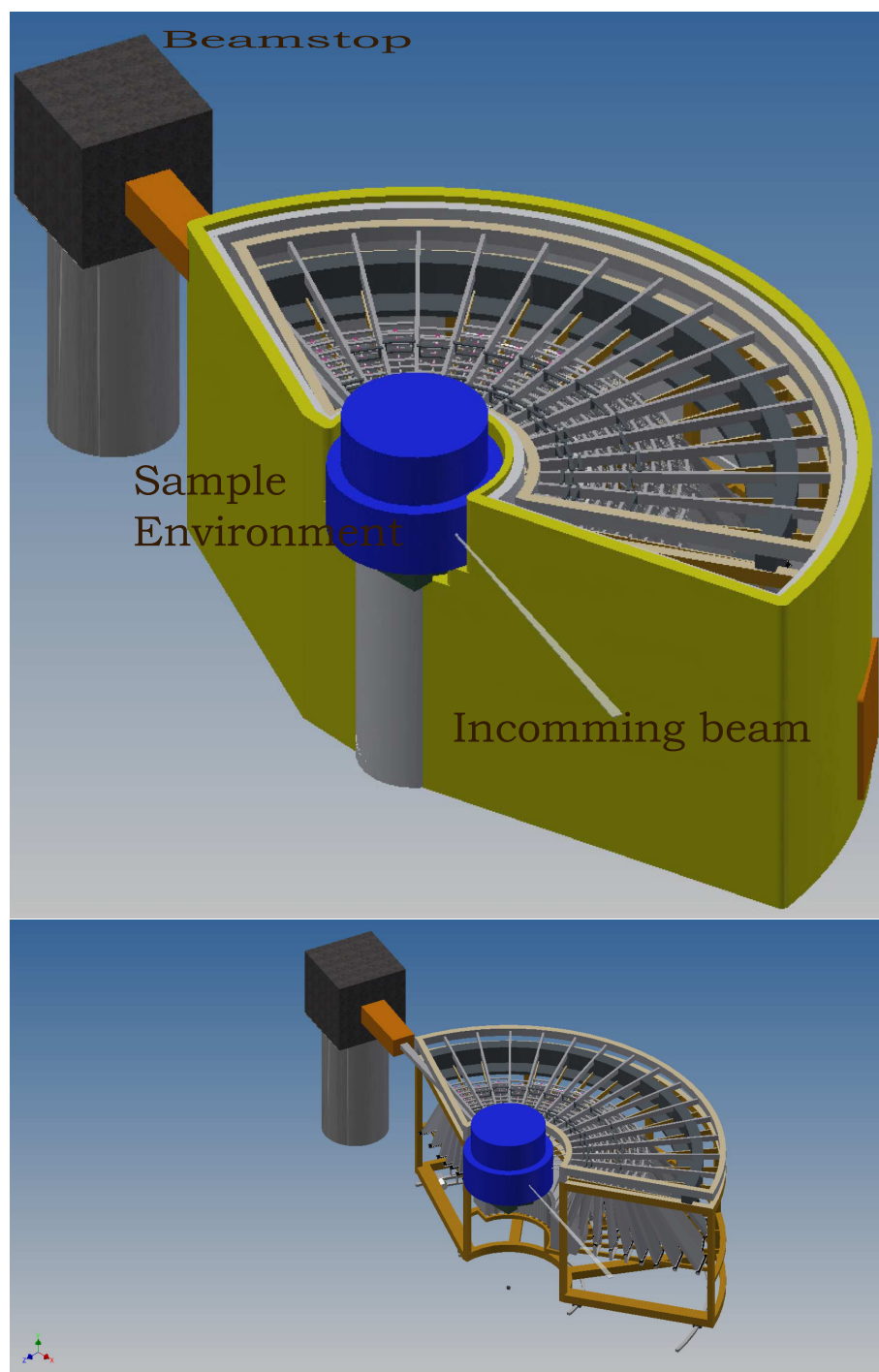


Figure 2: The detector tank with without its lid (top) and the analyser-detector modules inside it (bottom).

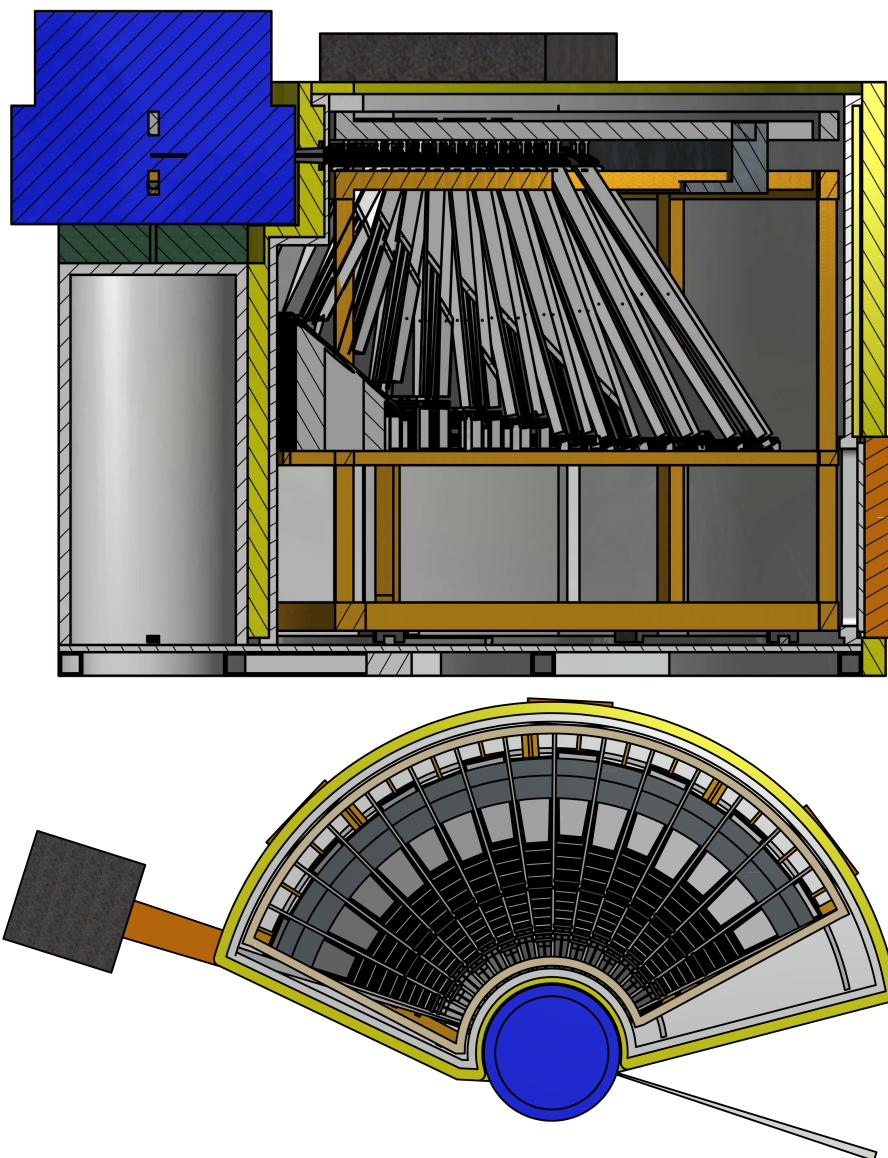


Figure 3: The tank seen from the side (top), and from the top (bottom panel).

4 Analysers

The analysers will be lowered down from above into predefined slots and locked into position. They will consist of an Al frame holding Silicon wafers with the PG crystals screwed in place. The design is such that the Al parts do not block line of sight from sample to analysers further back and all non-active elements can thus be hidden behind Cadmium sheets. It will be possible to remove or replace each analyser individually when the lid of the analyser tank is removed. Every second segment will have all analysers (and detectors) placed 4 cm further back than the standard segment. This zigzag pattern will be key in reducing the dark angles to at most 3 degrees per segment. The first segment will be constructed slightly differently with shorter analysers that is only mounted from one side in order to get as close to the direct beam as possible. In this way it is possible to get down to 3 degrees scattering angle which allows inelastic SANS measurements.

4.1 Aligning

The Al mounting will be machined to hold the Si wafers and thereby the analyser crystals in precalculated fixed angles so aligning is unnecessary. To check the alignment and as a backup if something is not aligned well enough the prototype testing showed that optical alignment and small air spacers will be a fast and permanent fix. Since the energy resolution comes from distance collimation (i.e. that the small sample height and analyser and detector width combined with the long distances limits the possible scattering angles) and not the mosaicity of the graphite the instrument is very robust to small analyser misalignments.

5 Beam vanes

Just below the analysers Al vanes with an inside Cd lining will lead down to the detectors and make sure that each detector group can only "see" one analyser. It will be possible to install radial collimators in these guides to decrease the solid angle seen by the detectors further.

6 Detectors

As the reflected signal from the analysers will become wider than the 9 degrees of each segment the detectors will overlap with the neighbour segment but thanks to the zigzag pattern and beam vanes no interference will be possible. The last 7 detector groups will each consist of 3 parallel detector tubes placed in a Al housing with Cd cladding. For the first 3 detectors the signals are so close that this will not leave space for the inactive ends of the detectors so instead the analysers will reflect down towards one big detector area. These are constructed from radially aligned detector tubes covering the entire cone. Figure 4 shows how the reflected signal will look on this detector setup. Below the detectors there will be an empty space so that it is possible to lower the 7 backmost detectors

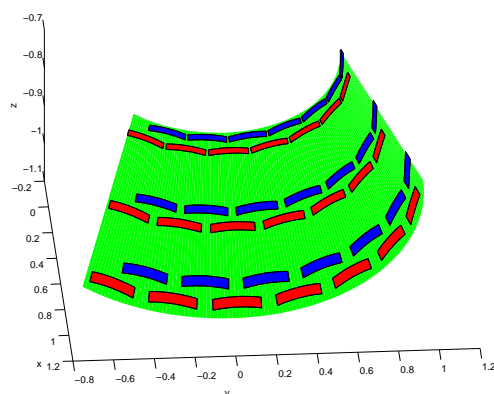


Figure 4: The first detectors. The green area is the total area covered by detectors while the red are the region illuminated by the 3 first analysers of the even analyser segments while the blue is illuminated by the odd analyser segments. It is possible to fill the unused parts of the detector tubes with a non-conducting ceramic material to reduce He_3 consumption.

from one segment down on a wagon and move it out of the tank through one of the hatches for maintenance.

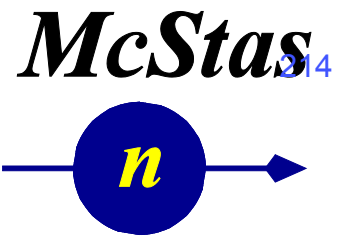
It will be possible to remove the front most detectors individually from the space below the detectors if maintenance is needed.

7 Magnetic materials

The tank and holders can be produced in nonmagnetic materials. Only the rails moving the analyser detector module needs some amount of steel. However this is more than two meters from the sample position and should cause no problems.



Technical University of Denmark



CAMEA

Costing report

Author:

N. B. Christensen



PAUL SCHERRER INSTITUT



ÉCOLE POLYTECHNIQUE
FÉDÉRALE DE LAUSANNE

CAMEA costing report

Executive summary: *The cost of the CAMEA spectrometer, involving guides and shielding, the spectrometer itself, key pieces of sample environment equipment needed to fulfill the science goals of CAMEA, and the manpower needed for construction, is estimated at 19.920 M€.*

Since we've attempted to make conservative estimates, this numbers should be seen as an upper limit. Out of the total construction cost, 33% is the cost of guides, shielding and shutters, 40% is the cost of the CAMEA-specific parts, i.e. choppers, analyzer tank, graphite analyzer crystals, ³He detectors, radial collimator, facilities for polarization analysis, Beryllium filter etc. 19% of the total cost corresponds to the estimate prices of the magnets and pressure cells foreseen for CAMEA but useable on other ESS instruments as well. Salaries corresponding to 21 man years are estimated to account for 7% of the total cost.

This document details the elements considered in the costing of the proposed CAMEA spectrometer for ESS, and is subdivided as follows

1. Guides and shielding
 - a. Guides
 - b. Mechanics and installation
 - c. Guide shielding
 - d. Instrument cave and beam stop
 - e. Shutters
 - f. Vacuum pumps for guides
2. CAMEA spectrometer
 - a. Choppers
 - b. Divergence jaws
 - c. Sample table
 - d. Vacuum tank
 - e. Vacuum pumps
 - f. PG analyzer crystals mounted on Si-wafers
 - g. Cooling machines for analyzers
 - h. Detectors
 - i. Be filter
 - j. Radial collimator
 - k. Electronics
 - l. Polarization analysis
3. Sample environment for CAMEA

- a. Magnets
- b. Pressure cells
4. Manpower
5. Summary of construction costs
6. Conclusion

The choice of subdivision is made to emphasize that a significant fraction of the full cost of CAMEA comes from the price of guides and various pieces of shielding. The total price of these will, to a significant extent, be similar for all long instruments at ESS.

We have attempted to give conservative estimates of all components, i.e. estimates that may turn out to be too high. For example, the cost of shielding of guides is highly uncertain and believed to be in the range of 1-2 times the price of the guides themselves. In this case, we have chosen to use the ratio 2. When available, information about the estimated uncertainties is included in individual subsections.

In each sub-section we indicate the sources of information lying behind the estimated cost of a given component. When possible we have used price estimates given by ESS staff members.

We have benefitted significantly from exchange of information with Felix Groitl, EPFL Lausanne, who has collected price estimates for the version of the CAMEA concept which will be built for the RITA-II spectrometer at PSI (PSI-CAMEA). In addition we are thankful to Pascal Manuel (ISIS), Christian Mammen (JJ X-ray), Peter Böni (Swiss Neutronics and TUM), Thomas Krist (Neutron Optics Berlin and HZB), Rasmus Toft-Petersen (HZB), Oleksandr Prokhnenko (HZB) and Uwe Filges (PSI) for information on the cost of various components.

For easy overview, all cost estimates are collected in a table in section 5. This table is reproduced in the costing section of the main proposal.

1. Guides and shielding

In this section, we estimate the cost of the CAMEA guide solution, the price of the guide shielding, and the price of additional shielding of the instrument beyond what is included in section 2d on the CAMEA vacuum tank. Also included is the cost of beam shutters and the pumps for the guides.

a. Guides

For the estimate of the price of the guide solution for CAMEA, we have used a price estimate provided by Swiss Neutronics [1].

The CAMEA guide solution is described in detail in the CAMEA guide report [2]. It can be divided into segments (each based on shorter tapered guide pieces) as indicated in Table 1 below.

Swiss Neutronics estimates the total price of this guide (Ni/Ti on float glass or borofloat glass) as follows:

Cost of guides **1.310 M€**

CAMEA guide				
Segment number	Segment length [m]	Distance from moderator face to the end of the segment [m]	m-value	Shape/Size
No guide				
1	2.16	2.16	No guide	No guide
Parabolic feeder				
2	1.74	3.90	3	Piecewise Straight
3	1.74	5.63	3.5	Piecewise Straight
4	0.87	6.50	3	Piecewise Straight
Chopper space. No guide				
5	0.10	6.60	No guide	No guide
Ellipse 1				
6	6.52	13.12	3.5	Piecewise Straight
7	6.52	19.64	2	Piecewise Straight
8	39.12	58.76	1.5	Piecewise Straight
9	6.52	65.28	2	Piecewise Straight
10	6.52	71.80	3	Piecewise Straight
Straight section (kink)				
11	13.94	85.74	2	Piecewise Straight
Ellipse 2				
12	15.73	101.47	2	Piecewise Straight
13	47.20	148.67	1	Piecewise Straight
14	7.87	156.53	2	Piecewise Straight
15	7.87	164.40	3.5	Piecewise Straight
Total length				

Table 1: CAMEA guide solution as described in the CAMEA Guide report [2]. The guide solution is based exclusively on straight tapered guide pieces forming the longer segments indicated. It consists of a parabolic feeder section (2.16-6.5 meters from the moderator face), and two elliptical sections (6.60 to 71.80 meters and 85.74 to 164.40 meters from the moderator face, respectively) with a straight kink section in between them (71.80 to 85.74 meters from the moderator face). Space has explicitly been allowed for the pulse shaping choppers at 6.5 meters from the moderator face, while choppers further downstream will not take up much space and have been excluded in the price estimate.

b. Mechanics and installation

Swiss Neutronics [1] estimates the following cost of the mechanical support pieces needed for the CAMEA guide (Special housing for the feeder section; Massive steel casing's for the two elliptical sections and for the kink section. I-beams and posts are included), and for installation by Swiss Neutronics using a laser tracker.

- Mechanics (housing, posts, I-beams) 1.209 M€
- Installation using laser tracker 0.086 M€

Cost of mechanics and installation 1.295 M€

c. Guide Shielding

For guide shielding we make the assumption that everything outside of the common bunker which ends at a distance of 30 meters from the moderator face is paid for by the CAMEA budget. Phil Bentley (ESS) estimates the ratio of the price of guides to shielding as being between 1:1 and 1:2. To be conservative we have chosen to use the ratio 1:2 for everything outside the first 30 meters.

With these assumptions and taking a constant price per meter of the CAMEA guide, our estimate for the price of guide shielding is $2 \cdot (1 - 30/164.4) \cdot 1.310 \text{ M€} = 2.142 \text{ M€}$

Cost of guide shielding 2.142 M€

d. Instrument cave and beam stop

According to Phil Bentley (ESS) all instruments are foreseen to sit in their own caves/hutches in order to shield neighboring instruments from each other. Combined with the cost of a beam stop, this additional shielding is estimated conservatively at 1 M€. The estimate is based on the experience from ISIS TS2 where the price was 700 kGBP.

Cost of instrument cave and beam stop 1.000 M€

e. Shutters

All instruments will have three shutters. It is at present not clear if one of these will have to be a heavy shutter. Phil Bentley (ESS) estimates the price of a heavy shutter as 0.75 M€, whereas a light shutter costs around 20 k€. Under the conservative assumption that CAMEA needs a heavy shutter, we estimate

the total price of shutters for CAMEA as 0.79 M€. With three light shutters, the price would be significantly less, 60 k€.

Cost of shutters	0.790 M€
------------------	----------

f. Vacuum pumps for guides

At the Paul Scherrer institute (PSI), a combination of backing and turbo pumps are used to pump the guides. We assume that this will also be the case for CAMEA. A combination of backing and turbo pumps comes to 10 k€. Adding a 4 k€ control unit, and assuming that one needs one such combination of pumps for every ~40 meters of guide, we arrive at an estimate of $4 \cdot 14 \text{ k€} = 56 \text{ k€}$ for the price of guide pumps for the 165 m CAMEA guide.

Cost of vacuum pumps for the guides	0.056 M€
-------------------------------------	----------

2. CAMEA spectrometer

In this section, we estimate the cost of the CAMEA spectrometer, excepting the parts directly related to guides and shielding, which were treated in the previous section. We also do not including sample environment, which will be treated in section 3.

a. Choppers

The CAMEA chopper solution is described in the Simulations and Kinematic Calculations report [3] and is reproduced in Table 2 below.

Iain Sutton (ESS) estimates the total cost of the above choppers at 1.425 M€ with an estimated uncertainty of $\pm 20\%$. This includes vacuum systems, cooling, control and integration into the instrument, but does not include installation. We note that Mirrortron [4] provided us with a quote of the above chopper solution of 1.050 M€. This does not include various support systems and integration.

Cost of chopper system	1.425 M€
------------------------	----------

Chopper section	Description
1	<p>Two pulse shaping choppers</p> <p>Rotation speeds: 14 to 210 Hz Angular openings: 170 degrees Distance: 6.5 m from the moderator. Radius: 35 cm</p>
2	<p>First frame overlap chopper</p> <p>Rotation speed: 14 Hz Angular opening: 20 degrees Distance: 8 m from the moderator. Radius: 35 cm</p>
3	<p>Second frame overlap chopper</p> <p>Rotation speed: 14 Hz Angular opening: 25 degrees Distance: 13 m from the moderator. Radius: 35 cm</p>
4	<p>Tail removal chopper</p> <p>Rotation speed: 14 Hz Angular opening: 157.6 degrees Distance: 78 m from the moderator. Radius: 35 cm</p>
5	<p>Two order sorting choppers</p> <p>Rotation speed: 180 Hz Angular opening: 2 times 80 degrees Distance: 162 m from the moderator. Radius: 35 cm</p>

Table 2: The CAMEA chopper solution as described in detail in Ref. [3].

b. Divergence jaws

We envisage the use of WISH-type jaws [5] to control the beam divergence for CAMEA. According to Pascal Manuel at ISIS, 5 sets of jaws and motor control cost 87500 GBP when they were purchased for WISH a few years ago. Assuming, conservatively, that cost has gone up by 20%, this amounts to 123 k€ on CAMEA.

Cost of divergence jaws	0.123 M€
-------------------------	----------

c. Sample table

A Huber sample table for CAMEA was estimated by the CAMEA team at 34 k€. This is somewhat higher than the 20 k€ paid for the EXED sample table at HZB (information from Oleksandr Prokhnenko, HZB) a

few years ago, and is therefore a conservative estimate. The EXED sample table is capable of supporting 1000 kilos and has 3 translational and 3 rotational degrees of freedom.

Cost of sample table	0.034 M€
----------------------	----------

d. Vacuum tank

For the vacuum tank hosting the analyzers and detectors, the CAMEA team has estimated a total cost of 0.908 M€. This includes the tank itself, shielding of the tank (Cast B₄C shielding on the outside; Cadmium shielding on the inside), holders and Cadmium shielding for detectors (See below for separate costing of detectors), mechanical holders for the analyzers (Pyrolytic graphite mounted on Si wafers. These are treated separately below), a beam stop inside the tank and Aluminum vanes, covered with Cadmium, designed to prevent cross-talk between different analyzer-detector pairs [6]. Finally, the costing of the vacuum tank includes the mechanics needed to rotate all analyzers around the sample positions.

For cooling of the analyzers, we have used cost estimates from the parallel PSI-CAMEA project for which cooling is being considered. For PSI-CAMEA this is achieved through cooled plates to which the analyzers are thermally anchored. The plates are thermally isolated from the tank (zirconium oxide isolation). Cooling is achieved by pulse tube cooling machines (see below for separate costing). Scaling the solution found by the PSI-CAMEA team, we estimate the cost of this arrangement to be 150 k€ at the ESS version of CAMEA.

Adding the cost of the vacuum tank and the cost of the solution for cooling the analyzers, we arrive at a total price for the analyzer tank (excluding detectors, Si wafers, graphite crystals and pulse tube cooling machines) of 1.058 M€.

Cost of vacuum tank	1.058 M€
---------------------	----------

e. Vacuum pumps

For the parallel project, PSI-CAMEA, PSI technicians have estimated that a single pump costing 25 k€ is needed for evacuating the vacuum tank. We assume the same price for the ESS version of CAMEA.

Cost of vacuum pump	0.025 M€
---------------------	----------

f. PG analyzer crystals mounted on Si-wafers

The price estimate of Si-wafers on which to mount the pyrolytic graphite analyzer crystals was collected by the CAMEA team. For 2m² of pyrolytic graphite, the price estimate is 362 k€.

The price of the PG analyzers themselves is estimated from the cost of the graphite purchased for the CAMEA prototype. A single 75 mm x 10 mm x 1 mm pyrolytic graphite piece of 60' mosaicity was priced by Panasonic at 55600 JPY in 2012. Scaling to 2 m² we arrive at 1.104 M€.

Note that we have not made allowance for a reduction in the total price of the graphite upon ordering a very large amount of graphite. Such a reduction should be negotiable and should bring the cost of graphite below 1 M€.

Cost of PG analyzers and Si-wafers	1.466 M€
------------------------------------	----------

g. Cooling machines for analyzers

The PSI-CAMEA project is considering 3 low-vibration pulse tube cooling machines to cool the analyzer crystals of the PSI-CAMEA analyzer box which covers 50 degrees in scattering angle. Scaling to the angular coverage of the ESS version of CAMEA, we conservatively estimate that 8 pulse tube cooling machines are needed. One such pulse-tube costs 44 k\$ according to quotes collected by Felix Groitl (EPFL and PSI-CAMEA). Hence we estimate that the cost of pulse tube cooling machines for CAMEA will be 255 k€.

Cost of cooling machines for analyzers	0.255 M€
--	----------

h. Detectors

The price of detectors was estimated by the CAMEA team based on information from Richard Hall-Wilton (ESS). The estimate combines hardware, vacuum seals and the ³He gas.

Hardware	353.500 €
----------	-----------

Vacuum Seals	293.000 €
--------------	-----------

³ He gas (24.7 liters, 7 bar)	250.500 €
--	-----------

Cost of detectors	0.897 M€
-------------------	----------

i. Be filter

For the Beryllium filter, we use numbers collected for the PSI-CAMEA project for their 50 degree Be filter. We imagine that CAMEA with its 130 degree angular coverage will use a similar filter (Length 10 cm; height 5 cm) and simply scale the cost estimate from PSI for the construction of the housing of the

filter and various pieces of shielding. By this procedure we reach a price for the housing and shielding of 126 k€.

For the Beryllium itself, we assume that CAMEA will use 260 half-degree Be blocks (Materion), each costing 368 € according to quotes collected by Felix Groitl (EPFL and PSI-CAMEA). In total, the purchase of Beryllium amounts to 96 k€, which has to be added to the cost of the housing and shielding of the filter.

Cost of Beryllium filter, housing and shielding	0.222 M€
---	----------

j. Radial collimator

We're using information received from JJ X-ray [7]. In the case of CAMEA, JJ X-ray estimates the price of a 130 degree, vacuum compatible, radial collimator (vertical coverage 3 degrees; 1.5 degree separation between Gd covered foils) at 50 k€.

Cost of radial collimator	0.050 M€
---------------------------	----------

k. Electronics

Using numbers received from Thomas Gahl, ESS, we estimates a total cost of 402 k€ for electronics for CAMEA. This includes motion control, wiring cabinets and basic power distribution, electronics for the personal safety and shutter systems, PLC control and control boxes for connection to the EPICS control layer. Finally, it also includes an estimated cost of design, installation and commissioning.

Cost of electronics	0.402 M€
---------------------	----------

l. Polarization analysis

CAMEA will be designed from the outset to have polarization analysis.

Incident beam polarization: Thomas Krist (HZB and Neutron Optics Berlin [8]), estimates the cost of a polarizer-bender at 4.5 k€ per square centimeter. At a distance of around 6.6 meters from the CAMEA sample position, the guide is approximately 8.2 times 10.8 centimeters. Assuming that 10% of the length along each axis is occupied by the mechanical support of the bender, we arrive at a price of 323 k€.

For comparison, Rasmus Toft-Petersen (HZB) informs us that the S-bender setup, including guide translation stage, recently purchased for FLEXX, cost 380 k€. Since the two estimates are very close and

the former does not include translation stage, we estimate that the correct price for CAMEA will be around 400 k€.

Polarization analysis of the scattered beam: The Paul Scherrer Institute has designed and built a polarization supermirror analyzer for the HYSPEC spectrometer at SNS. Scaling the price of this device to scattering angle coverage of CAMEA, we estimate a price of 1.7 M€.

Cost of polarization for CAMEA	2.100 M€
--------------------------------	----------

3. Sample environment for CAMEA

In this section, we estimate the cost of the essential pieces of sample environment required to fulfill some of the main science goals of CAMEA. Note that all pieces of sample environment equipment listed will also be available to other ESS instruments, if they can be accommodated on these.

a. Magnets

For the price of magnets, we use estimates from CAMEA team leader Henrik M. Rønnow. These are based on current quotes from providers of magnets and auxiliary equipment.

- High- T_c split coil magnet capable of going beyond 20T. Costing this device is extremely difficult, since the technology to build one for use on a neutron spectrometer is not fully developed. We tentatively estimate a price of 2.5 M€.
- 10T wide bore magnet for use in combination with pressure cells. Price estimate 500 k€
- Dysprosium boosters capable of adding 2T to the maximum field of a given magnet. Price estimate 50 k€
- Dilution insert for magnets. Price estimate: 180 k€

If the technology for the high- T_c split coil magnet is not mature two years before the construction of CAMEA is finalized, we will instead go for a 16T magnet with an estimated price tag of 1.4 M€

Combining the high- T_c split coil magnet, the 10T wide bore magnet, the Dy boosters and a dilution insert, we arrive at a total cost of 3.23 M€, which drops to 2.13 M€ if the high- T_c technology does not develop at a sufficiently rapid pace.

Cost of magnets and auxiliary equipment	3.230 M€
---	----------

b. Pressure cells

We are using price estimates received from Stefan Klotz, Université P. & M. Curie, France

- Paris-Edinburgh pressure cell for low-temperature research, including press, cryostat, CCR and He compressor. Estimated price: 250 k€.
- Diamond Anvil 30 GPa pressure cell for high temperatures. The cell itself and the facilities for external or laser heating, temperature and pressure measurement capabilities and He compressor. Total price estimate: 280 k€.
- High pressure cell for low-temperatures to fit into 10T wide bore magnet. High performance McWhan cell for the 2-3 GPa range. Price estimate 50 k€.

Cost of pressure cells and auxiliary equipment	0.580 M€
--	----------

4. Manpower

We estimate that the total personnel cost related to the CAMEA spectrometer will be 21 man-years, divided as 5 man year for a lead scientist, 5 man years for a lead engineer and 11 man years for various technical tasks, e.g. the construction of the analyzer tank, which was estimated to take up to 3 years. Using current typical Danish salaries for Scientists (Lead Scientist, Lead Engineer) and Technical Staff, we arrive at salary costs of 1.460 M€.

It is assumed that most of the hardware costs for major optical components include installation, as is the case, for example, for the guides. We also assume that electronic solutions are fully incorporated in the quotes for choppers and detectors.

Cost of manpower	1.460 M€
------------------	----------

5. Summary of construction costs

In table 3 we summarize the costing estimates from the previous sections. As can be seen from the table, the total construction cost of the proposed CAMEA instrument, excluding salaries, will be 18.460 M€, while inclusion of salaries brings the total cost to 19.920 M€. Out of the total cost, 33% corresponds to the price of guides, shielding and shutters, 40% corresponds to the cost of CAMEA-specific components such as the chopper system, vacuum tank, polarization analysis, cooled PG analyzers, ³He detectors etc. Finally, 19% of the total estimated cost comes from the specific magnets and pressure cells foreseen in order to be used on CAMEA, most notably a high- T_c split-coil magnet capable of going beyond 20 Tesla, and 7% is the manpower cost. We note that we have attempted to make conservative estimates throughout. Hence, we believe that the quoted cost, 19.920 M€ is an upper limit.

On the primary spectrometer side, the main cost drivers are guides and shielding of guides for the instrument. For the secondary spectrometer, the most costly item is polarization analysis. Finally, the combined price estimate for sample environment equipment is dominated by the cost of the large high- T_c split coil magnet.

Costing item	Price [M€]	Source of information and comments
Guides and shielding		
Guides	1.310	Swiss Neutronics.
Mechanics and installation	1.295	Swiss Neutronics.
Guide shielding	2.142	ESS. This assumes a ratio of guide cost to shielding cost of 1:2. The ratio is expected to be in the range 1:1 to 1:2.
Instrument cave and beam stop	1.000	ESS.
Shutters	0.790	ESS. MCNPX simulations are needed to decide on the need for a heavy shutter (0.75 M€)
Vacuum pumps for guides	0.056	CAMEA team.
Sum for guides and shielding	6.593	
CAMEA spectrometer		
Choppers	1.425	ESS.
Divergence jaws	0.123	ISIS.
Sample table	0.034	CAMEA team.
Vacuum tank	1.058	CAMEA team.
Vacuum pump	0.025	CAMEA team.
PG analyzer crystals and Si wafers	1.466	CAMEA team.
Cooling machines for analyzers	0.255	CAMEA team.
Detectors	0.897	ESS and CAMEA team.
Beryllium filter	0.222	ISIS.
Radial collimator	0.050	JJ X-ray.
Electronics	0.402	ESS.
Polarization analysis	2.100	Neutron optics Berlin, PSI and CAMEA team.
Sum for CAMEA spectrometer	8.057	
Sample environment for CAMEA		
Magnets	3.230	CAMEA team. This includes a 20+ Tesla split coil magnet estimated at 2.5 M€
Pressure cell	0.580	Stefan Klotz. Université P. & M. Curie, France.
Sum for sample environment	3.810	
CAMEA cost excluding manpower	18.460	
Manpower		
Lead scientist (5 years) Lead engineer (5 years) Technical staff (11 years)	1.460	CAMEA team.
Sum for manpower	1.460	
Total cost of CAMEA	19.920	

Table 3: Summary and overview of the cost of the proposed CAMEA spectrometer.

6. Conclusions

We conclude that the CAMEA spectrometer as proposed here, can be constructed at a total cost of 19.920 M€.

References

- [1] Swiss Neutronics web page <http://www.swissneutronics.ch/>
 - [2] J. O. Birk, CAMEA Guide report.
 - [3] J. O. Birk, CAMEA Simulations and Kinematic Calculations
 - [4] Mirrotron web page: <http://www.mirrotron.kfkipark.hu/>
 - [5] L. C. Chapon, P. Manuel, P. G. Radaelli, C. Benson, L. Perrott, S. Ansell, N. J. Rhodes, D. Raspino, D. Duxbury, E. Spill, J. Norris, Neutron News 22 (2), 22-25 (2011).
 - [6] J. O. Birk, CAMEA Technical solution report.
 - [7] JJ x-ray webpage: <http://www.jjxray.dk/>
 - [8] Neutron Optics Berlin webpage: <http://www.neutronopticsberlin.com/>
- CAMEA reports can be downloaded here: <http://infoscience.epfl.ch/search?ln=en&p=camea&f=>

Executive Summary of the CAMEA Project Achievements

In this report we have presented work in which we proposed the highly innovative neutron spectrometer CAMEA – Continuous Angle Multi-Energy Analysis – for the European Spallation Source (ESS). By combining indirect time-of-flight with multiple consecutive analyser arrays, this instrument will provide a massive flux on the sample and a strongly enhanced efficiency of detecting neutrons within the horizontal scattering plane.

This project commenced with the conception of CAMEA, outlining how this concept is an advancement in neutron instrumentation. Considering the advantage of this instrument concept we then identified the potential measuring capabilities, and the potential science cases that these capabilities can be used for. A key ability of CAMEA is enabling the study of samples smaller than 1 mm³ enabling extreme pressure studies, opening up neutron scattering to experimental fields such as material discovery, soft matter and geoscience studies. For established fields such as quantum magnetism, and strongly correlated electron systems the experimental opportunities advance by the high count rates that can be achieved, that will lead to breakthrough discoveries. Support for this project was then sort within existing neutron scattering communities, and from eminent researchers in experimental fields for which neutron scattering would be enabled by this instrument.

After determining the experimental possibilities and demand for CAMEA an instrument design was optimized. Computer simulations were performed to optimize both the primary and secondary spectrometer and establish the feasibility of the instrument. These simulations were backed up by analytical calculations of the key performances of the instrument. This optimization allows the concept to be compared to existing spectrometers, and complimentary spectrometers proposed for the ESS. Thus clearly establishing CAMEA's performance gains over existing instruments, and it's complementarity to direct time-of-flight instruments at the ESS.

Instrument prototyping was performed to confirm key results of the computer simulations. Prototyping also provides a key step in developing technical solutions for instrument design, optimization, alignment and instrument operation. Extensive experimental studies were performed to study the performance of consecutively positioned neutron analysers for transmission rates, and sources of background scattering, providing indisputable evidence of the feasibility of CAMEA concept.

With the aid of feedback from the Science and Technical Advisory Panel and ESS technical help, this work enabled the presentation of a proposal for CAMEA to be built at the ESS. The Science and Advisory Committee advised

the ESS Steering Committee that CAMEA should be constructed at the ESS, with the project accepted as an instrument for the ESS.